# STUDIES IN UNSTEADY FLAME PROPAGATION

BY

Z Y WU

1986

THESIS SUBMITTED FOR THE DEGREE OF

DOCTOR OF PHILOSOPHY

IN THE FACULTY OF ENGINEERING

UNIVERSITY OF LONDON

AND

FOR THE DIPLOMA OF MEMBERSHIP OF

IMPERIAL COLLEGE

Computational Fluid Dynamics Unit

Room 440, MED Building

IMPERIAL COLLEGE OF SCIENCE AND TECHNOLOGY

Exhibition Road

LONDON SW7 2BX

U.K.

## ABSTRACT

This thesis presents the result of an experimental and numerical investigation of unsteady, flame propagation through a pre-mixed combustible gas.

Photographs and qualitative descriptions of the flame wrinkling in a vented combustion chamber obtained for various operating conditions are presented.

The single-fluid approach developed by Spalding and Awn (1978) is refined to simulate wrinkled laminar flames. In this approach, a "particle-tracking technique" (Spalding 1974, and Maxwell 1977) is used to track the flame fronts. Predictions with the approach are compared with the photographs of propagating flames, and agreement in trends is found. The approach is subsequently used to obtain information on the flame wrinkling in simpler circumstances.

A novel turbulence model(Spalding 1982b), the two-fluid model of turbulent combustion is applied to a one-dimensional, unsteady, confined, premixed flame with an idealized character. The experimentally observed features of combustion oscillations have been plausibly simulated with qualitative realism; and the explanation of the "buzz"-phenomenon, by reference to the model, made.

## PREFACE

I joined the Computational Fluid Dynamics Unit (CFDU) of Imperial College in Sept. 1982. The work presented in this thesis is the main outcome of my research activities during past three years, on unsteady, premixed flame propagation.

During the first year of my studies, I followed the postgraduate lecture courses given by the Unit and engaged in the studying and application of the PHOENICS computer code of Spalding (1981) to familiarise myself with the numerical methods used in the Unit. Some of this work, including the computation of plane flame propagation (Wu 1984a) and 1-D, compressible, transient flow (Wu 1984b), have been reported.

The main research started in the second year when the two-fluid model of turbulence proposed by Spalding (1982b) has manifested itself the potential ability in representing some important aspects of reality (Spalding 1984a). As a member of the group for developing the two-fluid model in CFDU, I have the privilege to be the first student applying such a model to unsteady flames. The original plan of the research was to simulate a practically important phenomenon, namely "buzz", and to make comparison with experiments.

After this first stage of the research, on the one-dimensional study of the "buzz"-phenomenon depicting the ability of the two-fluid model in explaining the phenomenon, it became clear that some aspects of the two-fluid model, which are undetected in the one-dimensional calculations, need to be illuminated before the extension of its application to two-dimensional unsteady flames and the comparison with experiments quantitatively can be made. Therefore, an experimental investigation on flame wrinkling and its computer simulation was envisaged to study the influence of the pressure gradient on the combustion rate as the second and necessary stage of the research.

In the experimental programme, laboratory flames in which the Rayleigh-Taylor instabilities have a measurable effect are sought. However, this objective has not yet been achieved, because the Rayleigh-Taylor instability, if it was present at all, was overshadowed by the Landau instability in the present series of experiment, as will be described in this thesis. In order to advance the understanding of the Landau instability, after the prediction of experiments for the validation of the computer-based, numerical model used in this study was made, a theoretical investigation, by way of the above model, of unsteady flames under simpler conditions was carried out.The work reported in this thesis spans both stages.

I would now like to acknowledge my gratitude to all those who have provided help and coorperation in various ways during my years at Imperial college. First of all, I am deeply grateful to my supervisors, Professor D B Spalding and Dr A S C Ma for their skillful quidance, constant encouragement and financial support. They have quided me not only in the main direction of my research topic, but also helped me on how to overcome difficulties arising from various aspects of the work. It is indeed a privilege to have worked with them.

I should also like to thank Dr W M Pun for his very useful advice and discussions. His suggestions and willingness to help is highly appreciated. I am very grateful.

Discussions with Dr H Q Qin have been particularly valuable. She has helped me to gain experience with CFDU computer system and the numerical procedure. I owe a great debt to her.

The day-to-day exchange of ideas with other research workers has been most helpful. These include M Andrews, S B Jia, J Liu, S Lo, F Villasenor, S T Xi and all other members of the research team in CFDU.

Thanks are due to Mrs Frith Oliver and Mrs Catherine Webb for their assistance in various administrative matters.

The help of Mr Bob King on all aspects of my experimental programme and his endeavour in the laboratory are highly appreciated. So too am I grateful to Mr Peter Dale for helping me with computer problems.

I would also like to thank Miss E M Archer and her staff for providing very efficient library services.

Space does not permit me to list all the names of individuals who has contributed towards my work. It is to all these people that I wish to offer my sincere thanks.

I would like to extend my gratitude to all the members of my family who have supported me in one way or another.

Finally, I wish to acknowledge the Education Ministry of China and the Health & Safety Executive of Great Britain for providing financial support during my studies, and Xi'an JiaoTong University for making it all possible.

London

Jan. 1986

Z Y Wu

CONTENTS


| | | PAGE NUMBER |
|---|---|---|
| ABSTRACT | | 1 |
| PREFACE | | 2 |
| CONTENTS | | 6 |
| LIST OF FIGURES | | 12 |
| LIST OF TABLES | | 20 |
| CHAPTER 1 - INTRODUCTION | | 21 |
| 1.1 | The Problem Considered | 21 |
| 1.2 | Practical Relevance | 22 |
| 1.3 | Present Study | 24 |
| 1.3.1 | Objectives of the Present Study | 24 |
| 1.3.2 | Present Contribution | 24 |
| 1.4 | Layout of the Thesis | 29 |
| PART 1 | WRINKLED LAMINAR FLAMES | 32 |
| CHAPTER 2 - | EXPERIMENTAL INVESTIGATION OF FLAME WRINKLING IN A VENTED COMBUSTION CHAMBER | 33 |
| 2.1 | Introduction | 33 |
| 2.2 | General Background | 34 |
| 2.3 | Experimental Apparatus | 38 |
| 2.4 | Experimental Procedure | 43 |

| | | PAGE NUMBER |
|---|---|---|
| 2.5 | Test Cases and Experimental Conditions | 45 |
| 2.6 | Presentation of Results | 49 |
| 2.7 | Accuracy of the Experimental Results | 59 |
| 2.8 | Discussions | 59 |
| 2.9 | Closure | 64 |
| CHAPTER 3 - MATHEMATICAL FORMULATION | | 66 |
| 3.1 | Introduction | 66 |
| 3.2 | The Differential Equations | 66 |
| 3.3 | Auxiliary Information | 69 |
| 3.3.1 | Interface Tracking | 70 |
| 3.3.2 | Combustion Model | 70 |
| 3.3.3 | Initial and Boundary Conditions | 72 |
| 3.4 | Closure | 73 |
| CHAPTER 4 - THE NUMERICAL SOLUTION PROCEDURE | | 75 |
| 4.1 | Introduction | 75 |
| 4.2 | Formulation of the Finite-Domain Equations | 77 |
| 4.2.1 | The Finite-Domain Grid | 77 |
| 4.2.2 | Derivation of the Finite-Domain Equations | 79 |

| | | PAGE NUMBER |
|---|---|---|
| 4.3 | Incorporation of Auxiliary Information | 83 |
| 4.4 | The Solution of the Finite-Domain Equations | 89 |
| 4.4.1 | The GALA Method | 89 |
| 4.4.2 | General Features of the Solution Method | 91 |
| 4.4.3 | The Hydrodynamic Solution Procedure | 91 |
| 4.5 | Resolving the Fluid Interface | 92 |
| 4.5.1 | General Background | 92 |
| 4.5.2 | Flame-Front Tracking | 94 |
| 4.5.3 | Addition and Deletion of Particles | 97 |
| 4.6 | Closure | 99 |
| CHAPTER 5 - | The NUMERICAL SIMULATION OF EXPERIMENT | 100 |
| 5.1 | Introduction | 100 |
| 5.2 | Computational Details | 102 |
| 5.3 | Presentation of Results | 106 |
| 5.3.1 | Horizontally Propagating Flame | 106 |
| 5.3.2 | Upwards Propagating Flame | 111 |
| 5.3.3 | Downwards Propagating Flame | 113 |
| 5.3.4 | The Effects of the Grid Number and Time-Step Size | 115 |
| 5.4 | Convergence | 117 |
| 5.5 | Discussions | 119 |

| | | PAGE NUMBER |
|---|---|---|
| 5.6 | Closure | 122 |
| CHAPTER 6 - | NUMERICAL STUDIES OF PROPAGATING FLAMES EXHIBITING THE LANDAU INSTABILITY | 124 |
| 6.1 | Introduction | 124 |
| 6.2 | General Background | 124 |
| 6.3 | Description of the Problem | 125 |
| 6.3.1 | Physical Process | 125 |
| 6.3.2 | Mathematical Details | 126 |
| 6.4 | Presentation of Results | 128 |
| 6.5 | Convergence | 151 |
| 6.6 | Computer Storage and Time | 151 |
| 6.7 | Discussions | 152 |
| 6.8 | Closure | 156 |
| PART 2 | UNSTEADY TURBULENT FLAME PROPAGATION | 158 |
| CHAPTER 7 - | THE APPLICATION OF TWO-FLUID MODEL OF TURBULENT COMBUSTION TO AN IDEALIZED, ONE-DIMENSIONAL, UNSTEADY, CONFINED, PRE-MIXED FLAME(I) - INVESTIGATION ON A SUDDEN INCREASE IN THE RESISTANCE TO THE FLOW AT THE DUCT EXIT | 159 |

| | | PAGE NUMBER |
|---|---|---|
| 7.1 | Introduction | 159 |
| 7.2 | Experimental Evidence | 161 |
| 7.3 | The Concept of the Two-Fluid Model | 162 |
| 7.4 | Mathematical Formulation of the Two-Fluid Model | 165 |
| 7.5 | Description of the Problem | 170 |
| 7.5.1 | Physical Process | 170 |
| 7.5.2 | Mathematical Details | 172 |
| 7.6 | Presentation of Results | 177 |
| 7.6.1 | The Steady-State Flame | 177 |
| 7.6.2 | The "Stable" Oscillation Case | 182 |
| 7.6.3 | Parametric Study | 196 |
| 7.6.4 | The Effect of Numerical Parameters | 207 |
| 7.7 | Convergence, Computer Storage and Time | 213 |
| 7.8 | Discussions | 213 |
| 7.9 | Closure | 218 |

CHAPTER 8 - THE APPLICATION OF TWO-FLUID MODEL OF TURBULENT COMBUSTION TO AN IDEALIZED, ONE-DIMENSIONAL, UNSTEADY, CONFINED, PRE-MIXED FLAME (II) - INVESTIGATION ON THE OSCILLATORY MASS FLOW RATE AT THE INLET 219

| | | |
|---|---|---|
| 8.1 | Introduction | 219 |

| | | PAGE NUMBER |
|---|---|---|
| 8.2 | Problem Specification | 219 |
| 8.3 | Dimensionless Parameters | 221 |
| 8.4 | The Cases Investigated | 222 |
| 8.5 | Presentation of Results | 223 |
| 8.6 | Discussions | 235 |
| 8.7 | Closure | 238 |
| CHAPTER 9 - CONCLUSIONS | | 239 |
| 9.1 | Experimental Work | 239 |
| 9.2 | Theoretical work | 240 |
| 9.3 | Suggestions for Future Work | 244 |
| REFERENCES | | 248 |
| NOMENCLATURE | | 258 |
| APPENDIX A: | Listings of the PHOENICS Computer Code for the Single-Fluid Computations in Part 1 | 264 |
| APPENDIX B: | Interface-Tracking and Density-Calculation Subroutines | 278 |
| APPENDIX C: | Listings of the Q1 File and the GROUND File for the Two-Fluid Computations in Part 2 | 298 |

## LIST OF FIGURES


| FIGURE NUMBER | TITLE | PAGE NUMBER |
|---|---|---|
| 2-1 | Schematic Diagram of the Experimental Rig | 39 |
| 2-2 | Spark Circuit | 41 |
| 2-3 | Vent Arrangement | 42 |
| 2-4 | Vent and Sparking-Plug Position for the Investigation of the Effect of Gravity | 46 |
| 2-5 | Vent Lay-out for the Investigation of the Effect of Vent Arrangement and Size | 48 |
| 2-6 | Obstacle Arragement | 49 |
| 2-7 | Flames Propagating in Various Directions Relative to Gravity | 52 |
| 2-8 | The Development of Flame Wrinkling with Methane/Air Volume Ratio 12% | 53 |
| 2-9 | Initially Covered Vent Opening | 54 |
| 2-10 | The Development of Flame Wrinkling for the Effect of Vent Lay-out and Size | 55 |
| 2-11 | The Flame Propagating in the Vented Chamber with an Obstacle | 58 |
| 2-12 | The Development of Cusp Traces during and after Flame Propagation | 63 |

| FIGURE | TITLE | PAGE NUMBER |
|---|---|---|
| 4-1 | A Two-Dimentional Control Cell | 77 |
| 4-2 | Grid Showing Location of Variables and their Control Volume | 79 |
| 4-3 | Density Calculation from the Particle Locations | 86 |
| 4-4 | Flame-Front Tracking | 95 |
| 4-5 | Velocities Used in the Evaluation of Particle Velocity | 96 |
| 4-6 | Particle Addition and Deletion Procedures | 99 |
| 5-1 | The Flow Geometry | 101 |
| 5-2 | Flame Location at the start of Preliminary Calculation | 103 |
| 5-3 | The Calculation Domain and a Typical Grid Distribution (20x20) | 105 |
| 5-4 | The Predicted Location and Shape of the Flame Propagating Horizontally with a Grid Number of 20x20 | 106 |
| 5-5 | The Location and Shape of the Flame Propagating Horizontally | 107 |
| 5-6 | The Velocity Field in the Unburned-Gas Region at Three Different Flame Locations Corresponding to Fig.5-4 | 110 |
| 5-7 | The Predicted Location and Shape of the Flame Propagating Upwards with a Grid Number of 20x20 | 111 |

| FIGURE | TITLE | PAGE NUMBER |
|---|---|---|
| 5-8 | The Location and Shape of the Flame Propagating Upwards | 112 |
| 5-9 | The Predicted Location and Shape of the Flame Propagating Downwards with a Grid Number of 20x20 | 113 |
| 5-10 | The Location and Shape of the Flame Propagating Downwards | 114 |
| 5-11 | The Effect of Grid Number on the Results at the Time Equal to 0.32 sec. | 116 |
| 5-12 | The Effect of Time-Step Size on the Results at the Time Equal to 0.32 sec. | 117 |
| 5-13 | The Effect of Grid Number | 120 |
| 6-1 | The Model Cosidered | 126 |
| 6-2 | The Flame-Front Location and Shape at Successive Time, Separated by 0.02 s Intervals | 130 |
| 6-3 | The Combustion-Induced Flow for the Standard Flame | 131 |
| 6-4 | The Flame-Front Location and Shape at Successive Times, Separated by 0.02 s Intervals, under a Large Body Force | 136 |
| 6-5 | The Combustion-Induced Flow for the Flame under a Large Boby Force | 137 |

| FIGURE | TITLE | PAGE NUMBER |
|---|---|---|
| 6-6 | The Flame-Front Location and Shape with g=-100m/s$^2$ at Successive Times, Separated by 0.02 s Intervals | 141 |
| 6-8 | The Flame-Front Location and Shape with the Density Ratio Equal to 0.15 at Successive Times, Separated by 0.02 s Intervals | 143 |
| 6-9 | The Flame-Front Location and Shape at Different Times with the Density Ratio Equal to 0.2 | 143 |
| 6-10 | The Flame-Front Location and Shape at Different Times with the Density Ratio Equal to 0.3 | 144 |
| 6-11 | The Flame-Front Location and Shape at Different Times with the Burning Velocity Equal to 0.3 m/s | 145 |
| 6-12 | The Flame-Front Location and Shape at Different Times with the Burning Velocity Equal to 0.4 m/s | 145 |
| 6-13 | The Flame-Front Location and Shape at Different Times with the Burning Velocity Equal to 0.5 m/s | 146 |
| 6-14 | The Flame-Front Location and Shape at Different Times with the Wavelength of the Initial Perturbation Equal to 2xWidth of the Chamber | 147 |

| FIGURE | TITLE | PAGE NUMBER |
|---|---|---|
| 6-15 | The Flame-Front Location and Shape at Different Times with the Wavelength of the Initial Perturbation Equal to 0.667xWidth of the Chamber | 147 |
| 6-16 | The Effect of the Grid Number on the Flame-Front Location and Shape at t= 0.1s | 150 |
| 6-17 | The Effect of Time-Step Size on the Flame-Front Location and Shape at t= 0.1s | 151 |
| 6-18 | Successive Locations of a Curved Flame-Front Constructed with the Aid of Huygens' Principle | 153 |
| 7-1 | A Turbulent Flame is "Spotty" | 163 |
| 7-2 | A Baffle Stabilized Flame in a Duct | 171 |
| 7-3 | The Pressure Distribution of the Steady-State Flame along the Duct | 178 |
| 7-4 | The Velocity Distribution of Fluid 1 & 2 of the Steady-State Flame along the Duct | 179 |
| 7-5 | The Volume Fraction Distribution of Fluid 2 of the Steady-State Flame along the Duct | 180 |

| FIGURE | TITLE | PAGE NUMBER |
|---|---|---|
| 7-6 | The Interfluid Mass Transfer Rate Distribution of the Steady-State Flame along the Duct | 181 |
| 7-7 | The Variation of the Pressure at Half-Length of the Duct with Time after Sudden Change of Resistance at the Outlet | 183 |
| 7-8 | The Pressure Distribution along the Duct at a succesion of Instants through a "Stable" Cycle | 185 |
| 7-9 | The Distributions of Velocities U1 and U2 along the Duct at Various Instants through a "Stable" Cycle | 191 |
| 7-10 | The Volume Fraction Distributions of the Hot Gas along the Duct at Various Instants through a "Stable" Cycle | 193 |
| 7-11 | The Distributions of the Entrainment Rate along the Duct at Various Instants through a "Stable" Cycle | 195 |
| 7-12 | A Case in which the Initial Pressure Oscillation Dies out | 196 |
| 7-13 | The Instability Region in Terms of LCm-Cm/Cf | 198 |

| FIGURE | TITLE | PAGE NUMBER |
|---|---|---|
| 7-14 | The Characteristics of Oscillations with Different Cm/Cf at a Fixed LCm =100 | 200 |
| 7-15 | The Instability Region in Terms of LCm-$\rho_2/\rho_1$ | 201 |
| 7-16 | The Characteristics of Oscillation with Different$\rho_2/\rho_1$at a Fixed LCm =100 | 203 |
| 7-17 | The Instability Region in Terms of LCm-Ma | 205 |
| 7-18 | The Characteristics of Oscillations with Different Ma for a Fixed LCm =100 | 207 |
| 7-19 | The Effect of Grid Number | 210 |
| 7-20 | The Effect of Time-Step Size | 212 |
| 8-1 | The Variation of Mass Inflow Rate with Time at the Inlet | 220 |
| 8-2 | The Dependence of the Amplitude of Pressure Oscillation on the Frequency at Intake | 223 |
| 8-3 | The Variation of Pressure with Time for Different Frequencies Referring to Fig.8-2 | 225 |
| 8-4 | The Oscillation Characteristics with the Oscillatory Boundary Condition Removed at t*= 0.4 | 227 |

| FIGURE | TITLE | PAGE NUMBER |
|---|---|---|
| 8-5 | The Dependence of the Amplitude of Pressure Oscillation on the Frequency at Intake | 228 |
| 8-6 | The Variation of Pressure with Time for Differnet Frequencies | 230 |
| 8-7 | The Oscillation Characteristics with the Oscillatory Boundary Condition Removed at t*= 3 | 232 |
| 8-8 | The Dependence of the Amplitude of Pressure Oscillation on the Frequency at Intake | 233 |
| 8-9 | The Dependence of the Amplitude of Pressure Oscillation on the Frequency at Intake | 234 |
| 8-10 | The Oscillation Dies away after the Oscillatory Boundary Condition Removed at t*= 0.4 | 235 |
| 9-1 | Velocities used in the Evaluation of the Particle Velocity | 246 |

## LIST OF TABLES


| TABLE NUMBER | TITLE | PAGE NUMBER |
|---|---|---|
| 5-1 | Specification of the Cases | 101 |
| 5-2 | Cases Tested for the Effect of Grid Number | 115 |
| 5-3 | Cases Tested for the Effect of Time-Step Size | 116 |
| 5-4 | Convergence Details for Case 1 | 118 |
| 6-1 | Cases Tested for the Effect of Grid Number | 148 |
| 6-2 | Cases Tested for the Effect of Time-Step Size | 149 |
| 7-1 | Cases Tested for the Effect of Numerical Parameter, NX | 208 |
| 7-2 | Cases Tested for the Effect of Numerical Parameter, $\delta t^* u_o / L$ | 208 |
| 8-1 | Conditions for the Cases Investigated | 222 |

# CHAPTER 1 - INTRODUCTION

## 1.1 The Problem Considered

The present investigation is concerned with studies, by way of computer simulations and experiments, of unsteady, flame propagation through a premixed combustible gas involving both wrinkled laminar flames and oscillatory turbulent flames.

A laminar flame may become unstable during its propagation through a combustible mixture. At the initial stage, the flame only corrugates and the continuous laminar flame sheet still exists. The phenomenon is referred to as the laminar flame wrinkling. It may arise from two origins (Markstein 1964): hydrodynamically due to the interaction between flames and flow fields, and diffusively due to the preferential-diffusion in non-homogeneous mixtures. It is the hydrodynamically originated flame wrinkling which is to be considered in the present investigation.

In turbulent flames, the flame front becomes highly fragmented, consisting of a fairly thick matrix of burned gases interspersed with small eddies of unburned mixture. The unsteady, turbulent flame propagation then shows different characteristics. In the case of turbulent flames enclosed in a duct, the unsteady flame propagation often

manifests itself in an oscillatory mode (Campbell et al 1983). These combustion oscillations are accompanied by excursions in pressure and velocity within the combustion chamber. There are many types of combustion oscillation, and views on its classification vary from investigator to investigator (see for example: Barrere & Williams 1969, and Harrje 1972). The present investigation is mainly concerned with the low-frequency or "buzz"-type oscillation.

This study consists of the following three main parts :

(1) The experimental investigation of laminar flame wrinkling in a vented combustion chamber;

(2) Developing and validating of a computational procedure by the numerical simulation of the above experiment and idealised wrinkled flames in simpler circumstances both in two dimensions; and

(3) Testing of the two-fluid model of turbulent combustion (Spalding 1982b) by applying it to one-dimensional, unsteady, turbulent flames in ducts.

## 1.2 Practical Relevance

Flow problems in which the unsteady flame propagation is present, occur in many areas of interest in the

engineering field. For example,

- In unsteady-flow combustors such as the spark-ignition engine. Performance of the engine depends largely on the behaviour of propagating flames in the cylinder.

- In steady-flow combustors such as rocket engines and gas turbines, unexpected oscillatory combustions may easily occur and threaten their successful operations.

- In accidental gas explosions, which constitute a major hazard in coal mines and other industries, their intensity depends mainly on the development of unsteady flame propagation.

Practising engineers require an accurate knowledge of the behaviour of these unsteady flames in above systems and circumstances. However, these combustion processes are often exceedingly complex and difficult to ascertain by experimental technique. Therefore, it is highly desirable to develop validated numerical simulation approaches with the ability to predict accurately the unsteady flame propagation.

## 1.3 Present Study

### 1.3.1 Objectives of the Present Study

The objectives of the present study are :

(1) To investigate flame wrinkling in a vented combustion chamber experimentally and to compare the experimental results with predictions so as to test the credibility of a mathematical model and solution procedure for predicting the flow under consideration.

(2) To use the numerical procedure in parametric studies which reveal influences of various experimental factors in an idealised circumstance.

(3) To apply the two-fluid model of turbulent combustion to the one-dimensional, unsteady, premixed flames in ducts in order to demonstrate its ability to explain a practically important phenomenon, namely "buzz".

### 1.3.2 Present Contribution

Experimental Work

A simple experimental apparatus for the creation and observation of a variety of transient combustion and flow phenomena with a two-dimensional appereance is designed

and constructed.

In the experiment, the effects of various experimental factors such as the gravity force, the mixture ratio, the initially covered vent opening, the vent lay-out and size are investigated in comparative isolation; a preliminary investigation on the effect of obstacle is also included.

The phenomena of flame wrinkling under various operating conditions are recorded by motion pictures and still photographs; and the results presented can be compared with predictions for the testing of computational procedure.

## Theoretical Work

The computer simulations employed in this study involve both the single-fluid theory and the two-fluid theory.

### (a) Single-Fluid Theory

The single-fluid theory involves the conventional, simultaneous solution of a set of non-linear partial-differential equations. It focuses on one set of flow quantities such as velocity components, temperature, pressure etc. The approach employed in this study has been developed by Spalding and Awn (1978) and applied by Awn (1979) to the flame propagation in tubes. Three main

features introduced into the approach are:

(i) The use of a particle-tracking technique (Spalding 1974, and Maxwell 1977) to track interfaces;

(ii) The treatment of combustion by the simple prescription of the burning velocity and the density ratio; and

(iii) The use of volumetric continuity equation instead of the customary mass continuity equation. This is the GALA (Gas And Liquid Analyser) concept due to Spalding (1974). The use of GALA permits to solve difficulties encountered in a flow with density discontinuities between the two fluids, such as between lighter, burned gas and heavier, unburned gas (see Section 4.4.1 for explanation).

Devices (i) and (ii) enable the combustion problems to be handled in a simple and efficient manner by the introduction of the effect of combustion into the hydrodynamic calculations without the explicit solution of the energy equation. This will be explained in detail in Chapters 3 & 4.

In order that the above single-fluid approach may represent the flows, in which a "fragmentary character" is

in prominence such as the wrinkled laminar flames in the present study, a set of subroutines for the tracking of the fragmented flame fronts and for the density calculation is written. The novel methods employed in these subroutines are:

(1) The calculation of the percentage of the burned gas in a cell;

(2) The calculation of the particle velocity;

(3) The treatment of intersection of the particle string; and

(4) The determination of the contents of cells in which only the burned gas or the unburned gas is present.

These subroutines are used together with the PHOENICS computer code (Spalding 1981) to predict the wrinkled laminar flames, both for the comparison with the present experiments and for the investigation of influences of various experimental factors in an idealised circumstance; and they constitute a form of numerical flow visualization and provide a valuable tool for the study of flame behaviours, as will be seen later.

This part of the thesis is the first numerical study reported on the wrinkled laminar flame; although further

improvements are necessary, the foundations for such analysis have been laid.

(b) Two-Fluid Theory

The two-fluid theory involves the use of the two-fluid model of turbulent combustion (Spalding 1982b). The model permits the "fragmentary character" of turbulent flow to be described by a mathematical apparatus developed primarily for the analysis of two-phase flows; it, therefore, focuses on the volume fractions of the two fluids, $r_1$ and $r_2$, and two sets of velocity components and other flow quantities. In the present model, however, both fluids are subject to the same pressure. The model ceases to attempt to track interfaces, employing instead a statistical representation of the intermingling of two fluids. It is more applicable to the turbulent flows with a high fragmentation of interfaces, with which the single-fluid approach is unable to cope. The earlier investigation on combustion phenomena with the model (Spalding 1984a) has shown its ability in representing some important aspects of reality.

In the present study, the model has been tested for its ability in simulating oscillatory combustions in ducted flames.

Two types of boundary conditions to initiate disturbances are explored resulting in the establishment of the "stable" oscillation and a "resonance"-phenomenon.

Parametric studies are performed to establish the instability conditions under which combustion oscillations may occur.

Some of the important aspects of such a complex phenomenon as "buzz" have been plausibly explained with the model which shows its potential ability in directing towards the quantitative understanding of the phenomenon.

## 1.4 Layout of the Thesis

This thesis contains eight further chapters, which are divided into two parts excluding the last chapter as a conclusion.

Part one, Chapters 2 through 6, is concerned with wrinkled laminar flames, including the experimental investigation of flame wrinkling in a vented combustion chamber, item (1) and the computational simulation of experiments and simpler idealized wrinkled flames, item (2), as listed in Section 1.1.

In Chapter 2, is first described the experimental investigation on flame wrinkling.

The partial-differential equations governing the flow considered in this part are presented in Chapter 3, along with the auxiliary information needed to complete the mathematical formulation; these include the incorporation of the particle tracking and the manner in which combustion is simulated.

Chapter 4 is concerned with the outline of the solution procedure embodied in PHOENICS. The merits of GALA are also discussed in this chapter, together with a detailed description of the interface-calculation presented.

Chapter 5 presents the numerical simulation of experiments. The theoretical study is the application of the approach developed in Chapter 4 to an experimental situation.

In Chapter 6, numerical studies are made of flames exhibiting the Landau instability as a further application of the prediction procedure. At the end of this chapter, Part 1 is concluded.

Part two, Chapters 7 & 8, is concerned with unsteady, turbulent flames. The work presented in this part describes the application of the two-fluid model of turbulent combustion to a propagating one-dimensional, unsteady, confined, premixed flame. Two types of boundary

conditions to incorporate the disturbance on the flame are explored.

Chapter 7 investigates a sudden increase in the resistance to the flow at the duct exit while an oscillatory mass inflow rate at the duct inlet is investigated in Chapter 8.

The last chapter, Chapter 9, summarises the conclusions of this thesis and proposes some possible topics for future research.

# PART 1

## WRINKLED LAMINAR FLAMES

# CHAPTER 2 - EXPERIMENTAL INVESTIGATION OF FLAME WRINKLING IN A VENTED COMBUSTION CHAMBER

## 2.1 Introduction

The test of a computational procedure requires the comparison of its predictions with experimental data. In addition, the insight into a physical process can be improved if a pattern produced by or related to this process is made visible.

Some experimental results for the flame wrinkling are available in the literature; however, to complement the computational part of this study, an experimental investigation on flame wrinkling in a vented combustion chamber is carried out and described in this chapter.

An experimental rig is designed and constructed in such a way that the flame wrinkling can be readily visualized and recorded. In the experiment, effects of various factors such as the gravity force, the mixture ratio, the initially covered vent opening, the vent lay-out and size and the obstacle placed in the chamber are investigated in comparative isolation. Photographs of the flame wrinkling under various operating conditions are presented, which can be used to compare with the computed results.

The objectives of the experimental investigation may,

therefore, be summarised as:

(1) To provide information on the flame wrinkling using a visualization technique; and

(2) To test the computational procedure.

## 2.2 General Background

The wrinkled laminar flame has been a subject in the research on turbulent premixed flames, and its description is essential and necessary for the phenomenological aspects of the turbulent combustion theory (Libby & Williams 1981).

Damköhler (1947) has made the first attempt to interpret the effect of turbulence on the laminar flame and suggested a "wrinkled laminar flame structure"; briefly, the eddies, large compared to the flame thickness, would merely wrinkle the laminar flame,and the eddies, small compared to the flame thickness, would increase the effective transport properties within the flame.

Williams, Hottel & Scurlock (1949) in their studies of flame propagation in high velocity gas streams have found that the intensity of turbulence in the combustion zone exceeds the level of turbulence in the approach stream by more than one order of magnitude. which reveals that there

are other factors present in a turbulent flame than the above-mentioned eddy-effect; this stimulates subsequent experimental investigations to identify these unknown factors, i.e. studies on hydrodynamic flame wrinkling.

Experimental investigations have fallen into two broad categories : a) the qualitative visualization of flows, and b) the quantitative measurement of flow properties such as the flame speed and the wavelength of wrinkles.

Qualitative investigations require fast recording equipment to detect main features of the flow. For example, Markstein (1949) has made flow visualization studies in the flame wrinkling induced by small disturbances at the lower part of laminar flames. He has observed that the amplitude of disturbances increases as they move up along the flame and concluded that the intensity of turbulence present in the unburned gas may be considerably increased by the flame due to the hydrodynamic flame instability.

The methods used for measuring the flame speed vary from investigator to investigator, and often flow visualization is carried out simultaneously to diagnose the effect of flame wrinkling. Petersen & Emmons (1961) have investigated the flame wrinkling on laminar propane-air V-flames stabilized on a wire flameholder. The photographs

taken of flames have shown that some amplication of disturbances in the flame front takes place. The particle-track measurement has been used to obtain the flame-front curvature dependence of flame speed. Palm-Leis & Strehlow (1969) have studied the structural change in outwardly propagating spherical flames in laminar and isotropic turbulent flow fields. The flame speed has been measured from schlieren photographs. In addition, Yoshida & Tsuji (1984) have used instantaneous temperature measurements to determine the mean wavelength of eddy distribution in turbulent flames. The results show that it is determined by the wrinkle size which appears in the wrinkled laminar flame, which suggests the role of laminar flame instability in the flame wrinkling.

The hydrodynamic flame instability in the initial stage of turbulence development at a propagating premixed flame-front has also received attention recently in the research on gas explosions. In experimental investigations, the global pressure is measured to map the pressure variation with the flame behaviour. For example, the experiments on vented gas explosions performed in a 35 $m^3$ prismatic steel module by Solberg et al (1981) have shown the flame-front instability development during the venting process. The pressure signature shows that the instabilities result in a pressure rise. Edwards et al (1985) have performed an investigation on vented gas explosions in two cubical vented vessels of internal sides of 18 cm & 38 cm

respectively. The schlieren photographs and the pressure recording show that the onset of instability gives rise to an increased rate of pressure growth or to pressure oscillations.

Although the laminar flame wrinkling has been observed under attainable experimental conditions and some of its gross features and effects have been explored experimentally, little information on the interaction between flames and flow fields, which are responsible for the flame wrinkling, can be deduced from these experiments.

Owing to the complexity of the phenomena, the previous theoretical work relies largely on the linearized perturbation treatment (Landau 1944, Markstein 1951, Eckhaus 1961, Zeldovich et al 1980). They have established the hydrodynamic role in the onset of instabilities; however, the linearized treatment can not provide information on the flow field that follows the onset of instability.

The present invetigation is intended to demonstrate the flame wrinkling experimentally and to obtain the detailed information on the formation of wrinkled flame-fronts by way of the computer simulation. To the author's knowledge no such study has been reported to date.

Firstly, attention is now paid to the experimental investigation.

## 2.3 Experimental Apparatus

The experimental rig described below has been prepared and assembled in the CFDU laboratory, Imperial College, and shown schematically in Figure 2-1.

### Combustion Chamber

The combustion chamber consists of a rectangular box of internal dimensions 500X500X12 mm standing on a base plate; its narrowness gives the phenomena a two-dimensional appearance. All components are made of perspex plates. The front and back walls are both 12 mm thick. A side hole has been drilled and threaded at each corner of the chamber. They serve as vents or controlled passages for mixture-preparation as described later. A sparking-plug may be positioned close to the left bottom corner or right upper corner, as required for flame propagation in different directions, to ignite the charge; the ignition system will be described in detail later. Along the right side of the front wall a scale has been drawn as an aid for obtaining a predetermined mixture ratio during mixture preparation.

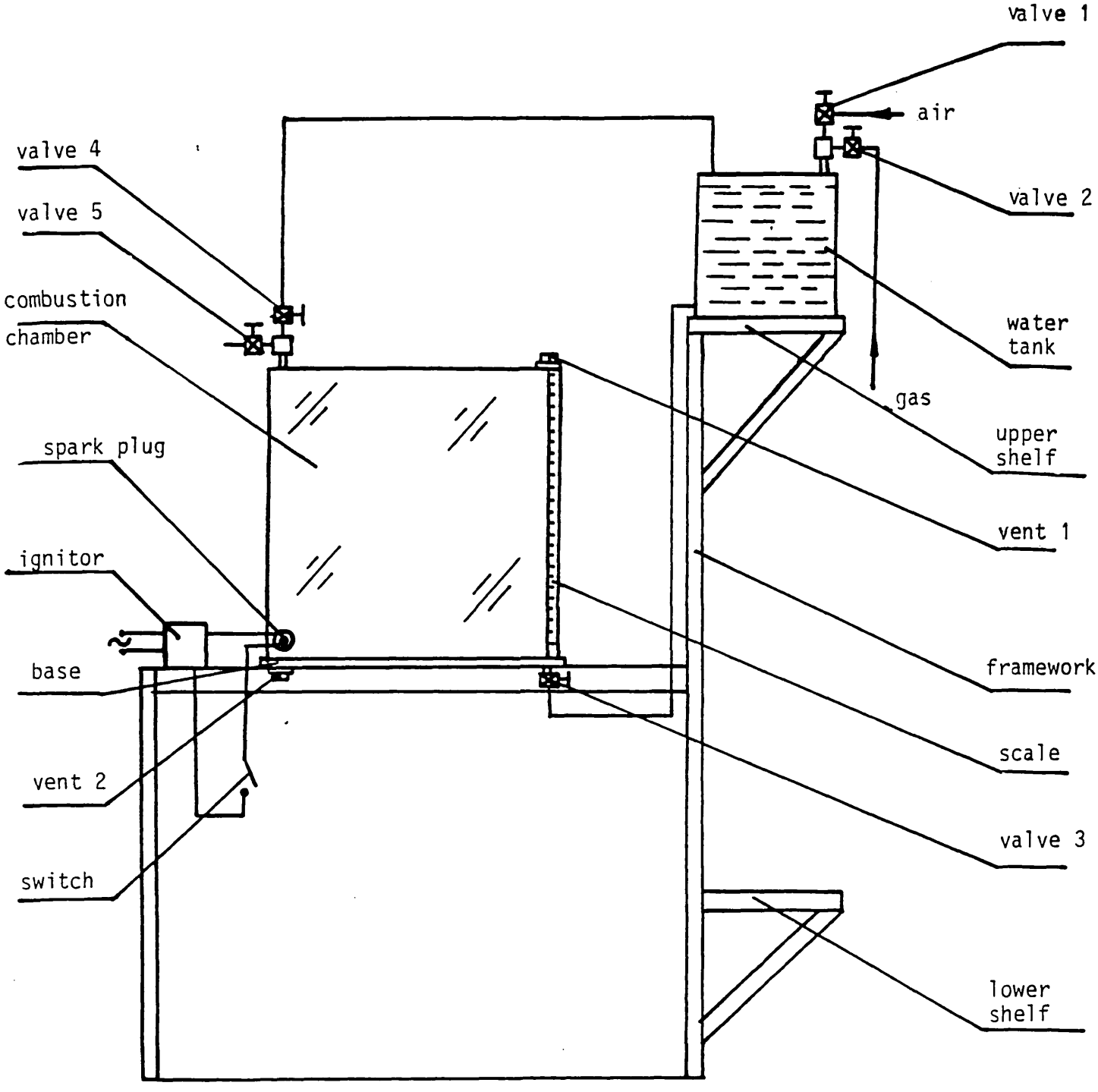



Figure 2-1 Schematic diagram of the experimental rig

Combustible Mixture Supply System

The fuel used is the natural gas taken from the town-gas supply, and air is taken directly from the laboratory atmosphere. The fuel and air are introduced into a perspex water tank placed in the upper shelf (see Figure 2-1), as the water feeds into the chamber by gravity during the preparation of mixture. The water tank has a capacity 1.5 times that of the chamber so that remaining water can be used to mix the gas and air in the tank thoroughly by shaking the water tank. Then the water tank is moved down to the lower shelf; and the homogeneous mixture is introduced into the combustion chamber, as the water returns from the chamber into the water tank by gravity. The detailed procedure of the mixture preparation will be described in Section 2.4.

Ignition System

A re-shaped sparking-plug is arranged as shown in Figure 2-2.

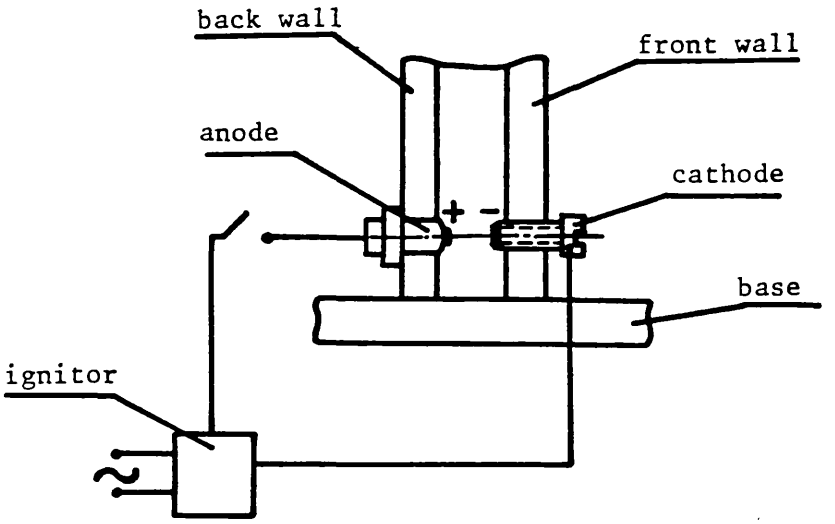



Figure 2-2 Spark circuit

A bolt wired to the ignitor is mounted on the front wall of the combustion chamber serving as the cathode, while the plug is mounted on the back wall of the chamber with its original electrode functioning as an anode. A button switch is placed to close the circuit.

Venting System

The vents can be placed at all corners of the combustion chamber and are covered by bolts during mixture preparation. They are uncovered as required before ignition. For cases employing initially covered vents, after the bolts have been removed, vents are covered by papers of various stiffness and thickness. Venting areas

may be changed by using hollow bolts with various sizes of holes, as shown in Figure 2-3.

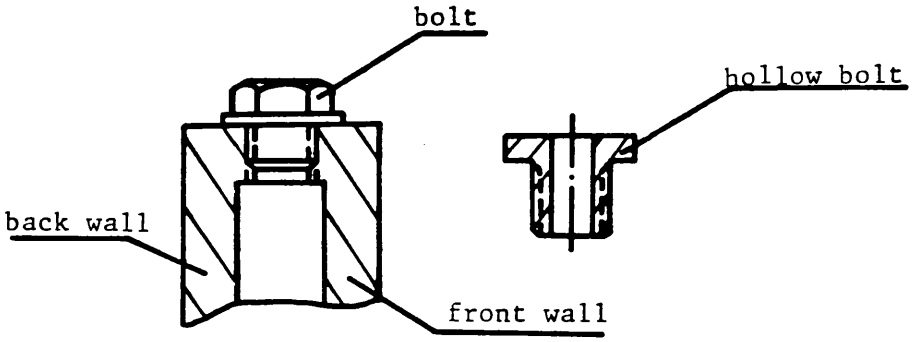



Figure 2-3 Vent arrangement

The Framework

The whole experimental apparatus is supported by a metal framework made of handy angles. The water tank has two positions, one above and the other below the combustion chamber so that the contents in the combustion chamber can be filled with or replaced by that in the water tank.

Photographic Recording

The experiments are carried out in a dark room. The development of flame fronts is recorded by means of a video-camera and cassette recorder at a speed of 25 frames per second. An aluminium foil is pasted over the back wall of the chamber to illuminate the flame without producing

an image. Still photographs of frozen frames are taken from the T.V. screen by means of a still camera. For a film rated at 100 ASA the exposure is generally set to 4 seconds at f8.0.

The development of the entire experimental investigation has been recorded in video-cassettes and the still records are used only to exhibit the highlights in document presentation.

## 2.4 Experimental Procedure

### Preparations

Before performing an experiment, following procedure is carried out :

(i) To check the water tank, the combustion chamber and all connections to ensure that there is no leakage in the system;

(ii) To fill up the water tank with distilled water;

(iii) To close all valves and vents before opening the gas tap; and

(iv) To set the video cassette recorder.

After doing these, the experiment rig is ready for a run, as will be described below.

Operations

The sequence of operations is :

(a) To place the water tank on the upper shelf and open valves 1, 3 & 5 (Figure 2-1). As water feeds into the chamber from the water tank through valve 3 by gravity, air is introduced into the water tank; the contents in the chamber, at the same time, are being pushed out of the chamber through valve 5;

(b) To observe the water level rising in the chamber to the required height on the scale for a predetermined mixture ratio before closing valve 1 and opening valve 2 for introducing gas into the water tank while water level in the combustion chamber rises further;

(c) To close valves 3, 5 & 2 as soon as the chamber is filled with water; then to shake the water tank using the remaining water to mix the gas and air thoroughly;

(d) To place the water tank on the lower shelf and open

valves 3 & 4. As the water returns to the water tank by gravity, the homogeneous gas-air mixture is introduced into the combustion chamber through valve 4;

(e) To close valves 3 & 4 having evacuated all water in the chamber, and to open vents;

(f) To switch off the light in the dark room and to start the recording system;

(g) To ignite the mixture. The burning process lasts much less than a second.

(h) To stop the recording system and to switch on the light for the preparations of the next run.

## 2.5 Test Cases and their Experimental Conditions

The present investigation is programmed to study the effects of different factors on the flame wrinkling, so as to permit some features of the phenomena to be observed in comparative isolation. These factors are : gravity, mixture-ratio, initially covered vent opening, layout of the venting arrangement, and obstacle.

The experimental conditions for the investigation of effects of each factor are described below.

## The Effect of Gravity

In order to reveal the effect of gravity on the flame wrinkling, three cases are investigated locating a single vent at the corner from which the flame propagates. In the first case, the ignition point is located at the left bottom corner so that the flame travels upwards. In the second, the chamber is placed horizontally. In the third, the ignition point is located at the left upper corner, then the flame travels downwards. The vent arrangement and the location of the ignition point are shown in Figure 2-4. The methane-air volume ratio used in this series of investigation is 9.8 %; the vent size is 0.01 m dia.

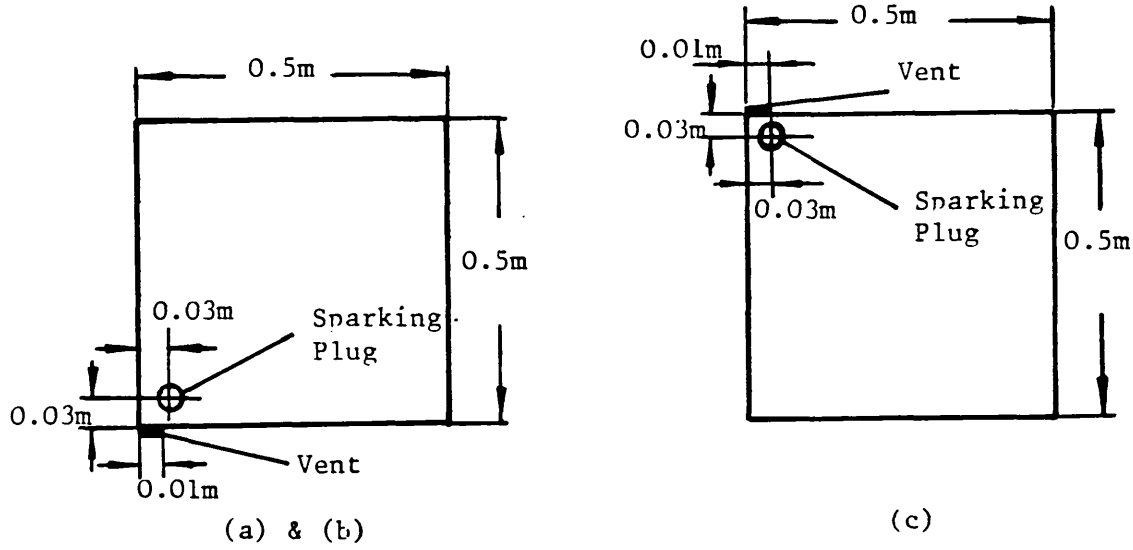



Figure 2-4 Vent and sparking plug position for the investigation of effects of gravity

(a) Flame propagates upwards
(b) Flame propagates horizontally ( the chamber is laid flat )
(c) Flame propagates downwards

The Effect of Mixture Ratio

In order to investigate the effect of mixture ratio, the venting and ignition point are fixed on a vertically standing combustion chamber, as shown in Figure 2-4(a).

The methane-air volume ratios investigated are 9.8 % and 12 %; the vent size 0.01 m dia.

The Effect of Initially Covered Vent Opening

For this series of investigations, the vent shown in Figure 2-4 (a) is initially covered by papers of various quality and thickness.

The methane-air volume ratio used is 9.8 %; the vent size 0.01m dia.

The Effect of Vent Lay-out and Size

For this series of investigations, the mixture ratio employed is 9.8 %, and the layout of the venting arrangement is shown in Figure 2-5.

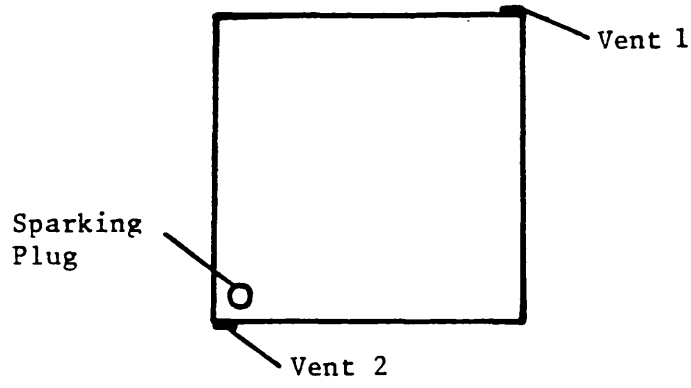



Figure 2-5 Vent layout for the investigation of the effect of the vent arrangement and size

The size of vent 1 located at the right upper corner is fixed at 0.01 m dia. In addition, the different sizes, 0.004 m dia. and 0.01 m dia., for vent 2 close to the point of ignition have also been employed. In extreme, vent 2 has been completely covered during flame propagation.

The Effect of Obstacle

For this investigation, an obstacle is placed inside the chamber forming a inner box, as shown in Figure 2-6.

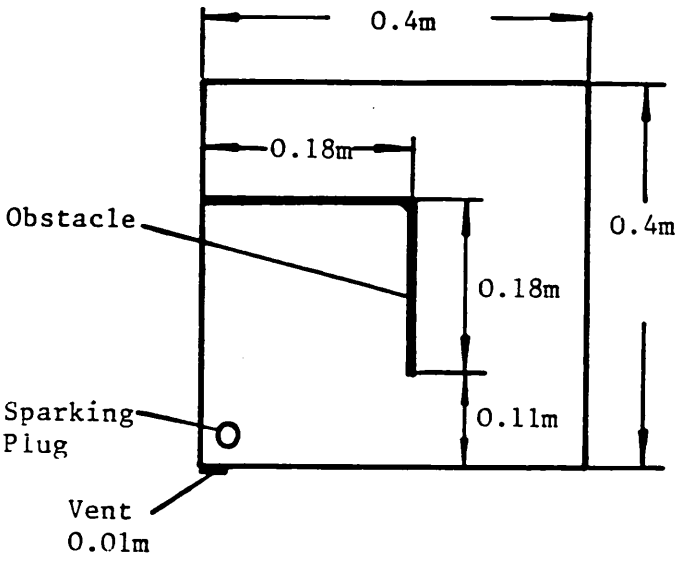



Figure 2-6 Obstacle arrangement

A single open vent is used and located in the left bottom corner from which the flame propagates.

The methane/air volume ratio used in this investigation is 9.8 %, the vent size 0.01 m dia.

## 2.6 Presentation of Results

The results obtained from the experimental investigation are mainly concerned with flame shapes, especially the wrinkled flame-fronts; they are presented under headings : effects of gravity, the effect of mixture ratio, the effect of initial covered vent opening, the effect of vent layout and size, the effect of obstacle. Only typical

results selected from the investigations are presented photographically for discussion in the next section. Other results exhibiting similar behaviours have been recorded in video-cassettes.

Effects of gravity

The results for flame propagation in various directions are given photographically in Figure 2-7 (a-c).

Figure 2-7 (a) shows that the flame propagates upwards.

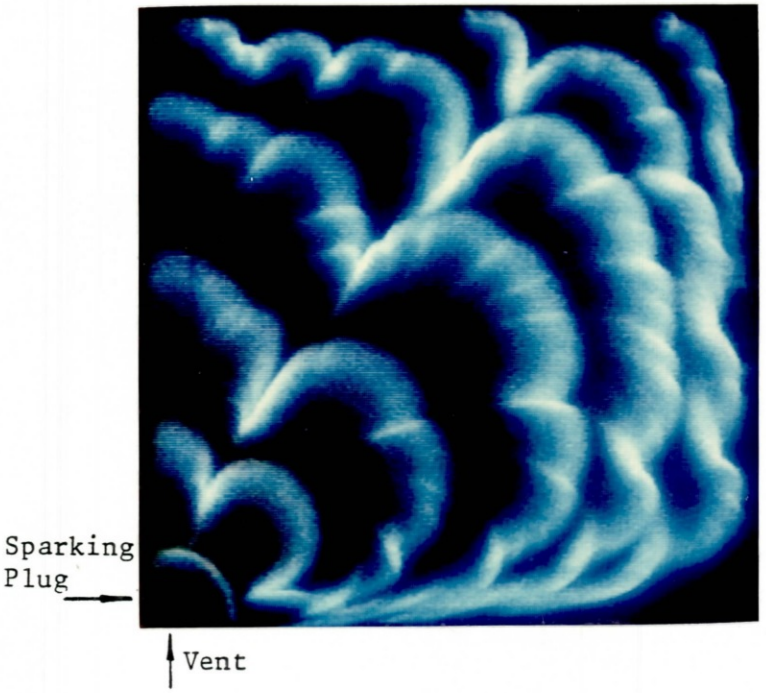
Figure 2-7 (b) shows that the flame propagates horizontally.

Figure 2-7 (c) shows that the flame propagates downwards.

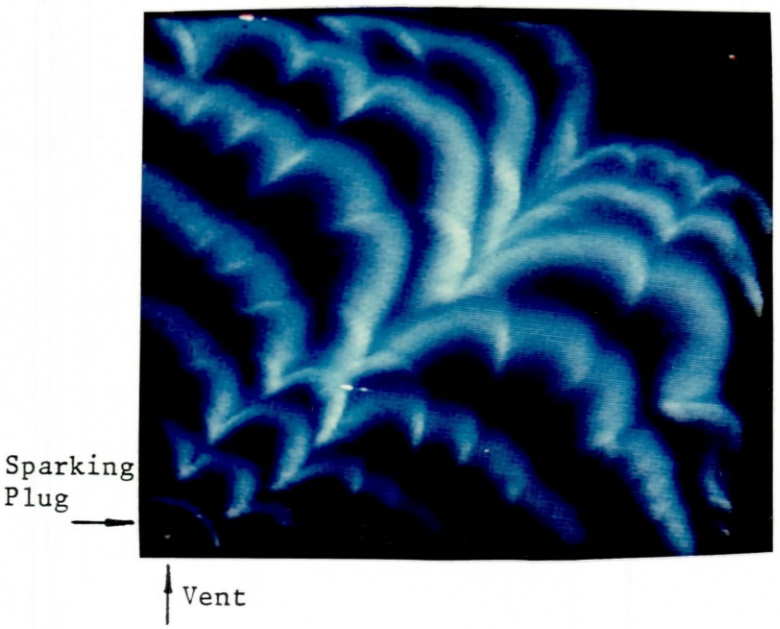
The corresponding experimental conditions for these three cases have been given in Section 2.4.

In the photographic prints the interval between any two flame positions is 2/25 sec.

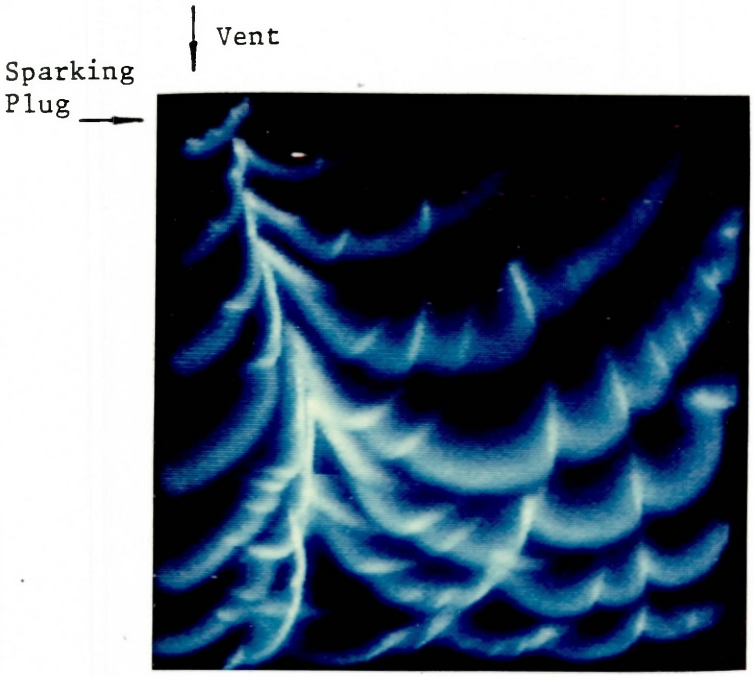
It can be seen that although the patterns are different under obvious influences of gravity, similar characteristics of flame wrinkling are revealed in all of them. The effects of gravity can be seen from the flame-tilting in Figure 2-7 (a) & (c).




(a) Flame propagates upwards




(b) Flame propagates horizontally




(c) Flame propagates downwards

Figure 2-7 Flames propagate in various directions relative to gravity

## The Effect of Mixture Ratio

The photograph of the development of flame wrinkling with the mixture ratio of 9.8 % has been already given in Figure 2-7 (a), the photograph with the mixture ratio of 12 % is now shown in Figure 2-8.

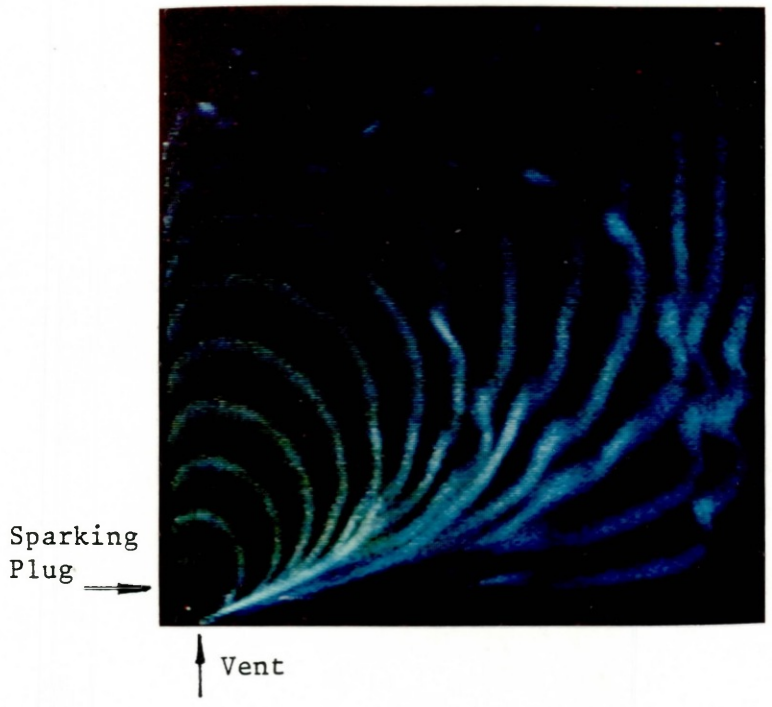



Figure 2-8 The development of flame wrinkling with the methane/air volume ratio of 12 %

The figure shows that the development of flame wrinkling is much slower and weaker compared with that in Figure 2-7 (a).

The Effect of initially covered vent opening

A typical results from this series of investigations is shown in Figure 2-9. All other conditions are the same as that in Figure 2-7 (a).

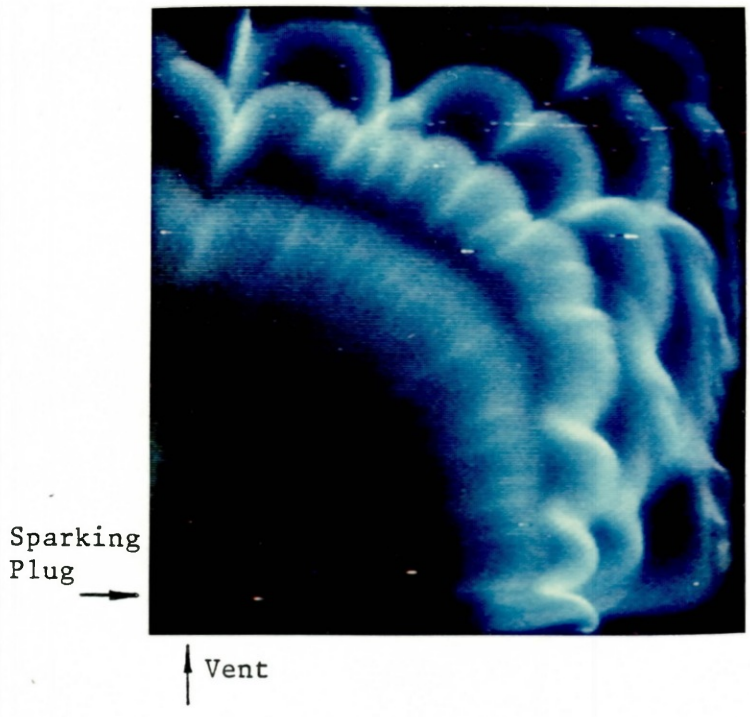
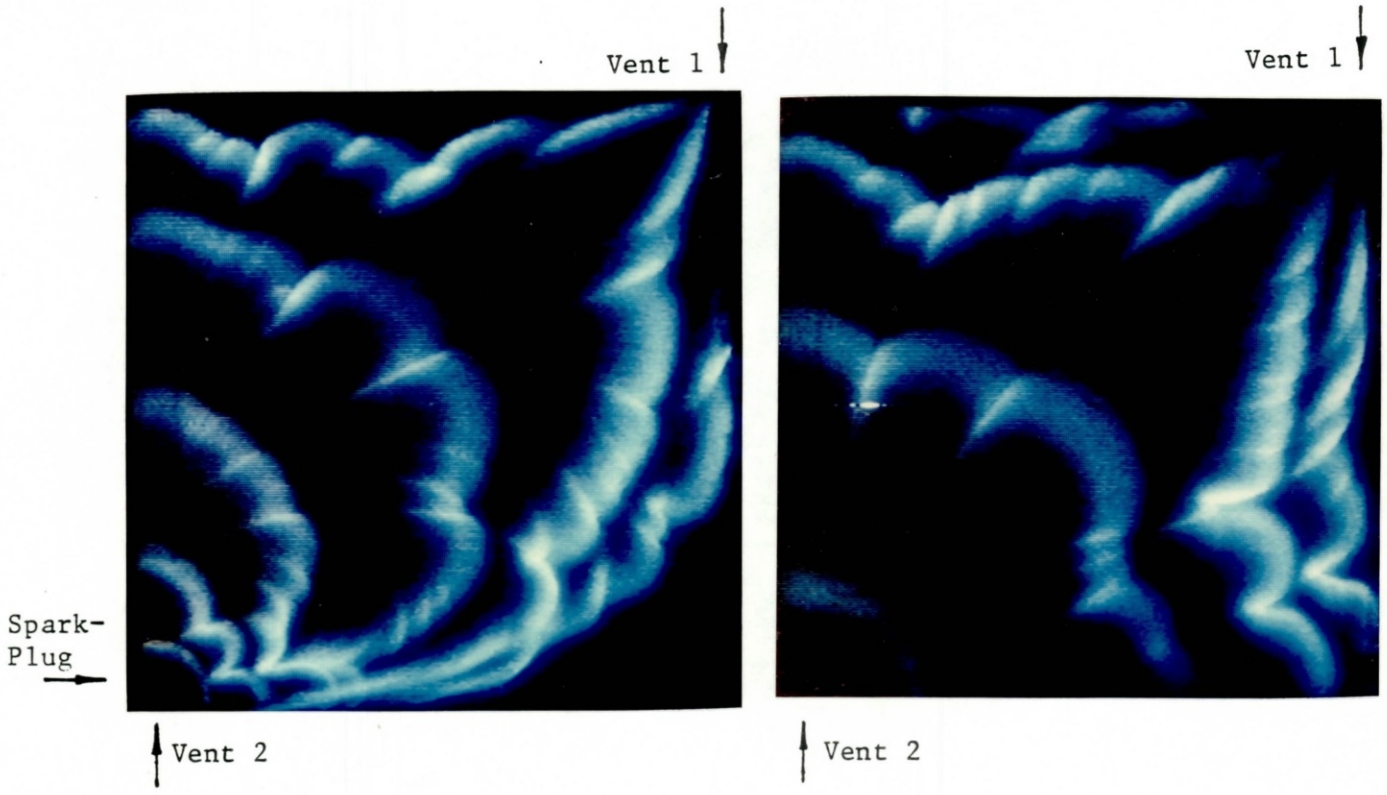



Figure 2-9 Initially covered vent opening

The occurrance of vent-cover rupture is estimated after the second flame position in the photograph. It can be seen that the strong flame wrinkling starts following the vent-cover rupture.

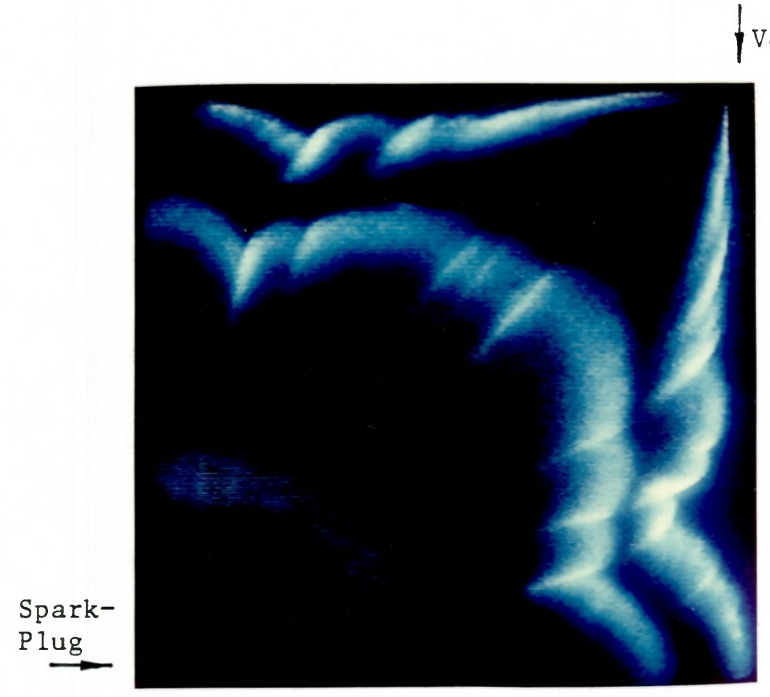
The Effect of Vent Lay-out and Size

The photographs showing the flame development for different vent sizes are shown in Figure 2-10 (a-c). They depict that the smaller the bottom vent, the higher the flame speed; and venting of the hot gas favours the flame wrinkling.




(a) vent 1 - 0.01 m
vent 2 - 0.01 m

(b) vent 1 - 0.01 m
vent 2 -0.004 m



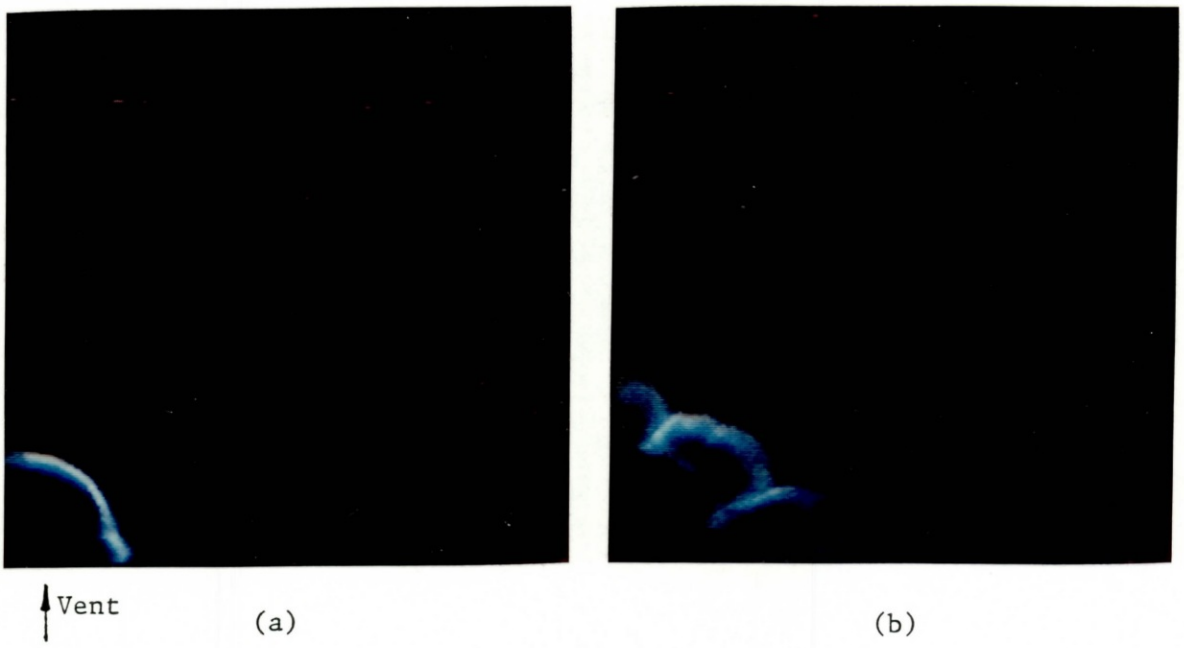

(c) vent 1 - 0.01 m
vent 2 - 0.0 m

Figure 2-10 The development of flame wrinkling under various vent arrangement

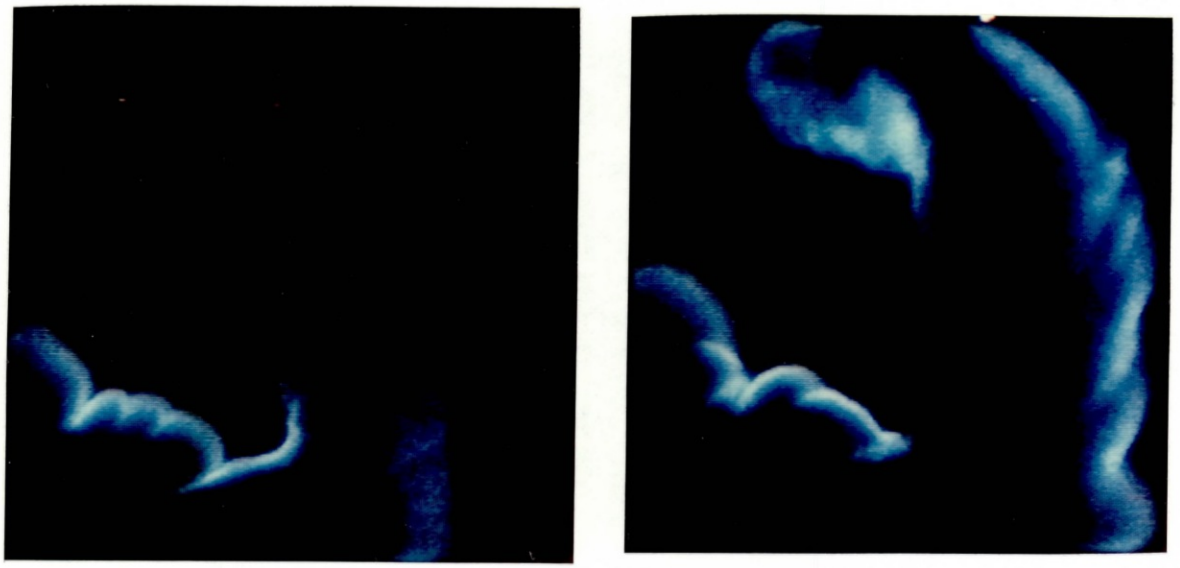
## The Effect of Obstacle

The photographs of flame propagating over the obstacle at a successive time with interval of 1/25 s are given in Figure 2-11 (a-g).

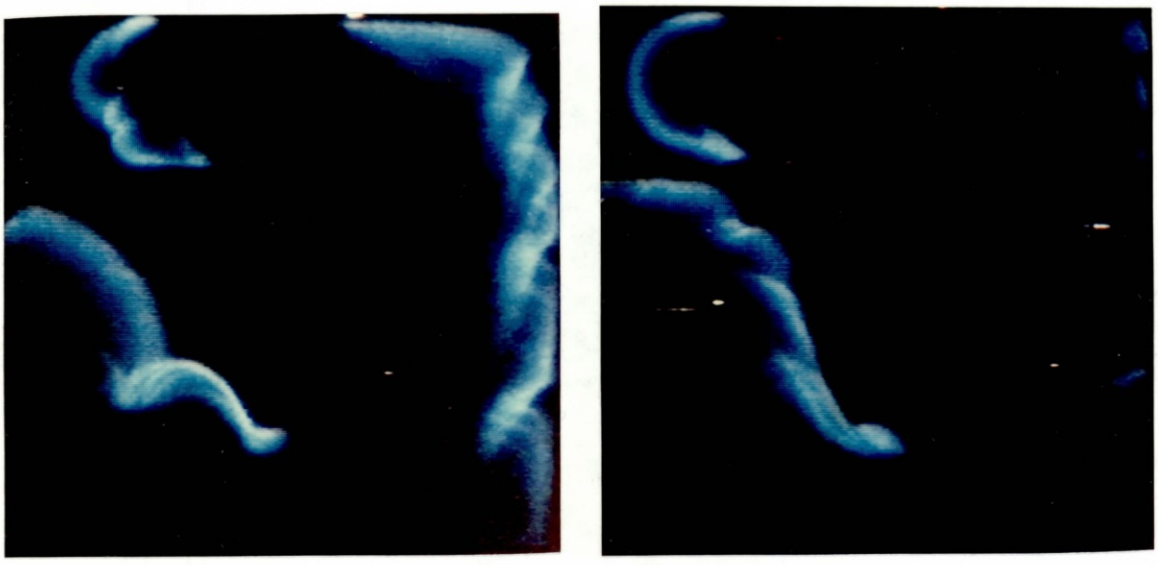
It can be seen from the photographs that part of the flame is pushed out of the inner box by the pressure generated there due to the obstacle as the flame propagates away from the ignition point. Then the flame is separated by the obstacle into two parts with different characteristics. In the region inside the obstacle, the flame demonstrates the characteristics of a wrinkled laminar flame similar to that in Figure 2-7 (a). In the region outside the obstacle, a strong turbulent flame acceleration can be seen instead of flame wrinkling.



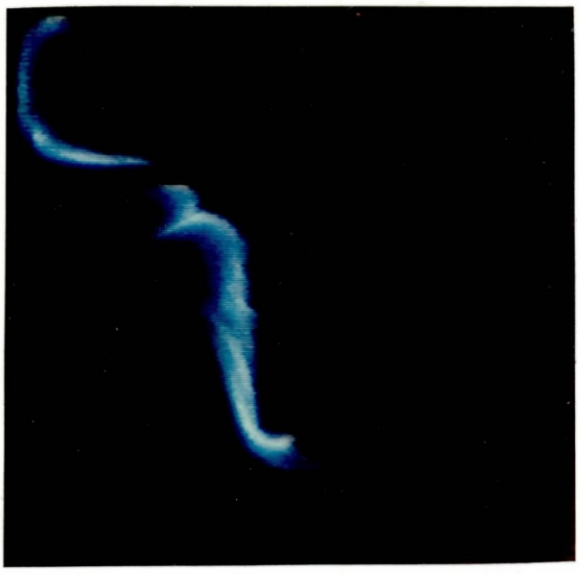

(a) (b)



(c) (d)



(e) (f)



(g)

Figure 2-11 Flame propagates over an obstacle placed in the vented combustion chamber.

## 2.7 Accuracy of the Experimental Results

Since this experimental investigation is mainly intended to visualize the flame wrinkling, there are very few things to be measured quantitatively. The achievement of predetermined mixture ratio has been described through the sequence of operation in Section 2.3, and timing, i.e. the interval between any two flame positions shown in the photographs presented, is determined by the speed of video-cassette recorder, i.e. 25 frames per second. The shape and position of the flames shown in the photographs are only relative to the combustion chamber. It deserves to be mentioned that the degree of reproducibility of the results is low but reasonable. The shape and position of the flames are different for various experiments performed under the same operation conditions; however, the agreement in trends has been found. These differences are attributed to the random behaviour of flame wrinkling and uncertainty of the exact ignition. Therefore, the drawing of a conclusion about quantitative accuracy of the results is not attempted in the present investigation.

## 2.8 Discussions

### Landau instability

The flame wrinkling, as shown in Figure 2-7 (b), in which the flame propagates horizontally, is free from the effect

of the gravity force. The flame is characterized by its cellular structure with a large intrusion towards the burned gas. An explanation of the phenomenon may be offered by the description of Lewis & Von elbe (1964), who has used the theory of Landau (1944) and Markstein (1964) to qualify the wrinkled flame : "the wrinkled flame is attributable to mass acceleration due to thermal expansion of the combustion products". The phenomenon is thus referred to as the Landau instability.

Effects of Gravity

When flames travel downwards or upwards, it is usually expected that the effect of gravity force on the flame wrinkling through the Rayleigh-Taylor instability may operate. It may be easier to envisage this effect in isolation by supposing that the burning rate tends to zero, i.e. the thermal expansion rate is negligible. Then, in the case of upward flame-travelling, the Rayleigh-Taylor instability would dominate as the heavier, unburned mixture rests on top of the lighter, burned gas; on the other hand, when the flame propagates downwards, the gravity force would resist the development of instability as the light, hot gas rests on top of the heavy, cold one.

However, the flame wrinkling shown in Figure 2-7 (c) is as strong as that in Figure 2-7 (a). Furthermore,

characteristics of the flame wrinkling in all three records, Figure 2-7 (a), (b) and (c), are similar regardless of the direction of flame propagation, indicating that the Rayleigh-Taylor instability has been overshadowed by the Landau instability in the present series of experiments. The only visible effect of the gravity force in Figure 2-7 is the flame-tilting.

The Effect of Mixture Ratio

A comparison between Figure 2-8 with Figure 2-7 (a) reveals that there is also the effect of mixture ratio on the flame wrinkling which mainly operates through the burning rate and the density ratio between the hot and cold gases. For the near-stoichiometric mixture, its thermal expansion rate is higher than that of the rich or lean mixture during the combustion process because of its higher burning rate and larger density difference between the hot and cold gases. The higher thermal expansion rate favours the development of the Landau instability, as shown in Figure 2-7 (a).

The Effect of Initially Covered Vent Opening

In cases employing initially covered vent opening, the venting of the hot gas following the vent-cover rupture results in a sudden pressure drop in the hot gas region leading to an acceleration of the flame front towards the

hot gas. This acceleration acts as a strong disturbance on the flame front for instabilities to develop, as shown in Figure 2-9.

## The Effect of Flame Wrinkling on the Burning Rate

It is clear that when a flame wrinkles the total area of the flame is augmented leading to an increase in the volumetric burning rate; besides, the results presented above show a local increase of burning rate in the cusps of wrinkled flame front. It is evidented by the brighter colour there, as shown in the photographs. It is also demonstrated by the vapour traces left on the walls of the combustion chamber, as described below.

## Description of the Traces Left on the Walls of the Chamber

After each run of the experiment, traces have been left on the walls of the chamber, as shown in Figure 2-12.

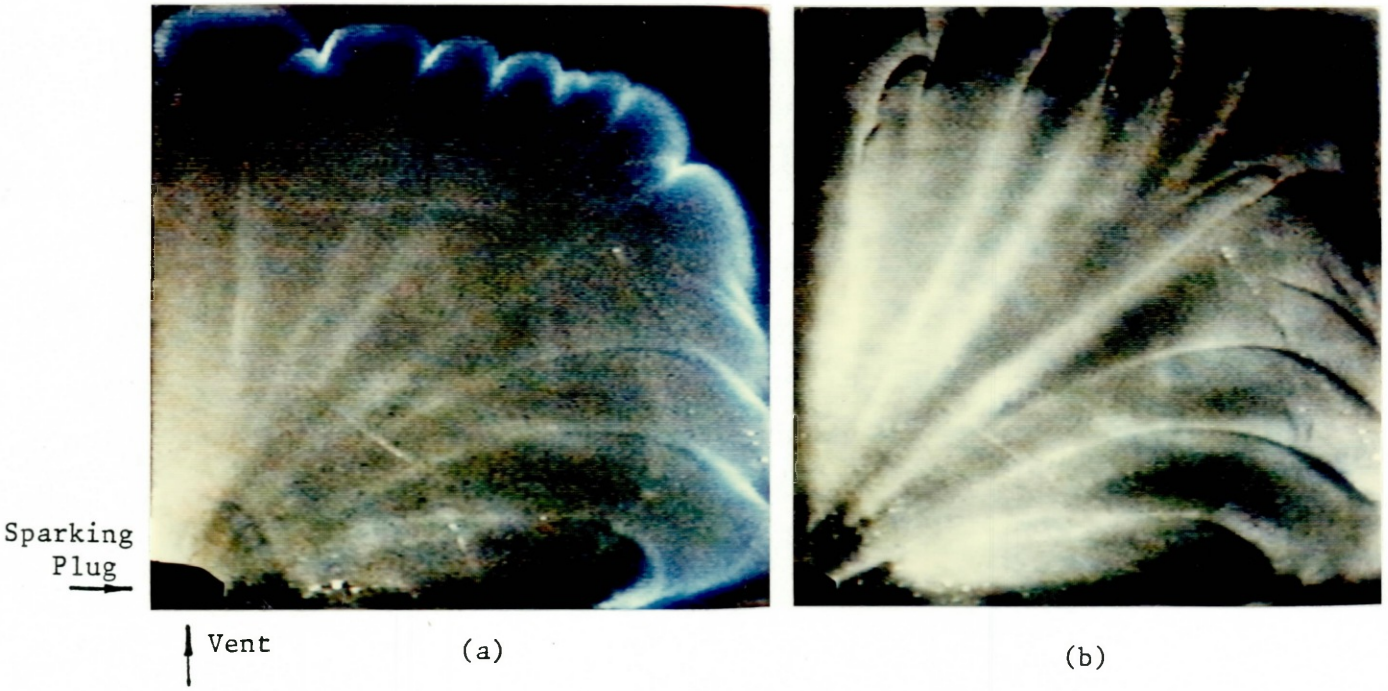



Figure 2-12 The development of cusp traces during (a) and after (b) flame propagation

The water vapour generated by combustion is condensed on the walls of the combustion chamber as the flame propagates. Inspection of Figure 2-12 reveals that these traces are those of the cusps of the flame front during flame propagation. The dark lines on the right side in Figure 2-12 (b) indicate that an increase of burning rate in the cusps of the flame prevents condensation by heating the walls. However, as the walls cool down, more vapour, generated near the cusps due to the higher burning rate, condenses on these regions resulting in bright lines, as shown on left side in Figure 2-12 (b).

### The Effect of Vent Arrangement and Size

Figure 2-10 suggests that for smaller vents, a high pressure in the chamber is built up much faster resulting in a high flame speed. Comparison of Figure 2-10 (c) with Figure 2-7 (a) shows that although the vent sizes are the same, it is more efficient to vent the low density hot gas behind the flame in order to reduce overpressure in the combustion chamber.

### Flame Acceleration Over an Obstacle

Figure 2-11 shows how flame accelerates when propagating over an obstacle. It is known that the shear-generated instability or Kelvin-Helmholtz instability plays an important role in flame acceleration through obstacles. It appears that the process is too fast to be given the detailed information by the video-camera used in this investigation; however, the results obtained are interesting, and the topic deserves further work to pursue.

## 2.9 Closure

The experimental investigation on the flame wrinkling in a vented combustion chamber has been performed. The typical results of the experiments, which show the flame wrinkling, are presented photographically and discussed.

The recorded observations have shown that the flame wrinkling in the present experiments demonstrates mainly the characteristics of the Landau instability due to the thermal expansion of gas during combustion processes.

The flame wrinkling may augment the total area of the flame leading to an increase in the volumetric burning rate; besides, a local increase of burning rate in the cusps of wrinkled flame fronts has been observed.

The results obtained have provided a challenge to the computational procedure.

# CHAPTER 3 - MATHEMATICAL FORMULATION

## 3.1 Introduction

Since the intention of study in this part is to predict the wrinkled flames both for comparison with the experimental results presented in Chapter 2 and under idealized simpler conditions, a numerical study of the Landau instability, the first step is to consider the mathematical formulation of the physical laws which govern the phenomena under consideration.

Although the physical laws for the conservation of mass, momentum and energy are very general in nature, it is sometimes reasonable to make some assumptions for certain problems under particular conditions. This chapter provides the set of differential equations that describe unsteady laminar flames and states the assumptions required to formulate these equations for the specific problems under consideration. Also, the auxiliary information necessary to complete the formulation is included.

## 3.2 Differential Equations

### Assumptions

(i) The flow is laminar and two-dimensional.

(ii) The flow is treated as incompressible; and the process adiabatic.

(iii) Viscosity effects are negligible.

(iv) The flame may be adequately represented as a discontinuity of density which advances relative to the gas at a fixed velocity towards the higher density side.

(vi) Friction at and heat transfer to chamber walls are neglected.

The set of differential equations for unsteady laminar flames with above assumptions is as follows :

The Continuity Equation

$$\frac{\partial u}{\partial x} + \frac{\partial v}{\partial y} = -\frac{1}{\rho}\frac{D\rho}{Dt} \quad ; \qquad (3.1)$$

where, the term $(-\frac{1}{\rho}\frac{D\rho}{Dt})$ represents the rate of reduction of fluid volume and $\frac{D\rho}{Dt}$ is the "substantial" derivative and defined as,

$$\frac{D\rho}{Dt} = \frac{\partial \rho}{\partial t} + u\frac{\partial \rho}{\partial x} + v\frac{\partial \rho}{\partial y} \quad . \qquad (3.2)$$

Equation (3.1) is the differential equation which is used in the GALA method (see Section 4.4).

## Momentum Equations

### Momentum in the X-direction

$$\frac{\partial(\rho u)}{\partial t} + \frac{\partial(\rho uu)}{\partial x} + \frac{\partial(\rho uv)}{\partial y} = -\frac{\partial P}{\partial x} \quad , \qquad (3.3)$$

### Momentum in the Y-direction

$$\frac{\partial(\rho v)}{\partial t} + \frac{\partial(\rho uv)}{\partial x} + \frac{\partial(\rho vv)}{\partial y} = -\frac{\partial P}{\partial y} + \rho g_y \quad ; \qquad (3.4)$$

where, t stands for time,

x and y stand for distance coordinates aligned with u and v respectively,

$\rho$ is the density,

u and v are the velocity components in the x-direction and y-direction respectively,

P is the pressure,

$g_y$ is the body-force component in the y-direction.

The left-hand sides of Equations (3.3) and (3.4) contain the unsteady and convective flux terms, while the pressure-gradient terms and the body-force term appear on the right-hand sides.

In accord with the combustion model, which will be described in Section 3.3.2, the energy equation is not solved, but the effect of the combustion on the flow is included via the density calculation.

## The general Transport Equation

In the interest of computational efficiency and convenience, Equations (3.3) and (3.4) can be presented in the following general form :

$$\underbrace{\frac{\partial}{\partial t}(\rho\phi)}_{\substack{\text{unsteady}\\ \text{term}}} + \underbrace{\text{div}(\rho\vec{U}\phi)}_{\substack{\text{convection}\\ \text{term}}} = \underbrace{S_\phi}_{\substack{\text{source}\\ \text{term}}} \quad ; \qquad (3.5)$$

where $\phi$ identifies the dependent variable, $S_\phi$ is the sum of any other terms which cannot be included in the convection or diffusion terms in the equation. Therefore, $S_\phi$ is the pressure-gradient term for Equation (3.3) and the sum of the pressure-gradient term and body-force term for Equation (3.4). This term forces all the equations into the standard form, which is solved by the numerical procedure ,as described in the next chapter.

## 3.3 Auxiliary Information

In this section, the auxiliary information necessary to complete the mathematical formulation will be specified. However, details of its implementation in the solution procedure will be described in the next chapter.

### 3.3.1 Interface Tracking

The particle-tracking technique (Maxwell 1977) is used to track the interface separating the hot burned gas from the cold gas. In this method, a string of massless particles is distributed at some initial time on the interface, and assumed to remain on it throughout the calculation. Each particle moves in the flow domain with the local interface-velocity calculated according to the following equation :

$$\frac{\partial x_p}{\partial t} = u_p \quad , \tag{3.6a}$$

$$\frac{\partial y_p}{\partial t} = v_p \quad ; \tag{3.6b}$$

where $x_p$ and $y_p$ are coordinates of the particle, and $u_p$ and $v_p$, components of its local velocity. The particles are connected by straight-line segments to form the interface surface. Particles can be generated or deleted according to the interface variation as needed and a more detailed description of this technique will be given in Section 4.5.2.

### 3.3.2 Combustion Model

In view of the fact that the chemical reaction takes place in a region much smaller than the grid size employed in the present study, a simple combustion model is introduced

into the solution procedure. Such a has been developed by Awn & Spalding (1978) and successfully applied by Awn (1979) to flame propagation in tubes.

The main features of the model are :

(i) The flame front is assumed to be a hydrodynamic discontinuity in density.

(ii) The burning velocity is assumed to be constant and the flame speed, $\vec{U}p$ , expressed as :

$$\vec{U}p = \vec{S}b + \vec{U}unb \; ; \qquad (3.7)$$

where Sb is the burning velocity normal to the flame front, and $\vec{U}unb$ is the velocity of the unburned gas at the head of the flame. All quantities in Equation (3.7) are vectors.

(iii) Away from the flame front the process is considerd isentropic.

(iv) The thermal expansion of gas due to combustion is accounted for by a surface source at the flame front.

With this combustion model, there is no need to solve the

energy equation at all; for the effect of combustion process on the hydrodynamic properties is included through the density calculation. The flame front is the interface that separates the burned gas from the unburned gas; the particle-tracking technique allows the flame-front shape and location to be determined.The local density distribution in the field is also determined from the location of the interface, as will be described in detail in the next chapter.

### 3.3.3 Initial and Boundary Conditions

To complete the specification of the mathematical formulation, both initial and boundary conditions are needed. The necessary initial conditions include the starting values of all dependent variables and initial positions of all interface marker particles. The required boundary conditions are either the value of dependent variables or their gradients along the the boundaries of the calculation domain.

#### Initial Conditions

For the prediction of experiments, the initial field values and initial position of the interface are obtained from a preliminary calculation, as will be discussed in Section 5.2. For numerical studies of the Landau

instability, the initial conditions are specified by assigning guessed values, and will be described in Section 6.3.2.

Boundary Conditions

The following physical boundaries will be encountered in the present study and their treatments are listed as follows :

Vent Opening or the Open End of Combustion Chamber

A constant and uniform pressure, P= O $N/m^2$, is specified on this boundary.

Walls

All walls are stationary, frictionless and impervious.

## 3.4 Closure

In this chapter, the information presented may be summarized as follows :

(a) The coordinate system has been defined.

(b) The assumptions for the flow under consideration have been listed and resulting differential equations

presented. These equations have been written in the form of a general transport equation.

(c) The auxiliary information required to complete the mathematical formulation has been outlined, which includes the location and shape of a moving interface, the combustion model, initial and boundary conditions for the flow.

# CHAPTER 4 - THE NUMERICAL SOLUTION PROCEDURE

## 4.1 Introduction

In the previous chapter, the differential equations along with the necessary auxiliary information have been set out. These equations are coupled and non-linear and are seldom amenable to an analytical solution. The task in this chapter is to present a numerical procedure employed for the solution of these equations and to track interface movement.

The equations are solved by means of the PHOENICS code (Spalding 1981), which embodies a version of the finite-domain procedure developed by Patankar and Spalding (1972). Details of PHOENICS have been widely described by Spalding (1982a); therefore, here only an outline is given for the sake of completeness and the reader's reference. All listings and their explanation related to the present problem are given in Appendix A.

In addition, a particle-tracking procedure is incorporated into the solution procedure in order to track the flame-front (interface) and to evaluate local densities due to the combustion model adopted in this study. This will be described in detail in this chapter, and the listings of relevant subroutines are given in Appendix B.

The solution procedure consists of the following major steps :

(a) The flow domain is divided into a finite number of discrete regions by constructing a staggered grid system. This yields "control volumes" or "cells" for each flow variable.

(b) The partial-differential equations are transformed into finite-domain equations for each variable at each cell. This is accomplished by integrating these equations over each control volume and using appropriate assumptions for the determination of variable values between grid nodes.

(c) The resulting finite-domain equations are solved by means of an appropriate algorithm.

(d) The tracking of the flame-front and the evaluation of densities are performed by means of the particle-tracking procedure already mentioned.

(e) The solution of the finite-domain equations can be influenced by the number of grid-nodes employed. The number required for "grid-independent" solution to be obtained varies as the physical process. The only way to determine the optimum number of grids is to perform the calculation several times with differing

numbers of grid nodes.

The remainder of this chapter consists of five sections. In Section 4.2 the finite-domain equations are given, and a detailed account of the auxiliary information is contained in Section 4.3. The solution procedure is outlined in Section 4.4; this is followed by Section 4.5 where the particle-tracking technique is described. Section 4.6 is the closure of this chapter.

## 4.2 Formulation of the Finite-Domain Equations

### 4.2.1 The Finite-Domain Grid

#### (a) General Concept

The integration domain is filled by a set of non-overlapping cells which are constructed by orthogonal grid lines, as shown in Figure 4-1.

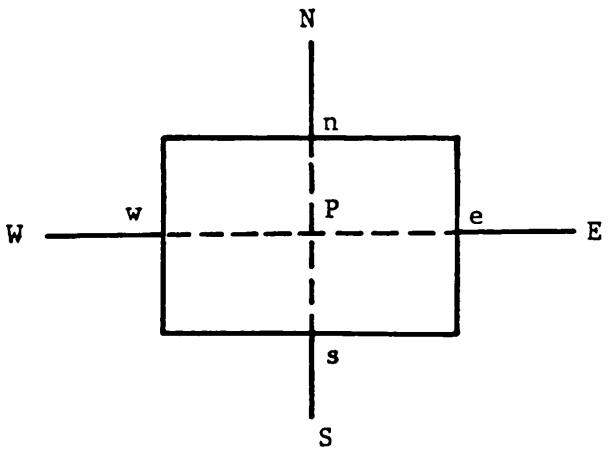



Figure 4-1 A two-dimensional control cell

The cell-centre point,P (called the grid node), is located at the geometrical centre of a cell. The neighbour nodes are referred to as points N, S, E and W (North, South, East and West); n, s, e and w are used to denote the north, south, east and west faces of the cell respectively. The values of variables at P, N, E and W are regarded as the representing values within the cells concerned while the values at n, s, e and w are regarded as the representing values over the faces of a cell.

The grid may be non-uniformly spaced, but once the grid number and dimensions have been chosen, they remain fixed during the solution process.

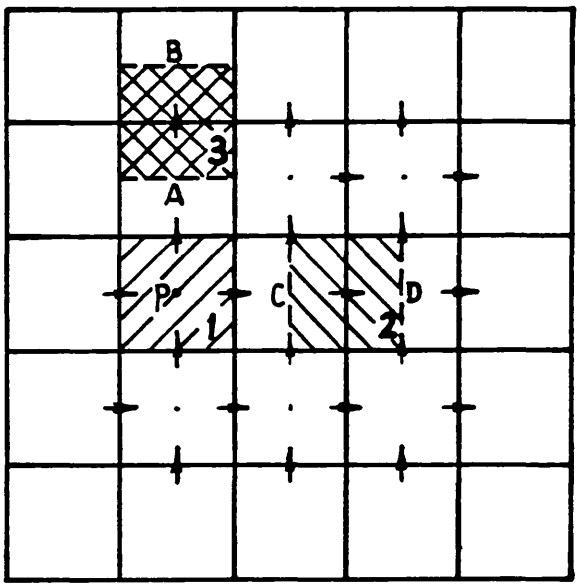
(b) Location of Flow Variables

Scalar variables such as pressure and density are stored at the location P; the velocity components are stored at the cell-face locations, e, w, n, s and are denoted by : Ue, Uw, Un, Us.

(c) Control Volumes

The term "control volume" refers to those imaginary regions over which the partial-differential equations are integrated so as to convert these equations into their finite-domain forms. Because there are three different locations for the variables in the "staggered-grid", there

are three types of control volumes staggered , as shown in Figure 4-2 : (i) main-control volumes for the scalar variables stored at each grid node; (ii) u-velocity control volumes for the u-velocities storage locations; and (iii) v-velocity control volumes for the v-velocities storage locations.




| Symbol | Location | Control-Volume for |
|---|---|---|
| 1 | • | P,ρ |
| 2 | — | u |
| 3 | \| | v |

Figure 4-2 Grid showing locations of variables and their control volume

### 4.2.2 Derivation of the Finite-Domain Equations

The derivation of the finite-domain equations has been described by Spalding (1982a). Therefore, it is only briefly outlined here. It is done by integrating differential transport equations over each of control volumes that subdivide the flow domain. The integrations

entail "interpolation assumptions" which are commonly referred to as the "fully-implicit" and "upwind" formulations.

Integration of the general conservation Equation (3.5) over the control cell P (see Figure 4-2) gives :

$$\iiint_V \frac{\partial(\rho\phi)}{\partial t}dV + \iint_A (\rho\vec{U}\phi)\cdot d\vec{A} = \iiint_V S_\phi dV \quad ; \qquad (4.1)$$

where V denotes the cell volume, A its total surface area.

The transport of a variable, $\phi$ , across the faces and throughout the time, yields transient and convection terms. Other terms which result from the integration of the general transport equation over the control volume are included in source terms. Each one of these terms are now discussed.

Transient Term

Since the variable, $\phi$ , is assumed to be uniformly distributed throughout the control cell, the transient term can be written as :

$$\iiint \frac{\partial(\rho\phi)}{\partial t}dV = V\frac{\partial(\rho\phi)}{\partial t} = \frac{V}{\Delta t}(\rho_p\phi_p - \rho_{p,o}\phi_{p,o}) \quad ; \qquad (4.2)$$

where the subscript o refers to values prevailling at the start of the time interval.

The transient procedure adopted is fully implicit in that all neighbouring $\phi$'s of $\phi_p$ and related values are late-time values, i.e. present values.

Convection Term

Variables in the surface integral are presumed to be constant over each cell face, thus :

$$\iint (\rho\vec{U}\phi)\cdot d\vec{A} = \sum_{n,s,e,w} (\rho\vec{U}\phi)\cdot\vec{A} \qquad (4.3)$$

Since $\phi_p$ is the value associated with the nodal point P, interpolations are required for each cell-face value of $\phi$ to be used in the surface integral Equation (4.3). In the present study, the "upwind" scheme of Spalding (1972) is used to evaluate the convection fluxes across the control volume faces. This is that, for the convective term, the value of $\phi$ to be convected across a cell face is taken to be the nodal value prevailling at the upstream side of the face; for example, when the convective flux is calculated at the north face n, the value of $\phi_n$ specified is :

$$\phi_n = \phi_N \qquad \text{if } v<0$$

or

$$\phi_n = \phi_p \qquad \text{if } v>0 \qquad (4.4)$$

where v is the velocity component normal to the north

face; and similar rules apply for the other faces and directions.

Equation (4.3) can be expressed in terms of the convection flux, Ci where :

$$Ci\ \phi = \rho U_i A_i \phi \quad ; \tag{4.5}$$

where the subscript, i, refers to the cell faces.

Source Term

For constant variables assumed over each cell , the source term can be written as :

$$\iiint_V S_\phi dV = VS_\phi \quad . \tag{4.6}$$

The source term of $\phi$ may then be linearised to be written in the form :

$$VS\phi = VSu + VSp\phi_p \quad ; \tag{4.7}$$

where Su and Sp are the appropriate components numerically designed for the source term.

General Form of the Finite-Domain Equation

The equation that results from the sum of the various terms which have appeared in the derivation above can be written in the following general form :

$$a_p\phi_p = a_N\phi_N + a_S\phi_S + a_W\phi_W + a_E\phi_E + a_T\phi_T + S_u \quad , \qquad (4.8)$$

where $$a_p = a_N + a_S + a_W + a_E + a_T + (-S_p) \quad ; \qquad (4.9)$$

where $a_p$ ....$a_N$ etc. are the "coefficients" of the finite-domain equation; they are functions of Ci's. The formulation of all "coefficients" can be found in "Four Lectures on the PHOENICS Computer Code" (Spalding 1982a).

## 4.3 Incorporation of Auxiliary Information

Initial Conditions

The initial field of the dependent variables must be specified before the calculation procedure may begin. In the case of flows containing interface such as the flame-front in this study, the initial location of the interface should also be specified.

Boundary Conditions

The boundary conditions required to specify the flow

situations under consideration have been discussed in Chapter 3. The appropriate methods of implementing them in the solution scheme are given below.

Values of dependent variables must be specified at the boundaries before the finite-domain equations can be solved. These boundary conditions, which determine the uniqueness of the solution for a given flow situation, are usually of two types :

(i) The value of the variable is prescribed at the boundary; and

(ii) Its flux value at the boundary is prescribed (such as mass flux, momentum flux etc.).

In the present study, both conditions are handled by way of the linearised source terms. The details of this approach may be found in Spalding (1982a), and only a brief outline is described here.

The expression of the boundary condition in PHOENICS is a linear form. The total source is expressed as :

$$S = m\phi_{BC} + C(\phi_{BC} - \phi_p) \qquad (4.10)$$

where m is a prescribed inflow rate of mass to the cell,

$\phi_{BC}$ is the prescribed quantity having the dimensions of $\phi$;

$\phi_p$ is the unknown value of $\phi$ for the cell; and

C is a prescribed coefficient.

The required boundary conditions can be adequately specified by the appropriate combination of the coefficient, C, and quantity, $\phi_{BC}$, appearing in Equation (4.10).

Density Calculation

As discussed in Section 3.3.2, the local density in the field is determined by the interface location and shape. When a cell is totally immersed in either the unburned- or burned-gas region, its density is uniform and is directly specified appropriate to that region as $\rho_u$ or $\rho_b$. When the interface is partially located in a given cell, the density in that cell may be calculated as a proper weighted average of the burned- and unburned-gas densities according to :

$$\rho = \alpha\rho_b + (1-\alpha)\rho_u \quad ; \qquad (4.11)$$

where $\alpha$ is the ratio of the area of the cell occupied by the burned gas, Ab, to the total area of the cell, At, as expressed :

$$\alpha = Ab/At \qquad (4.12)$$

The area of a cell occupied by the burned gas, Ab, is calculated from the particle locations as follows:

(a) The procedure starts with the first particle at a boundary of the flow domain and moves along the particle string until a new cell is encountered. It is straightforward procedure to determine which cell contains particles by reference to the particle coordinates. Figure 4-3 illustrates a cell through which the particle string passes.

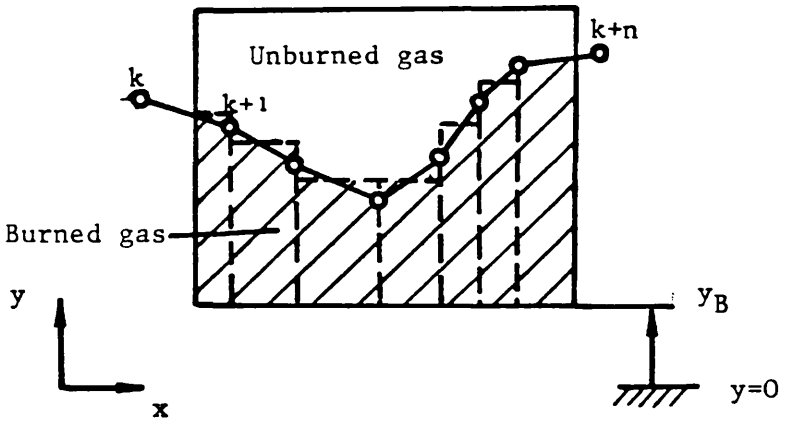



Figure 4-3 Density calculation from the particle locations.

(b) The area occupied by the burned gas (shaded area) between the particle string and the boundaries of the cell is divided into segments as shown. The area of these segments may be expressed as:

$$Aseg = (x_{k+1}-x_k)\left(\left(\frac{y_{k+1}+y_k}{2}\right)-y_B\right) \quad ; \qquad (4.13)$$

where the x's and y's are coordinate locations of particles.

Obvious adjustments to Equation (4.13) are necessary for the first and last segments in the cell. Then, it is only necessary to algebraicly sum the segment areas and divide the result by the total area of the cell to obtain the percentage of the burned gas, .

(c) Return to (a) starting with the first particle in the new cell.

To determine the contents of cells in which only the burned gas or the unburned gas is present, the present procedure sets the fluid in these cells as that which previously occupied the larger proportion (Andrew 1986). The Courant condition ensures the success of this practice for determining the contents of cells.

The above described procedure have been programmed in Subroutine DENXY given in Appendix B; and comments are made in the listing.

The method used for tracking the interface will be fully described in Section 4.5.

Volumetric Source for the Continuity Equation, Sr

The source term in Equation (3.1), $(-\frac{1}{\rho}\frac{D\rho}{Dt})$ needs to be specified based on the combustion model adopted in this

study.

This source term is zero throughout the entire field, except for cells containing the flame front where combustion occurs.

The expression for the source term is :

$$Sr = Sb*L_{fl}*\left(\frac{\rho_u}{\rho_b}-1\right) \; ; \qquad (4.14)$$

where, Sb is the burning velocity;

$\rho_u$ , $\rho_b$ are the densities of the unburned and burned gas respectively.

$L_{fl}$ is the length of the flame front lying inside the cell, and calculated from the particle coordinate locations as follows:

$$L_{fl} = \sum_k \sqrt{(x_{k+1}-x_k)^2+(y_{k+1}-y_k)^2} \qquad (4.15)$$

The above expression is programmed between statement labels 330 and 331 in the listing of Subroutine DENXY given in Appendix B.

## 4.4 The Solution of the Finite-Domain Equations

### 4.4.1 The GALA Method

In the numerical study of wrinkled laminar flames, it is necessary to simulate the motion of flame-fronts causing density discontinuities between the lighter, burned-gas and heaver, unburned-gas regions. Difficulties have been encountered in determining the density of a cell with a flame-front crossing it because of those arising from evaluating average face-densities of such cells near the flame-front.

The problem can be solved if the mass conservation equation is written as follows (Spalding 1974) :

The mass-continuity equation,

$$\frac{\partial \rho}{\partial t} + \mathrm{div}(\rho \vec{U}) = o \qquad (4.16)$$

can also be written as

$$\frac{1}{\rho}\frac{D\rho}{Dt} + \mathrm{div}(\vec{U}) = o \quad ; \qquad (4.17)$$

where D/Dt represents the operator ( $\partial / \partial t + \vec{U}$ * grad), i.e. the "substantial derivative", and the density disappears from the "div" term.

Now it become clear that the evaluation of div($\vec{U}$) requires no knowledge of densities for cell boundaries, whereas evaluation of $(\frac{1D\rho}{\rho Dt})$ merely requires knowledge of how the densities of identified particles of fluid vary with time, which is easier to come by.

The numerical procedure built upon Equation (4.17) is called GALA (for GAs-Liquid Algorithm). The GALA method has been extensively exercised by Maxwell (1977) for the numerical simulation of phenomena such as the rise of a bubble through a liquid, the transient motion of a water wave, and its "breaking" over an obstacle; the agreement with experimental data has proved to be excellent. It has been also successfully used by Awn (1979) for the investigation of flame propagation in tubes.

GALA is adopted as an option incorporated in the PHOENICS code and is used for investigations of the wrinkled laminar flame in this study.

### 4.4.2 General Feature of the Solution Method for the Finite-Domain Equations

The finite-domain equations for the velocity components and scalar property $\phi$ are expressed in the general form, Equation (4.8). They are only linear in appearance, because the coefficients and sources are function of $\phi$'s. In addition,the momentum equations are coupled through the unknown pressure field; thus an iterative procedure must be employed for their solution.

In the present study, the finite-domain equations for u and v are solved in PHOENICS by the Jacobi point-by-point procedure. Most of the equation (scalar ) sets are solved, slab-by-slab, by means of "a slab-wise linear solver".

The GALA algorithm mentioned above is embodied in PHOENICS. The purpose is to solve the pressure-correction equation,which takes the form of Equation (4.8) with its own appropriate coefficients. It ensures that the continuity equation is satisfied as the pressure field is calculated. These details have been described by Spalding (1982a).

### 4.4.3 The Hydrodynamic Solution Procedure

The main steps of the computational procedure for solving the flow field based on GALA can be summarized as follows:

(a) guess the pressure field; setting it equal to the pressure at the starting of the solution procedure. Calculate source term for the continuity equation from appropriate physical models adopted.

(b) Calculate all coefficients in the finite-domain equations and solve momentum equation, using the guessed pressure distribution.

(c) The resulting velocity and the guessed pressure distribution are used to calculate the source term of the pressure-correction equation which is now solved.

(d) The resulting pressure-corrections are used to correct the pressure and velocity fields so that local continuity is satisfied in all control volumes.

(e) This completes one iteration; Steps (a) to (d) are repeated until convergence is obtained at any given time step.

## 4.5 Resolving the Fluid Interface

### 4.5.1 General Background

The successful calculation of flows containing interfaces

requires a detailed knowledge of the instantaneous shape and location of the fluid interface. In the present study the particle-tracking method has been used to obtain this information. The use of this method is also able to calculate two different densities as a supplement to the combustion model described in Sections 3.3.2 and 4.3.

The development of the MAC (Marker and Cell) method at Los Alamos Scientific Laboratory by Welch, Harlow, Shannon and Daly (1966) has been the first extensive use of a numerical procedure to solve free-surface flows with the use of marker particles to denote the location of the free surface. Daly (1969) has used the same method to study the effects of surface tension in time-dependent hydrodynamic calculations. Maxwell (1977) has used the particle-tracking technique to investigate the behaviour of the free surface in different flow situations, Awn (1979) has made use of this method for studying flows with combustion, Castrejon (1984) has used this technique to investigate free-convection heat transfer inside an annular cavity, and Qin (1984) has used the same method to trace vortex patterns downstream of valves.

In the present study the basic principles of the particle-tracking method used by Maxwell (1977) and Awn (1979) have been incorporated into the PHOENICS code so as to generate a numerical flow-visualization procedure which proves to be a valuable tool for comparing numerical predictions

with experimental results, and for a better understanding of the flow under consideration, as will be seen later.

The mathematical basis of the particle-tracking technique has been discussed in Section 3.3.1. The details of the interface tracking are described below.

### 4.5.2 Flame-Front Tracking

A string of imaginary particles is distributed at an initial time, along the flame-front. Each of these particles is characterised by coordinates $x_p$ and $y_p$, where p denotes a certain particle. Then the variation of the particle location with time is deduced from the finite-difference equations,

$$x_p = x_{p,o} + u_p \Delta t \quad , \tag{4.18a}$$

$$y_p = y_{p,o} + v_p \Delta t \quad , \tag{4.18b}$$

where $x_{p,o}$ and $y_{p,o}$ are the coordinates of the particle at the beginning of the time interval and $u_p$ and $v_p$ are the instantaneous velocity components with which the particle is moved through the finite-domain mesh, and are evaluated at the old location $x_{p,o}$ and $y_{p,o}$.

The velocity $\vec{U}p$ of the particle on the flame front is calculated from the burning velocity $\vec{S}b$ which is defined

to be the velocity relative to the unburned gas. This velocity is always normal to the interface surface and directed towards the unburned gas. So, $\vec{U}p$ is given by :

$$\vec{U}p = \vec{S}b + \vec{U}unb \quad ; \qquad (4.19)$$

where $\vec{U}unb$ is the velocity of the unburned gas immediately ahead the flame, as shown in Figure 4-4. All quantities in Equation (4.19) are vectors.

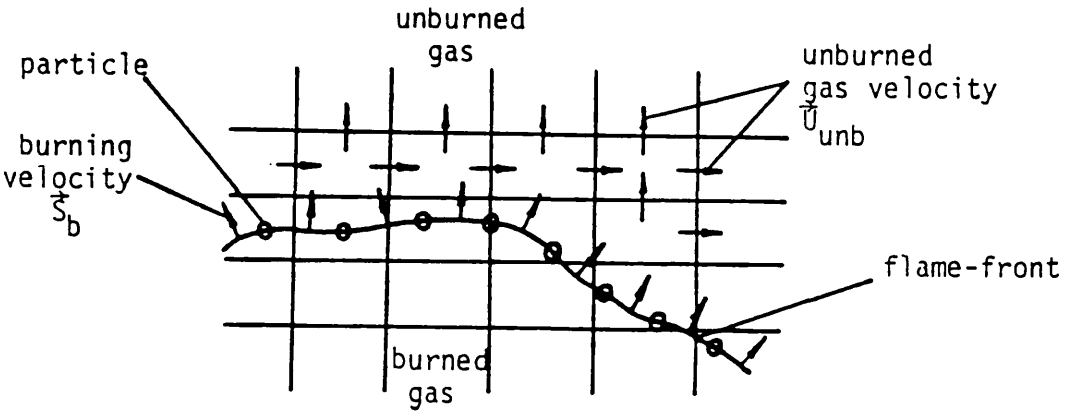
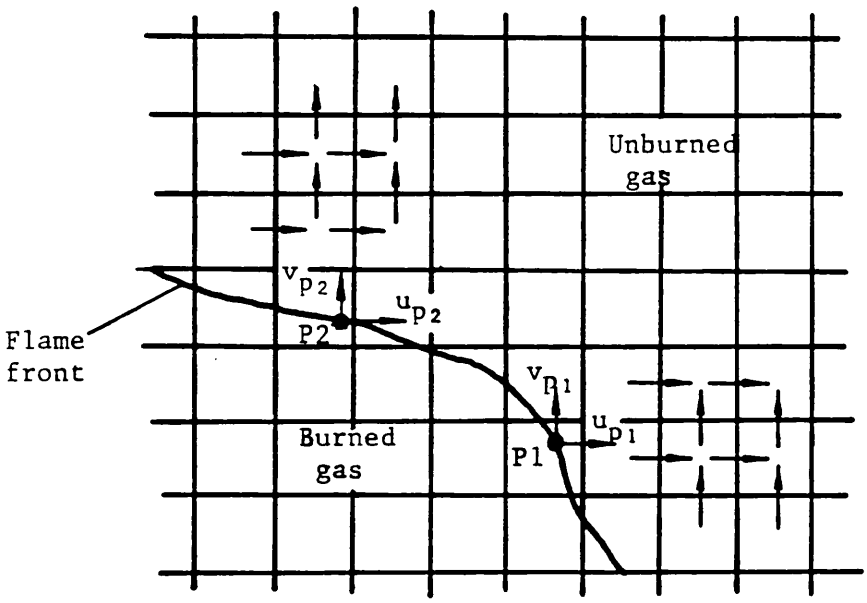



Figure 4-4 Flame-front tracking

The components of $\vec{U}unb$ are calculated by linear extrapolation or interpolation from the velocities surrounding the particle on the unburned-gas, i.e. higher-density side only. The procedure may confirm that all the cells from which the velocity components employed are totally immersed in the unburned-gas region by checking the density values in those cells. For the cases in which

the particle string passes through a cell from the north-face to the south-face, or from the east-face to the south-face, or from the east-face to the west-face, the components of $\vec{U}unb$ are taken from those on the right side of the particle, for example, particle P1 shown in Figure 4-5; for all other cases, the components of $\vec{U}unb$ are taken from those on the upper side of the particle, for example, particle P2 shown in the figure.




—— u-velocities used in the interpolation or extrapolation procedure to obtain $u_p$

| v-velocities used in the interpolation or extrapolation procedure to obtain $v_p$

Figure 4-5 Velocities used in the evaluation of particle velocity

The procedure for calculating the components of $\vec{U}unb$ is programmed between statement labels 332 and 345 in Subroutine DENXY given in Appendix B.

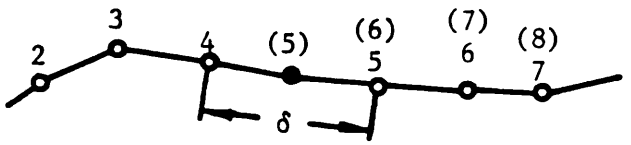
### 4.5.3 Addition and Deletion of Particles

Because of the fluid motion, the interface particles do not always remain evenly spaced. Even parts of the interface may intersect. Therefore, a check on the distances between adjacent particles for the sake of accuracy becomes the first step in the tracking calculation. If a pair of particles is separated by more than a given distance $\delta_1$, a new particle is inserted between them (see Figure 4-6 (a)). The coordinates of the new particle are taken to be the average coordinates of its neighbours, and the particle storage array is adjusted to accommodate the new particle. If the spacing between successive particles is less than a prescribed distance $\delta_2$, one of the particles is deleted ,as shown in Figure 4-6 (b). Under the circumstance of wrinkled flame-fronts investigated in this study, some parts of the interface may often intersect, which creates a serious problem for the particle-tracking technique. When it happens, the practice adopted in this study is to delete those particles which form a closed loop at the flame front assuming that the gas in this region has been burned, as described in Figure 4-6 (c).

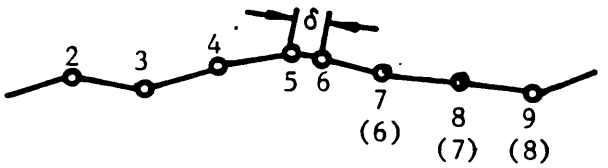
Also, if the particles reach the walls, they are deleted assuming that the flame extinquishes.

The procedure described in this section is programmed in

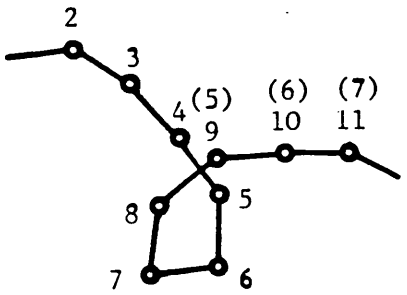
Subroutine TRKXY given in Appendix B; and comments are made in the listing.



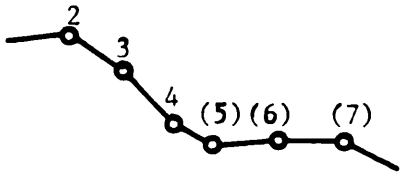

(a) Particle addition midway between two existing particles (i.e. 4 & 5) if $\delta$ exceeds a given spacing $\delta_1$. The particles are then renumbered to account for the addition.




(b) Particle 6 is deleted if $\delta$ is less than the prescribed spacing, $\delta_2$. The particles are renumbered to account for the deletion.




Interface intersects




After particles 5, 6, 7 and 8 have been deleted

(c) Particles 5, 6, 7 and 8, which form a closed loop at the interface are deleted if the interface intersects. The particles are renumbered to account for the deletion.

Figure 4-6 Particle addition and deletion procedures

## 4.6 Closure

In this chapter, the derivation of the finite-domain form of the partial-differential equations and their method of solution have been presented.

With this chapter, the theoretical formulation for the computer simulation of the phenomena under consideration is completed and attention will now be paid to the prediction of experiments.

# CHAPTER 5 - THE NUMERICAL SIMULATION OF EXPERIMENT

## 5.1 Introduction

The present chapter deals with the computations which are compared with the experimental results for the testing of the prediction procedure described earlier.

### The Cases to be Predicted

Three cases have been selected for the simulation exercise, which involves the effect of gravity. They correspond to photographs in Figure 2-7 (b) (flame propagates horizontally), Figure 2-7 (a) (flame propagates upwards) and Figure 2-7 (c) (flame propagates downwards) respectively.

### Specifications of the Cases Tested

The dimensions of the combustion chamber and flow conditions employed in the calculations are identical to that of the experiments. All conditions for these cases are the same except for the direction of flame propagation; and details are given in Table 5-1.

Table 5-1 Specifications of the Cases Tested

| Case No. | Corresponding case in the experiment | No. of vents | Vent size (mm) | Vent location | Methane/air volume ratio |
|---|---|---|---|---|---|
| 1 | Fig. 2-7 (b) flame propagates horizontally | 1 | 10 | in the corner from which flame propagates | 9.8 % |
| 2 | Fig. 2-7 (a) flame propagates upwards | 1 | 10 | in the corner from which flame propagates | 9.8 % |
| 3 | Fig. 2-7 (c) flame propagates downwards | 1 | 10 | in the corner from which flame propagates | 9.8 % |

The geometry of combustion chamber is shown in Figure 5-1.

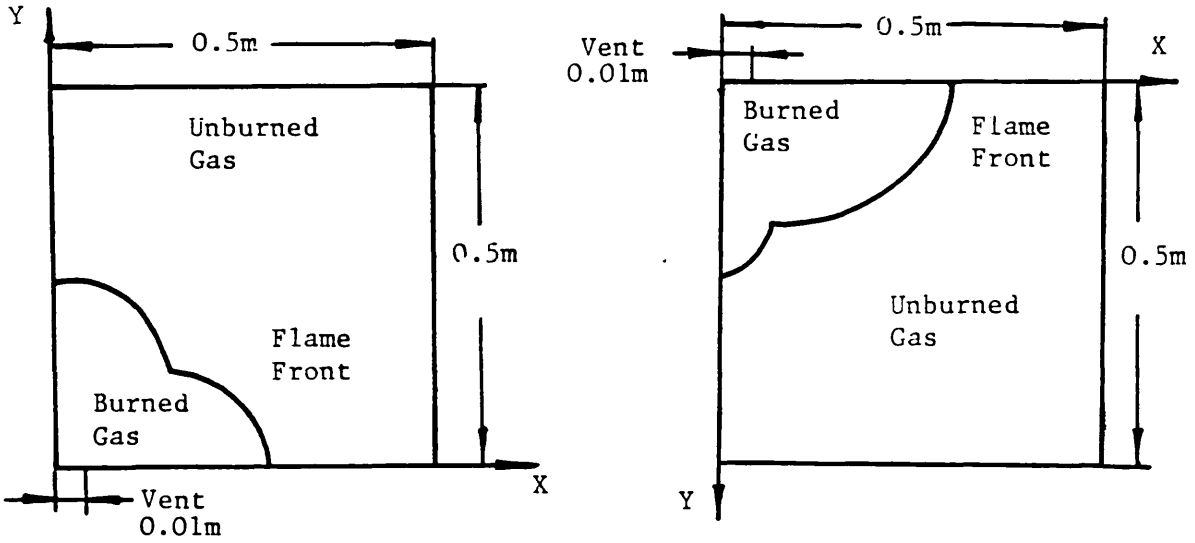



Figure 5-1 The geometry of flow region
(a) Flame propagates horizontally (the chamber is laid flat) - Case No.1
(b) Flame propagates upwards - Case No.2
(c) Flame propagates downwards - Case No.3

The prediction is mainly concerned with the location and shape of the flames. In addition, other specific information such as the velocity field in the unburned-gas region for Case 1, will also be presented to allow the characteristics of the flow to be examined. Details of this investigation and results obtained will be discussed in the succeeding sections and listings of the PHOENICS code and relevant subroutines are given in Appendices A & B respectively.

## 5.2 Computational Details

### Initial and Boundary Conditions

As already mentioned in Section 3.3.3, the velocity & pressure fields and flame location obtained from a preliminary calculation serve as initial conditions for the simulation of process. This preliminary calculation is really a kind of assumption for uncertainty about the exact ignition, and is described below.

The preliminary calculation starts from the flame of a quarter-circular arc of radius equal to 0.01 m and centred on the origin of the coordinates, as shown in Figure 5-2.

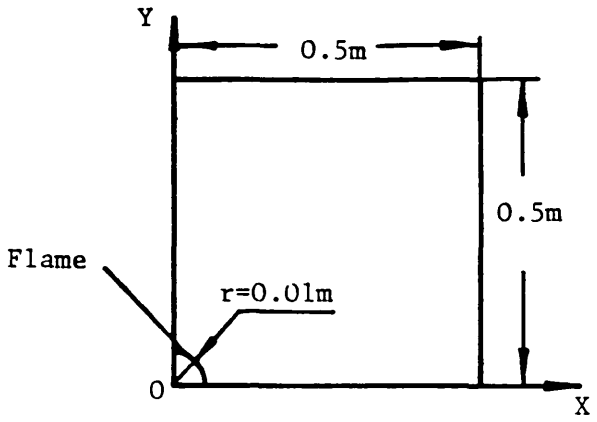



Figure 5-2 Flame location at the start of preliminary calculation

The vent is closed for this calculation and the flow is compressible. The tracking particles are placed uniformly along the flame surface. Since the flame location is known, the starting density-field throughout the flow domain may be prescribed. The initial distribution of velocity components and pressure for the preliminary calculation are set to zero and the atmospheric respectively. As the flame propagates, the radius of flame-arc increases. The calculation is to end at the moment when the radius of flame-arc reaches 0.05 m. Then the vent is opened, and a uniform pressure, P = 0 $N/m^2$ (relative to the atmospheric pressure) is specified at the vent opening. The results thus obtained are used as the initial conditions for the prediction process to start.

The above treatment can be easily performed by using "SAVE" and "RESTRT" options in PHOENICS. "RESTRT" is to provide as initial conditions the solution fields created

and stored by a previous run in which "SAVE" is used.

Density and Burning Velocity

The density calculation has been described in Section 4.3. The data of the density of the burned gas, $\rho_b$ and the density of the unburned gas, $\rho_u$ in Equation (4.11) are obtained from Karim et al (1967) who has investigated the thermodynamic properties of the combustion of methane under the assumption of chemical-equilibrium conditions. The values of $\rho_b$ and $\rho_u$ pertaining to the mixture ratio of 9.8% used in the present calculation are 0.19 and 1.08 respectively.

The burning velocity, Sb is specified from the data pertaining to the mixture ratio used. In the present calculation, the data obtained by Andrews and Bradley (1972) are adopted for the burning velocity of laminar flames. Its value for the cases calculated in this study is 0.4 m/s.

Grid Distribution and Time-Step Size

The grid lines are distributed non-uniformly over the flow domain with two columns of finer grids near the walls,as shown in Figure 5-3.

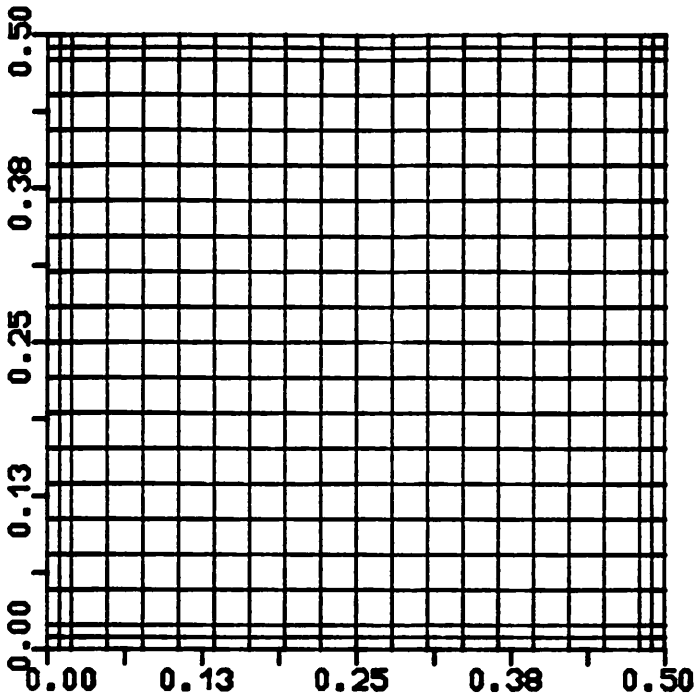



Figure 5-3 The calculation domain and a typical grid distribution (NX x NY : 20 x 20)

Computations have been made with grid numbers of 20x20 and 30x30. In addition, four different grid systems have been investigated for Case 1 at a chosen flame location.

The time-step size used in this investigation is 0.004 sec throughout. The effect of time-step size has been also investigated for Case 1 at a chosen flame location.

## 5.3 Presentation of Results

### 5.3.1 Horizontally Propagating Flame (Case 1)

#### The Location and the Shape of Flame

Figure 5-4 shows the predicted location and shape of the flame propagating horizontally with a grid number of 20x20.

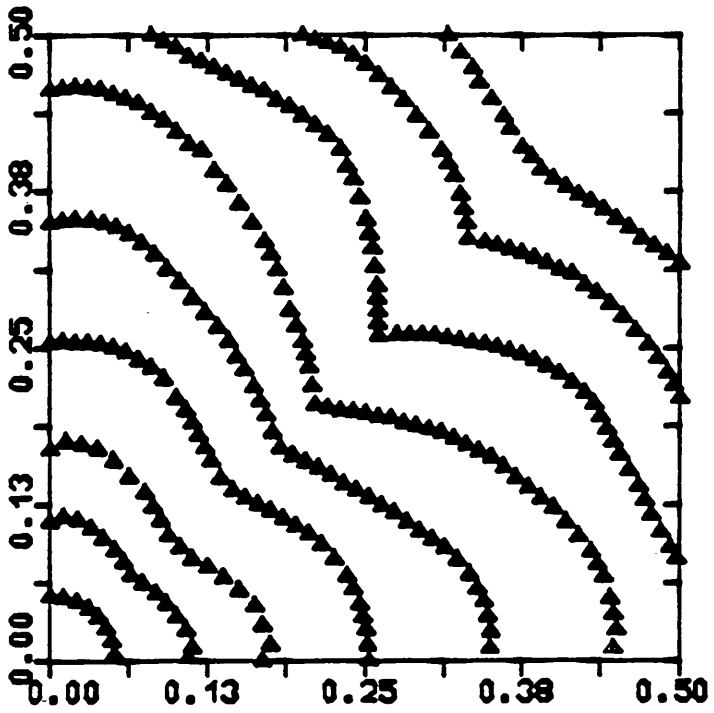
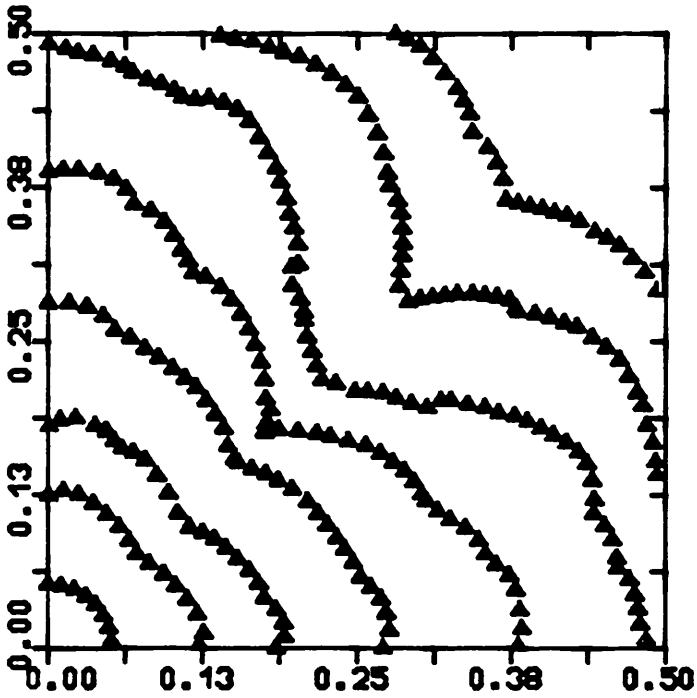


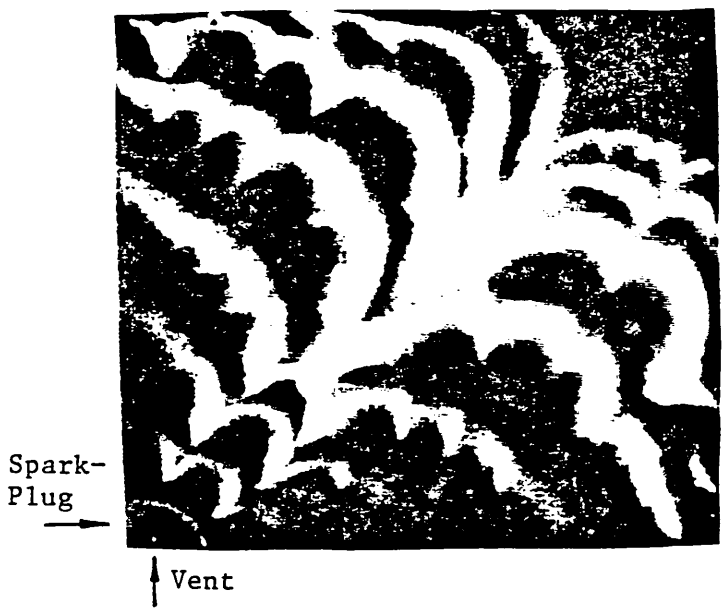

Figure 5-4 The predicted location and shape of the flame propagating horizontally with a grid number of 20x20

The interval between any two flame positions is 0.08 sec. Figure 5-5 (a) shows the same flame but with a grid number of 30x30. A photo-copy of the experimental flame is given

in Figure 5-5 (b) for a comparison. The interval between any two flames in both figures are the same (0.08 sec.).




(a) The predicted flame




(b) The experimental flame

Figure 5-5 The location and shape of the flame propagating horizontally (grid number 30x30) - Case 1

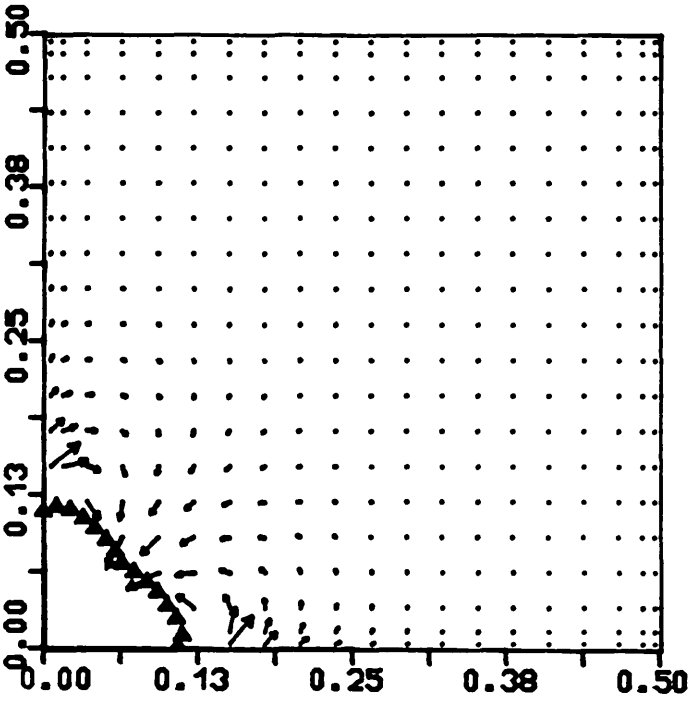
The flame propagation in this case is free from the effect of gravity. Therefore, the body-force term in Equation (3.4) has been set to zero in this calculation.

It can be seen from above figures that there is an agreement in trends between the prediction and experiment. The development of flame wrinkling in the prediction is slower than that in the experiment; but more details appear in the computational results as the grid number increases.

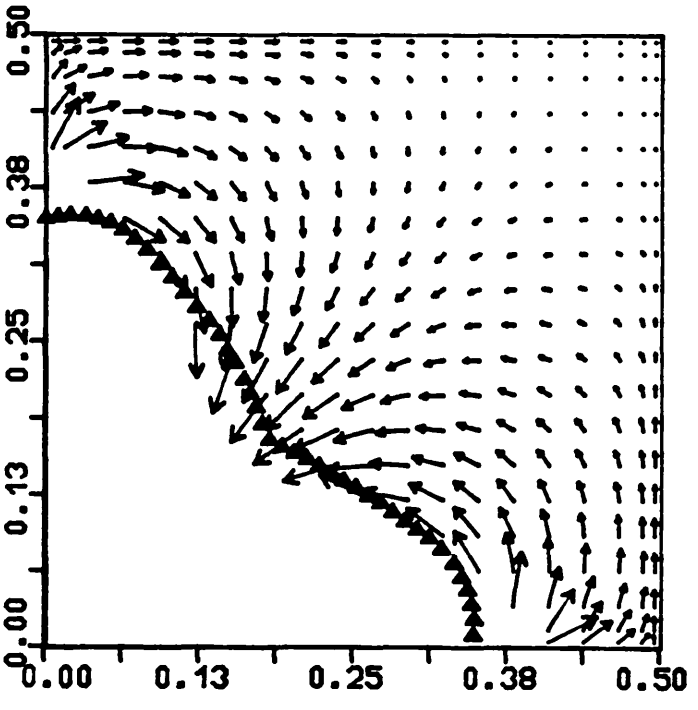
Velocity Field in the Unburned Gas Region

As there is a significant change in the velocity field across the flame front. The velocity in the burned-gas region is very large in comparison with that in the unburned-gas region in the present calculation. In order to show the variation in the velocity magnitudes of the head of the flame front, only the velocities in the unburned-gas region have been plotted. In this way the regions of interest may be studied more closely.

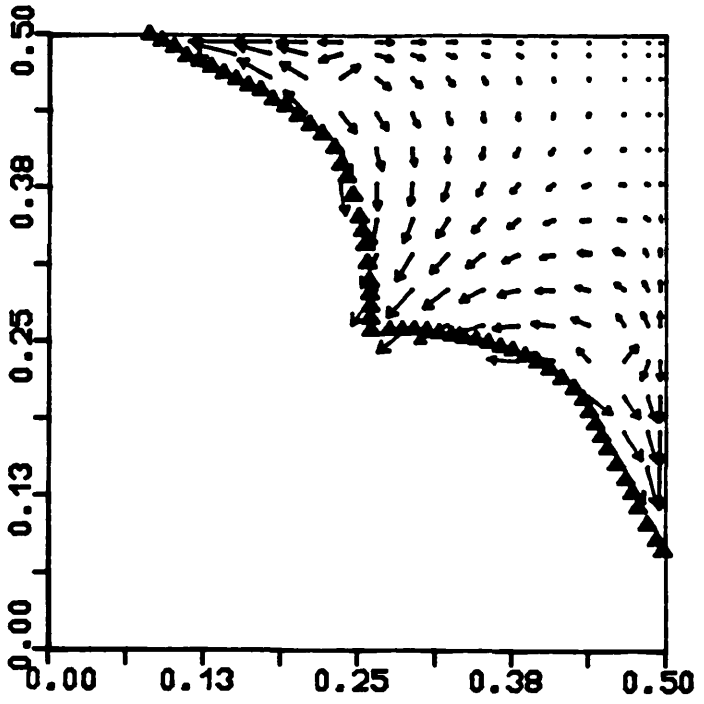
Figure 5-6 (a-c) shows the velocity fields in the unburned-gas region at three different flame locations corresponding to Figure 5-4. In these figures, the triangle-line represents the flame front while the arrows represent the velocity vectors, which are scaled relative to the maximum velocity in the field.




(a) The velocity field corresponding to the second flame position in Fig.5-4.




(b) The velocity field corresponding to the fourth flame position in Fig.5-4.




(c) The velocity field corresponding to the sixth flame position in Fig.5-4.

Figure 5-6 The velocity field in the unburned-gas region at three different locations corresponding to Fig.5-4.

As is seen from the figures 5-6 (a) & (b), the thermal expansion within the combustion waves generates a thrust, which pushes the unburned gas ahead of the flame towards the central region of the chamber, facing the vent opening, and resulting in the flame identation in the direction of the burned gas. In the dent the flow of unburned gas converges to increase the thrust which would tend to deepen the cavity.

### 5.3.2 Upwards Propagating Flame (Case 2)

Figure 5-7 shows the predicted location and shape of a flame propagating upwards with a grid number of 20x20.

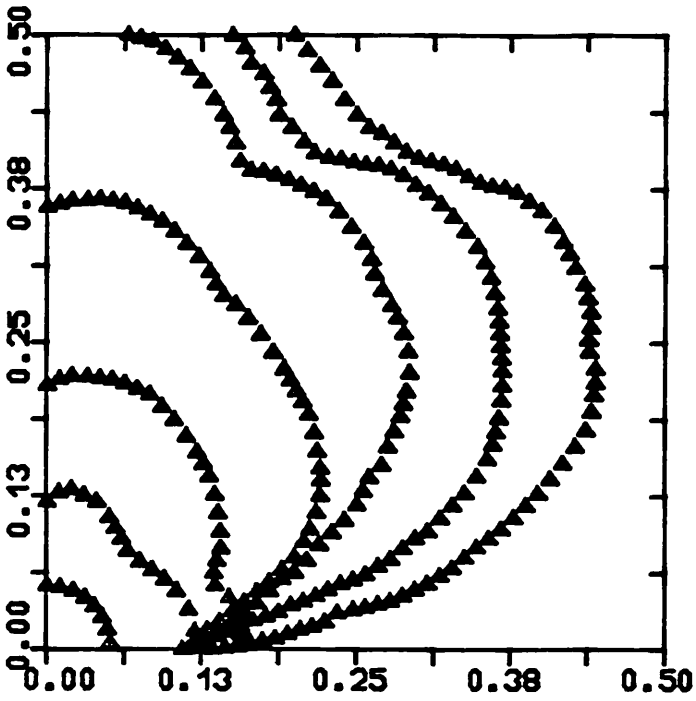
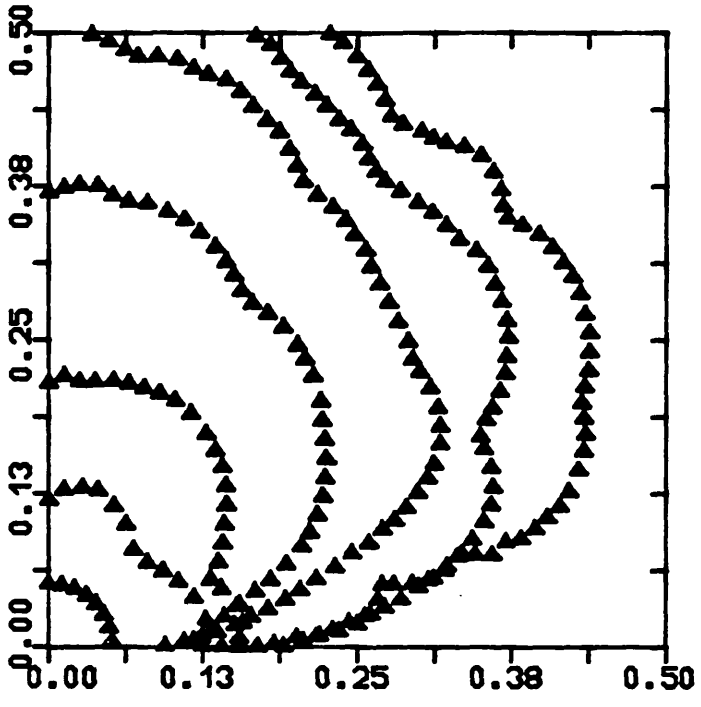



Figure 5-7 The predicted location and shape of the flame propagating upwards with a grid number of 20x20

Figure 5-8 (a) shows the same flame but with a grid number of 30x30. A photo-copy of the experimental flame is given in Figure 5-8 (b).

The interval between any two flames in both figures are the same (0.08 sec).




(a) The predicted flame




(b) The experimental flame

Figure 5-8 The location and shape of the flame propagating upwards (grid number 30x30) - Case 2

The effect of gravity can be clearly seen from these figures that flames are tilted to the left. However, the numerical procedure underpredicts the flame speed, as will be discussed later.

### 5.3.3 Downward Propagating Flame

Figure 5-9 shows the predicted location and shape of the flame propagating downwards with a grid number of 20x20.

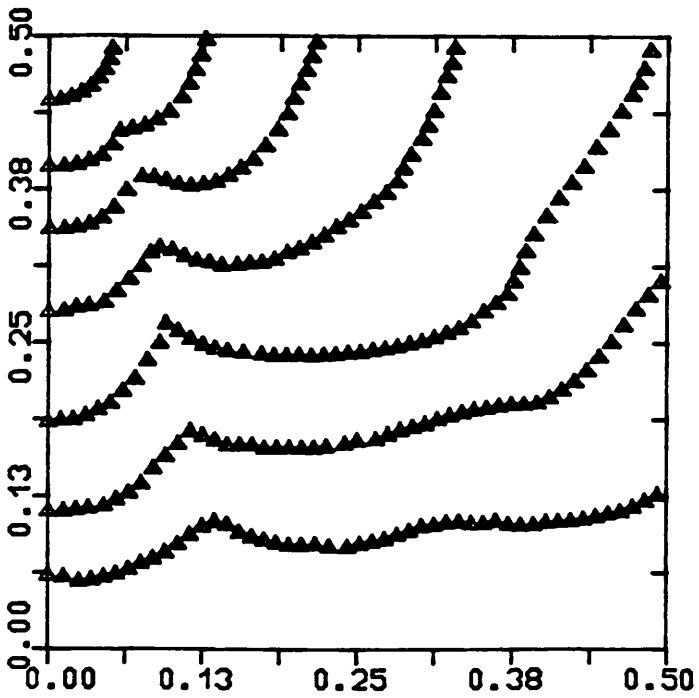
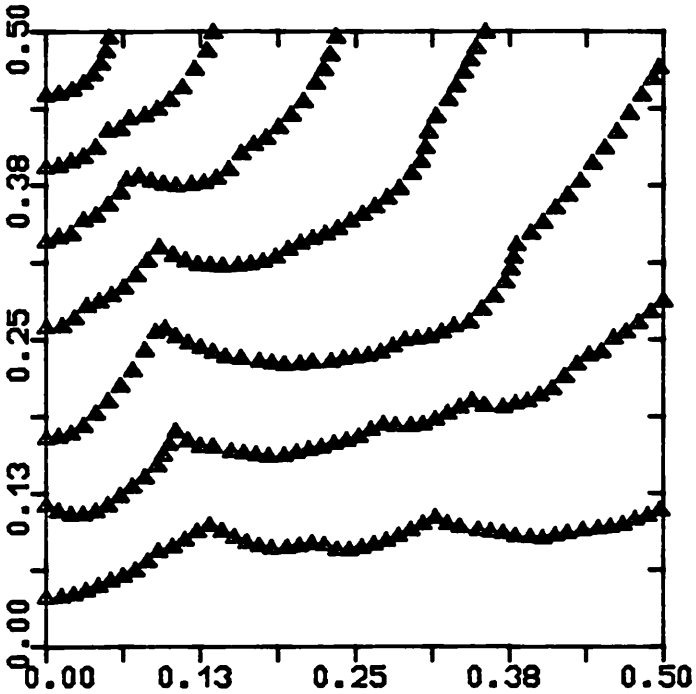
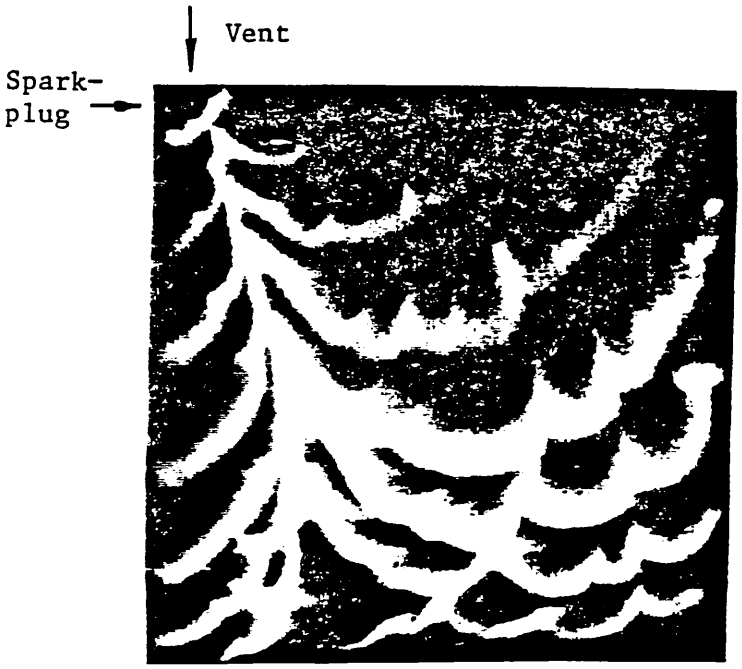



Figure 5-9 The predicted location and shape of the flame propagating downwards with a grid number of 20x20

Figure 5-10 (a) shows the same flame but with a grid number of 30x30. A photo-copy of the experimental flame is given in Figure 5-10 (b).




(a) the predicted flame




(b) The experimental flame

Figure 5-10 The location and shape of the flame propagating downwards (grid number 30x30) - Case 3

The results presented above show that the gross feature of the flames have been predicted for all three cases. The contribution of gravity to the flame behaviour has been well predicted, as shown in Figure 5-8 and Figure 5-10. However, the small-scale wrinkles have not yet been successfully obtained; it will be discussed in Section 5.5.

### 5.3.4 Effects of the Grid Number and Time-Step Size

This investigation has been performed for Case 1. The tests for the effect of grid number are listed in Table 5-2.

Table 5-2 Tests for the Effect of Grid Number

| No. | NX | NY | $\Delta t$ ( sec.) |
|---|---|---|---|
| 1 | 20 | 20 | 0.004 |
| 2 | 24 | 24 | 0.004 |
| 3 | 30 | 30 | 0.004 |
| 4 | 32 | 32 | 0.004 |

Figure 5-11 shows the influence of grid number on the location and shape of the flame at the time equal to 0.32 sec.

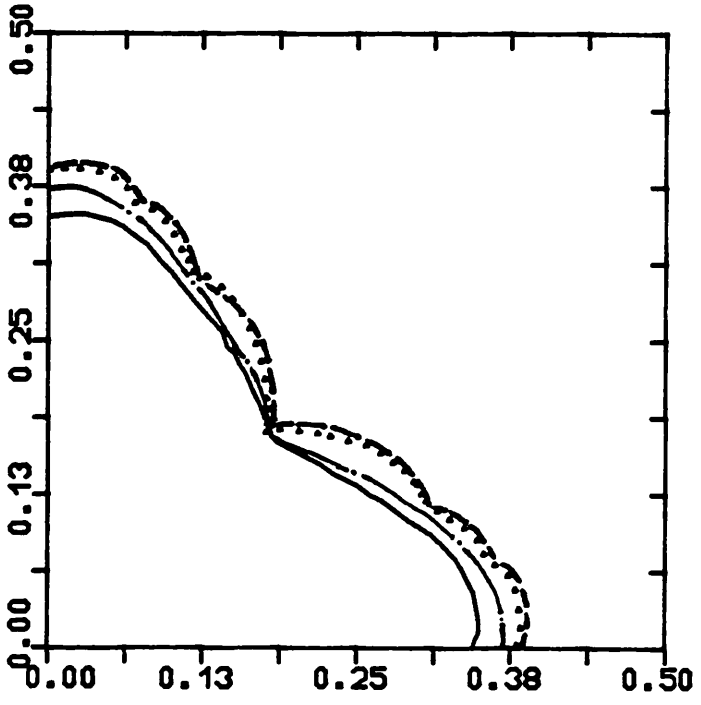



Figure 5-11 The effect of grid number on the results at the time equal to 0.32 sec.

———— 20x20 ..... 30x30
———— . ———— 24x24 ---------- 32x32

The investigation on Case 1 for the effect of time-step size is listed in Table 5-3.

Table 5-3 Tests for the Effect of Time-Step Size

| No. | NX | NY | $\Delta t$ ( sec.) |
|---|---|---|---|
| 1 | 20 | 20 | 0.008 |
| 2 | 20 | 20 | 0.004 |
| 3 | 20 | 20 | 0.002 |

Figure 5-12 shows the influence of the time-step size on the location and shape of the flame at the time equal to 0.32 sec.

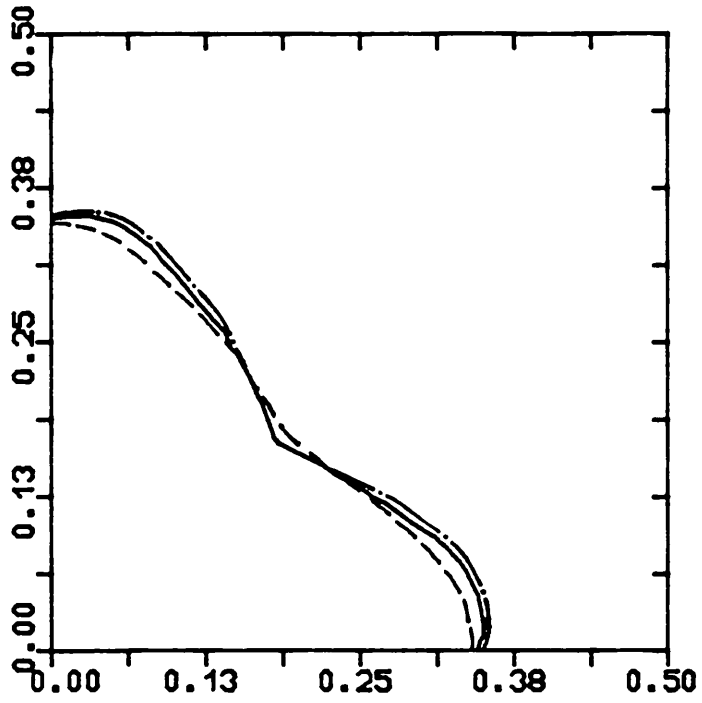



Figure 5-12 The effect of time-step size on the location and shape of the flame at t = 0.32 sec.

_____ . _____ . _____ t = 0.002 sec

_____ t = 0.004 sec

---------- t = 0.008 sec

## 5.4 Convergence

It is important to identify whether or not the solution is converging, and if it is, whether it has sufficiently converged for practical purposes. The presence of systematic behaviour of a particular set of monitored

variables between successive sweeps (or iterations), with the differences of their successive values diminishing, is one sign of convergence.

The convergence is also quantitatively monitored through the use of residuals. A residual of a variable $\phi$ at a node P, denoted by $R_\phi$, is defined as :

$$R_\phi = a_p\phi_p - \Sigma a_i\phi_i - S_u \quad ;$$

where $a_p$ is the denominator of Equation (4.8). The simultaneous-existing residuals are defined as those present for each cell for each variable when the whole variable field has been "frozen" at the most-recently calculated value.

The convergence details of the run for Case 1 are given in Table 5-4.

Table 5-4 Convergence Details for Case 1

| | |
|---|---|
| Grid | 20x20 |
| Number of sweep | 20 |
| Relaxation | FALSDT for u & v is 0.01 |
| Time-step size | 0.004 sec |
| Typical non-normalised absolute volumetric error (order) | 1.E-06 $m^3/s$ |

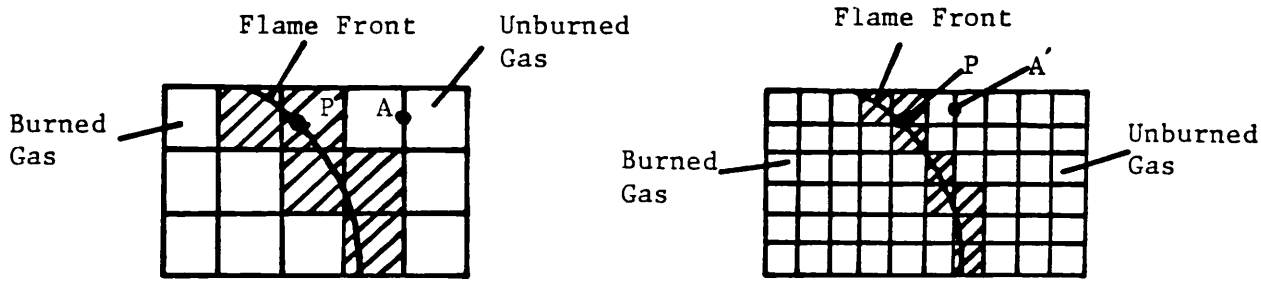
## 5.5 Discussions

The results presented above reveal the main features of the computational procedure. On the whole, agreements between predictions and experiments are encouraging. The influence of some factors on the results are apparent; they may be clarified through the following discussion.

### The effect of Grid Number

In the present calculation, the density and flame propagation speed are computed, the results are, therefore, expected to be sensitive to the grid number employed due to the following reasons.

(i) In the numerical scheme adopted,the densities in those cells which contain the flame-front are calculated as weighted averages of $\rho_b$ and $\rho_u$ , as described in Section 4.3. The number of cells, hence the relative area affected by the flame in a coarse grid-system is different from that in a fine one, as shown shaded in Figure 5-13 (a) & (b). This area diminishes with increasing fineness of the grid.




(a) coarse grid (b) fine grid

Figure 5-13 The effect of grid number

(ii) The flame propagation speed is calculated from the burning velocity and the velocity of the unburned gas in the cell immediately ahead of the flame. For example, in Figure 5-13 (a), the velocity at point A serves to determine the interface speed at point P; however,in the fine mesh depicted in Figure 5-13 (b), the flame speed at the same point, P, is evaluated from the velocity at A'. Clearly, since A and A' are at different location relative to the flame front, the velocities at these points will not, in general, be the same, in turn, it will lead to a discrepancy in the interface speed at point P although linear extrapolation or interpolation has been used.

(iii) As described in Section 4.5.2, in the calculation

of particle velocity, the components of $\vec{U}$unb may be taken from the different sides relative to the particle position depending on the direction in which the flame front passes through a cell. It may result in numerical velocity-discontinuity along the flame front. The use of finer grid may reduce the errors.

(iv) A severe property variation exists across the flame front. Since linear interpolation has been employed in the formulation of the finite-domain equations, the accuracy of the latter is strongly dependent on the cell size used in the region surrounding the flame front.

(v) The results presented show that the flow direction in most regions of the flow domain is oblique to the grid lines and even makes an angle of $45^0$ with the grid lines, as shown in Figure 5-6, which is the most serious situation for the numerical diffusion (Patankar 1980). This situation occurs because the ignition is placed at the origin of the coordinate system.

Flame Propagation Speed

As is seen from Figures 5-5,5-8 and 5-10, the predicted

area of the flame front is less than the experimental results. The underpredicted flame speed in the present calculations may be attributed to the underestimated flame area, because the motion of flames largely depends on the thermal expansion of the gas due to combustion, the rate of which is proportional to the area of the flame front in the present model. The underestimated flame area by the present procedure also tends to reduce the effect of the buoyancy force in the case of upward flame propagation, as shown in Figure 5-8.

### The Effect of Walls

In the experiments, the influence of walls exists; for example, the wall exerts a viscous drag on the flow, and also there is heat transfer through the walls, which tends to reduce the burning rate near the walls. These effects are not included by the present numerical procedure, since not only isentropic conditions are assumed, but also the burning velocity is taken as uniform over the entire flame front.

## 5.6 Closure

In this chapter, the numerical predictions have been compared with the experimental results presented in Chapter 2. The conclusions of these comparison may be summarized as follows :

(a) The agreement in trends for all three cases is found encouraging; and the effects of gravity force have been well predicted. It may be concluded that the numerical procedure can be used for simulating the experimental flow.

(b) Some discrepancies are apparent. In particular, the small-scale wrinkles have not successfully been predicted; the possible reasons have been discussed.

Predicted velocity field for the horizontally propagating flame has been also presented; it appears to be realistic. Some further information will be given in the next chapter, where the wrinkled laminar flames in simpler circumstances will be investigated for the better understanding of their formation.

# CHAPTER 6 - NUMERICAL STUDIES OF PROPAGATING FLAMES EXHIBITING THE LANDAU INSTABILITY

## 6.1 Introduction

In the last chapter, predictions have been compared with experimental evidence to test the credibility of the mathematical model and solution procedure. This chapter continues to demonstrate the ability of the computational procedure by studying the propagating flames exhibiting the Landau instability, so as to provide detailed insight into the mechanism. The investigation concentrates on the visualization of the formation of the wrinkled flame-front. The effects of various parameters on the flame behaviour are investigated. The results obtained will be presented and discussed in this chapter, and listings of the PHOENICS code (Q1 and GROUND) and relevant subroutines are given in Appendices A & B.

## 6.2 General Background

The problem of the stability of a plane flame front was first formulated and solved by Landau (1944). His investigation led to an unexpected result : a plane flame turns out to be absolutely unstable. The problem is later called Landau instability. The Landau instability does not appear to be observed very often experimentally. Subsequent analyses by Markstein (1951) and Istratov and

Librovich (1969) and experiments by Peterson and Emmons (1961) have been devoted to explain the experimentally observed stable laminar flames by incorporating the effects of flame curvature, heat conduction and viscosity on the flame propagation.

All previous theoretical studies on Landau instability are based on the linearized perturbation analysis; however, this method can give no information on the events that follow the onset of instability. Moreover, the nonlinear effects remain undetected in a linear treatment. It is ,therefore, desirable to use numerical simulations to advance the understanding of Landau instability.

## 6.3 Description of the Problem

### 6.3.1 Physical Process

The phenomenon studied here is the idealized premixed flame propagating upwards in a two-dimensional rectangular combustion chamber, closed at the top and open at the bottom, as shown in Figure 6-1.

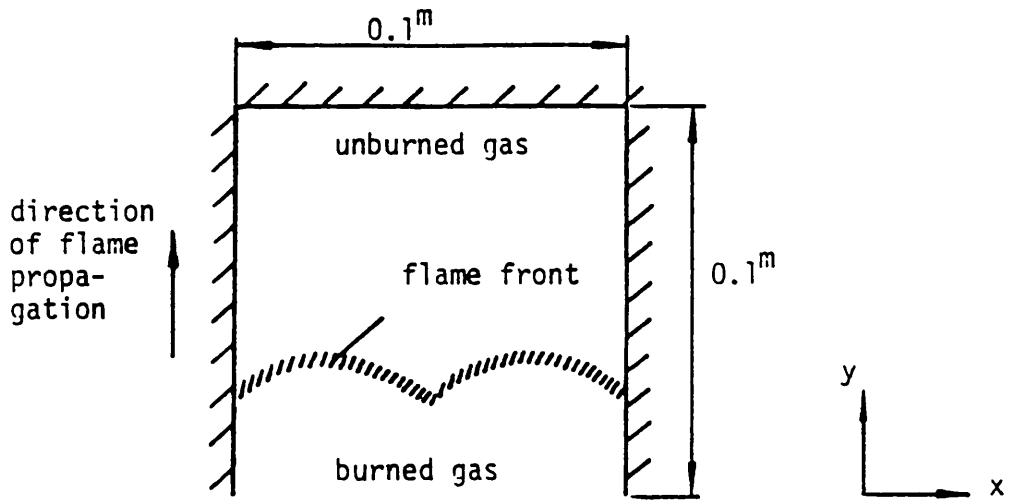



Figure 6-1 The model considered

Initially, the plane flame is assumed to be distorted by a artificial perturbation; the response of the flame and resultant flow field are to be simulated numerically.

### 6.3.2 Mathematical Details

#### The Differential Equations

Equations (3.1), (3.3) & (3.4), which govern the unsteady laminar flames with the assumptions stated in Section 3.2, are applicable to the problem. In accord with the approach employed here, the energy equation is not solved, but the effect of combustion on the flow is included via

the density change.

Flame-Front Tracking and Density Calculation

The flame-front tracking and density calculation have already been described in Section 4.5.2 and Section 4.3 respectively.

Volumetric Source for the Continuity Equation

The source term, $(-\frac{1}{\rho}\frac{D\rho}{Dt})$ in Equation (3.1) has been expressed by Equation (4.14).

Initial Conditions

An initial sinusoidal configuration of the flame-front, which represents the distortion of the flame by a perturbation, is given as follows :

$$y = A \sin(kx) + C \quad ; \qquad (6.1)$$

where : A = -0.0025 m;
k = 31.416 rad/m;
C = 0.0028 m.

Particles are distributed uniformly along the initial flame surface. Since this initial location is known, the

starting density throughout the flow-domain may be prescribed.

The initial velocities are set to zero, and the initial pressure is set to the atmospheric one,.i.e.

at t = 0, u = 0.0 m/s;

v = 0.0 m/s;

P = 0.0 $N/m^2$ (pressure is measured as excesses above 1.E5 $N/m^2$).

Boundary Conditions

At the open side, a uniform pressure is specified. There is no flow through walls.

Grid Number and Time-Step Size

A uniform grid, with 20x20 nodes, and a time step of 0.002 sec. is employed, in the majority of runs. The effects of grid number and time step size are demonstrated in Section 6.4.

## 6.4 Presentation of Results

The investigation has been performed through the parametric studies. The investigated parameters are the gravity force, the density ratio, the burning velocity and the wavelength of the initial perturbation. The first run

is taken as the "standard run", and others differ from the "standard run" by changing one parameter only.

Standard Run

For this case, conditions are as follows :

| | | | |
|---|---|---|---|
| density ratio | : | $\rho_b/\rho_u$ | = 0.2; |
| burning velocity | : | $S_b$ | = 0.4 m/s; |
| gravity force | : | g | = 0.0 $m/s^2$; |
| the wavelength of initial perturbation | : | L | = 2xwidth of the chamber. |

The flame-front location and shape at different times are given in Figure 6-2.

The interval between any two curves is 0.02 sec, and first curve from the bottom is the initial interface, as is true of all the subsequent diagrams.

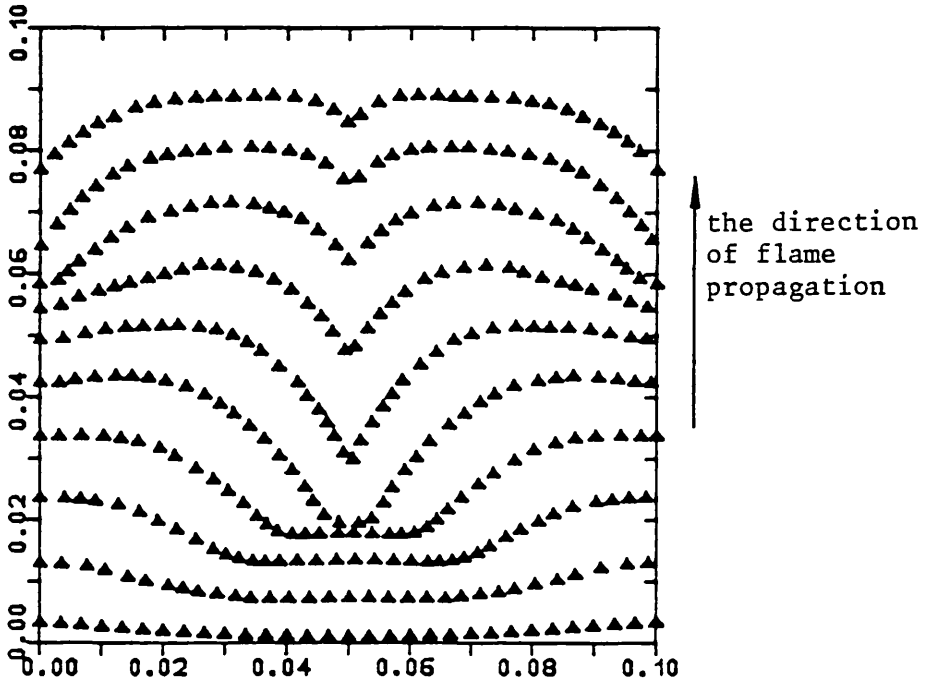



Figure 6-2 The flame-front location and shape at successive times, separated by 0.02 s intervals.

It can be seen that the instability continues to grow from a single sinusoidal perturbation; and the flame front grows from the initial shape to the one with sharp ridge pointing towards the burned gas and smooth curves towards the unburned gas. The wrinkled flame-front becomes flat as the flame approaches the top, under the effect of the confinement, as will be discussed in Section 6.5.

A good way to understand the development of instabilities is by viewing the combustion-induced flow ahead of the flame front, which is made visible by particles distributed on grid lines in the region of unburned gas

and computed to move with the fluid.

The computer-generated movement of the grid is shown, by this means, in Figure 6-3 (a-i).

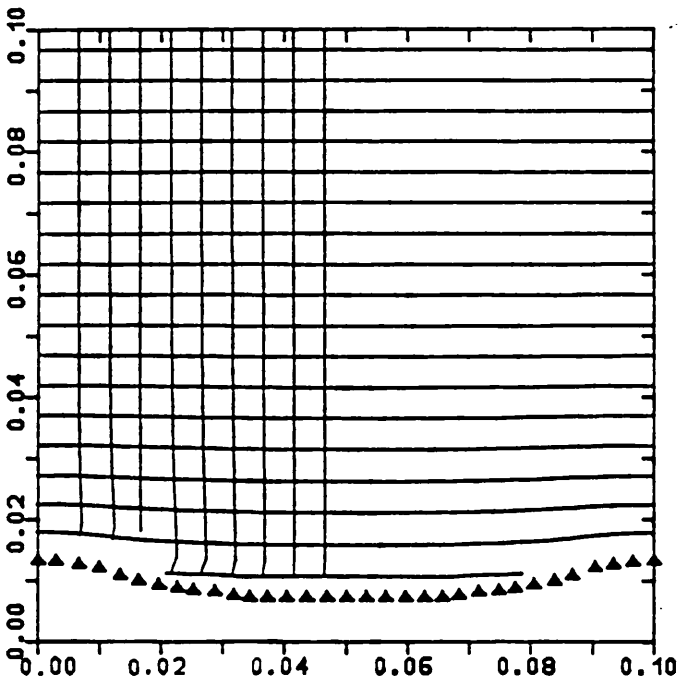



Figure 6-3 (a) Standard flame location at t = 0.02 s

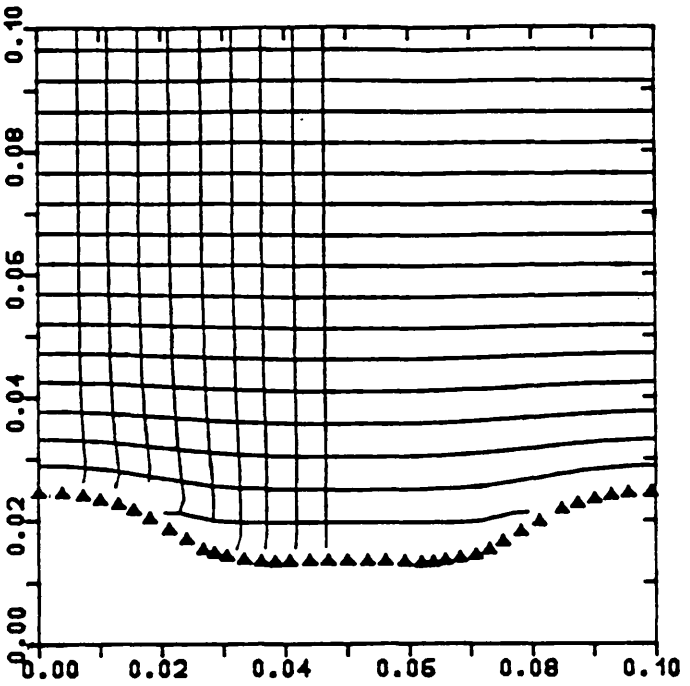



Figure 6-3 (b) Standard flame location at t = 0.04s.

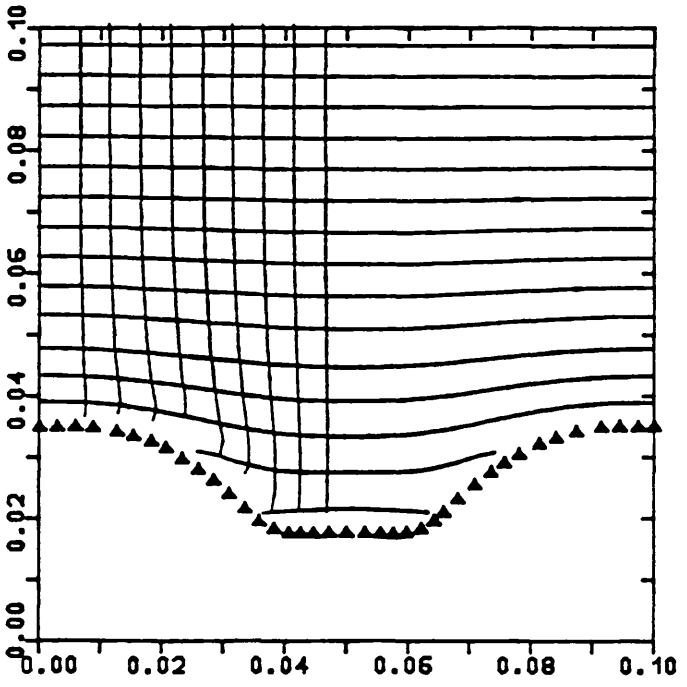



Figure 6-3 (c) Standard flame location at t = 0.06s.

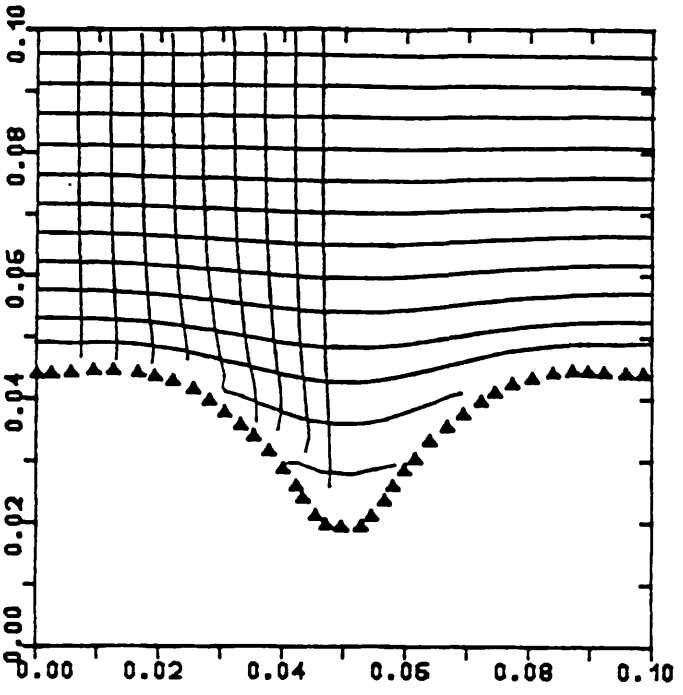



Figure 6-3 (d) Standard flame location at t = 0.08s.

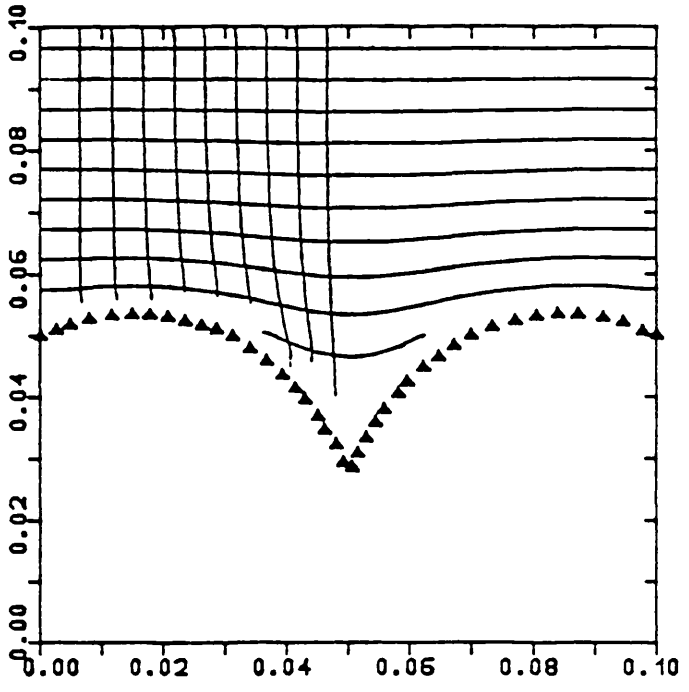



Figure 6-3 (e) Standard flame location at t = 0.10s.

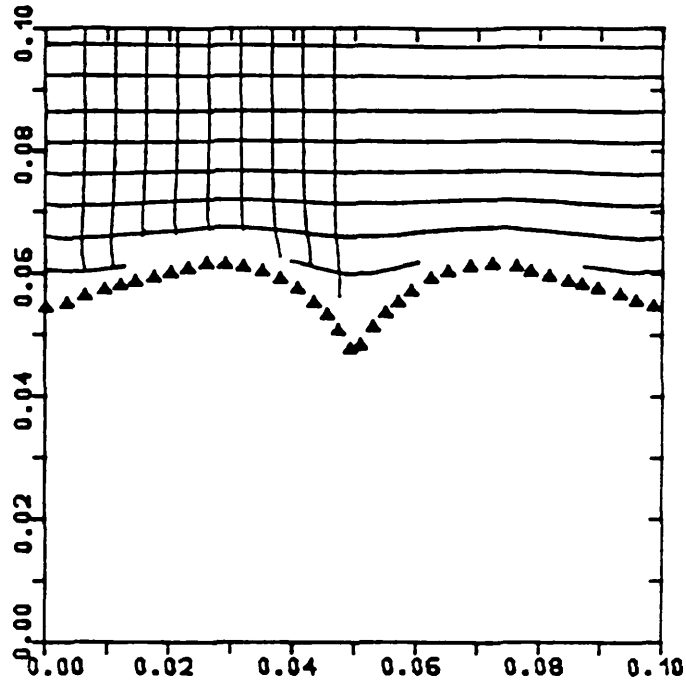



Figure 6-3 (f) Standard flame location at t = 0.12s.

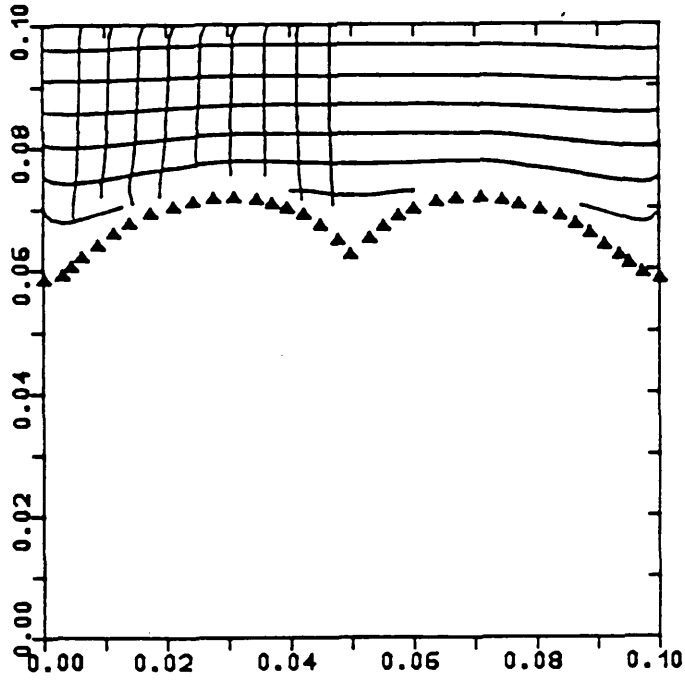



Figure 6-3 (g) Standard flame location at t = 0.14s.

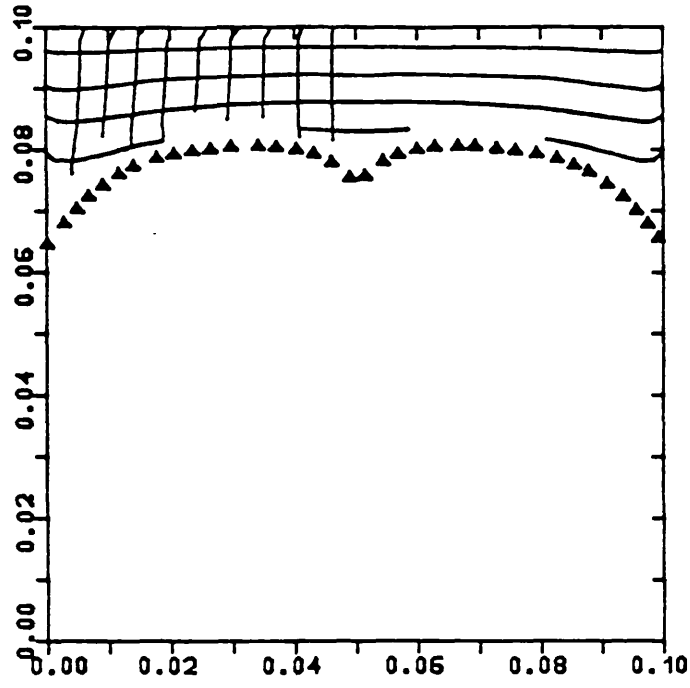



Figure 6-3 (h) Standard flame location at t = 0.16s.

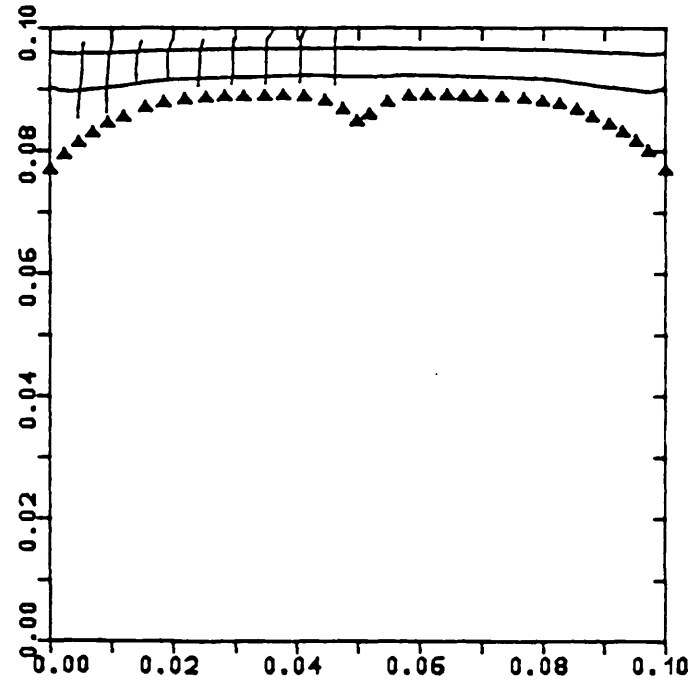



Figure 6-3 (i) Standard flame location at t =0.18s.

These figures show that the unburned gas ahead of the flame is pushed away from the side-walls into the region where the flame front is concave towards the burned gas, resulting in convection currents which lead to the formation of the wrinkled flame-front.

The Effect of the Gravitational Force

Figure 6-4 represents the effect of using a large body force ($g=100\ m/s^2$) on the flame pattern during its upward propagation.

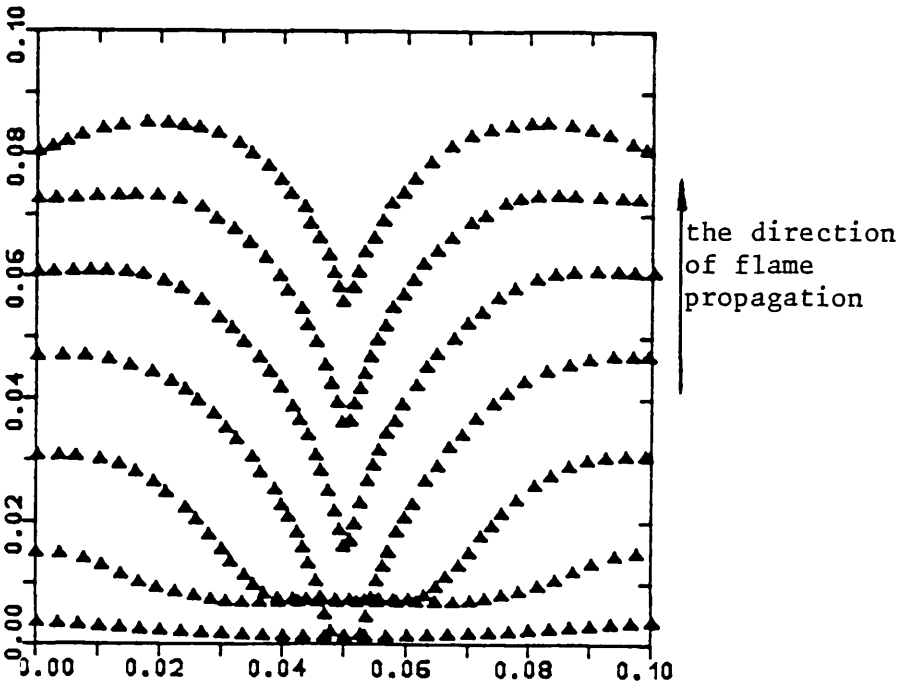



Figure 6-4 The flame-front location and shape at successive times, separated by 0.02s intervals, with a large body force. Conditions are : $\rho_b/\rho_u = 0.2$; Sb = 0.4 m/s; g = 100 $m/s^2$.

As is seen from the comparison between Figure 6-2 and Figure 6-4 that the instability under a large body force develops much faster than without it.

Figure 6-5 (a-f) show the movement of the particles in the region of the unburned gas as a consequence of the combustion.

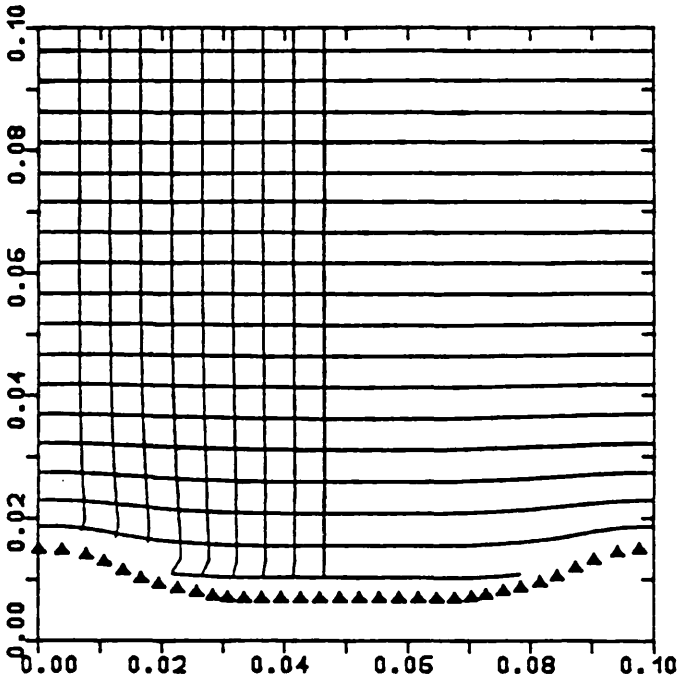



Figure 6-5 (a) The flame under a large body force (t= 0.02 s) (g=100 m/s$^2$)

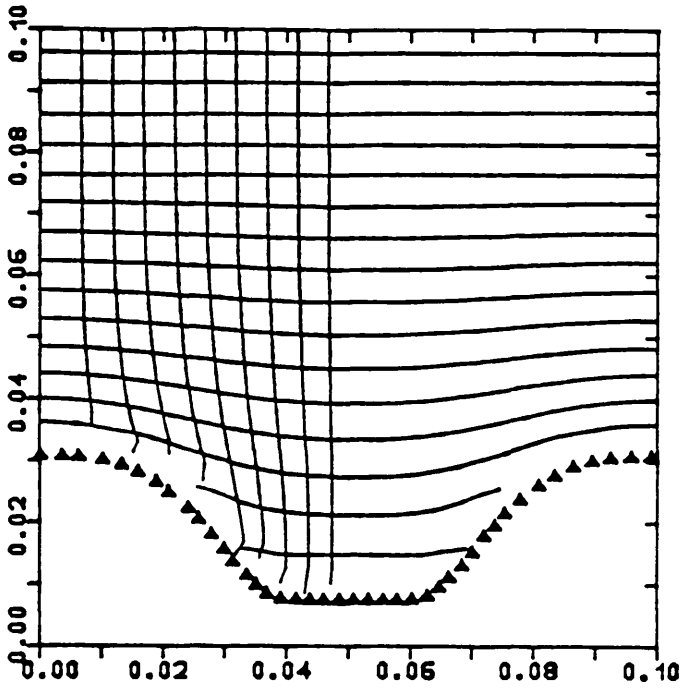



Figure 6-5 (b) The flame under a large body force ($g=100m/s^2$) at t=0.04s.

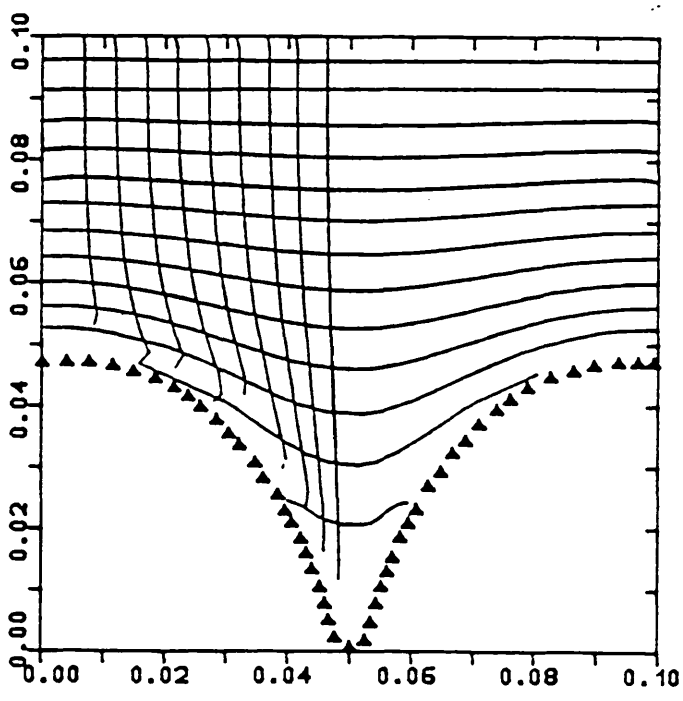



Figure 6-5 (c) The flame under alarge body force($g=100m/s^2$) at t=0.06s.

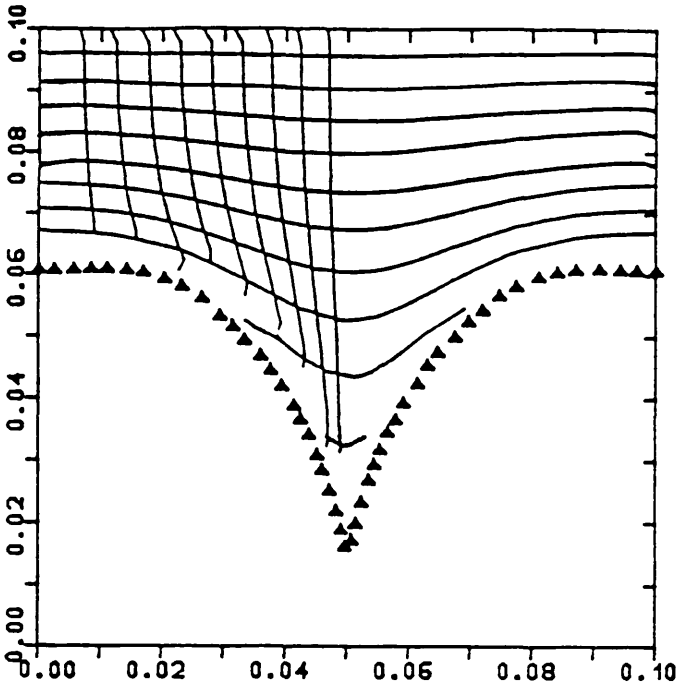



Figure 6-5(d) The flame under a large body force($g=100m/s^2$) at t=0.08s.

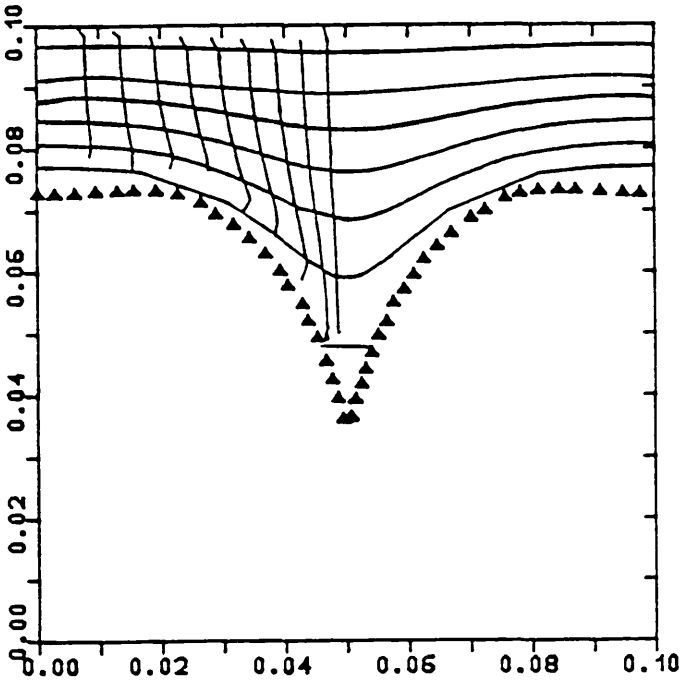



Figure 6-5(e) The flame under a large body force($g=100m/s^2$) at t=0.10s.

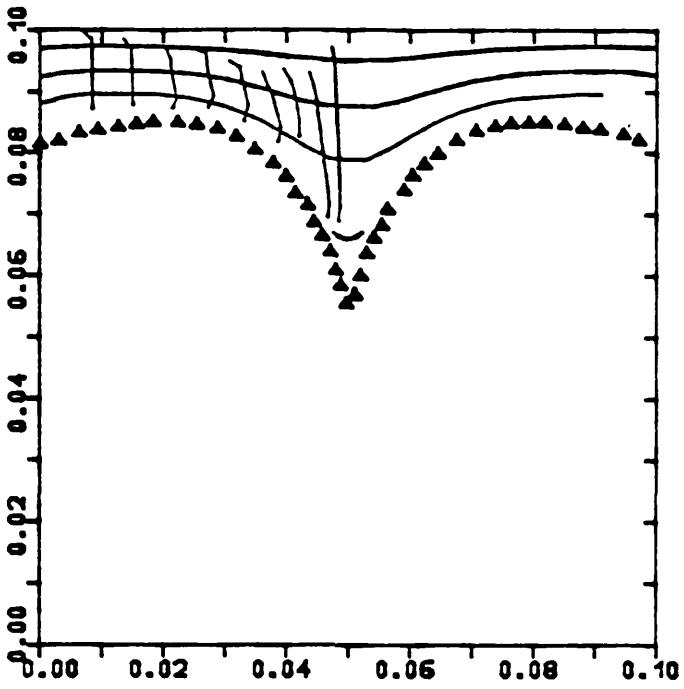



Figure 6-5 (f) The flame under a large body force (t= 0.12s) (g=100 $m/s^2$)

It can be seen from these figures that much stronger convection currents of the unburned gas appear ahead of the flame, because of the large buoyancy force; and a stronger indentation persists as the flame propagates upwards.

## The Effect of the Direction of Flame Propagation under a Large Body Force

Figure 6-6 shows the flame-front location and shape with g= -100 $m/s^2$, corresponding to downward flame propagation with a large buoyancy force.

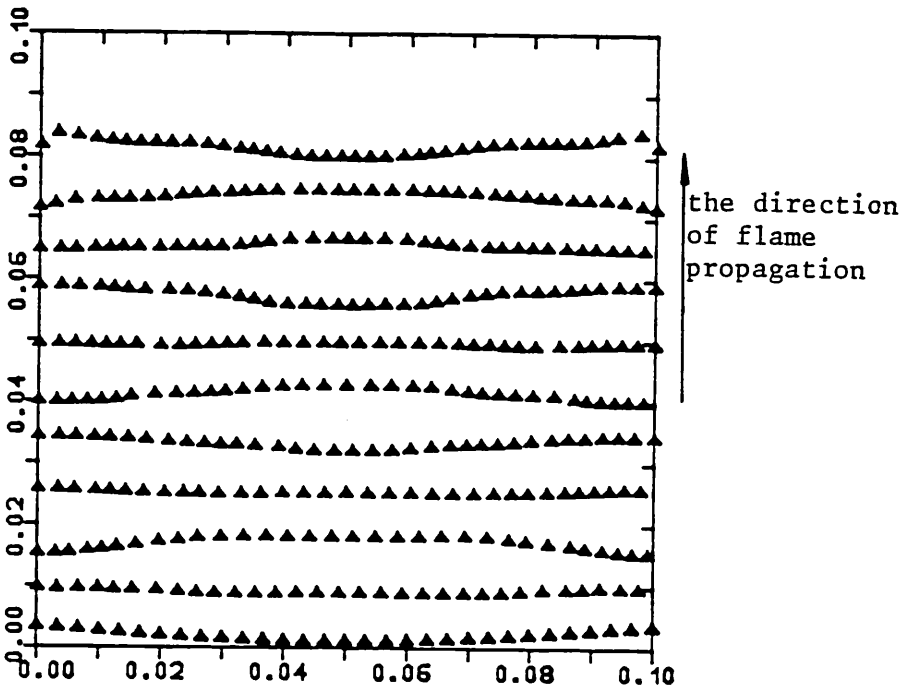



Figure 6-6 The flame-front location and shape with $g = -100\ m/s^2$ at successive times, separated by 0.02 s intervals. Conditions are : $\rho_b/\rho_u = 0.2$; $Sb = 0.4\ m/s$; $g = -100\ m/s^2$.

The figure indicates that the flow becomes oscillatory with the amplitude close to the initial one and a frequency equal to about $16.7\ s^{-1}$

If the gravitational force is further increased, the instability disappears eventually, which is shown in Figure 6-7.

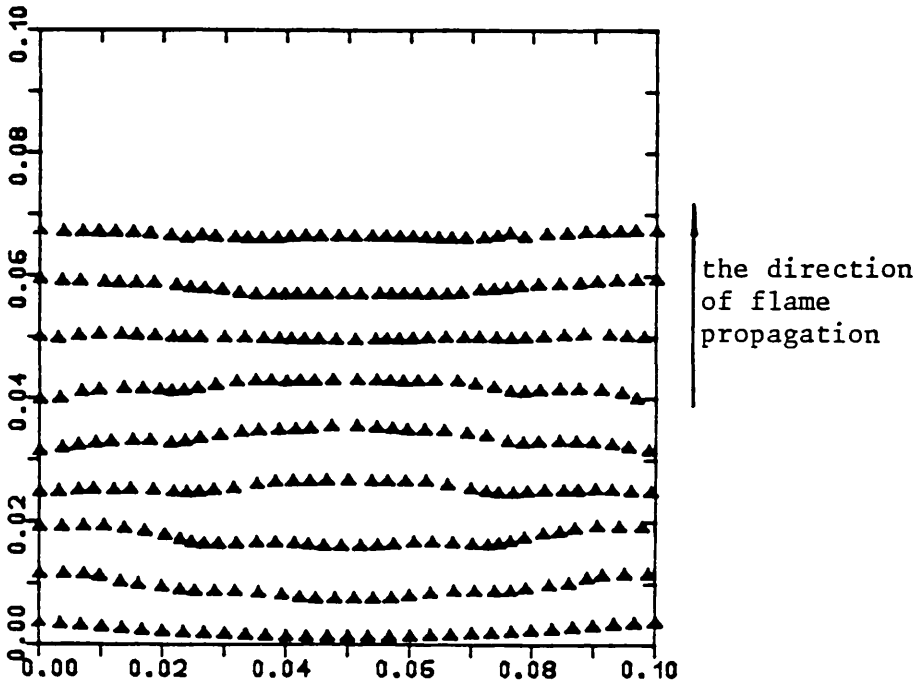



Figure 6-7 The flame-front location and shape with $g = -300\ m/s^2$ at successive times, separated by 0.02 s intervals. Conditions are : $\rho_b/\rho_u = 0.2$; $Sb = 0.4\ m/s$; $g = -300\ m/s^2$.

## The Effect of the Density Ratio, $\rho_b/\rho_u$

The characteristics of instabilities with different $\rho_b/\rho_u$ are given in Figures 6-8 to 6-10. All other conditions are kept the same in these figures.

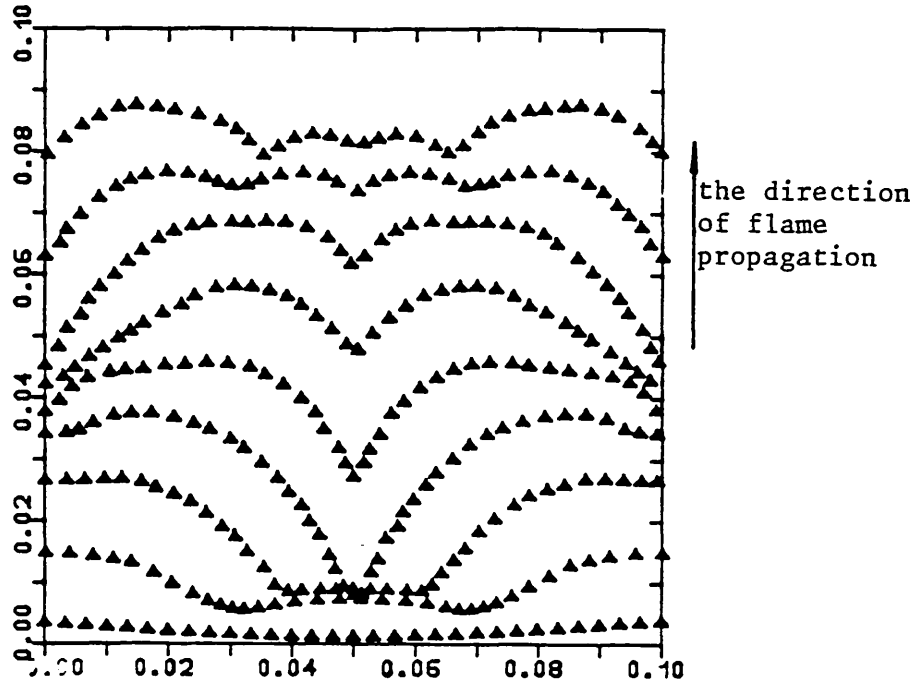



Figure 6-8 The flame location and shape with $\rho_b/\rho_u$=0.15 at successive times,separated by 0.02s intervals. Conditions are: $S_b$=0.4m/s; g=0.0m/s$^2$; $\rho_b/\rho_u$=0.15.

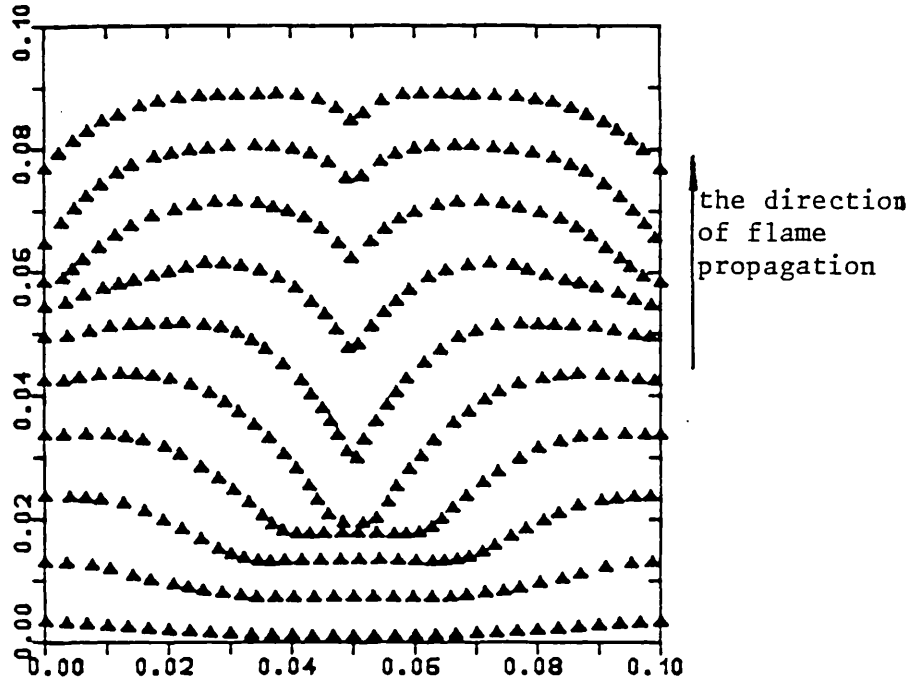



Figure 6-9 The flame-front location and shape with $\rho_b/\rho_u$=0.20.

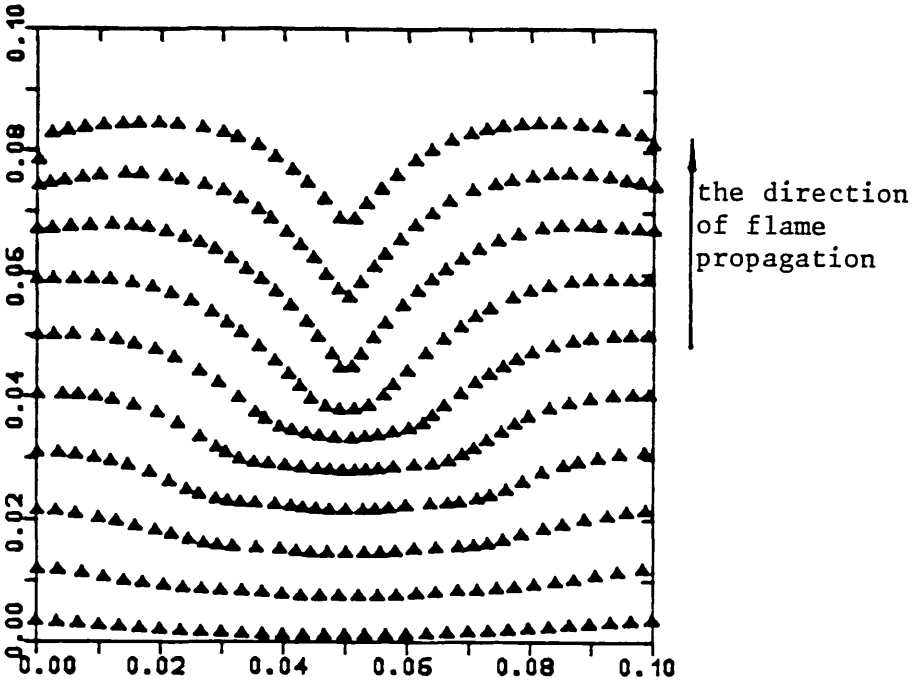



Figure 6-10 The flame location and shape with $\rho_b/\rho_u$ =0.3

It can be seen from these figures that the development of instabilities increases as the value of the density ratio, $\rho_b/\rho_u$, decreases.

The Effect of the Burning Velocity, Sb

The characteristics of instabilities with different burning velocities are shown in Figures 6-11 to 6-13. All other conditions are kept the same in these figures.

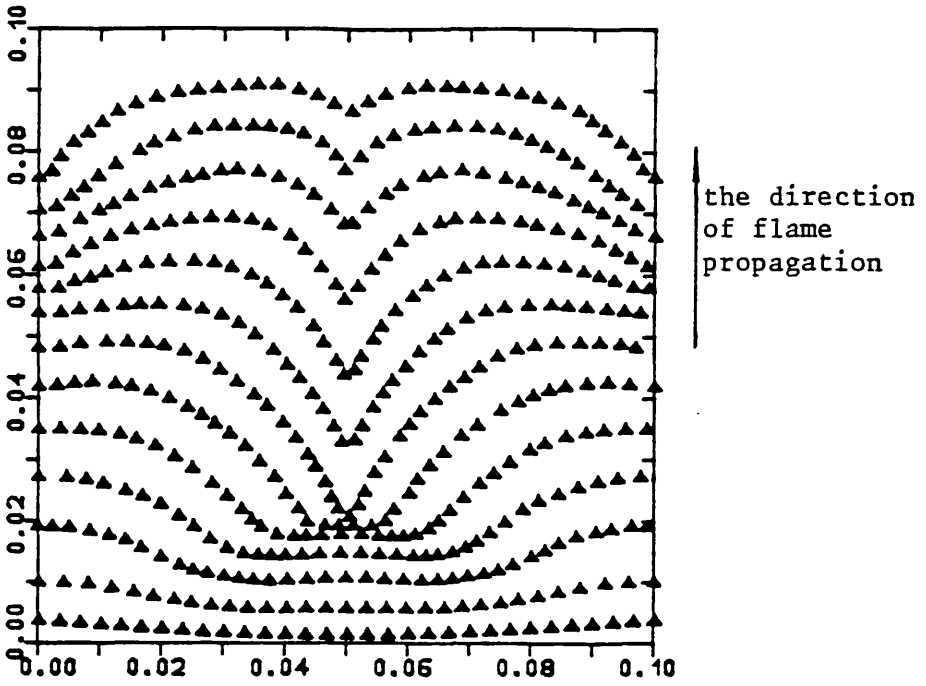



Figure 6-11 The flame-front location and shape at different times with the burning velocity, $S_b$=0.3m/s. Conditions are: $\rho_b/\rho_u$=0.20; $S_b$=0.3m/s; g=0.0m/s$^2$.

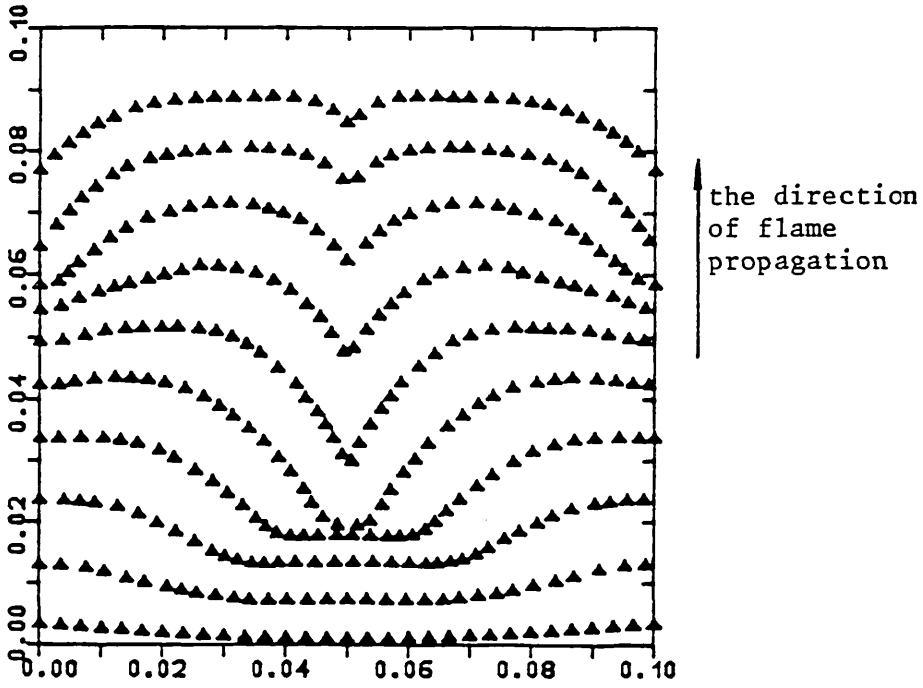



Figure 6-12 The flame-front location and shape with $S_b$=0.4m/s. Conditions are: $\rho_b/\rho_u$=0.20; $S_b$=0.4m/s; g=0.0m/s$^2$.

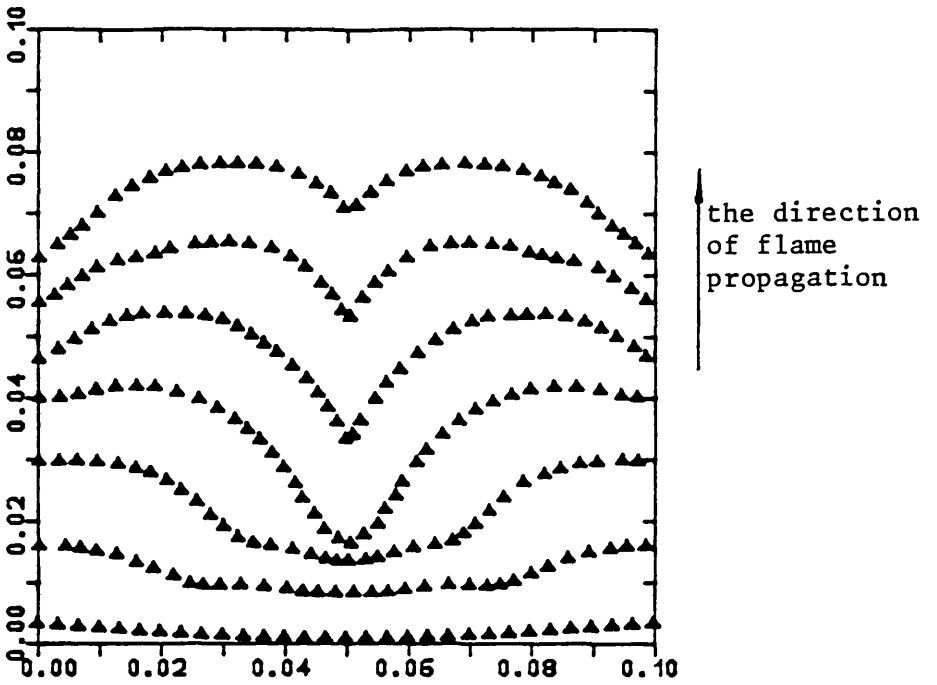



Figure 6-13 The flame-front location and shape at different times with the burning velocity, Sb = 0.5 m/s. Conditions are $\rho_b/\rho_u$ = 0.2, Sb = 0.5 m/s, g = 0.0 m/s$^2$.

As is seen from these figures, the development of instabilities increases as the burning velocity, Sb, increases.

## The Effect of the Wavelength of the Initial Perturbation

Figures 6-14 to 6-15 show the characteristics of instabilities with different wavelengthes of the initial perturbation.

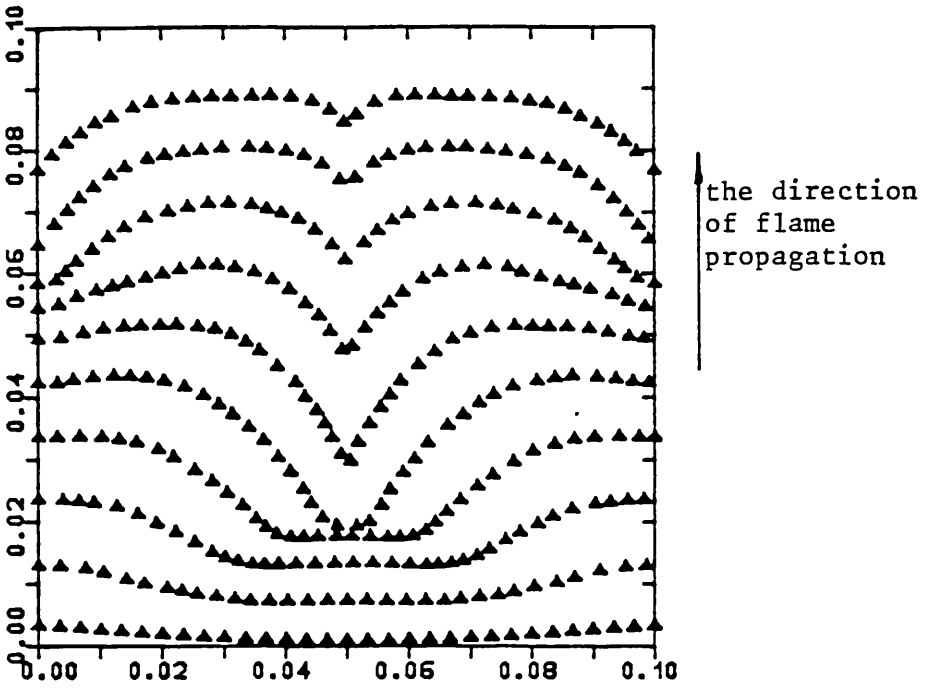



Figure 6-14 The flame-front location and shape with the wavelength of the initial perturbation equal to 2xwidth of the chamber.

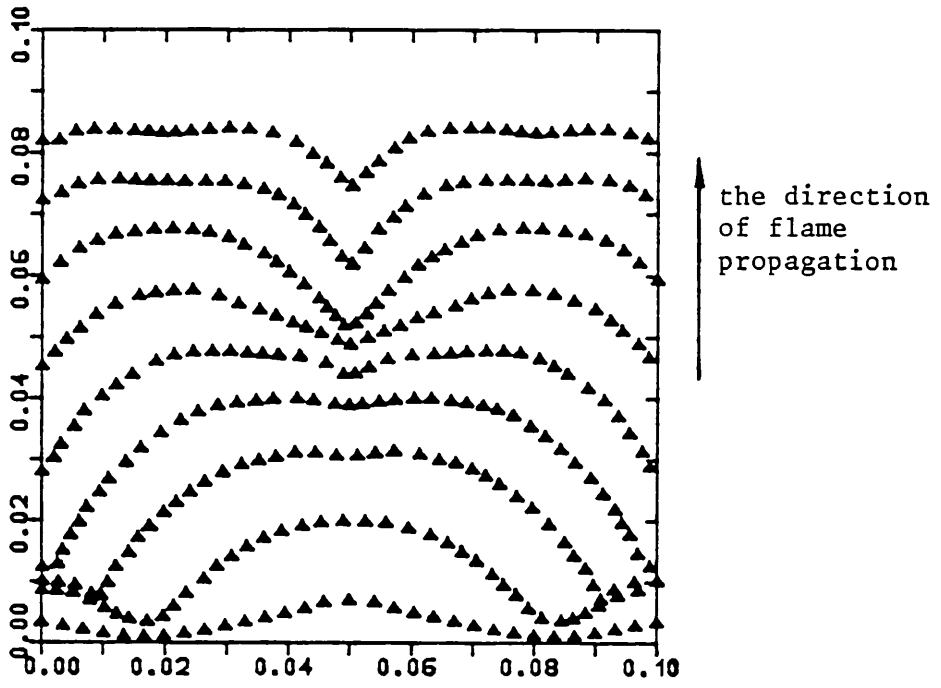



Figure 6-15 The flame-front location and shape with the wavelength of the initial perturbation equal to 0.667xwidth of the chamber.

Figures 6-14 & 6-15 show that the rate of the instability development increases as the wavelength of perturbation decreases.

## The Effects of Grid Number and Time-Step Size

The cases tested for effects of the grid number and time-step size are listed in Tables 6-1 & 6-2. For all cases the physical conditions are same as those of the "standard run".

Table 6-1 Cases Tested for the Effect of the Grid Number

| No. | NX | NY | $\Delta t$ (sec.) |
|---|---|---|---|
| 1 | 10 | 10 | 0.002 |
| 2 | 20 | 20 | 0.002 |
| 3 | 30 | 30 | 0.002 |
| 4 | 40 | 40 | 0.002 |

Table 6-2 Cases Tested for the Effect of the Time-Step Size

| No | NX | NY | Δt (sec.) |
|---|---|---|---|
| 1 | 20 | 20 | 0.005 |
| 2 | 20 | 20 | 0.002 |
| 3 | 20 | 20 | 0.0013 |
| 4 | 20 | 20 | 0.001 |

The results are given in Figure 6-16 & Figure 6-17.

Figure 6-16 shows the effect of the grid number on the results. The curves are the flame-front location and shape at the time equal to 0.1 sec. It can be seen from the figure that more details appear as the grid number increases.

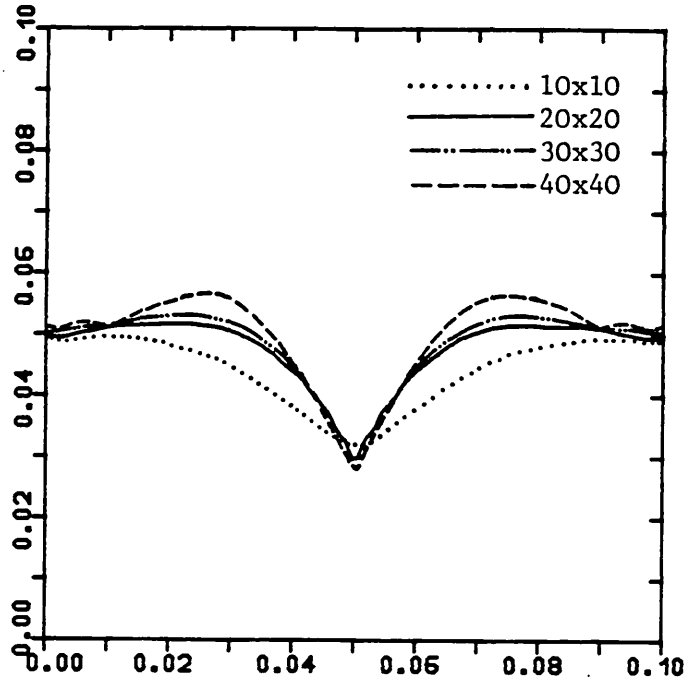



Figure 6-16 The effect of the grid number on the flame-fron location and shape at t = 0.1 sec.

Figure 6-17 shows the effect of the time-step size on the flame-front location and shape at t = 0.1 sec.

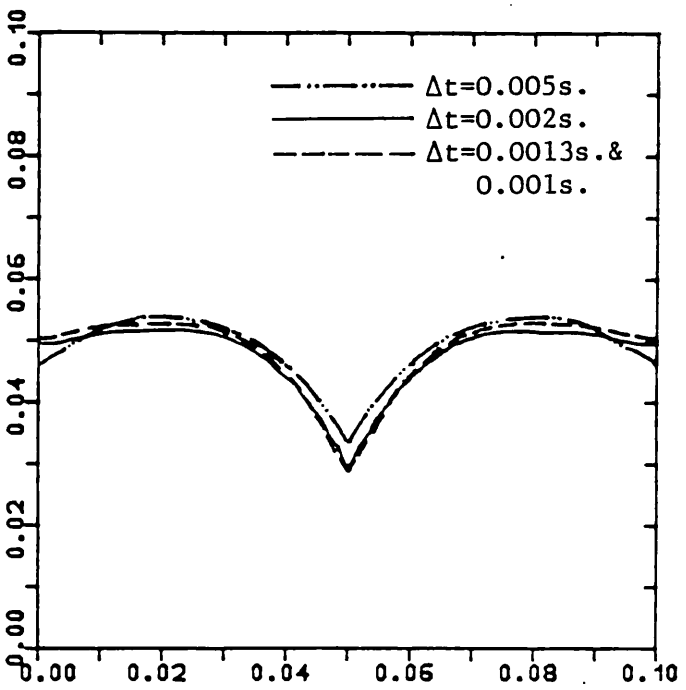



Figure 6-17 The effect of the time-step size on the results at t = 0.1 sec.

## 6.5 Convergence

The solutions above are converged. The non-normarized absolute volumetric error is of the order of 1.E-06 for all runs. No relaxation technique has been needed.

## 6.6 Computer Storage and Time

(i) Essential in-core space used is 21068 for grid number of 20x20.

(ii) For the "standard run", a 80 time-step run with 15

sweeps for each time-step takes approximately 4021 sec on a Perkin Elmer 3220 mini-computer.

## 6.7 Discussions

### The Formation of a Wrinkled Flame Front

Under conditions specified for the investigation, when the flame propagates from the open to the closed end of the chamber, if the idealized plane flame is not disturbed, it would remain flat throughout its propagation and ahead of the flame front the unburned gas would be at rest. When, as Figure 6-2 shows, the plane flame front is initially distorted with a concavity towards the burned gas, then the thermal expansion of burnt gas produces a thrust against the unburned gas in such a way that the unburned gas is pushed away from the region where the flame front is convex towards the unburned gas into the region where the flame front is concave towards the burned gas, which results in convection currents of the gas ahead of the flame. The converged flow pattern of the unburned gas in the concave region decreases the thrust of the burned gas against the unburned gas, causing instabilities to develop, as shown in Figure 6-3 (a-i). The damping effect which prevents the growth of perturbations in the present model is attributed to the "self-closing of a wave identation", as described by Lewis & Von Elbe (1964) and by Zeldovich et al (1985), and this self-closing nature is

due to the propagation of a wave from the side to the middle of a cavity, it can be visualized by means of Huygens' principle from geometric optics, as shown in Figure 6-18. The same effect has been achieved by the particle-tracking technique in the present calculations.

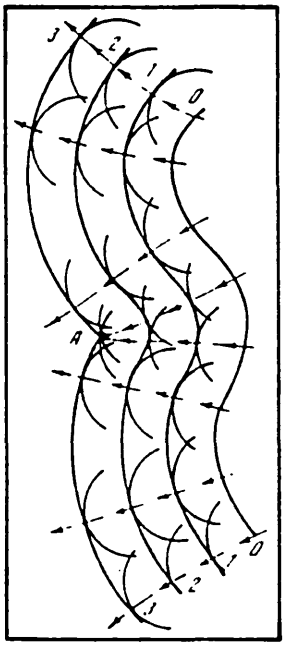


Figure 6-18 Successive locations of a curved flame front constructed with the aid of Huygens' principle. The dashed curves denote the trajectories of points in the flame front. ( Zeldovich et al )

The Effect of Confinement

As described above, the perturbation grows during the flame propagation upward as a result of the nonuniform motion of the gas caused by the thermal expansion of gas. As the flame approaches the top of the chamber, the

movement of the unburned gas is restricted becuase of confinement. The development of instability is diminished and the wrinkled flame front begins to change shape. The amplitude of the existing instability in the flame front thus decreases as Figures 6-2 & 6-8 show.

The Effect of the Gravitational Force

Figures 6-4, 6-6 and 6-7 show that gravitational forces have strong effect on the instability of a plane flame front. The effect is different depending on whether the flame propagates upwards or downwards. When a flame propagates upwards the heavier unburned gas lies above the lighter burned gas. Because of the Rayleigh-Taylor instability, the interface between the unburned gas and the burned gas is unstable even if no material flows through it. We may thus expect that the instability develop faster in a upward-moving flame with gravity than without it, as shown in Figure 6-4. On the other hand, when the flame propagates downwards, the gravitational force keeps the heavy gas from rising or the light gas from sinking, therefore, to resist the growth of the initial perturbation. If the force of gravity is sufficiently large, the initial perturbation will die out and the flame front eventually returns to smooth shape as Figure 6-7 shows.

The Effect of the Density Ratio and the Burning Velocity

The flow velocity induced by combustion is determined by the burning velocity and the degree of the thermal expansion of gas, as described by Equation (4.14).

Figures 6-8 to 6-10 show that the growth rate of the perturbation increases as the density ratio, $\rho_b/\rho_u$ , becomes smaller.Figures 6-11 to 6-13 indicate that the growth rate of the perturbation increases as the burning velocity, Sb, increases. These tendencies have been supported by the author's experiment indirectly through the investigation of effects of the mixture ratio (Figure 2-7 (a) & Figure 2-8)

The Effect of the Wavelength of Initial Perturbation

A comparison between Figure 6-14 and Figure 6-15 suggests that the perturbation with a smaller wavelength develops faster than with larger wavelength.

Restriction

In the present model, the flame front is treated as a hydrodynamic discontinuity in density with a constant burning velocity. It is valid when the wavelength of the perturbations much greater than the diffusive-thermal

width of the flame front. When the wavelength of perturbations becomes comparable with the diffusive-thermal width of a flame front, the change in its structure under the influence of gas dynamic perturbations and the resulting change in the burning velocity have to be taken into account, which is not under present consideration.

## 6.8 Closure

In this chapter, the ability of the prediction procedure in handling the wrinkled laminar flame has been demonstrated. This is accomplished by presenting the valuable information on the hydrodynamic flame-wrinkling, as summarized below :

The detailed calculations of formation of the wrinkled flame-front presented in Section 6.4 clearly confirm that the wrinkling is caused by the combustion-induced flow.

The effect of the gravitational force on the flame behaviour is that of the Rayleigh-Taylor instability.

The rate of the growth of instabilities is found to increase as the burning velocity or the density difference between the unburned gas and the burned gas increases respectively, or as the wavelength of the perturbations decreases.

The results from the present investigation provide further insight into the hydrodynamic instability of flames. Since the present model is based on the adopted assumptions and results are based on the adopted numerical precision, the explanation on the phenomena should be restricted to these conditions.

With this chapter, the investigations of wrinkled laminar flames by using the single-fluid approach employed in this study have been completed. As mentioned in Section 1.3.1, this approach may not apply to the unsteady flame propagation in turbulent flows, for which a novel approach, i.e. the two-fluid model of turbulent combustion, is needed. An application of the two-fluid model to turbulent unsteady flames will be presented in the next part of the thesis, where the temporal instabilities of stabilized flames in ducts are to be investigated.

# PART 2

# UNSTEADY TURBULENT FLAME PROPAGATION

# CHAPTER 7-THE APPLICATION OF TWO-FLUID MODEL OF TURBULENT COMBUSTION TO AN IDEALIZED, ONE-DIMENSIONAL, UNSTEADY,CONFINED,PREMIXED FLAME (I) - INVESTIGATION ON A SUDDEN INCREASE IN THE RESISTANCE TO THE FLOW AT THE DUCT EXIT

## 7.1 Introduction

Flame stabilized by baffles in ducts may be present in the exhaust ducts of aircraft jet engines which require extra thrust for short periods. The baffle-duct arrangement is then called an "after-burner" or "reheat" system.

Although the flow in such systems is intended to be steady, experience has shown that oscillations may easily occur, which is one of the most serious problems in the development of ramjets, after-burners and rockets.

The onset and characteristics of these oscillations have been investigated experimentally by a number of workers (see the next section); however, the nature of the process remains obscure. Theoretically, the difficulty lies in the description of interactions between turbulence, combustion and oscillations. Until fairly recently, the calculation of combustion-driven oscillations is still believed to be beyond the abilities of the existing turbulent combustion models (Jones & Whitelaw 1984). Therefore, it is desirable to develop a novel turbulence

model which may describe the turbulent combustion process more realistically and is capable of tackling some complex phenomena of turbulent combustion such as combustion oscillations. A general theory of the two-fluid model of turbulence has been proposed by Spalding (1982b) to meet the need.

The work presented in this part of the thesis describes the application of the two-fluid model of turbulent combustion to one-dimensional, unsteady, confined, premixed flames with idealized sets of initial and boundary conditions, so chosen as to identify significant factors responsible for combustion oscillations, and to establish the instability conditions under which combustion oscillations may occur, thereby, to explain the phenomena, particularly, the low-frequency, "buzz" phenomenon.

Two types of boundary conditions to initiate disturbances are explored. The first type is a sudden increase in the resistance to the flow at the duct exit, and the second type is an oscillatory mass inflow rate at the duct inlet. This chapter deals with the investigation of the first type of boundary condition; and the second one follows in Chapter 8.

The listings of the PHOENICS code related to the present

problem are given in Appendix C.

## 7.2 Experimental Evidence

The "buzz"-phenomenon has been observed in a number of experimental investigations (Stewart & Nesbitt 1953, Keller et al 1981, Campbell et al 1983, Heitor et al 1984). Among these investigations, the most extensive study is that of Campbell et al (1983), who have investigated the "buzz"-phenomenon in a propane-air premixed flame stabilized on a V-gutter located in a rectangular duct. They have observed that the "buzz"-type oscillation with the frequency of 60 HZ is initiated only when there is a minimum length of hot duct present (the section of duct from the stabilizer to duct exit). High-speed schlieren photographs have shown the violent cyclic pulsation of the flame during these oscillations; and simultaneous pressure and velocity measurements have been made showing their periodic variation accompanying the flame motion. Increasing the hot length of the duct is found to increase the amplitude of the pressure oscillation while having little effect on the frequency. Flow changes in the experiment show that raising the inlet flow velocity increases the frequency of oscillation, but decreases the amplitude.

The existing of a minimum length of hot duct for the onset of "buzz" is also observed by Heitor et al (1984), who has

found the oscillation with a predominant frequency of 100 HZ in a methane-air premixed flame stabilized on baffles located on the axis of a pipe.

In addition, the sensitivity of a flame anchored in a duct to an imposed disturbance with a resonant frequency of the burner resulting in a high-amplitude oscillation has been observed by Shonerd (1952) and Blackshear (1956).

## 7.3 The Concept of the Two-Fluid Model

As reviewed above, the experimental results have shown some characteristics of the "buzz" phenomenon. Now we shall turn our attention to the computer simulation to see how the two-fluid model can simulate and explain these experimental findings. Before doing so, it is advantageous to briefly outline the concept of the two-fluid model of turbulent combustion and its mathematical formulation, as introduced by Spalding (1982b,1985).

It has long been recognised that turbulent flame, like turbulent flows without combustion for that matter, are "spotty", i.e. fragments of the hot burned gas and the cold unburned gas intermingle within a flame in the manner of a lake system on land, as shown in Figure 7-1.

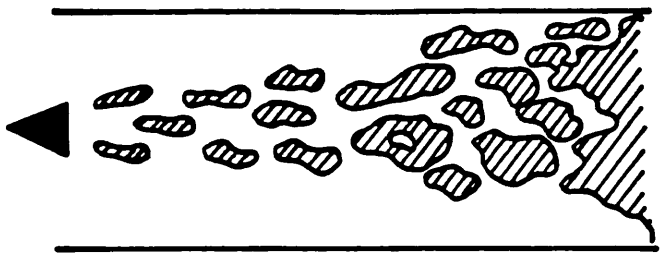


Figure 7-1 A turbulent flame is "spotty".

One of the major effects of the "spottedness" on the turbulent mixing can be described as a "sifting" process by the two-fluid model as follows. When a premixed combustible gas burns intermittantly within a duct due to "spottedness", the uneven density change as the result of exothermic reaction causes an uneven pressure distribution in the duct. This newly created pressure gradient drives the lighter burned gas to accelerate more than the heavier unburned gas, thus "sifting" it towards the duct outlet, where however the average temperature is the highest. Experimental investigations (Shepherd, Moss & Bray 1982) have revealed that the fragments may have significantly different velocities, i.e. "slip" exists between the two fluids.

Relative motion between intermingled fluids can also result from random movements of fluid fragments, the net magnitude of which are usually proportional to the

gradient of their concentration distribution.

These two phenomena, termed by Spalding (1984a) as "pressure-gradient diffusion" and "concentration-gradient diffusion" respectively, are governinig the turbulent mixing process.

The "concentration-gradient diffusion" has been embodied in conventional turbulence models, however, the "pressure-gradient diffusion" has been hitherto neglected in them. The dominant feature in the ducted combustion is that there exists a pressure gradient encountering a large density difference. The combustion processes there, therefore, largely depend on the "pressure-gradient diffusion" mechanism.

The two-fluid model of turbulent combustion idealized the "spottedness" phenomena; it allows for the co-existence of two-kinds of fluid which can occupy (in turn) any location; and the most interesting phenomena take place at the interface between the two fluids. Fluid fragments can be distinguished by reference to properties for each fluid, such as velocities, temperatures, and etc.

The concept described above has been realized by Spalding (1982b, 1984a, 1985), who has made use of the mathematical apparatus developed primarily for the analysis of two-phase flows, as briefly described below.

## 7.4 Mathematical Formulation of the Two-Fluid Model

### (a) Definitions

It is supposed that two fluids, 1 & 2, share occupancy of space. The proportions of time during which each fluid can be expected to occupy a particular location are the volume fractions, $r_1$ and $r_2$, which obey the relation:

$$r_1 + r_2 = 1 \qquad (7.1)$$

How the two fluids are distinquished from one another is arbitrary. In the present study, only premixed flames are considered; therefore, the two fluids are defined as "colder" (Fluid 1) and "hotter" (Fluid 2).

At any location and time, all gas fragments belonging to Fluid 1 are supposed to have the same values of temperature, velocity components and fragment size. All the above fluid properties will be represented by the symbol $\phi_i$, where i takes the value 1 or 2 according to the fluid. It will be supposed that both fluids have the same pressure at each point.

### (b) Differential Equations

#### Mass Balance

There are two mass-conservation laws to express. They can both be written in the form :

$$\frac{\partial}{\partial t}(\rho_i r_i) + \mathrm{div}(\rho_i r_i \vec{U}_i) = \dot{m}_i \quad ; \qquad (7.2)$$

where, t stands for time,

$\rho_i$ stands for the density of Fluid i,

$\vec{U}i$ stands for its velocity vector, and

$\dot{m}_i$ stands for the rate of transfer of mass into Fluid i from the other fluid, with which it is intermingled.

In Equation (7.2), instantaneous values of $\rho$ , r, $\vec{U}$ and $\dot{m}$ are in question. In numerical calculations, to compute the most rapid fluctuations of these quantities, time-average quantities are prefereable, in which case the quantity operated upon by div must be augmented by $\vec{D}i$, an effective diffusion flux. The equation then becomes :

$$\frac{\partial}{\partial t}(\rho_i r_i) + \mathrm{div}(\rho_i r_i \vec{U}_i + \vec{D}_i) = \dot{m}_i \quad , \qquad (7.3)$$

from which, however, overbars signifying time-averaging have been omitted so as to avoid needless clutter.

The $\partial/\partial t$ term represents the difference of outflow from inflow along the time dimension; div represents that difference along the space dimension; and $\dot{m}_i$ can be regarded as the negative of the difference between outflow

and inflow along an "interfluid dimension". If all these fluxes are denoted by $\vec{G}i$, and DIV is defined as a generalisation of div which makes reference to all their dimensions, Equation (7.3) can be finally expressed as:

$$DIV\ (\vec{G}_i) = 0 \qquad (7.4)$$

Balance of Other Quantities

The above nomenclature facilitates the compact writting of the differential equation governing the distribution of the fluid property $\phi_i$. The equation becomes:

$$DIV\ (\phi_i \vec{G}_i) = S_{\phi i} \quad , \qquad (7.5)$$

wherein $S_{\phi i}$ is the volumetric source of the entity $\phi$ in Fluid i, and $\phi_i$ is the value of $\phi$ associated with the flux which it multiplies.

In the momentum equations , for example, $\phi_i$ stands for a velocity component, and the volumetric-source quantity $S_{\phi i}$ consists primarily of pressure-gradient, body-force, interfluid-friction and wall friction terms. Thus, for the velocity $u_i$, the equation becomes:

$$DIV(u_i \vec{G}_i) = -(\frac{\partial p}{\partial x} + b_x \rho_i) r_i + f_{12}(u_2 - u_1) - f_{iw} u_i \ ; \qquad (7.6)$$

where, x is the distance coordinate aligned with $u_i$ ,

P is the pressure,

$b_x$ is the body-force component in the x-direction,

$f_{12}$ is the volumetric interfluid-friction coefficient,

$u_i$ is the velocity component in the x-direction,

$f_{iw}$ is the volumetric coefficient of friction between Fluid i and a nearby wall.

The particular formulation of the above general equations used to describe the specific problem considered in this study will be given following the physical description of the problem in the next section.

(c) Modeling Formulation

In order that the equation system above should be closed, mathematical expression must be devised for such inter-fluid transport quantities as $\dot{m}_i$ and $f_{12}$ . Since these questions have been discussed in detail by Spalding (1982b,1983a,1983b) elsewhere, only their expressions to be used in this study are quoted here.

Interfluid Friction Factor

The formulation used for $f_{12}$ which appears in Equation (7.6) is :

$$f_{12} = Kf\ r_1 r_2 \rho^* |u_1 - u_2| / l, \qquad (7.7)$$

where , Kf is a dimensionless constant,

$\rho^*$ is the density of the the lighter of the two fluids,

$|u_1 - u_2|$ is the local relative speed of the two-fluids,

l, the fragment size, is expressed for this study, as:

$$l = Y \quad , \qquad (7.8)$$

Y is the half duct width, the value is 0.05m in the present calculation.

Interfluid Mass Transfer Rate

The interfluid mass-transfer process is presumed to proceed only in one direction, namely from colder (Fluid 1) to hotter (Fluid 2). The formulation used here is as follows :

$$\dot{m}_i = Km\ r_1 r_2 \rho^* |\ u_1 - u_2\ | / l, \qquad (7.9)$$

where , Km is a dimensionless constant and Km/Kf is always greater than unity. Kf/l and Km/l, having a dimension of the reciprocal of length, are later designated as parameters, defined as Cf and Cm

respectively.

(d) Solution Procedure

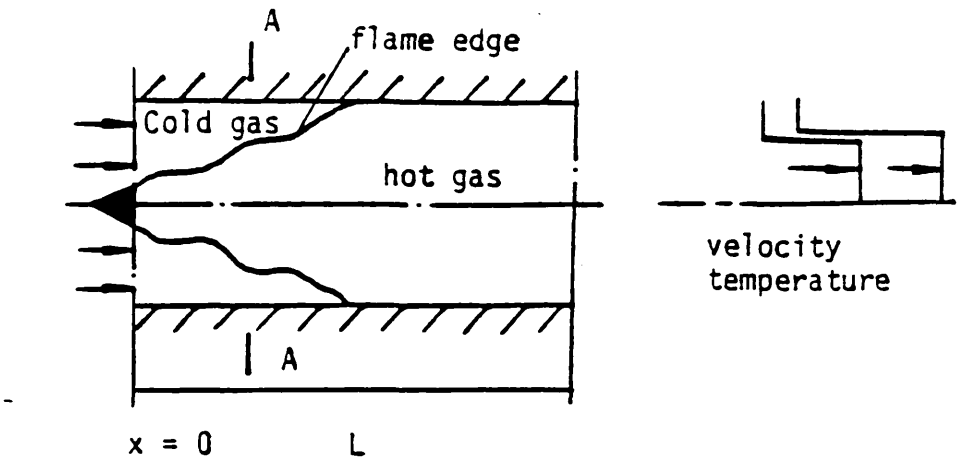
The solutions which are to be presented of the above system of equations have been obtained by straightforward application of the PHOENICS computer code (Spalding 1982a). The main features of what is embodied in PHOENICS have already been recited in Chapter 4.

A full account of the computational details using the 81 code of PHOENICS has been reported (Wu 1984c). The listings of the corresponding settings in the 84 code of PHOENICS related to the present problem are given in Appendix C.

## 7.5 Description of the Problem

### 7.5.1 Physical Process

The flame concerned here is imagined to spread from the wake of a flame holder mounted in a stream of premixed combustible gas, flowing at high speed through a duct of constant width formed by two plane parallel walls of large extent, as shown in Figure 7-2.




**(a) The model considered** **(b) Profiles at A-A**

Figure 7-2 A baffle stabilized flame in a duct

In this study, there are two fluids of interest, i.e.the cold, premixed unburned gas defined as Fluid 1 and the hot, completely burned gas defined as Fluid 2.

The transient process being investigated starts from the already established steady-state flame obtainable by setting a large time-step for the solution of transient equations. While the flame is burning steadily, a sudden increase in the resistance to the flow at the duct exit is introduced by raising the pressure there. The resultant response of the flow to the disturbance is in question.

### 7.5.2 Mathematical Details

(a) Assumptions

(i) The system is one-dimensional.

(ii) Friction at and heat transfer to the duct wall are neglected.

(iii) Viscosity effects are negligible.

(iv) The flow is considered compressible and the process isentropic.

(v) The interfluid heat transfer and diffusive transfer of chemical species have been neglected.

(vi) The cold gas, when entrained by the hot gas, burns instantly.

(b) Differential Equations

With above assumptions, Equations (7.3) and (7.6) given in Section 7.4 take following forms :

For Cold Gas

Continuity : $$\frac{\partial(r_1\rho_1)}{\partial t} + \frac{\partial(r_1\rho_1 u_1)}{\partial x} = -\dot{m} \quad , \qquad (7.10)$$

Momentum : $$\frac{\partial(r_1\rho_1 u_1)}{\partial t} + \frac{\partial(r_1\rho_1 u_1 u_1)}{\partial x} = -r_1\frac{\partial p}{\partial x}$$

$$+f_{12}(u_2-u_1)-\dot{m}\,|u_1-u_2| \quad , \qquad (7.11)$$

For Hot Gas

Continuity : $$\frac{\partial(r_2\rho_2)}{\partial t} + \frac{\partial(r_2\rho_2 u_2)}{\partial x} = \dot{m} \quad , \qquad (7.12)$$

Momentum : $$\frac{\partial(r_2\rho_2 u_2)}{\partial t} + \frac{\partial(r_2\rho_2 u_2 u_2)}{\partial x} = -r_2\frac{\partial p}{\partial x}$$

$$-f_{12}(u_2-u_1)+\dot{m}\,|u_1-u_2| \quad ; \qquad (7.13)$$

where : subscripts 1 & 2 represent the cold and hot gas respectively,

t stands for time,

x stands for distance coordinate,

$r_1$& $r_2$are the volume fractions for the cold gas and hot gas respectively;

$\rho_1$and $\rho_2$ are the densities,

$u_1$ and $u_2$ are the velocity components in the x-direction,

P is the pressure, which both fluids are subject to,

$f_{12}$ and $\dot{m}$ are the interfluid friction factor and the interfluid mass transfer rate respectively, and their formulations have already been given in Equations (7.7) and (7.9) respectively.

(c) Dimensionless Parameters

In order to make the numerical investigation systematic and to ensure that results have the widest possible significance, it is desirable to examine Equations (7.10) to (7.13) on the principle of similarity.

Parameters Characterising the Physical Process

According to the dimensional analysis (Schlichting 1960), dimensionless parameters on which the solution of Equations (7.10) to (7.13) depend are :

$$Ma, \quad LCm, \quad Cm/Cf \quad \text{and} \quad \rho_2/\rho_1$$

where , $Ma(= u_o/c_o)$ is the Mach number at inlet;

L is the duct length;

Cm(= Km/l) is a dimensional coefficient in the interfluid mass transfer term;

Cf(= Kf/l) is a dimensional coefficient in the interfluid friction term;

$\rho_2/\rho_1$ is the density ratio.

Numerical Parameters

Since the solution of these equations is to be obtained numerically, two additional parameters must be included; they are :

the number of grid cells, NX and

the magnitude of time step, $\delta t^* u_o/L$ .

Consequently, any performence variable for the process, $\phi$ , can be written as a function of following dimensionless parameters :

$$\phi = \phi \ ( \ Ma, \ LCm, \ Cm/Cf, \rho_2/\rho_1, \ NX, \ \delta t^* u_o/L \ ).$$

It will be seen in Section 7.6 that $\phi$ has been chosen as a dimensionless pressure, $(P-P_L)/(P_H-P_L)$, where $P_H$ & $P_L$ are the extreme values at high back-pressure and low back-pressure respectively. All values of the pressure are the local pressures taken at mid-duct section.

(d) Boundary Conditions

At the inlet, it is assumed that two percent of the constant mass inflow is supplied as hot gas to ensure flame holding.

$$x = 0 , \qquad m_1 = 0.9 \ u_1 \rho_1 , \qquad (7.14a)$$

$$m_2 = 0.1 \ u_2 \rho_2 , \qquad (7.14b)$$

$$u_1 = u_2 = u_o \quad ; \qquad (7.14c)$$

where $u_o$ is the approach flow velocity.

At the outlet, the back pressure is suddenly changed after a large first time-step ( t= 100 sec). Hence,

$$x = L \ , \quad 0 < t < 100 \text{ sec} \ , \quad P = 0 \ ;$$
$$t > 100 \text{ sec} \ , \quad P = 1.E3 \ N/m^2 .$$

All pressure are measured as excesses above 1.E5 $N/m^2$.

(e) Initial Conditions

The profiles in the steady-state flame established after the first large time-step as initial conditions for the process to start will be presented in Section 7.6.1.

The following initial values throughout the flow domain are used for the first time-step, i.e.,

at $t = 0$ ,
$u_1 = 20.m/s$ ,
$u_2 = 30.m/s$ ,
$r_1 = 0.2$ ,
$r_2 = 0.8$ ,
$\rho_1 = 1.0 \ kg/m^3$ ,
$\rho_2 = 0.2 \ kg/m^3$ ,
$P = 500.N/m^2$.

(f) Density Evaluation

The densities for both fluids are evaluated from the isentropic relation :

$$\rho_i = \rho_{i,o}\left(\frac{P}{P_o}\right)^{1/\gamma} \qquad (7.15)$$

where : P is the local pressure,

Po is the atmospheric pressure,

$\gamma$ is the ratio of specific heat at constant pressure to that at constant volume. It is 1.4 for a perfect gas which both fluids are assumed to be,

$\rho_{i,o}$ is the density of Fluid i(1 or 2) at the atmospheric pressure.

## 7.6 Presentation of Results

This section presents the results under headings : the steady-state flame, the "stable" oscillation case, parametric study, the effect of numerical parameters.

### 7.6.1 The Steady-State Flame

Firstly, the characteristics of the steady-state flame as specified by the distributions of its properties, which serve as the initial conditions at which the transient process starts, are given in Figures 7-3 to 7-6 below.

Figure 7-3 shows the pressure distribution of the steady-state flame along the duct.

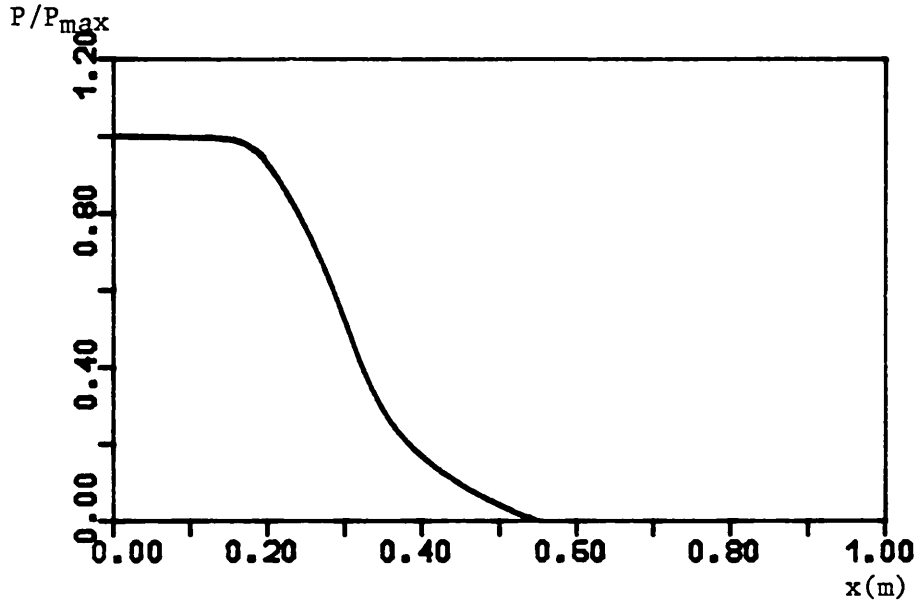



Figure 7-3 The pressure distribution of the steady-state flame along the duct. $P_{max}$ is the maximum pressure; x is the distance measured from the inlet.

Figure 7-4 shows the velocity distributions of Fluid 1 & Fluid 2 along the duct.

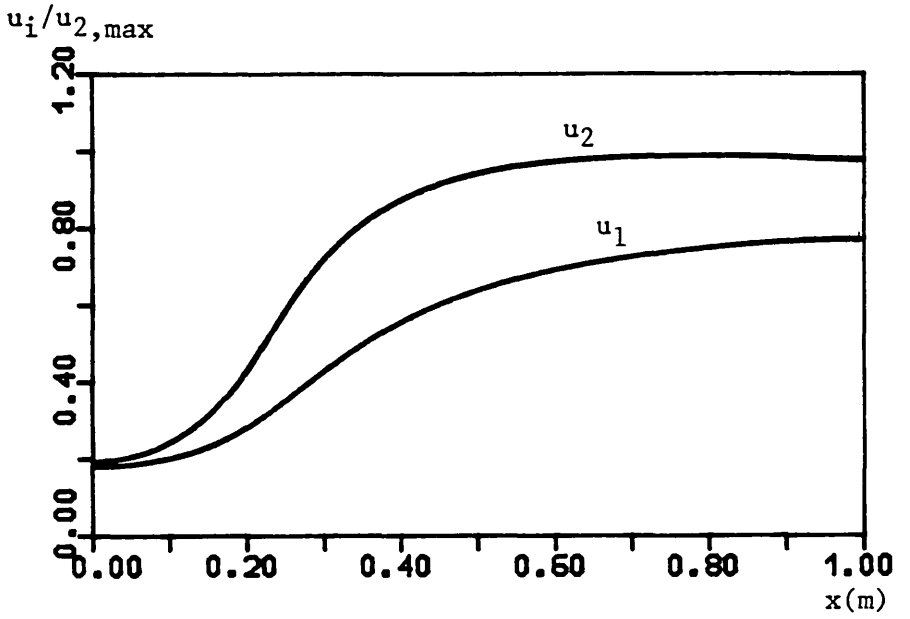



Figure 7-4 The velocity distributions of Fluid 1 & Fluid 2 along the duct. $u_{2,max}$ is the maximum velocity of fluid 2.

It can be seen from Figures 7-3 and 7-4 that the pressure falls in the direction of flow, because the gases accelerate as they move downstream due to the thermal expansion caused by combustion. The burned gas and unburned gas are subject to the same pressure fall, but the former accelerates more rapidly because of its lower density resulting in a velocity difference between the two fluids, which has been supported by experimental findings (Shepherd, Moss and Bray 1982). In the present model, this velocity difference is the dominant factor to cause the turbulent mixing through the "pressure-gradient diffusion" mechanism, as will be shown in Figure 7-6.

Figure 7-5 shows the volume fraction distribution of Fluid 2 along the duct.

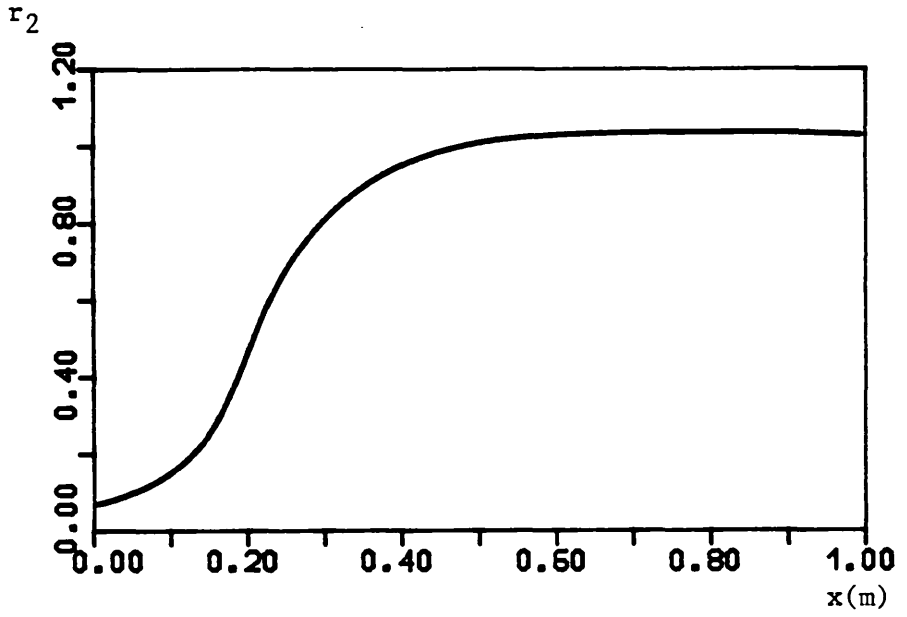



Figure 7-5 The volume fraction distribution of Fluid 2 along the duct.

In Figure 7-5, the values of volume fraction $r_2$ on both ends of the duct, 0 & 1, indicate the premixed gas and completely burned gas respectively. Therefore, the distance between the flame-holder and the section where the flame reaches the wall can be deduced from this distribution. As is seen from Figure 7-5, the distance is about 0.5m. In this calculation, the half-duct width implied in the fragment size is 0.05m; the flame length, therefore, is about 5 duct width; this value is close to the results of Scurlock (1956), which shows that the length for flame spread to the walls is about 4 duct width for a density ratio, $\rho_2/\rho_1$ =0.17.

Figure 7-6 shows the interfluid mass transfer rate distribution along the duct.

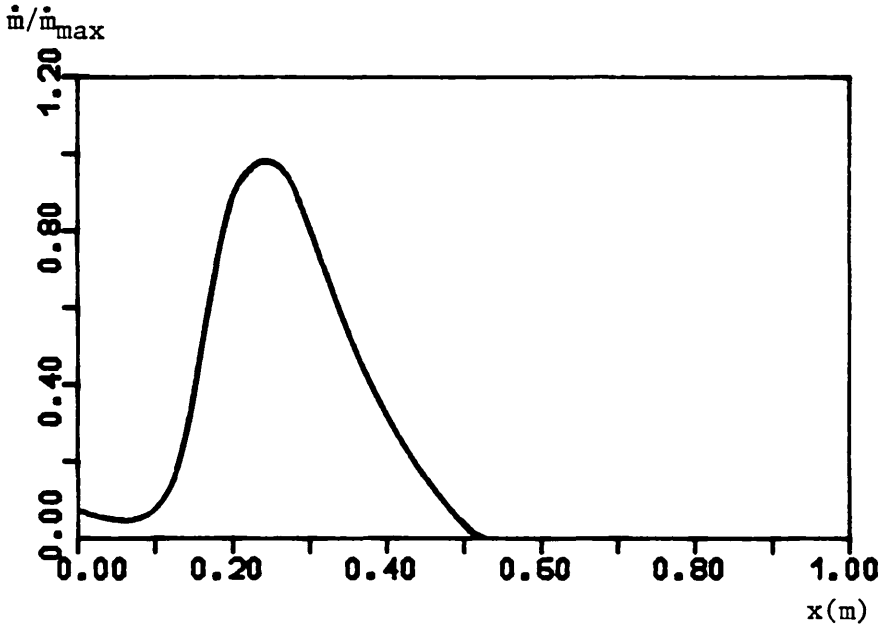



Figure 7-6 The interfluid mass transfer rate distribution along the duct. $\dot{m}_{max}$ is the maximum interfluid mass transfer rate.

As is seen, the interfluid mass transfer rate exhibits its peak at the point where the difference of velocity between hot and cold gases is a maximum and the volume fraction of the hot gas is about 0.5; as the latter tends to unity (x>0.5m), the entrainment rate becomes zero,meaning that the combustible mixture in the duct has been completely burned resulting in a homogeneous hot gas.

In the present model, the entrainment rate has been given a lower limit value to account for the random turbulent motion when the relative speed of the two fluids passes through zero, as shown near the duct inlet in Figure 7-6.

The results presented above have served as a useful preliminary study to show some of the attractive features of the two-fluid model, e.g. the "pressure-gradient diffusion", which is the essential ingredient of the flame acceleration in ducts.

### 7.6.2 The "Stable" Oscillation Case

The transient process starts after a sudden change of the back pressure at the outlet. Under certain conditions, the oscillations may become "stable". When it occurs, the variation of the pressure with time gives periodic cycles, as shown in Figure 7-7. Although in the figure only few cycles have been presented, they do last very long.

For this case, values of dimensionless parameters are :

Ma=0.027, LCm=100., Cm/Cf=4.348, $\rho_2/\rho_1$ =0.2, NX=40, $\delta t^* u_o/L$=0.01

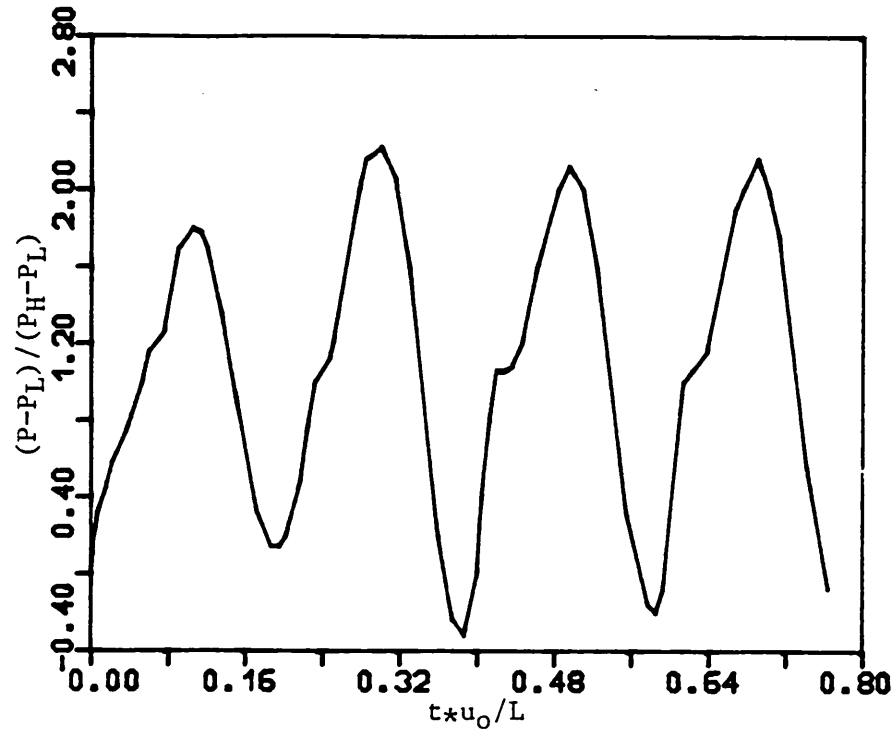
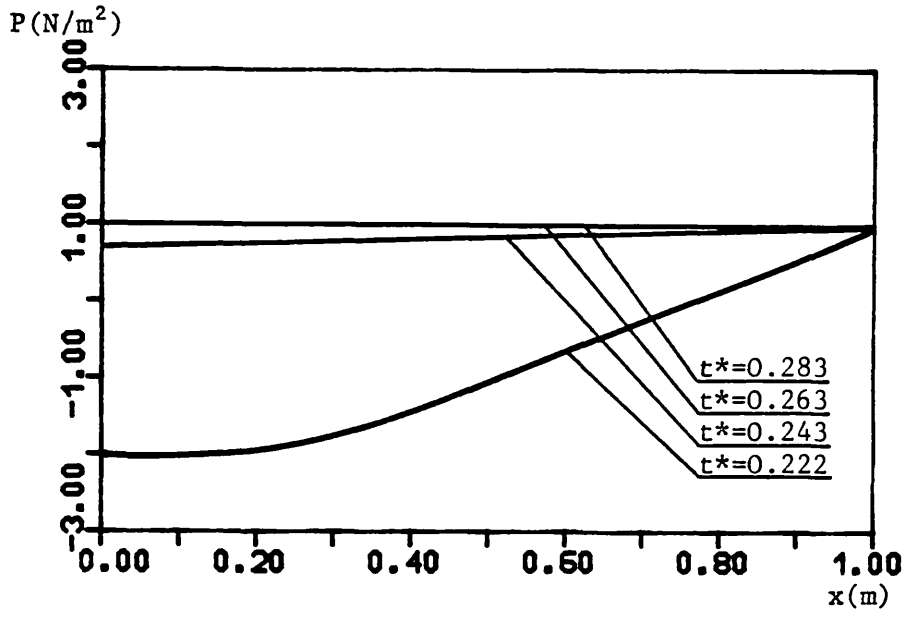


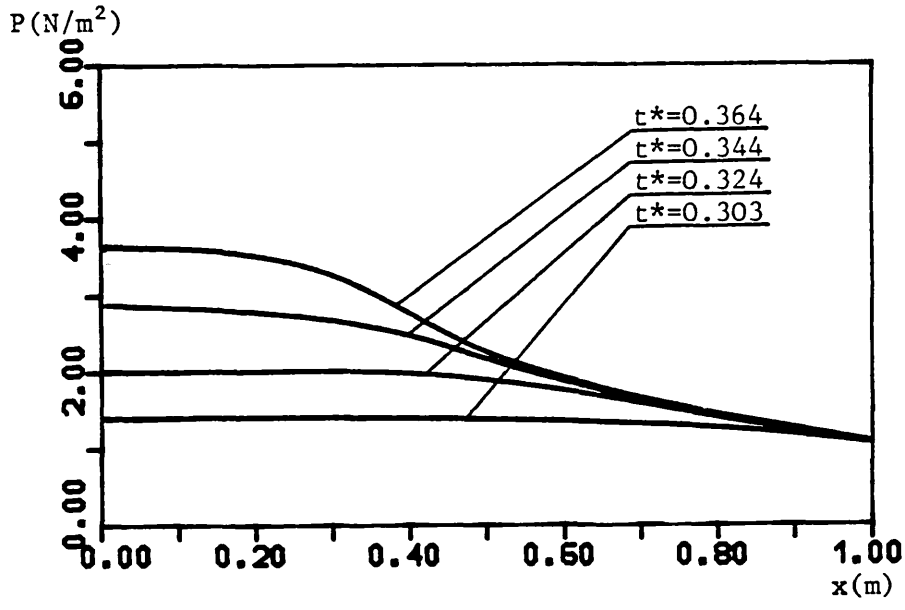

Figure 7-7 The variation of the pressure at half-length of the duct with time after a sudden change of resistance at the outlet.

The x-wise variations of variables, P, $u_1$, $u_2$, $r_2$, and $\dot{m}$ at various instants through a "stable" cycle are also provided in Figures 7-8 to 7-11.

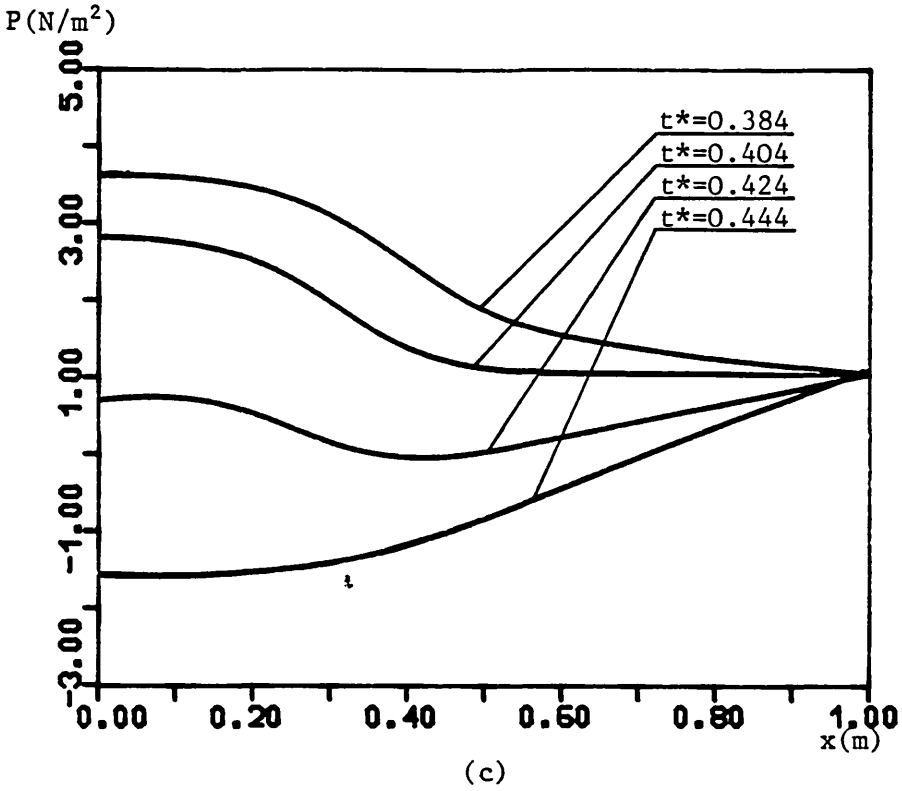
Figure 7-8 (a-c) shows the pressure distributions along the duct at various instants through a "stable" cycle.


P(N/m²)
3.00
1.00
-1.00
-3.00
0.00
0.20
0.40
0.60
0.80
1.00
x(m)
t*=0.283
t*=0.263
t*=0.243
t*=0.222

(a)


P(N/m²)
6.00
4.00
2.00
0.00
0.00
0.20
0.40
0.60
0.80
1.00
x(m)
t*=0.364
t*=0.344
t*=0.324
t*=0.303

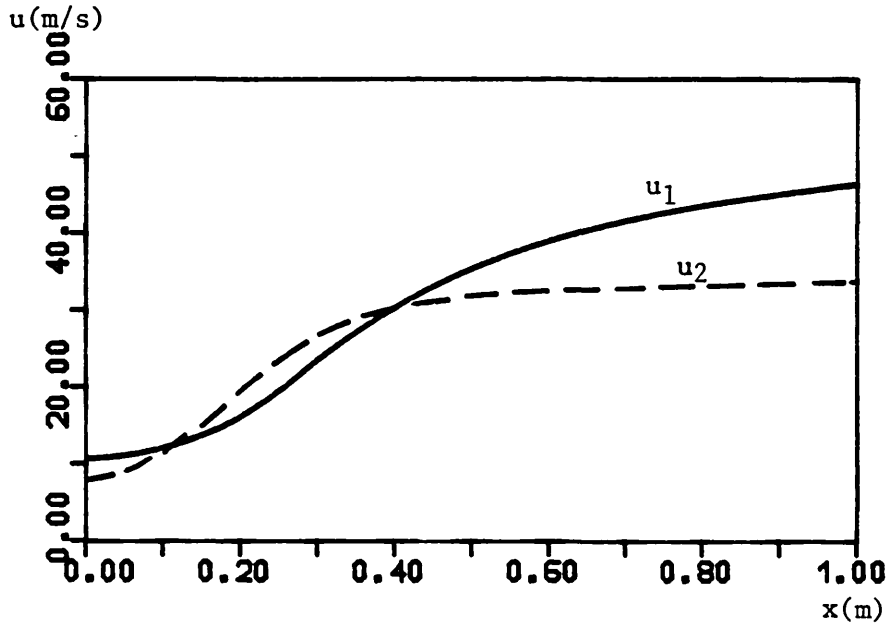
(b)



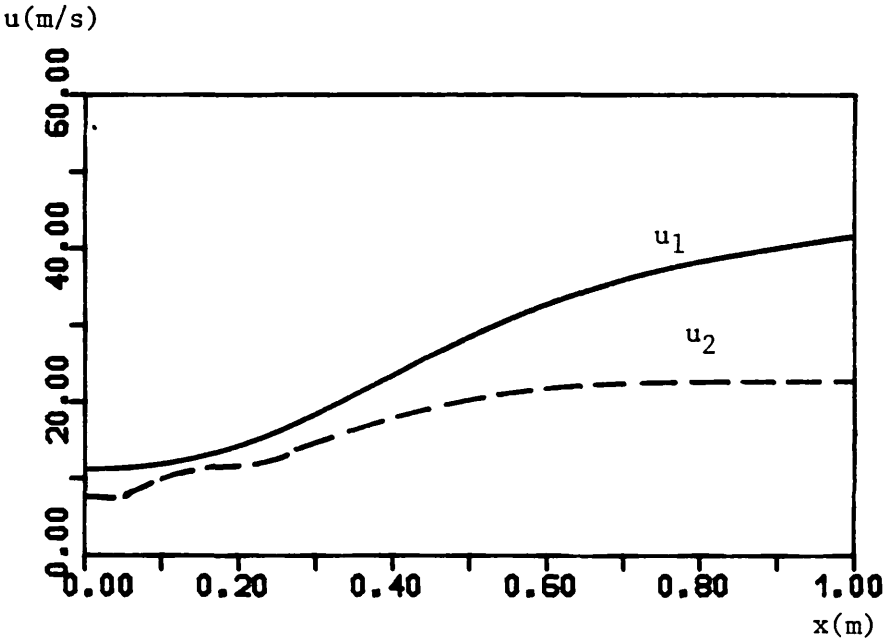

(c)

Figure 7-8 The pressure profiles along the duct at a sussession of instants through a "stable" cycle.

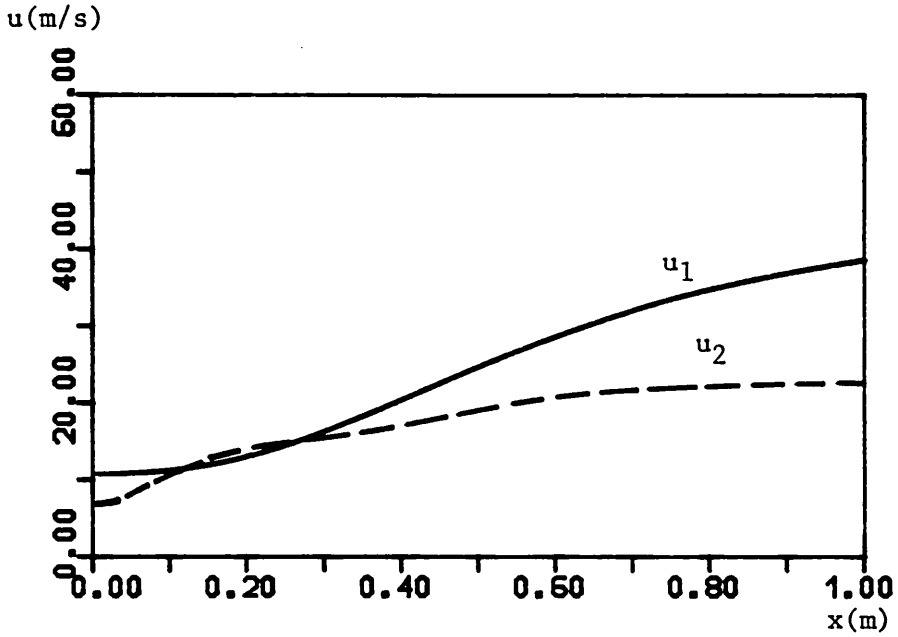
Figure 7-9 (a-1) shows the distributions of velocities $u_1$ and $u_2$ along the duct at a succession of instants through the cycle.



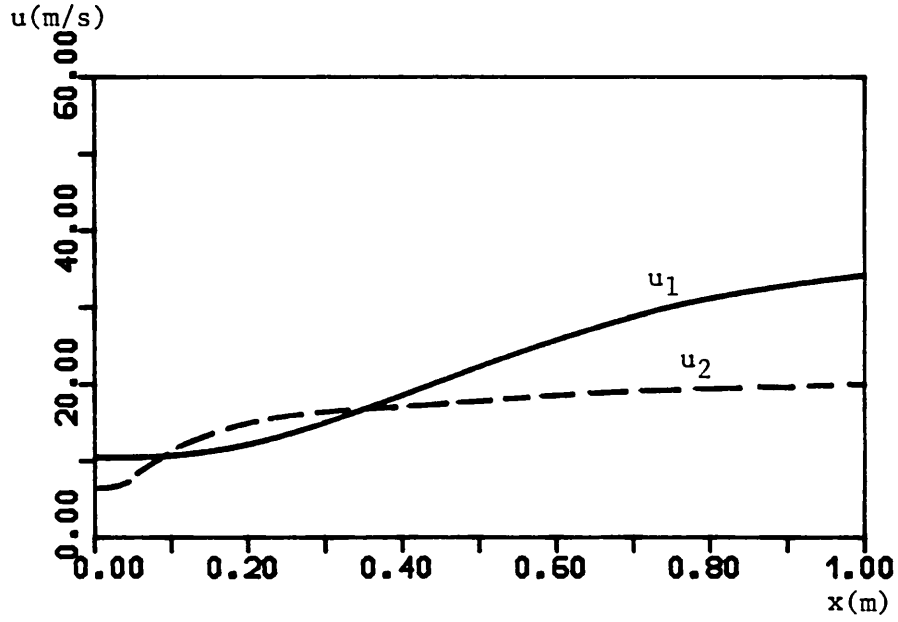

(a) t*=0.222



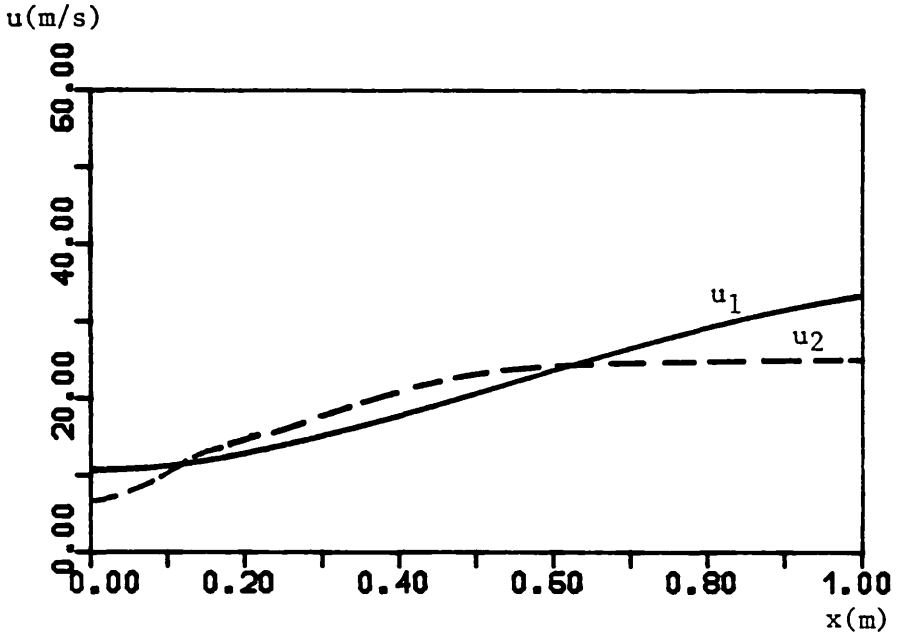

(b) t*=0.243



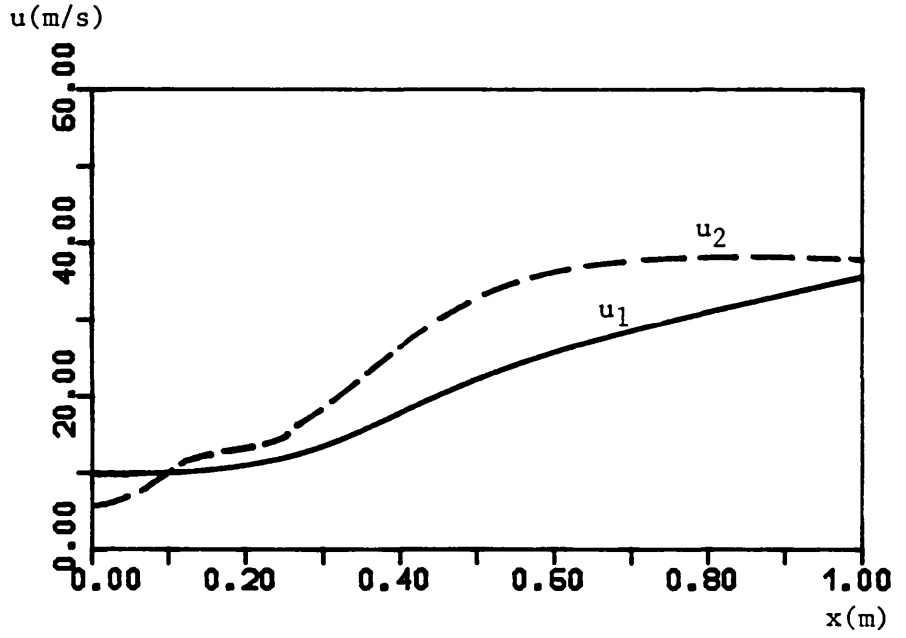

(c) t*=0.263



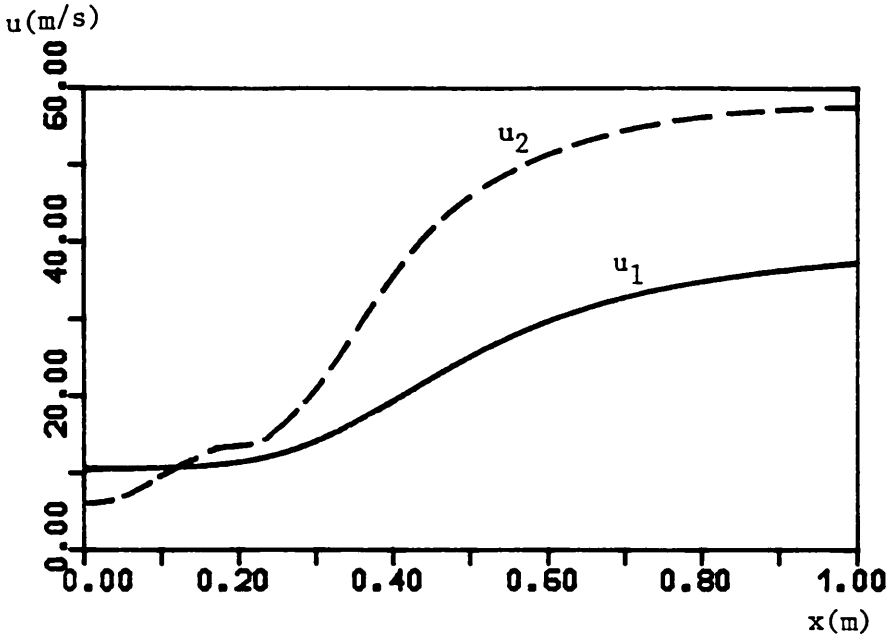

(d) t*=0.283



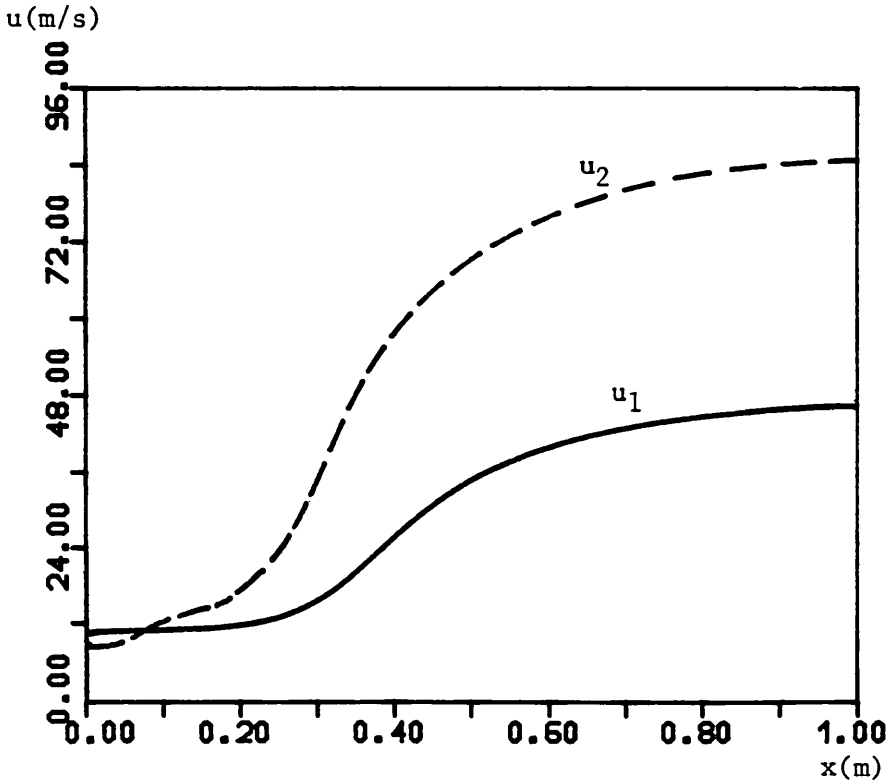

(e) t*=0.303



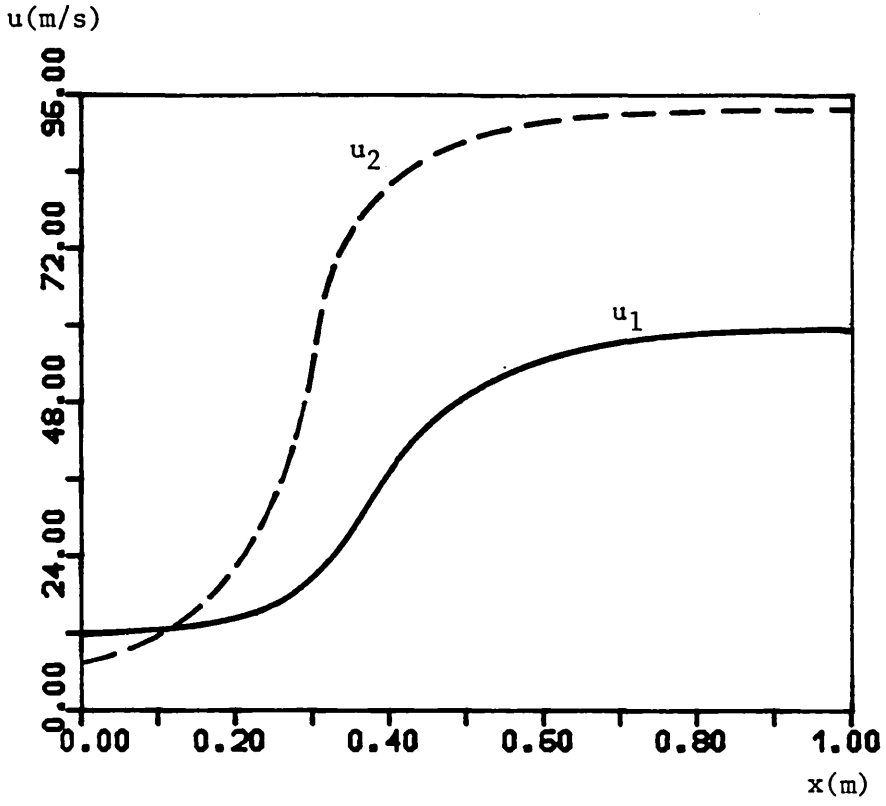

(f) t*=0.323



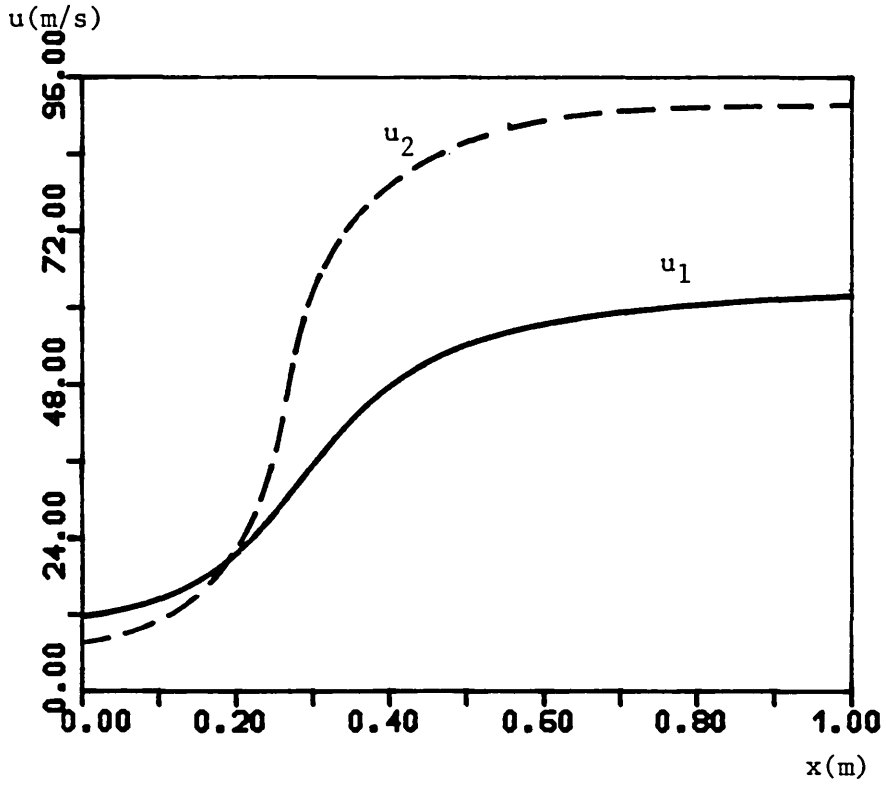

(g) t*=0.343



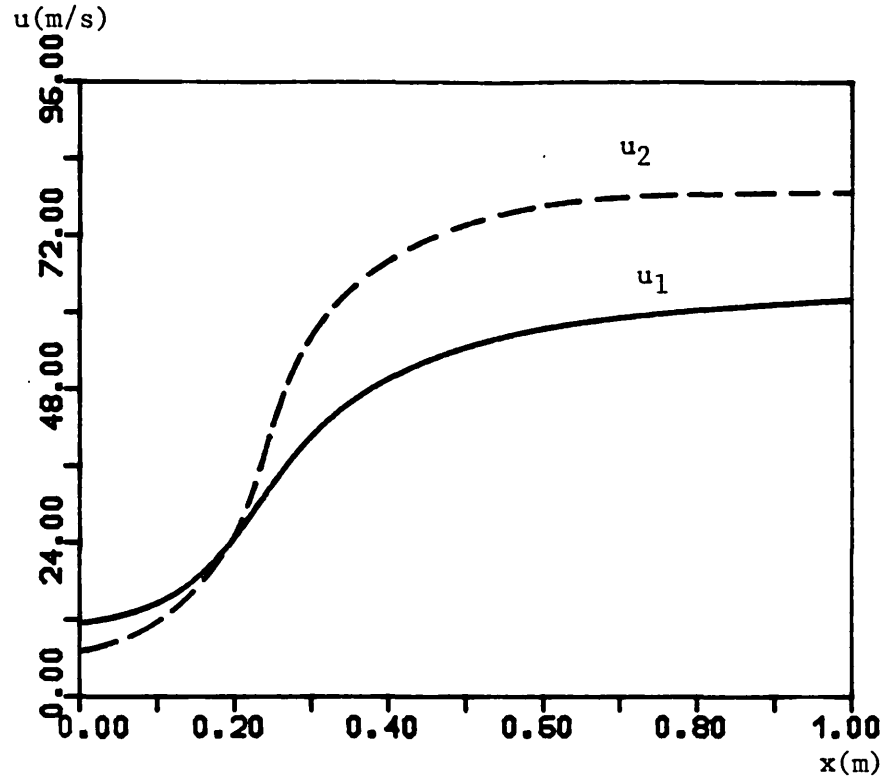

(h) t*=0.364



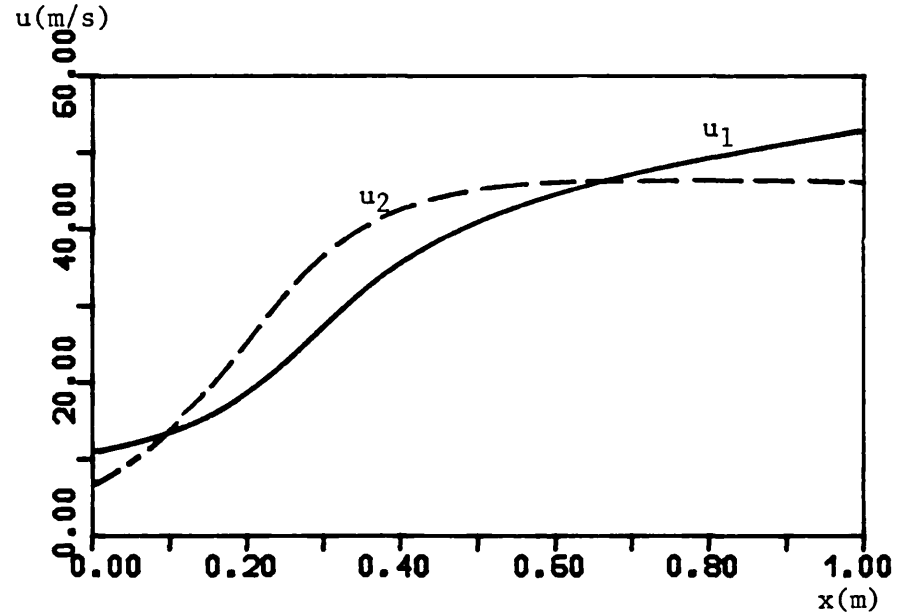

(i) t*=0.384




(j) t*=0.404



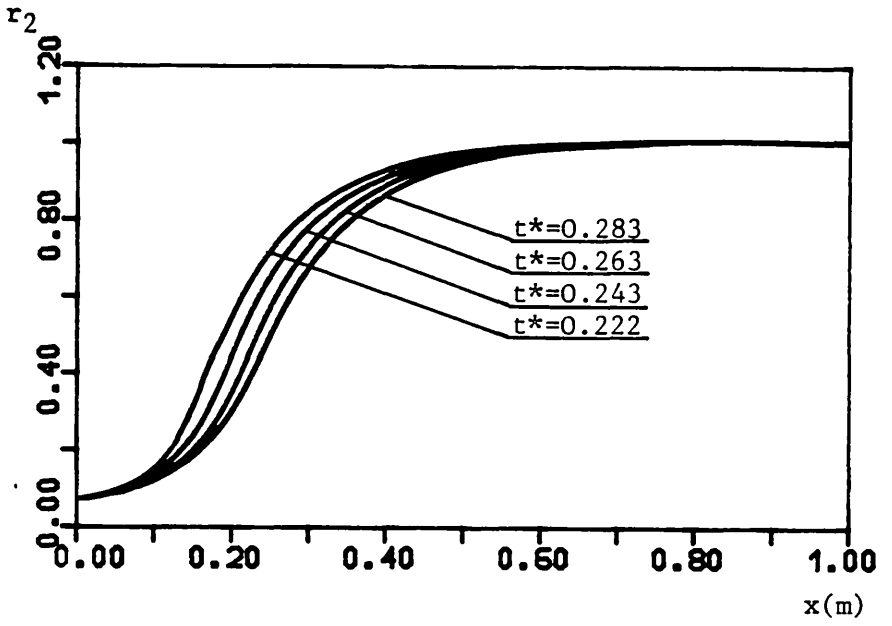

(k) t*=0.424



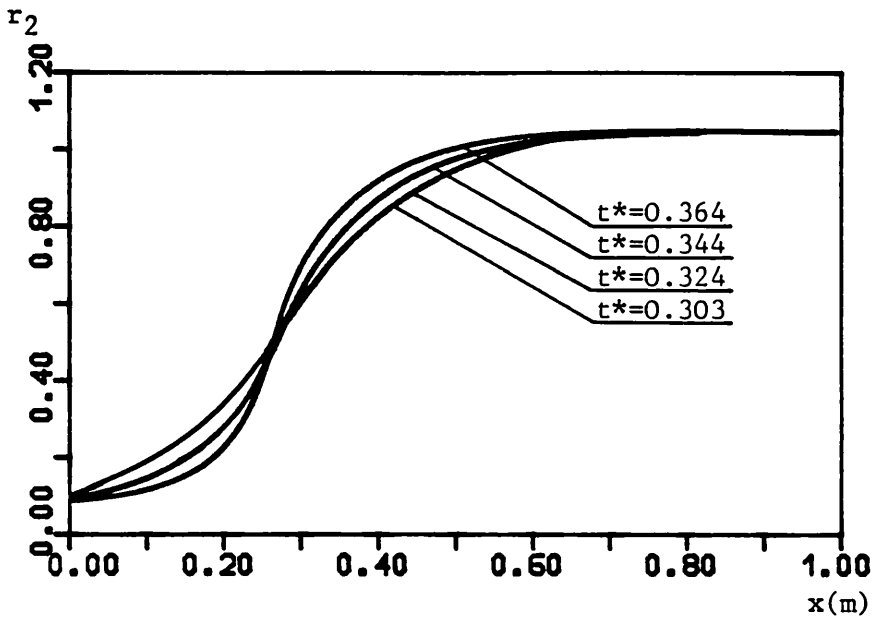

(l) t*=0.444

Figure 7-9 The distributions of velocities $u_1$ and $u_2$ along the duct at various instants through a "stable" cycle.

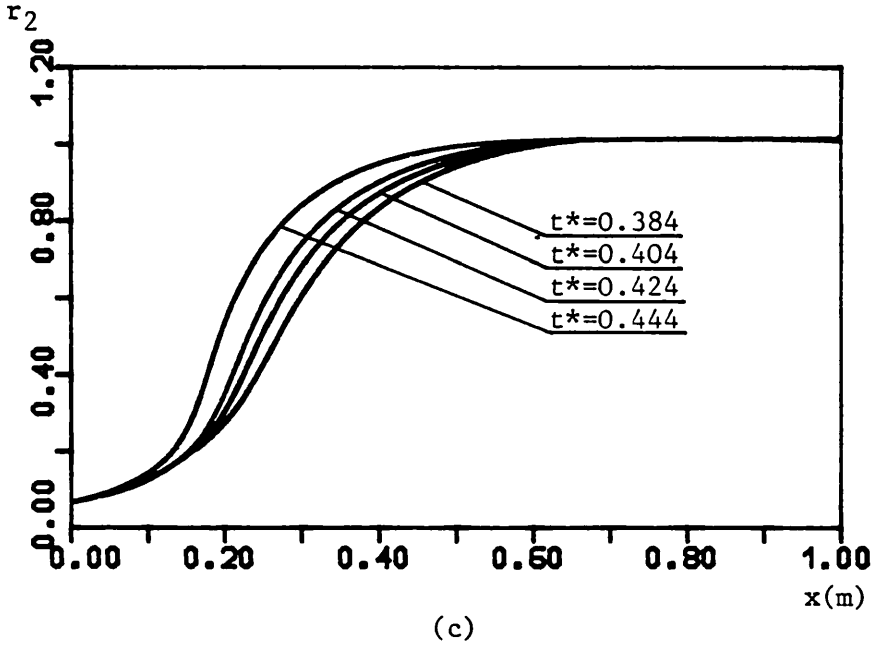
Figure 7-10 (a-c) shows distributions of the volume fraction of Fluid 2 along the duct at various instants through a "stable" cycle.




(a)



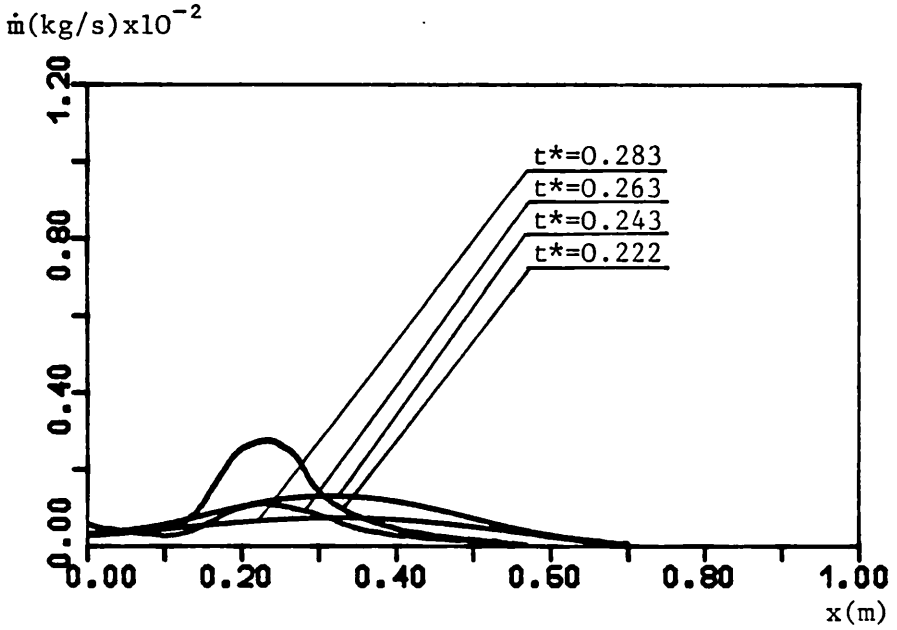

(b)



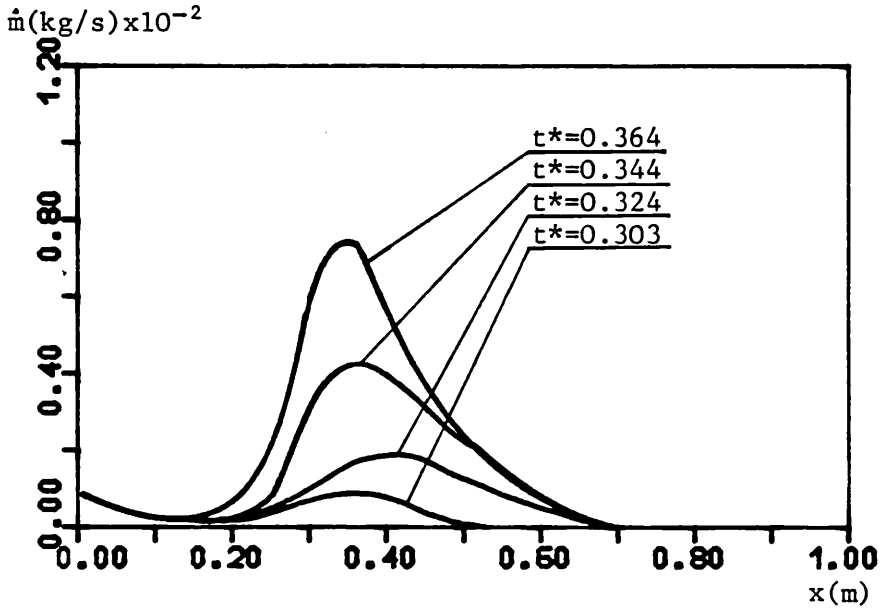

(c)

Figure 7-10 The volume fraction distributions of the hot gas along the duct at various instants through a "stable" cycle.

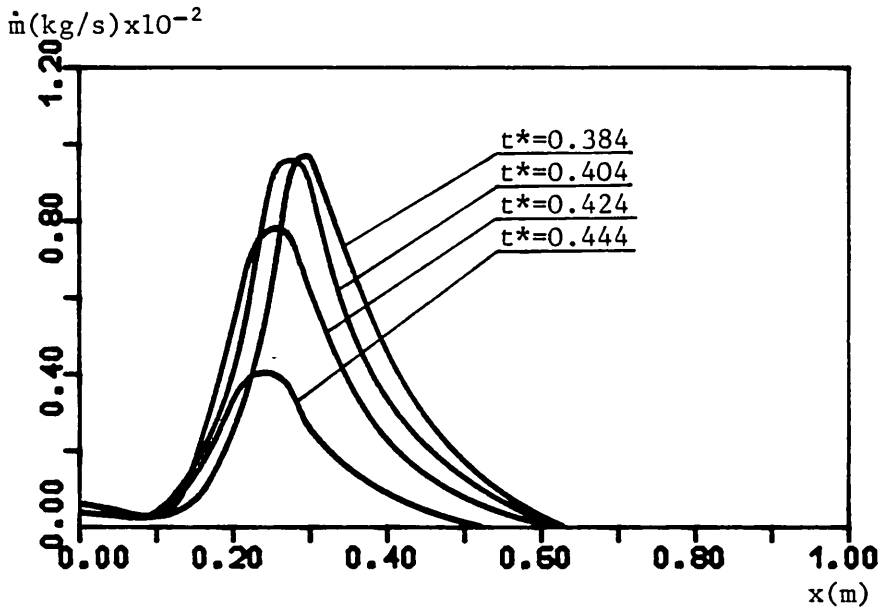
Figure 7-11 (a-c) shows the distributions of the interfluid mass transfer rate along the duct at various instants through a "stable" cycle.




(a)




(b)




(c)

Figure 7-11 The distributions of the entrainment rate along the duct at various instants through a "stable" cycle.

The results presented above show that all variables exhibit the periodic variation in a "stable" cycle following the pressure oscillation. It confirms that the interfluid mass transfer rate increases as the difference of velocity between the hot gas and the cold gas increases.

### 7.6.3 Parametric Study

In some of the cases investigated, "stable" oscillation could not be obtained within the range of calculations. An example is shown in Figure 7-12.

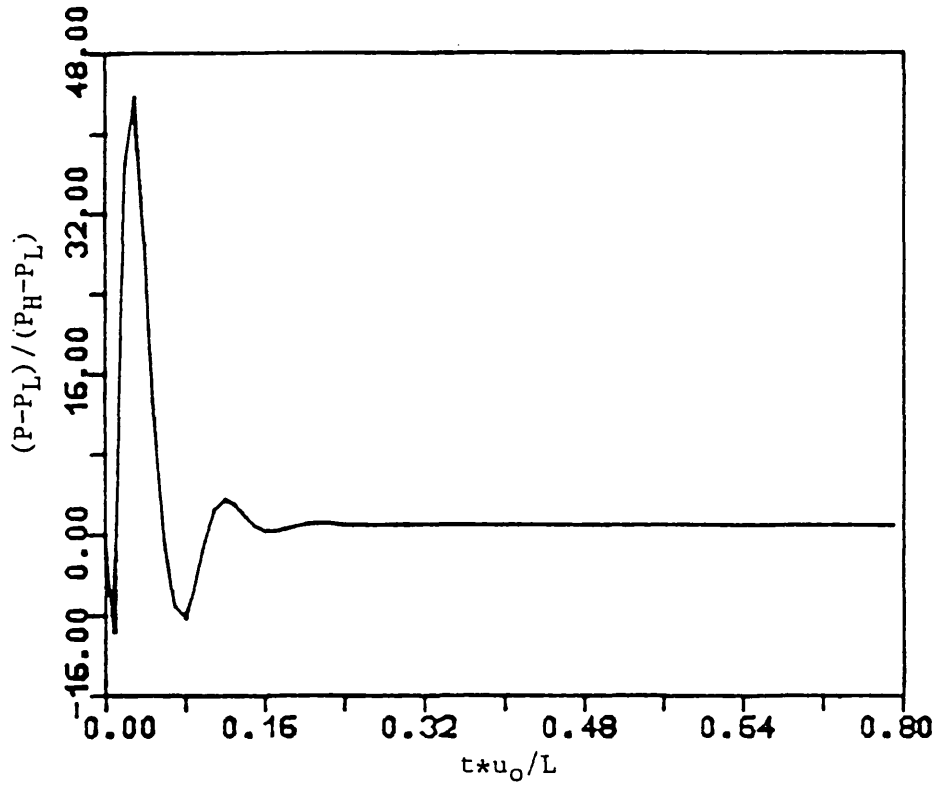



Figure 7-12 A case in which the initial pressure oscillation dies out. Conditions are : LCm=100, Ma=0.027, Cm/Cf=4.348, $\rho_2/\rho_1$=0.5, NX=40, $\delta t*u_o/L$=0.01.

It would ,therefore, be interesting and essential to delimit the instability region for further studies. An exercise to achieve this objective is described as the parametric study.

Instability regions are plotted in terms of LCm versus Cm/Cf, $\rho_2/\rho_1$ and Ma respectively. The effect of these numerical parameters will be discussed in Section 7.6.4.

The Instability Region Mapped on the Graph of LCm versus Cm/Cf

The instability region in terms of LCm-Cm/Cf is given in Figure 7-13 with other parameters fixed as :
Ma=0.027, $\rho_2/\rho_1$ =0.2, NX=40, $\delta t^* u_o/L$=0.01.

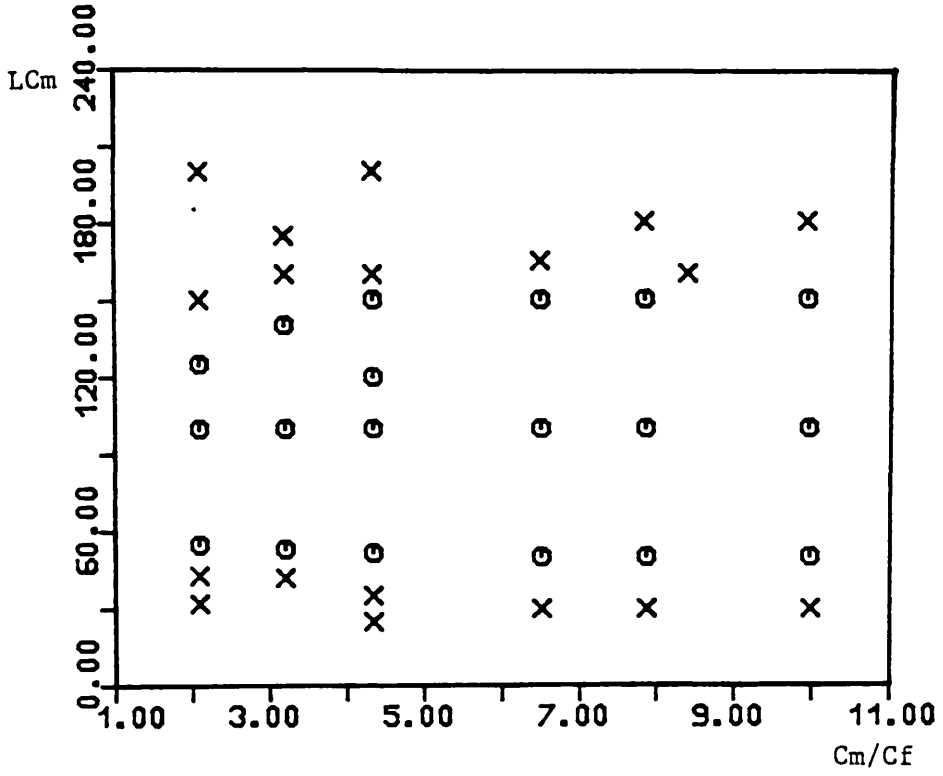



Figure 7-13 The instability region in terms of LCm-Cm/Cf

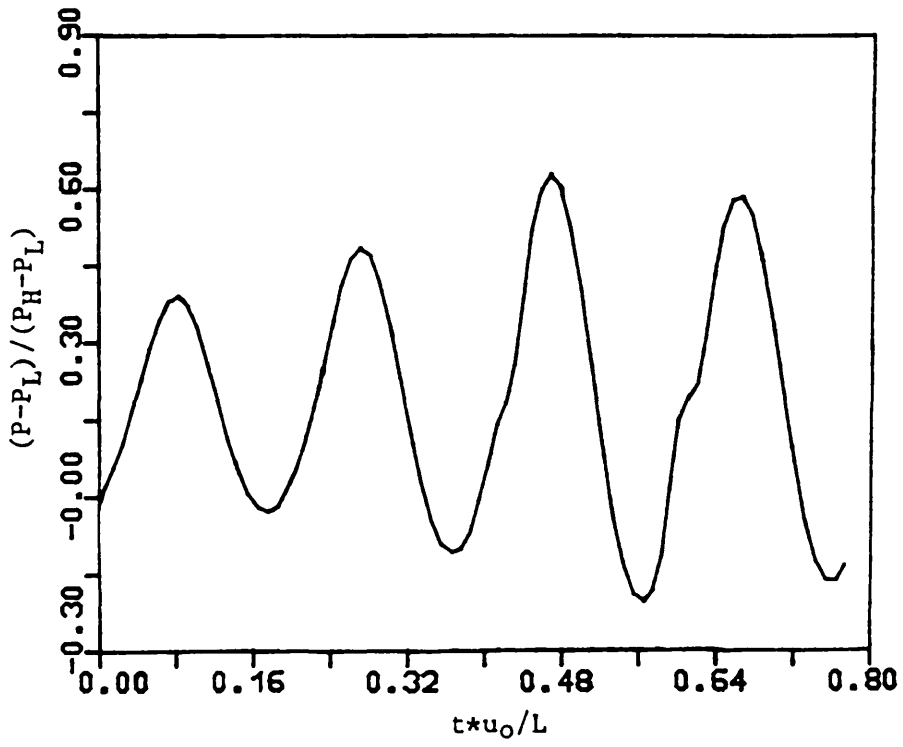
x diminishing oscillation
⊙ "stable" oscillation

The characteristics of oscillations at LCm=100 for three Cm/Cf values given in Figure 7-14 (a-c) show that :

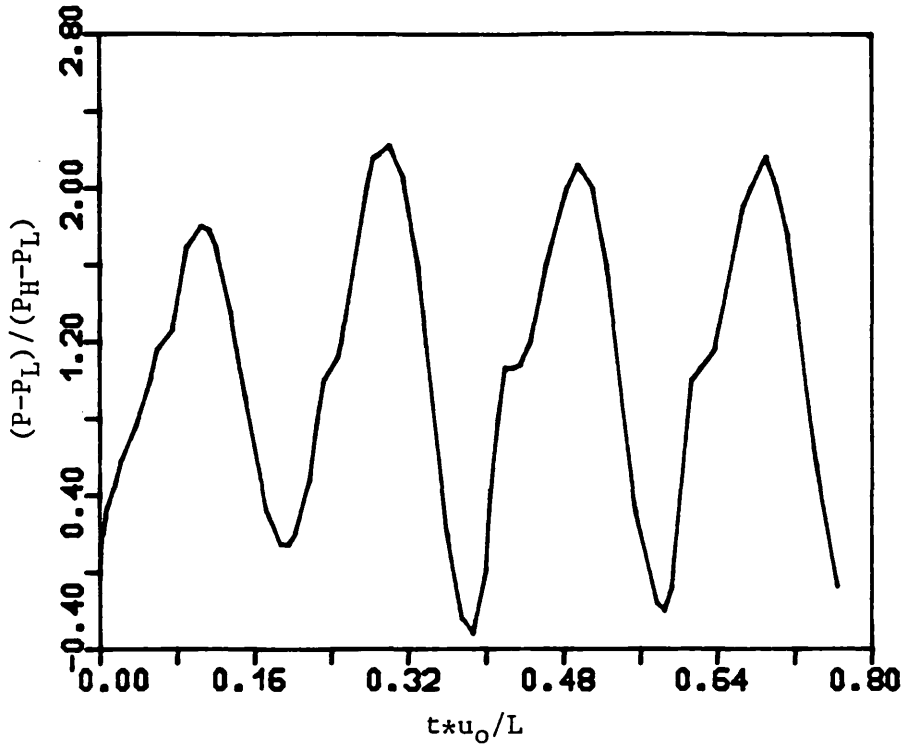
(i) Inside the instability region the pressure oscillations are "stable" after an initial starting period;

(ii) For Cm/Cf < 4.348, the dimensionless amplitude increases as Cm/Cf increases;

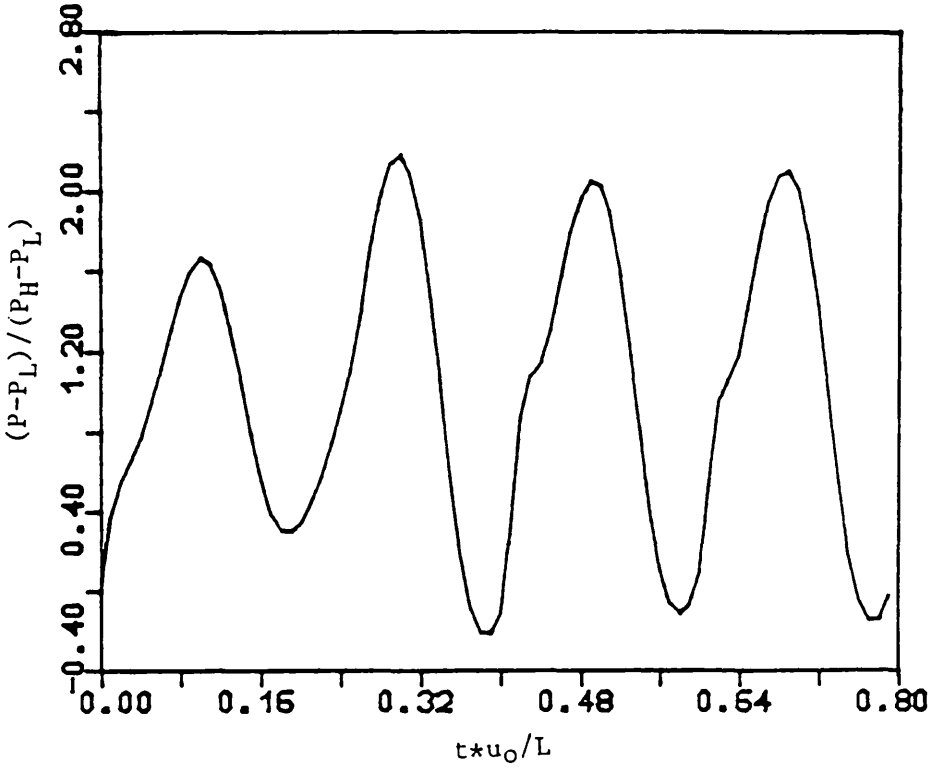
(iii) For Cm/Cf>4.348, no noticeable effect of Cm/CF on the amplitude.




(a) LCm=100, Cm/Cf=2.1




(b) LCm=100, Cm/Cf=4.348




(c) LCm=100, Cm/Cf=10.

Figure 7-14 The characteristics of oscillations with different Cm/Cf at a fixed LCm=100.

## The Instability Region Mapped on the Graph of LCm versus $\rho_2/\rho_1$

The instability region in terms of LCm-$\rho_2/\rho_1$, is given in Figure 7-15, which shows that oscillations occur within a closed region. For this case other dimensionless parameters are fixed as :

Ma=0.027, Cm/Cf=4.348, NX=40, $\delta t^* u_0 /L$=0.01.

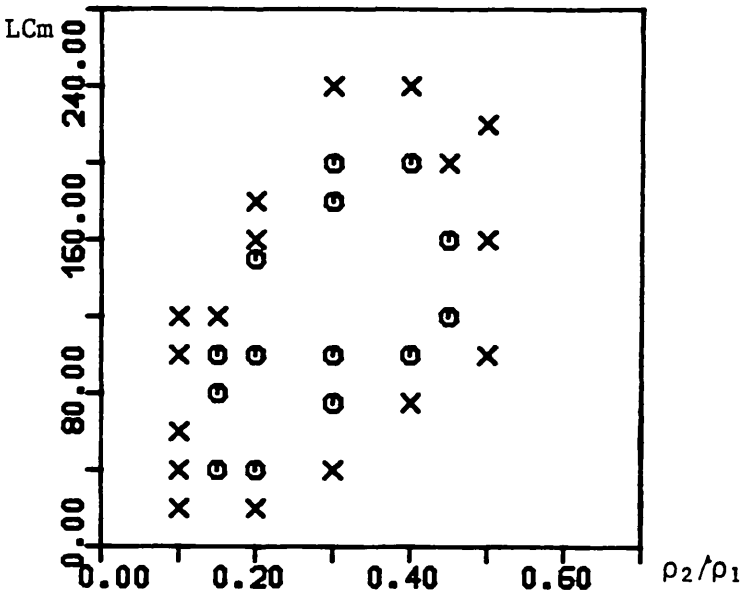
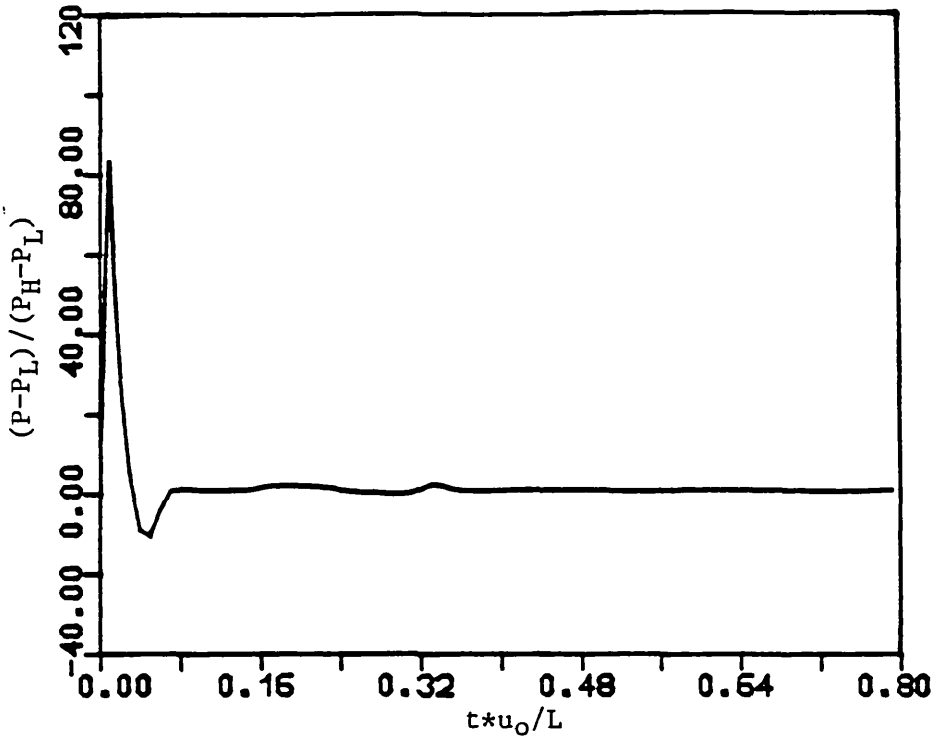
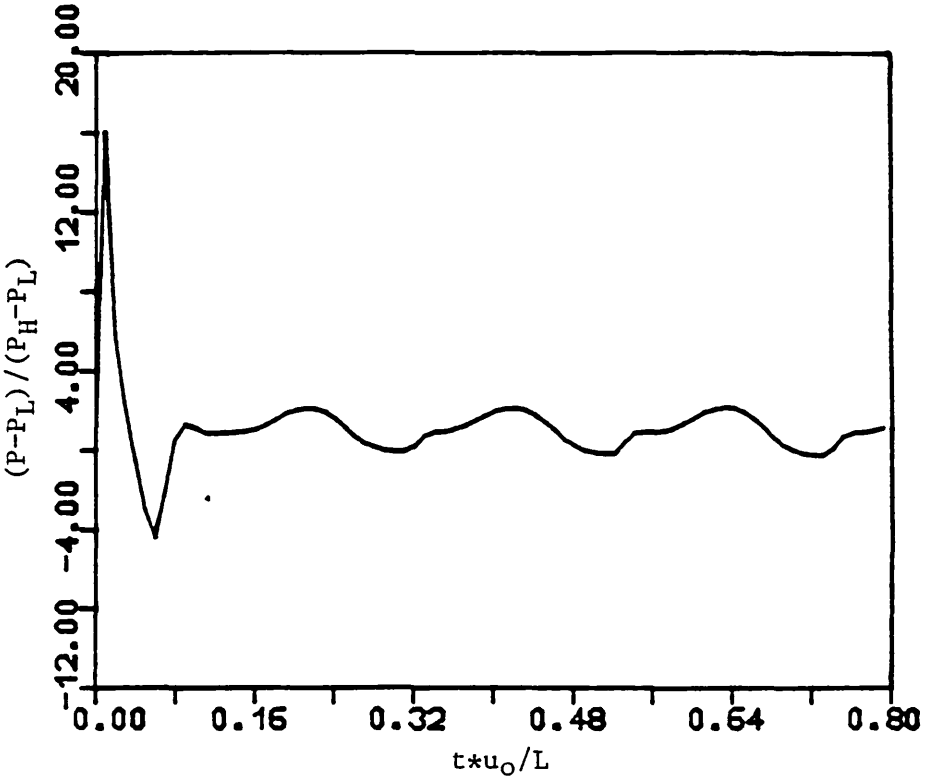



Figure 7-15 The instability region in terms of LCm-$\rho_2/\rho_1$

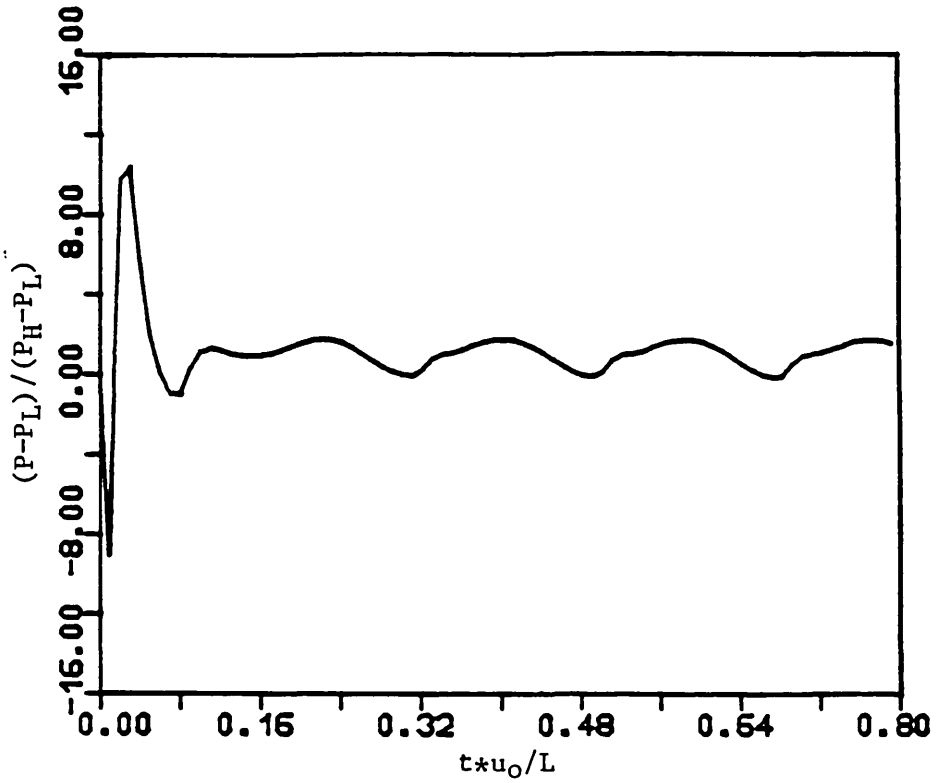
The characteristics of oscillations with different $\rho_2/\rho_1$ at a fixed LCm=100, are given in Figure 7-16 (a-d).



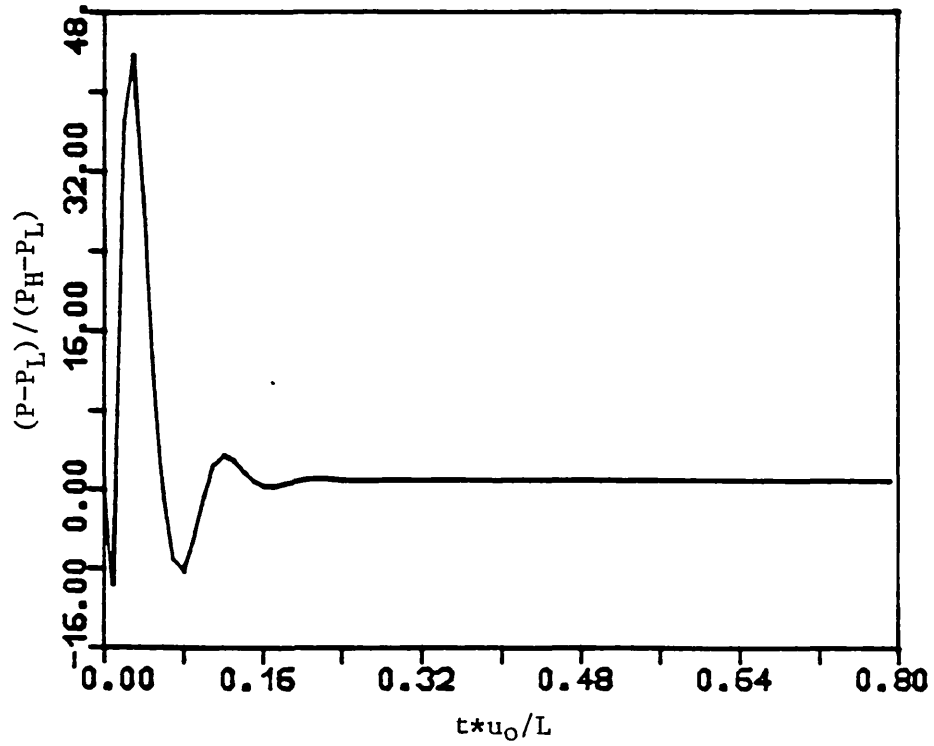

(a) LCm=100, $\rho_2/\rho_1$=0.1




(b) LCm=100, $\rho_2/\rho_1$=0.15




(c) LCm=100, $\rho_2/\rho_1$=0.3




(d) LCm=100, $\rho_2/\rho_1$=0.5

Figure 7-16 The characteristics of oscillations with different $\rho_2/\rho_1$ at a fixed LCm=100.

It can be seen that :

(i) Outside the instability region, $\rho_2/\rho_1 < 0.1$ and $\rho_2/\rho_1 > 0.5$, as shown in Figure 7-16 (a) & (d), the pressure oscillations die out;

(ii) Within the instability region, as shown in Figure 7-16 (b) & (c), the pressure oscillations are "stable"; and there is no noticeable effect of $\rho_2/\rho_1$ on the frequency and the amplitude.

The Instability Region Mapped on the Graph of LCm versus Ma

The instability region in terms of LCm-Ma is given in Figure 7-17, which shows that there is little effect of the Mach number on the occurance of instabilities. For this case, following dimensionless parameters are fixed as :

$Cm/Cf=4.348$, $\rho_2/\rho_1 =0.2$, $NX=40$, $\delta t^* u_o /L=0.01$.

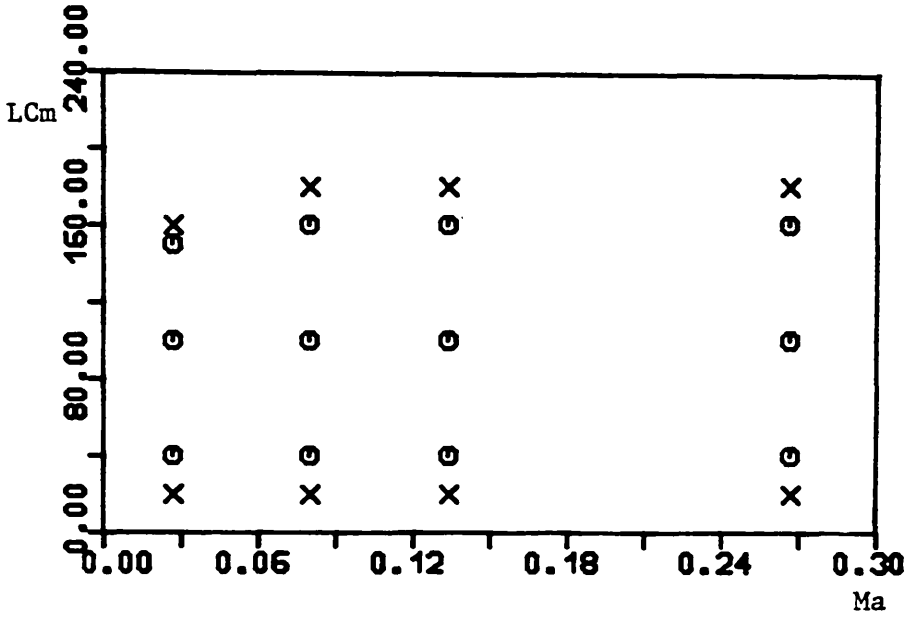
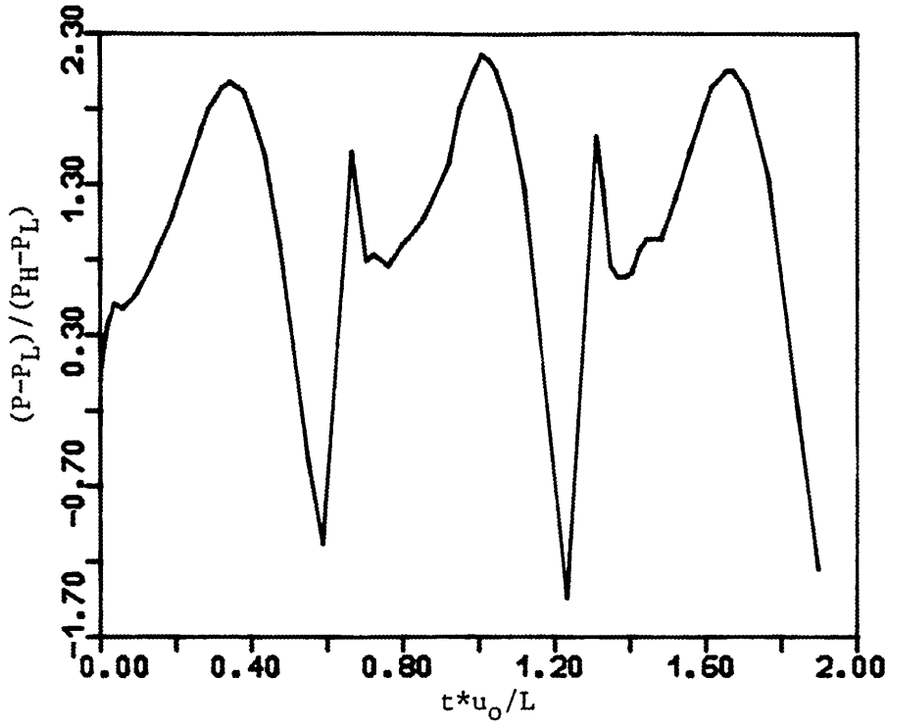
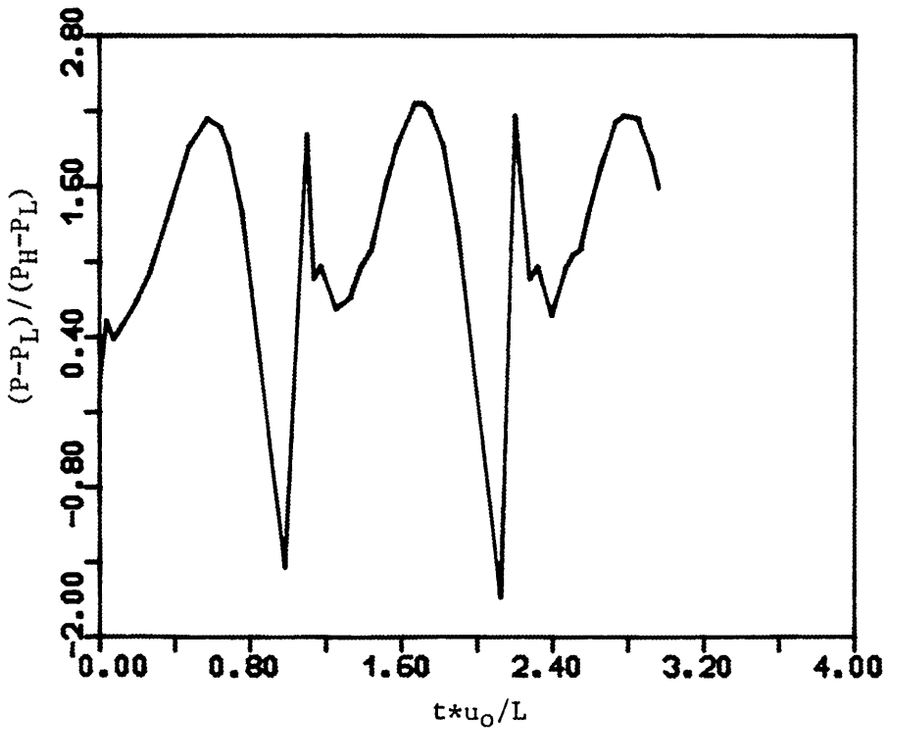



Figure 7-17 The instability region in terms of LCm-Ma

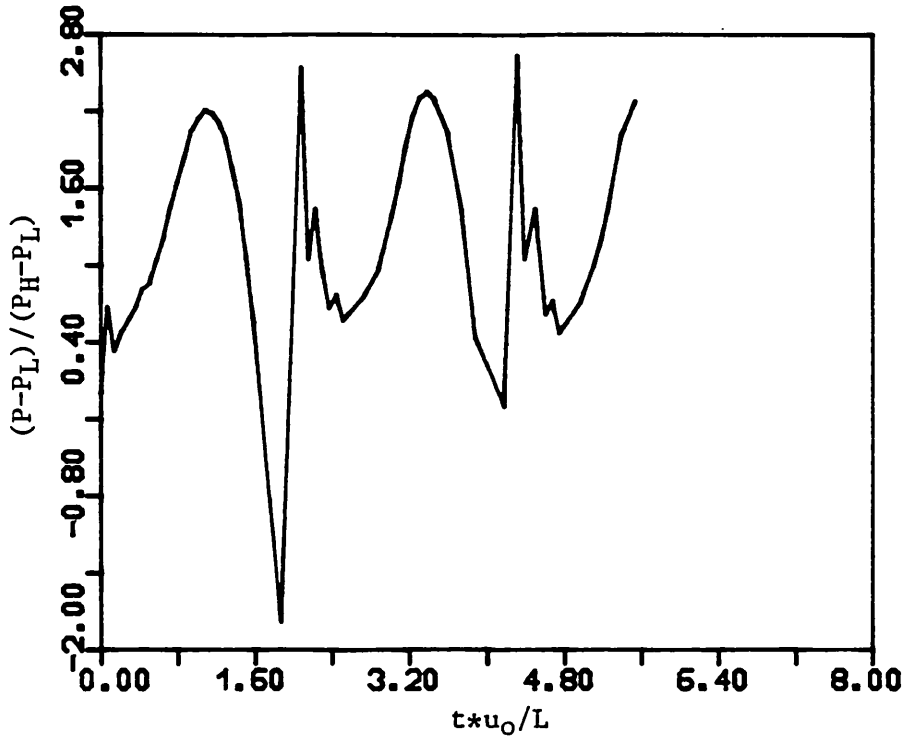
The characteristics of pressure oscillations at different Mach numbers for a fixed LCm=100, are given in Figure 7-18 (a-c).




(a) LCm=100, Ma=0.08




(b) LCm=100, Ma=0.134




(c) LCm=100, Ma=0.267

Figure 7-18 The characteristics of oscillations with different Ma for a fixed LCm=100.

It can be seen that the dimensionless frequency decreases as the Mach number increases while the dimensionless amplitude remains substantially the same.

### 7.6.4 The Effect of Numerical Parameters, NX and $\delta t*u_o/L$

The effect of numerical parameters, NX for the size of grid cells and $\delta t*u_o/L$ for the magnitude of time-step, has been investigated. The cases tested are listed in Tables 7-1 & 7-2. For all cases, the physical parameters are fixed as : Ma=0.027, LCm=100, Cm/Cf=4.348, $\rho_2/\rho_1$ =0.2.

Table 7-1 Cases Tested for the Effect of Numerical Parameter, NX

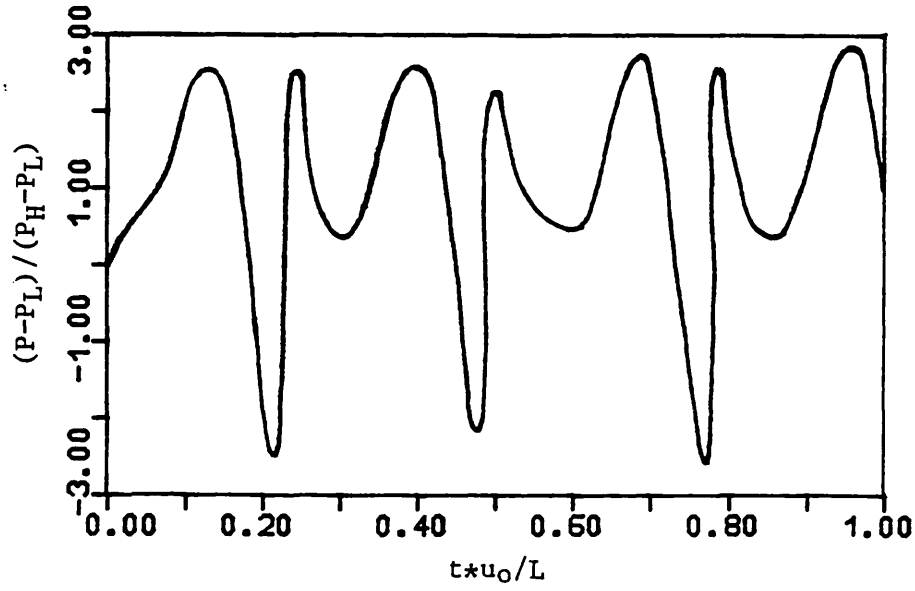
| No. | NX | $\delta t^* u_o / L$ |
|---|---|---|
| 1 | 50 | 0.001 |
| 2 | 40 | 0.001 |
| 3 | 30 | 0.001 |

Table 7-2 Cases Tested for the Effect of Numerical Parameter, $\delta t^* u_o / L$

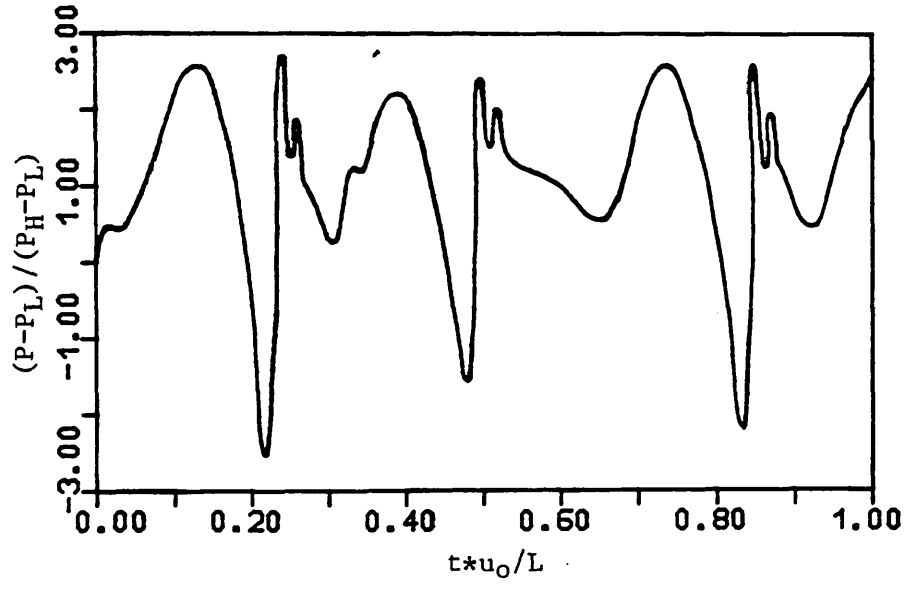
| No. | NX | $\delta t^* u_o / L$ |
|---|---|---|
| 1 | 40 | 0.05 |
| 2 | 40 | 0.03 |
| 3 | 40 | 0.01 |
| 4 | 40 | 0.001 |
| 5 | 40 | 0.0005 |

The results are given in Figures 7-19 and 7-20.

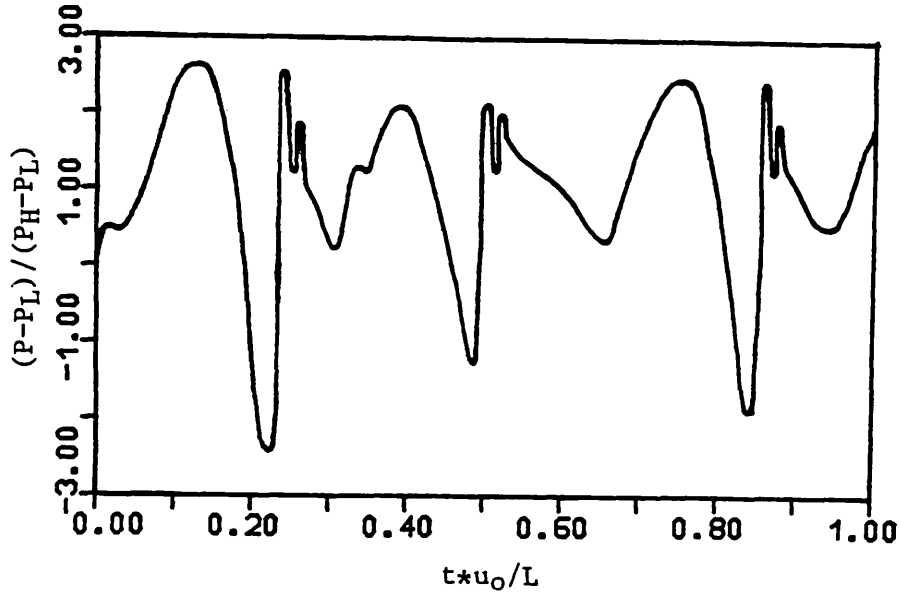
Figure 7-19 (a-c) shows the effect of grid number, NX.


3.00
1.00
-1.00
-3.00
$(P-P_L)/(P_H-P_L)$
0.00
0.20
0.40
0.60
0.80
1.00
$t*u_o/L$

(a) NX=30


3.00
1.00
-1.00
-3.00
$(P-P_L)/(P_H-P_L)$
0.00
0.20
0.40
0.60
0.80
1.00
$t*u_o/L$

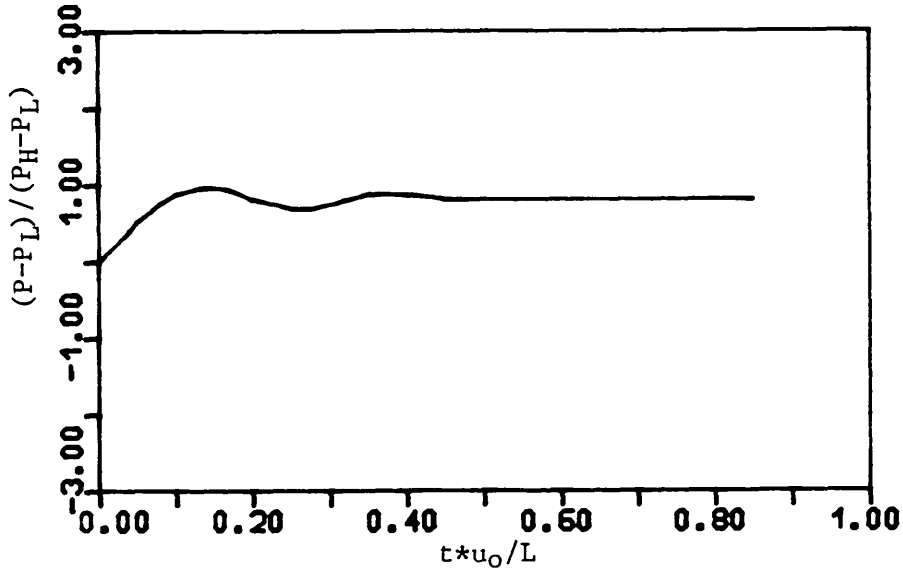
(b) NX=40



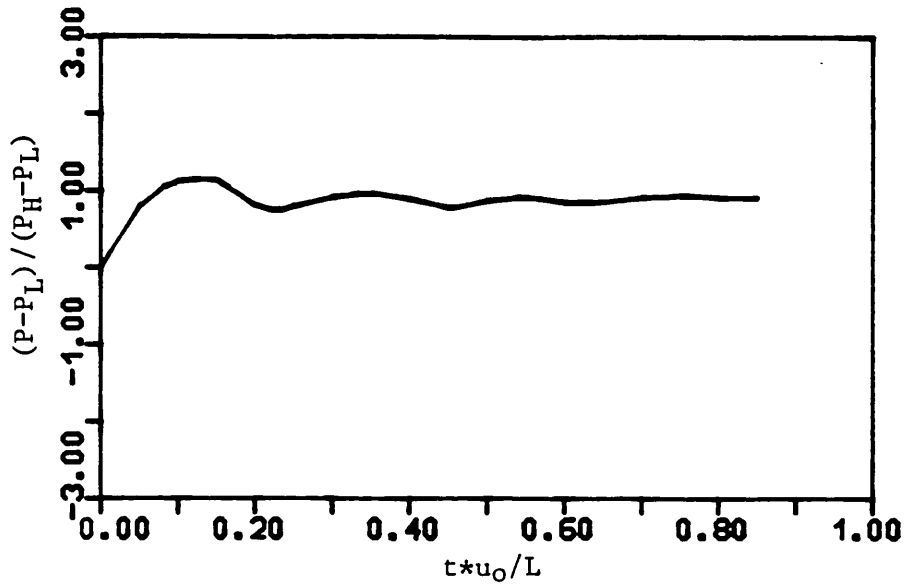

(c) NX=50

Figure 7-19 The effect of the numerical parameter,NX

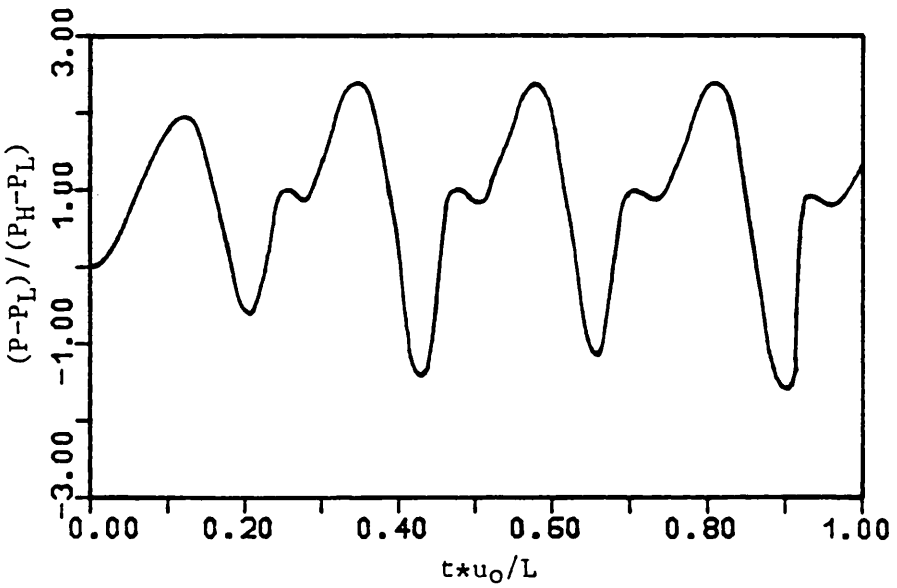
Figure 7-20 (a-e) shows the effect of the time-step size, $\delta t*u_o/L$.



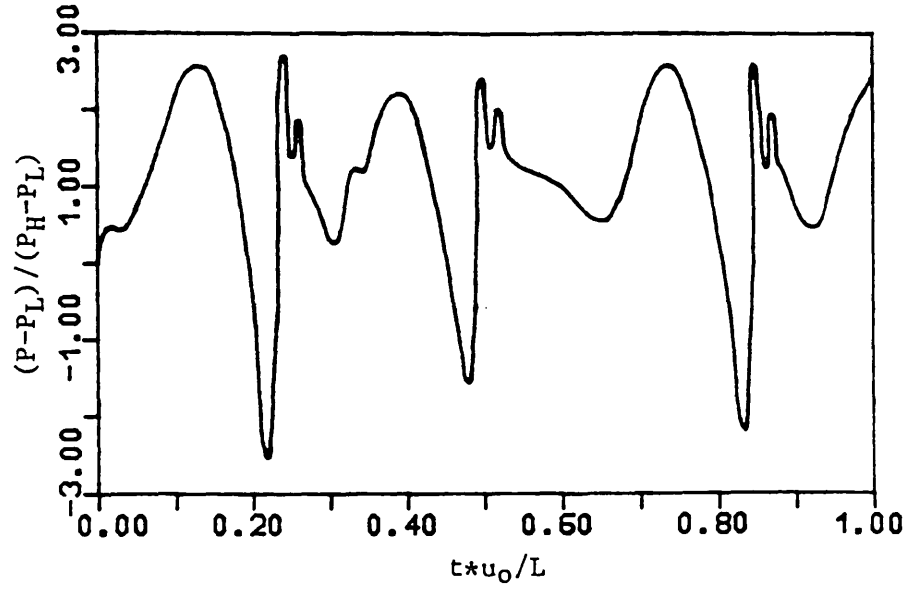

(a) $\delta t*u_o/L=0.05$



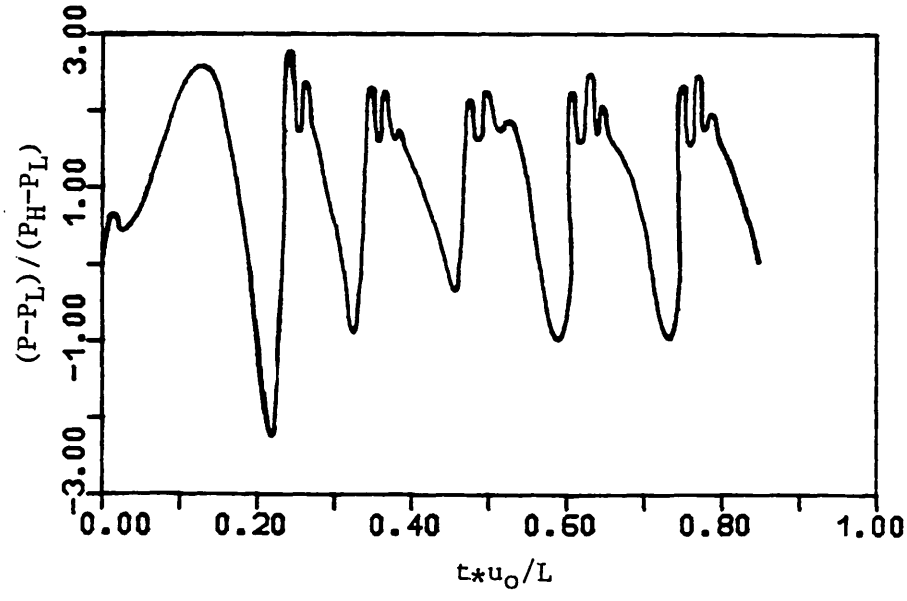

(b) $\delta t*u_o/L=0.03$




(c) $\delta t*u_o/L=0.01$




(d) $\delta t*u_o/L=0.001$




(e) $\delta t*u_o/L=0.0005$

Figure 7-20 The effect of the time-step size, $\delta t*u_o/L$.

As is seen from Figure 7-19 that there is little effect of the grid number, NX, on the results for NX greater than 40.

Apparent changes on the results can be seen from Figure 7-20 as the time-step size is changed; the oscillation, nevertheless, persists and more details appear as the time-step size decreases. A dimensionless time-step size of 0.01 has been used in majority of runs in the present investigation.

## 7.7 Convergence, Computer Storage and Time

The convergence is good. At each time step, the total continuity error on sweep 60 has reduced to an order of 1.E-3. The monitored values of all variables have converged to 4 decimal places.

The essential in-core space used is 4186 for NX=40.

For the case, which is No.3 in Table 7-2 of Section 7.6.4, a 150 time-step run takes approximately 6875 sec. on a Perkin Elmer 3220 mini-computer.

## 7.8 Discussions

The main interest in this investigation is to explain the oscillation-phenomena in the combustion system studied and

to identify the significant factors responsible for low-frequency, large-amplitude pressure oscillations. The results presented above provide the information to understand the mechanism of oscillations, which is now discussed.

Oscillation-Sustained Mechanism

It is evident in Figure 7-7 that "stable" oscillations may occur under favourable conditions after a steady-state flame has been disturbed.

An examination of property distributions at successive instants through a "stable" cycle, such as shown in Figure 7-8 to 7-11 suggests that the following mechanism seems to operate :

A pressure wave, travelling at sound speed upstream along the duct, has a greater effect on the velocity of the hotter gas than that of the colder one because of the density difference, resulting in an increase of relative velocity between them; in turn, it leads to a higher local burning rate. If the periodic component of the rate addition is in phase with the oscillating components of the pressure, the latter will be excited as indicated by the Rayleigh criterion (Rayleigh 1945). It needs only a few cycles of the oscillating pressure for it to become so

successively amplified, that a continuous increase of the burning rate results. The rise of the mean pressure caused by the increased burning rate is accompanied by the flame moving upstream. As the flame advances upstream its area reduces, which tends to decrease the burning rate, leading to a pressure drop, thus the flame is pushed downstream by the approach flow. Following that, the flame area increases, thence the burning rate accompanied by emission of further pressure wave, in such a way the process sustains itself.

It follows that the oscillation is a combined consequence of the accoustic oscillation and the non-accoustic interaction between flow field and heat release. The mean pressure oscillation coupling with the movement of the flame modulates the acoustic oscillation. The former is characterized by a low frequency and is often referred to as "buzz", which is just shown in Figure 7-7.

The Physical Meanings of Parameters

In the present investigation a systematic, parametric study has been performed to establish instability regions. It is convenient to introduce the physical meanings of these parameters before a discussion of the formation of instability regions. There is no need to explain the Mach number and the density ratio, $\rho_2 / \rho_1$ , which are familiar to readers.

Cm/Cf

In the present model the friction between the two fluids acts as one of the damping factors, while the entrainment rate of the cold gas into the hot gas acts as the energy for sustaining oscillations. Therefore, the parameter, Cm/Cf, represents the ratio of two interfluid exchange rates, that of the mass-transfer to that of the momemtum transfer. However, the mass-transfer is synonymous with the addition of combustion heat in the present model.

LCm

In the present model the fragment size is proportional to the duct width, as expressed in Equation 7.8, so that the dimensionless parameter, LCm is proportional to L/Y, a dimensionless duct length-width ratio.

Formation of Instability Region and the Effect of Physical Parameters

An inspection of Figures 7-13,7-15 and 7-17 shows that the instability occurs within defined limits of LCm, which implies that instability is likely to occur if L/Y exceeds a minimum value for a sufficiently small fraction of the gases to be burned for the minimum energy to excite the system, but is less than a much larger value which is great enough for the whole of the gas to be burned. The

existence of the lower-limit of L/Y has been supported by experimental findings (Campbell 1982, Heitor et al 1984).

As mentioned above, Cm/Cf represents the ratio between the energy input for sustaining oscillations and the damping factors; it will be, therefore, expected that the greater value of Cm/Cf results in a higher amplitude when oscillations occur, as shown in Figure 7-14 (a) & (b); and instability region becomes narrower as Cm/Cf decreases, as shown in Figure 7-13.

The effect of $\rho_2/\rho_1$ on the instability region appears more complicated. It is mainly through the gas expanding and the velocity difference between the two fluids. The former affects the pressure developing in the duct and the latter affects the entrainment rate and hence the energy input to the system. $\rho_2/\rho_1$ indicates :

(i) Gas expands more when higher combustion energy is available.

(ii) When the difference between $\rho_2$ & $\rho_1$ is higher, the "slip" velocity is higher, hence the entrainment and combustion energy is higher locally.

The effect of the Mach number are twofold. On one hand, the high flow velocity may enhance the entrainment rate

resulting in a pressure rise; and on the other hand, it will speed up the energy release by moving the hot gas out of the duct.

## 7.9 Closure

The two-fluid model of turbulent combustion has been applied to one-dimensional, unsteady, confined, premixed flames of an idealized character.

The first type of disturbance, i.e. a sudden change in back pressure, to the established steady-state flame has been explored. The instability regions and their conditions, under which combustion oscillations may occur, have been established through parametric studies.

The results obtained provide the information in understanding the mechanism of the "buzz"-phenomenon, thereby, the ability of the two-fluid model in representing some important aspects of reality has been demonstrated.

Further prediction will be performed in the next chapter, where the oscillatory boundary conditions will be explored, leading to a "resonance"-phenomenon.

# CHAPTER 8-THE APPLICATION OF TWO-FLUID MODEL OF TURBULENT COMBUSTION TO AN IDEALIZED,ONE-DIMENSIONAL, UNSTEADY, CONFINED, PREMIXED FLAME (II) - INVESTIGATION ON THE OSCILLATORY MASS FLOW RATE AT THE INLET

## 8.1 Introduction

In the last chapter, the ability of the two-fluid model in simulating combustion oscillations has been demonstrated by exploring a sudden change in resistance to the flow at the duct exit. This chapter presents further predictions, i.e. the exploration of oscillatory boundary conditions in the same flow system.

In this investigation, the maximum response in amplitude of the flow characteristics to the variation in frequencies at the inlet, i.e. "resonance", is searched.

The results obtained are presented and discussed leading to a definite conclusion on the two-fluid model.

## 8.2 Problem Specification

The physical and mathematical description of the problem has already been given in Section 7.5 of the last chapter; however, in this chapter, the oscillatory boundary condition for mass inflow at the duct inlet is employed

instead of the sudden change in back pressure at the outlet used in the last chapter.

The oscillatory boundary condition is set to conform to a cosine function of time, as shown in Figure 8-1.

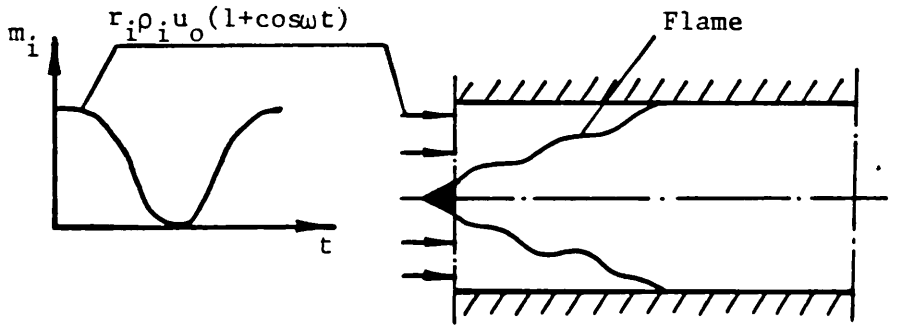



Figure 8-1 The variation of mass inflow with time at the inlet

Boundary conditions are given mathematically below.

<u>At the Inlet</u>, the mass inflow rate is suddenly changed from a constant value to an oscillatory one after a large first time-step.

$$x = 0\ ,\quad 0 < t < 100\ \text{sec}\ ,\quad m_1 = 0.9\ u_1\rho_1\ ,$$
$$m_2 = 0.1\ u_2\rho_2\ ,$$
$$u_1 = u_2 = u_o\ ;$$
$$t > 100\ \text{sec}\ ,\quad m_1 = 0.9\ u_1\rho_1\ ,$$
$$m_2 = 0.1\ u_2\rho_2\ ,$$
$$u_1 = u_2 = u_o(1+\cos\omega t)\ . \qquad (8.1)$$

At the Outlet, the atmospheric pressure is specified.

$$x = L \ , \qquad P = 0 \ N/m^2 \ \text{(relative to 1.E5 } N/m^2\text{)}$$

Initial conditions are the same as those set in Section 7.5.2.

## 8.3 Dimensionless Parameters

In addition to the parameters used in Section 7.5.2, another dimensionless parameter which characterizes the oscillatory boundary condition employed here is :

$$\frac{\omega * L}{u_o}$$

where , $\omega$ is the frequency of oscillatory mass inflow rate, $L$ is the duct length, $u_o$ is the mean value of the approach flow velocity.

Consequently, any performance variable for the process, $\phi$ , can be written as a function of following dimensionless parameters :

$$\phi = \phi \ ( \ Ma, \ LCm, \ Cm/Cf, \rho_2/\rho_1, \ NX, \ \delta t * u_o/L, \ \omega * L/u_o ).$$

It will be seen in Section 8.5 that $\phi$ has been chosen as a dimensionless pressure, $P_{max} \ / P_{ref}$ , where $P_{max}$ is the amplitude of pressure oscillation at a given frequency, $\omega * L/u_o$ ;and $P_{ref}$is the pressure at zero frequency of the

oscillatory boundary condition.

## 8.4 The Cases Investigated

For this type of boundary condition explored, the maximum response in amplitude of the flow characteristics to the variation in frequencies at the inlet, i.e."resonance", is searched. Therefore, under given conditions, the results will be plotted in terms of $P_{max}/P_{ref}$ versus $\omega*L/u_o$.

Four cases have been investigated, they are different from each other by only one parameter; and conditions of these cases are listed in Table 8-1 below.

Table 8-1 Conditions for the Cases Investigated

| Case No. | Conditions | | | | | |
|---|---|---|---|---|---|---|
| | LCm | Cm/Cf | Ma | $\rho_2/\rho_1$ | NX | $\delta t*u_o/L$ |
| 1 | 100 | 4.348 | 0.027 | 0.2 | 40 | 0.01 |
| 2 | 100 | 4.348 | 0.134 | 0.2 | 40 | 0.01 |
| 3 | 100 | 4.348 | 0.027 | 0.3 | 40 | 0.01 |
| 4 | 200 | 4.348 | 0.027 | 0.2 | 40 | 0.01 |

## 8.5 Presentation of Results

### Case 1

Figure 8-2 shows the dependence of the amplitude of the pressure oscillation on the frequency of the mass inflow rate.

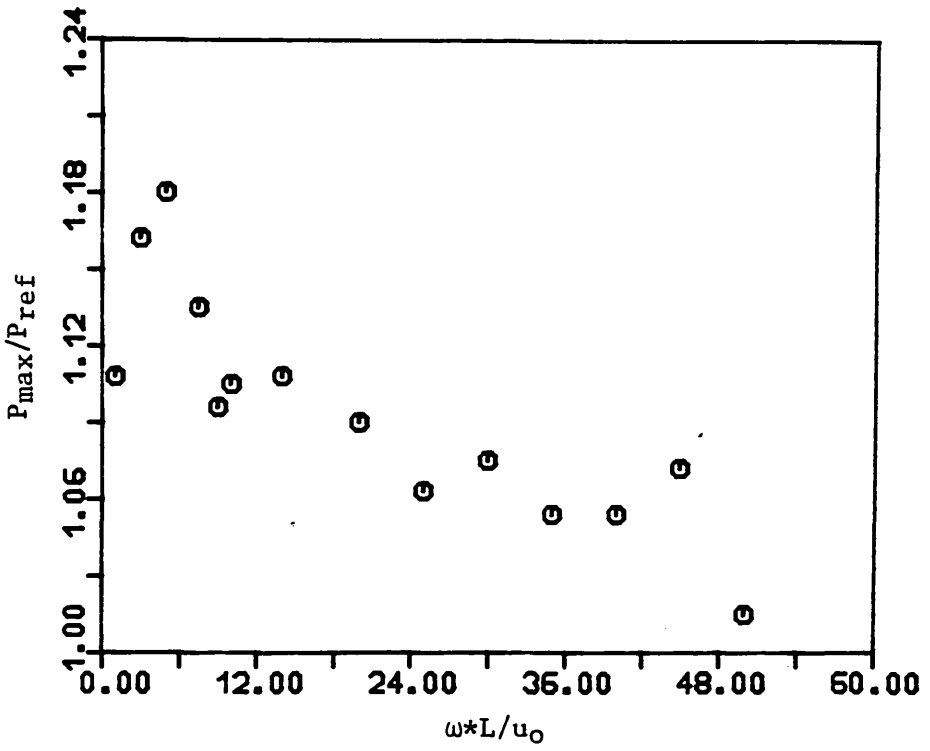
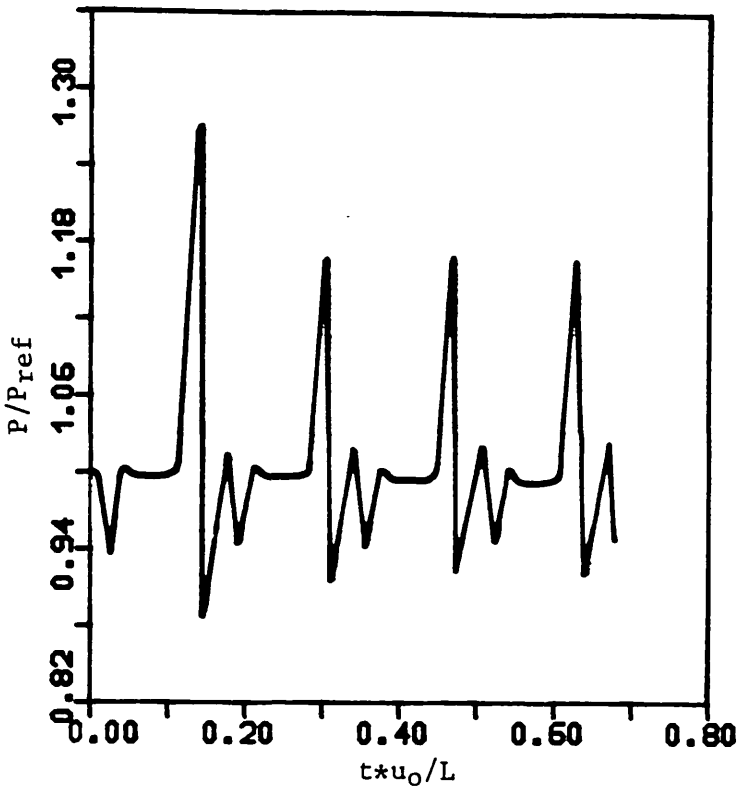
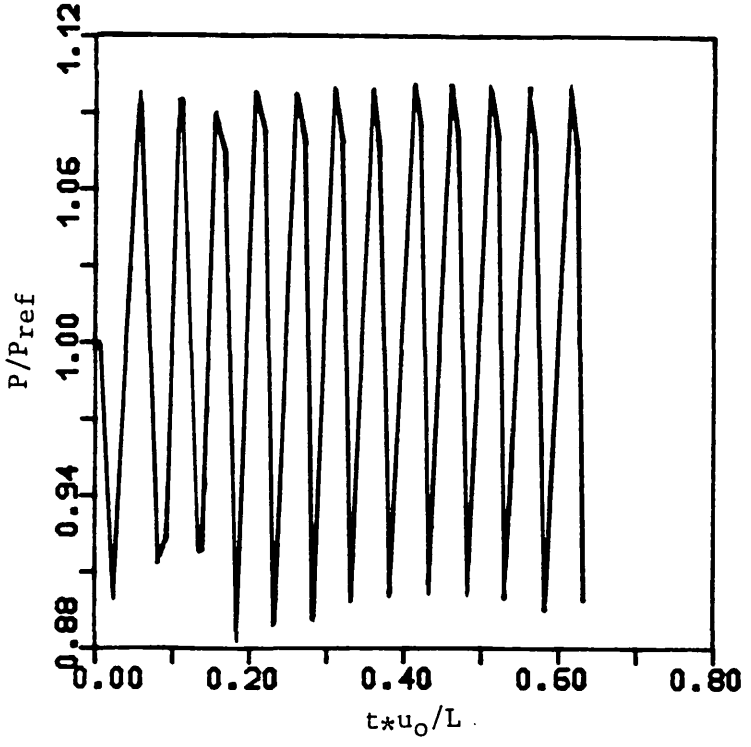



Figure 8-2 The dependence of the amplitude of pressure oscillation on the frequency at intake. Conditions are : LCm=100, Cm/Cf=4.348, Ma=0.027, $\rho_2/\rho_1$=0.2, NX=40, $\delta t*u_o/L$=0.01.

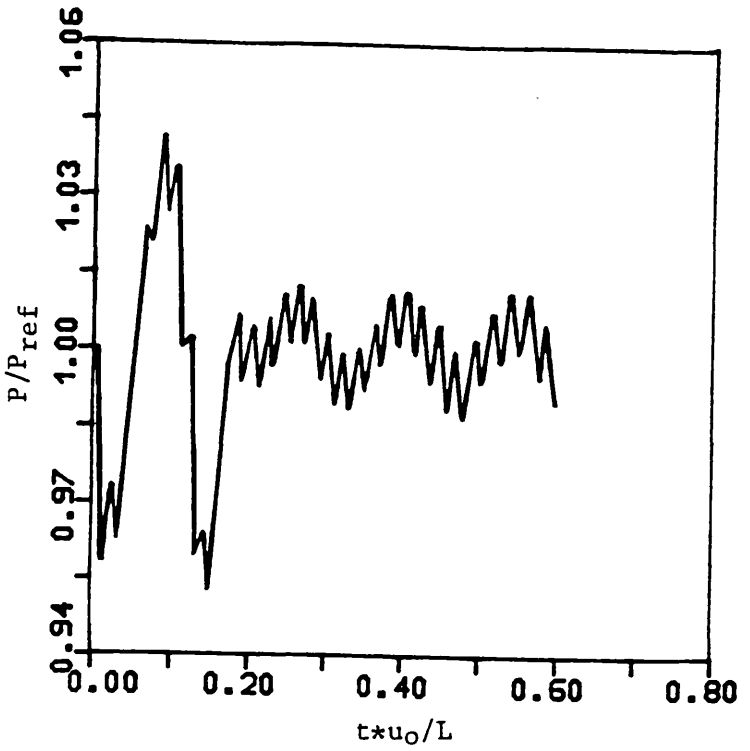
Characteristics of oscillations at different $\omega*L/u_o$ for the fixed parameters given above are shown in Figure 8-3 (a-c).




(a) $\omega * L / u_o = 5$




(b) $\omega * L / u_o = 20$




(c) $\omega * L/u_o = 50$

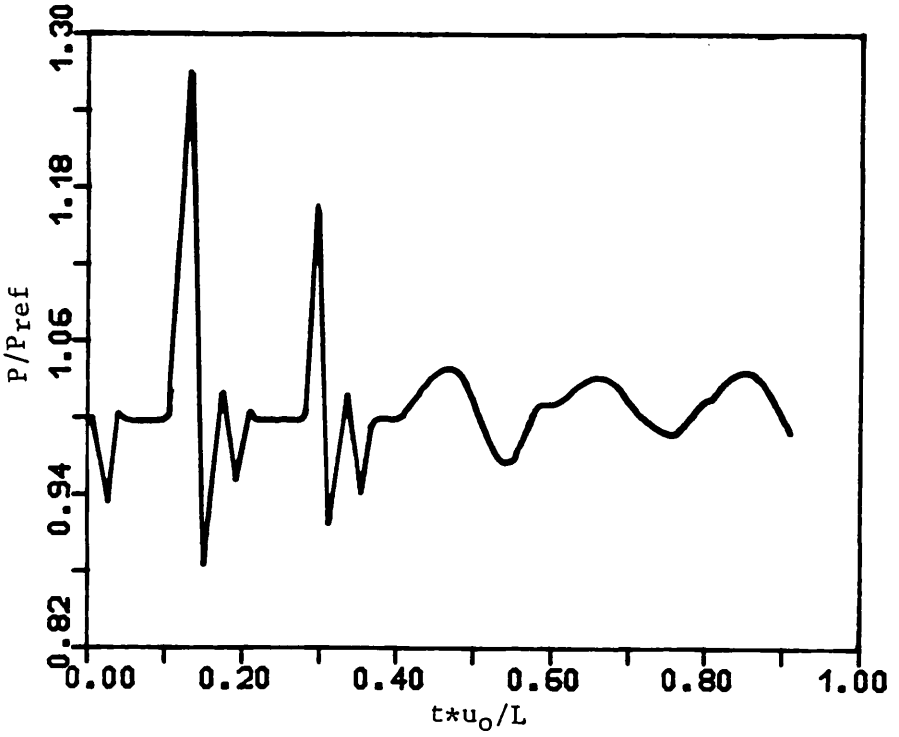
Figure 8-3 The variation of pressure with time for different frequencies referring to Figure 8-2.

It can be seen from Figure 8-2 that results indicate a kind of "resonance", i.e. a peaking of the amplitude when plotted against frequency.

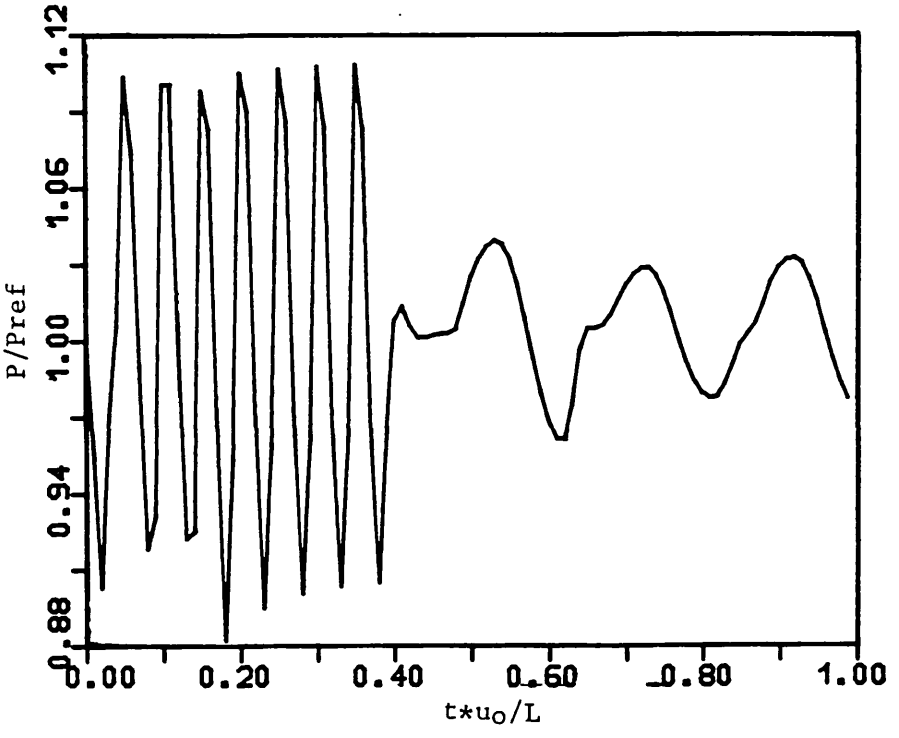
An inspection of the parameters employed in this case reveals that they fall into the "stable" oscillation region in Figure 7-12; it will be, therefore, expected that once oscillations have been induced by the imposed oscillatory boundary condition, they may continue even after the latter has been removed.

The oscillation characteristics with the sudden removal of

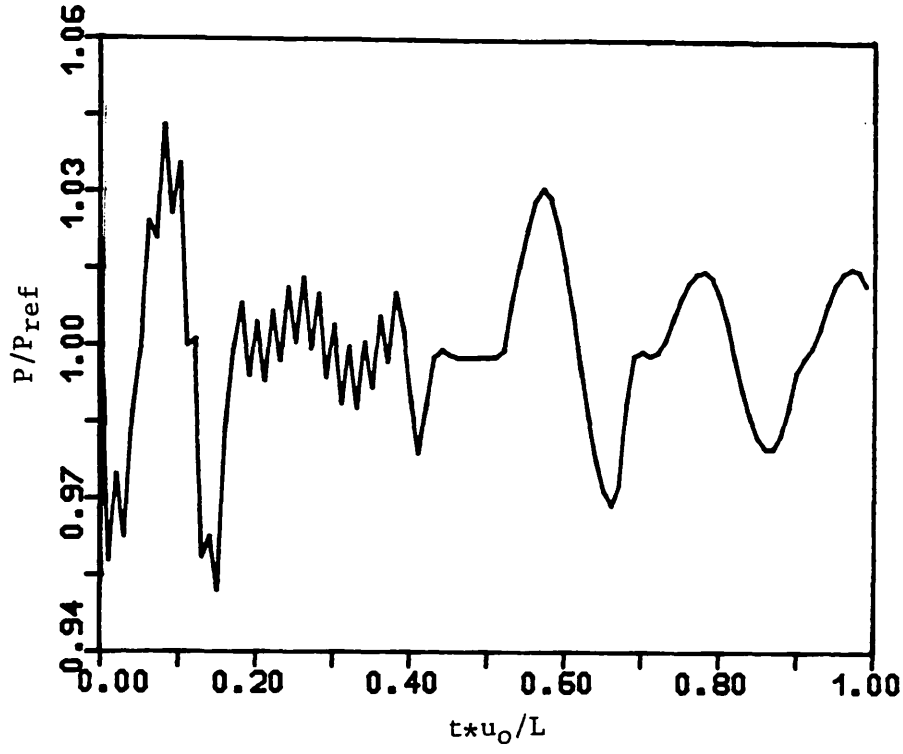
the oscillatory boundary condition (changed to a constant mass inflow rate) at t*=0.4 are shown in Figure 8-4 (a-c).




(a) $\omega^* L/u_o = 5$




(b) $\omega^* L/u_o = 20$




(c) $\omega * L/u_o = 50$

Figure 8-4 The oscillation characteristics with the oscillatory boundary condition removed at $t^* = 0.4$.

As is seen from Figure 8-4, the frequency and amplitude of continued oscillations after the oscillatory boundary condition has been removed are almost independent of the frequency imposed as the boundary condition. The frequency of these undamped oscillations is equal to 5 approximately. It turns out to be the "resonance" frequency in Figure 8-2.

Case 2

Figure 8-5 shows the dependence of the amplitude of the

pressure oscillation on the frequency of the mass inflow rate for case 2 in Table 8-1, in which only the Mach number is changed to 0.134, and other parameters remain the same as that of Case 1.

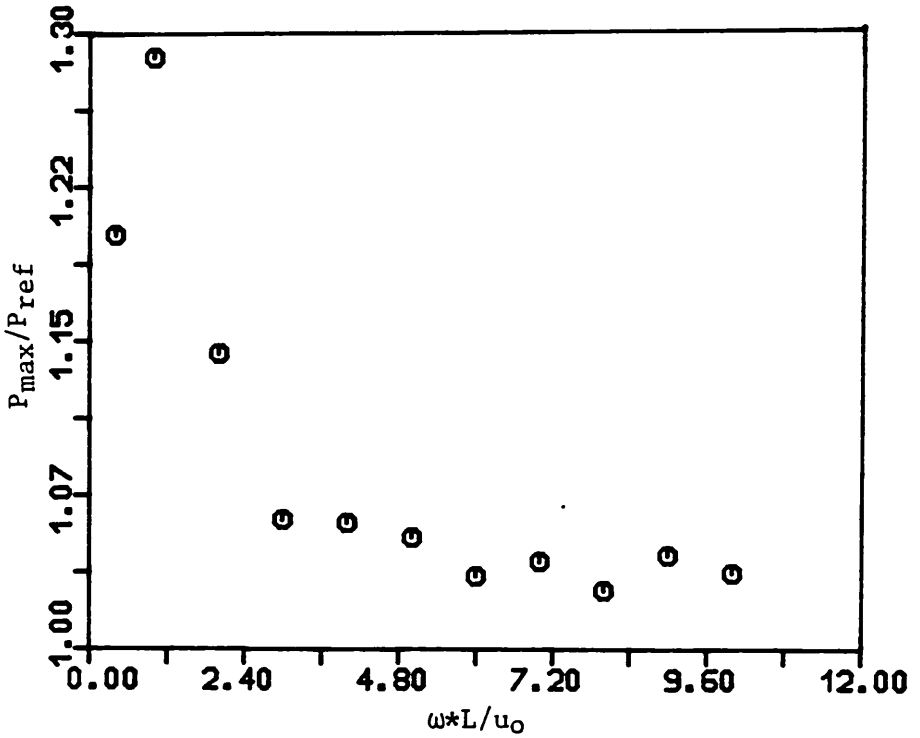
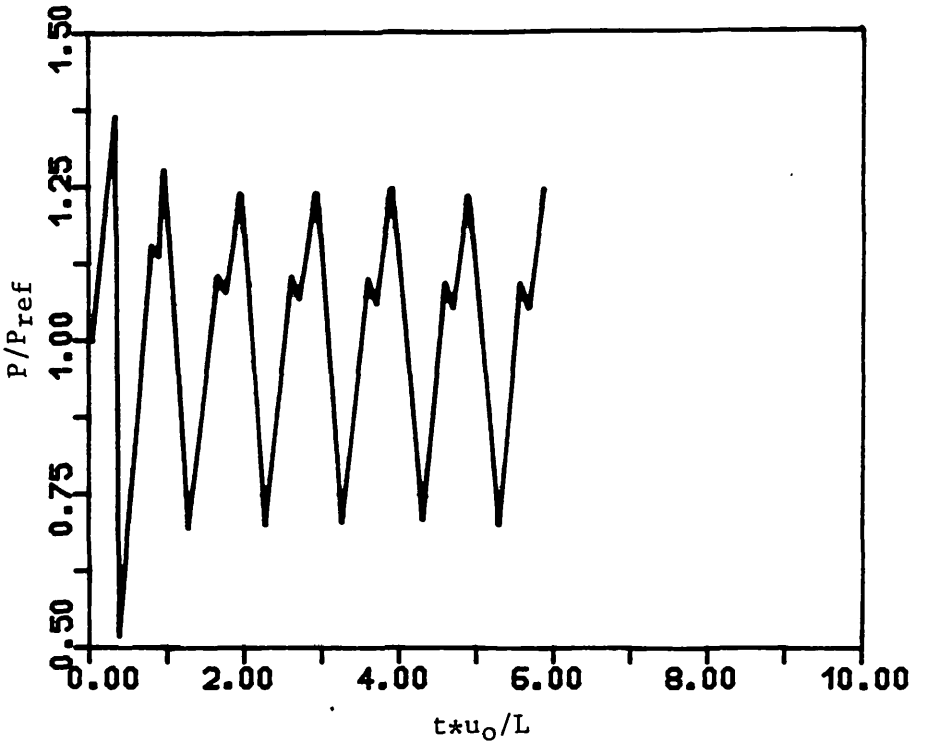
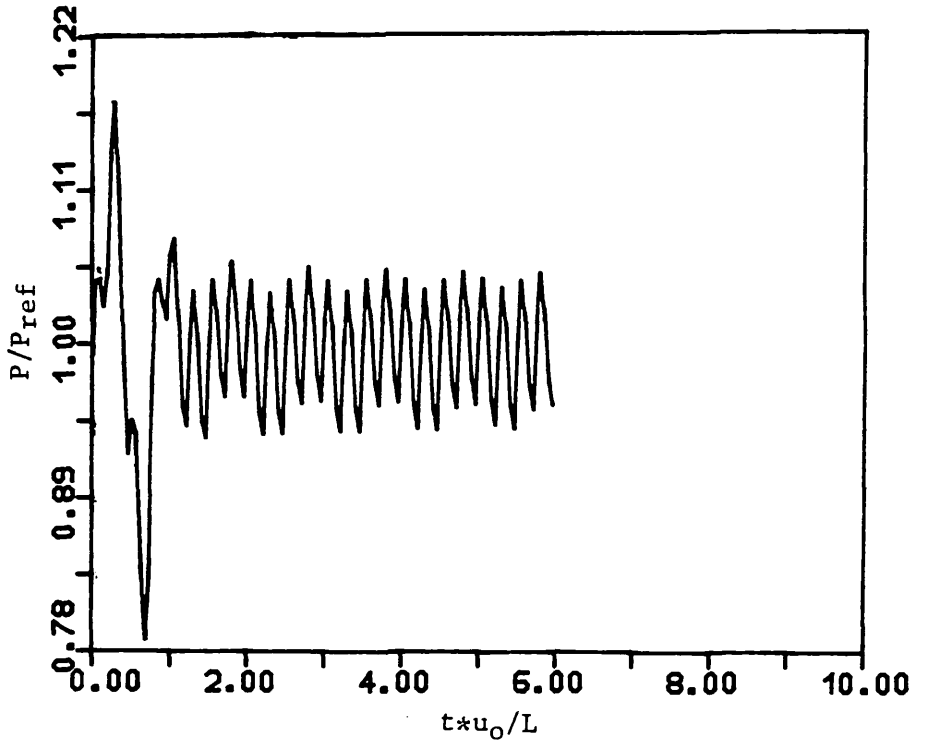



Figure 8-5 The dependence of the amplitude of pressure oscillation on the frequency at intake. Conditions are : LCm=100, Cm/Cf=4.348, Ma=0.134, $\rho_2/\rho_1$=0.2, NX=40, $\delta t*u_o/L$=0.01.

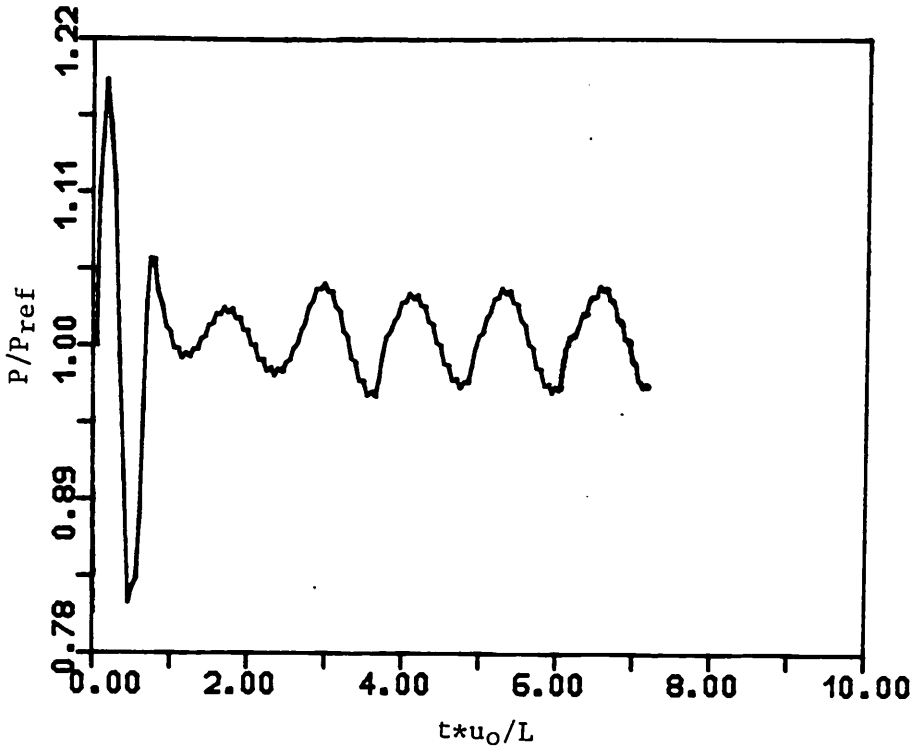
The characteristics of these oscillations at different $\omega*L/u_o$ for the fixed parameters given above are shown in Figure 8-6 (a-c).




(a) $\omega * L / u_o = 1$



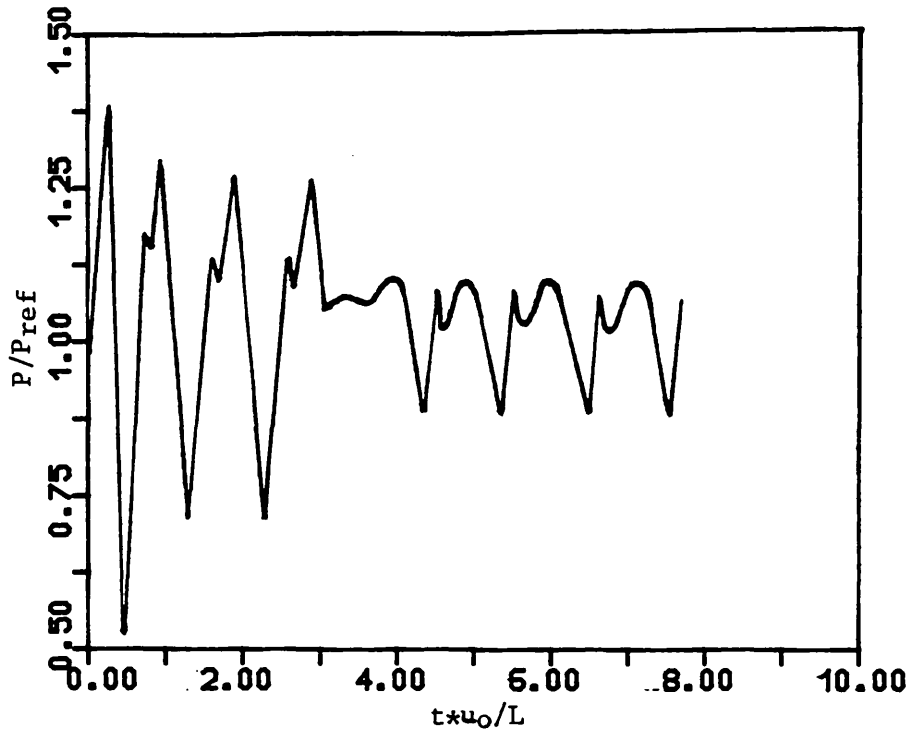

(b) $\omega * L / u_o = 4$



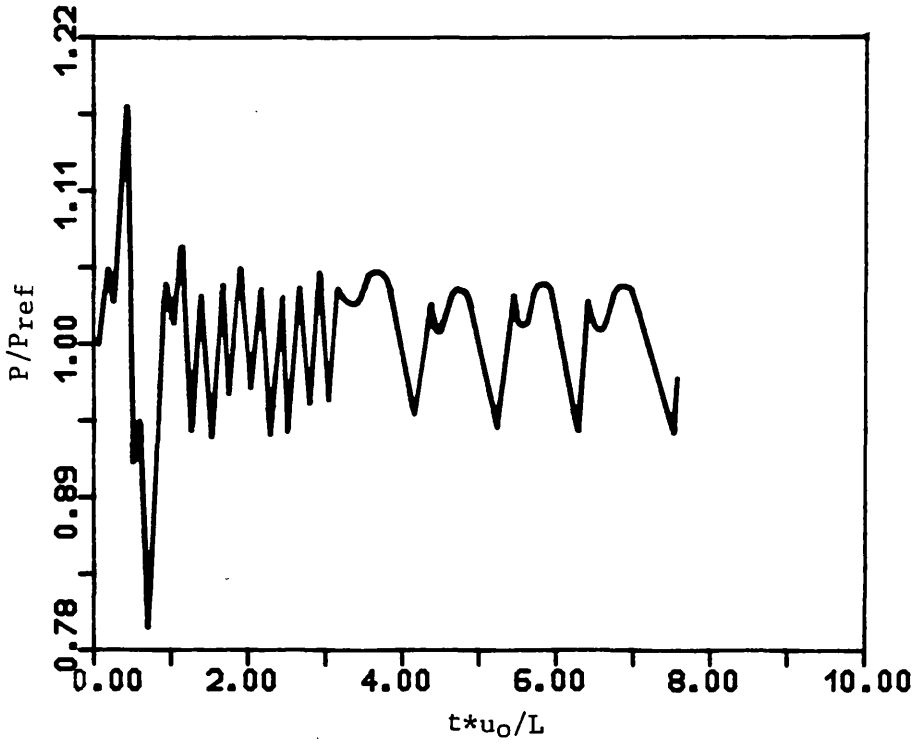

(c) $\omega * L/u_o = 10$

Figure 8-6 The variation of pressure with time for different frequencies referring to Figure 8-2.

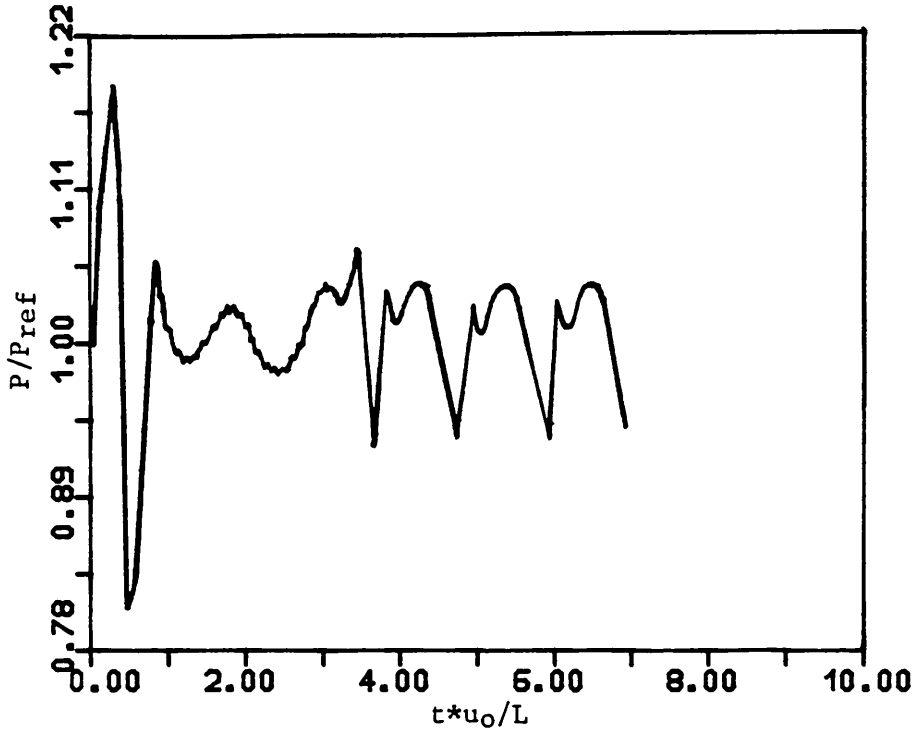
The oscillation characteristics with a sudden removal of the oscillatory boundary condition at t*=3 are shown in Figure 8-7 (a-c).




(a) $\omega * L/u_o$




(b) $\omega * L/u_o$




(c) $\omega * L/u_o = 10$

Figure 8-7 The oscillation characteristics with the oscillatory boundary condition removed at $t^*=3$.

Again, Figure 8-7 shows that the frequency of undamped oscillations after the oscillatory boundary condition has been removed is independent of the frequency imposed as the boundary condition. The frequency of undamped oscillations in this case is equal to 1 approximately, which is the "resonance" frequency in Figure 8-5.

Case 3

Figure 8-8 shows the dependence of the amplitude of pressure oscillation on the frequency at intake for Case 3

in Table 8-1; in this case, only $\rho_2/\rho_1$ is changed to 0.3 and other parameters remain the same as that of Case 1.

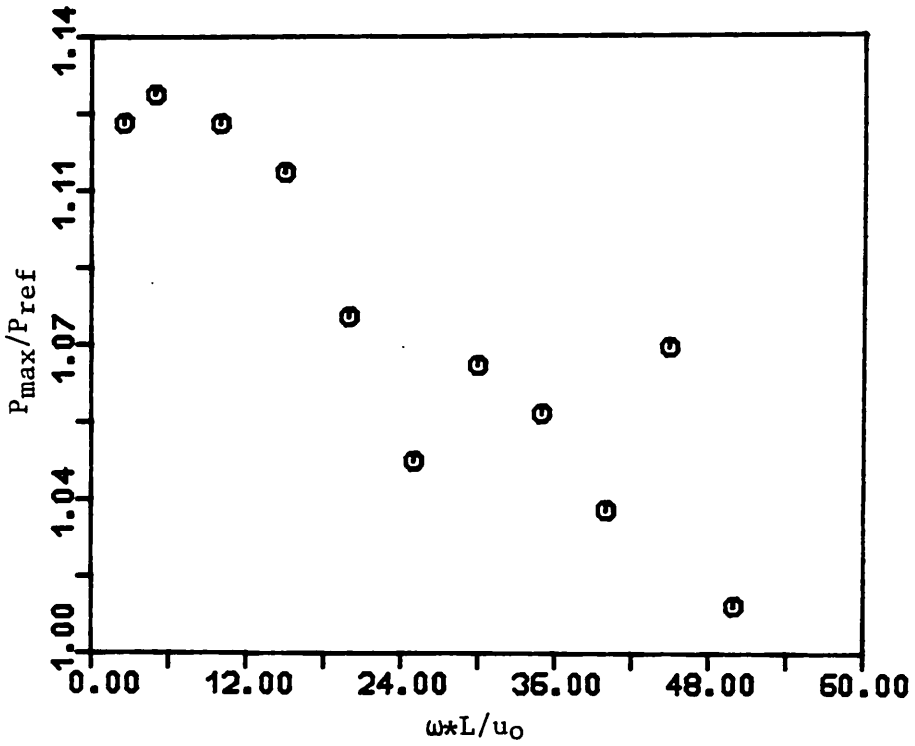



Figure 8-8 The dependence of the amplitude of pressure oscillation on the frequency at intake. Conditions are : LCm=100, Cm/Cf=4.348, Ma=0.027, $\rho_2/\rho_1$ =0.3, NX=40, $\delta t*u_o/L$=0.01.

As is seen, the results in Figure 8-8 still show the "resonance" phenomenon.

Case 4

Figure 8-9 shows the dependence of the amplitude of pressure oscillation on the frequency at intake for Case 4 in Table 8-1; in this case only LCm is changed to 200 and other parameters remain the same as that in Case 1.

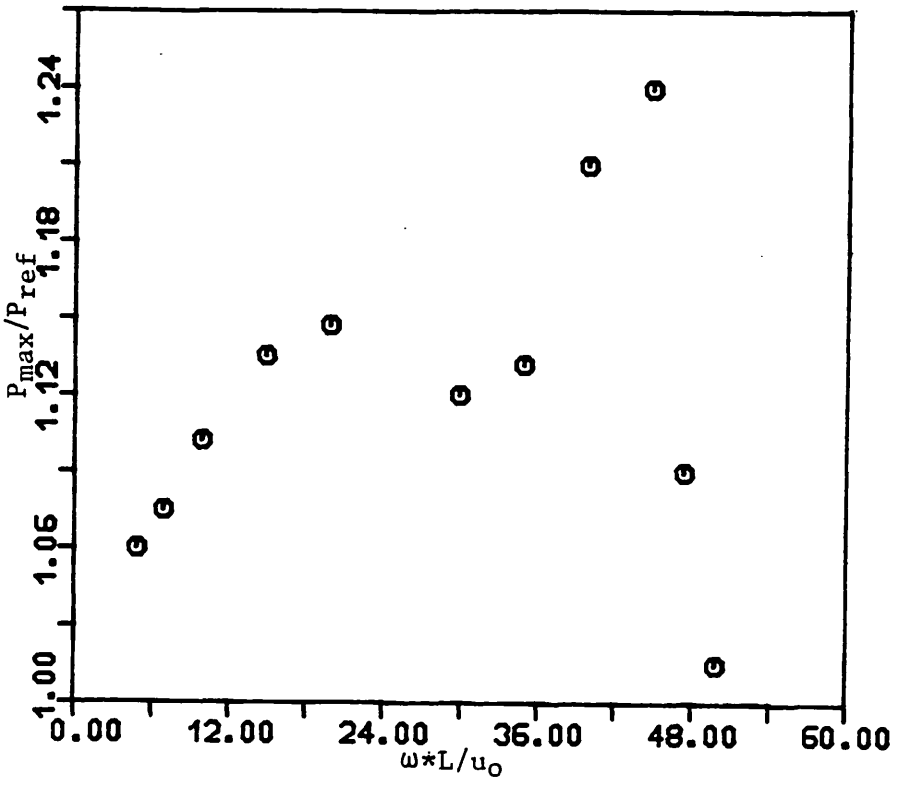



Figure 8-9 The dependence of the amplitude of pressure oscillation on the frequency at intake. Conditions are : LCm=200, Cm/Cf=4.348, Ma=0.027, $\rho_2/\rho_1$=0.2, NX=40, $\delta t*u_o/L$=0.01.

A peaking of the amplitude can be seen in Figure 8-9, and it is shifted to the higher frequency side.

The parameters employed in this case are outside the "stable" oscillation region in Figure 7-12; therefore, the oscillations induced by the oscillatory boundary condition will die away if the latter has been removed. An example for this situation is depicted in Figure 8-10, where $\omega*L/u_o$equal to 10 is chosen from Figure 8-9.

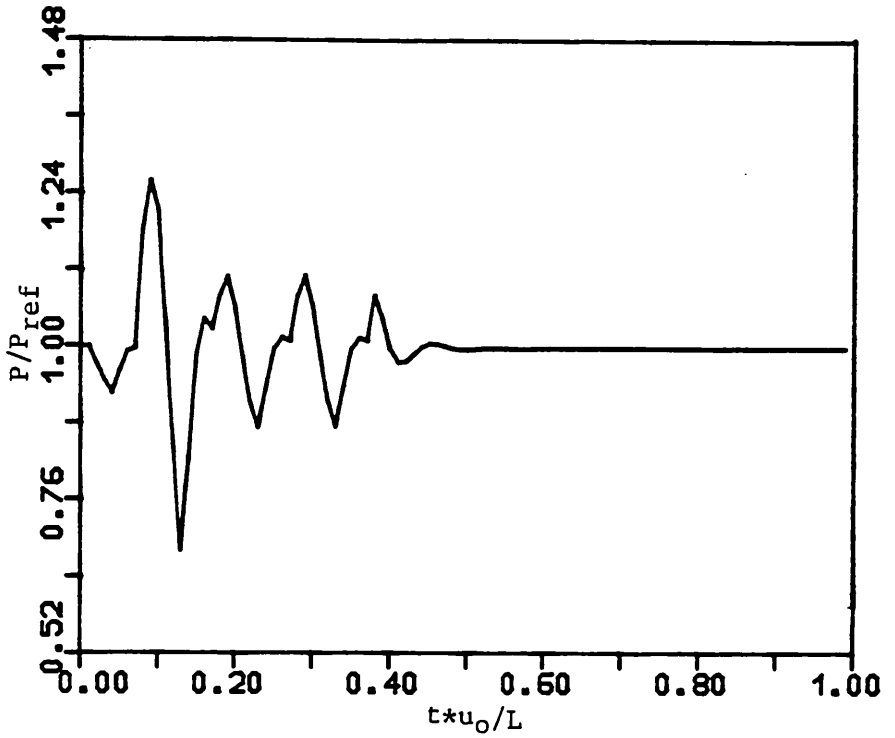



Figure 8-10 The oscillation dies away after the oscillatory boundary condition has been removed at $t^*=0.4$. ( $\omega^*L/u_o=10$)

## 8.6 Discussions

### "Resonance" Induced by Oscillating Flow

It is well known that in a forced vibration-system, if the frequency of the periodic force is equal to the natural frequency of the system upon which it acts in phase, then the force will always act in the direction of motion, hence energy will continually be added to the vibrating system, causing the amplitude to increase. This phenomenon is called the "resonance", and the value of the forced

frequency equal to the natural one is called the "resonance" frequency.

The results given in Figures 8-2, 8-5, 8-8 and 8-9 show the analogous phenomenon in the combustion system investigated, where a kind of resonance occurs when the oscillatory boundary condition is imposed. In such a case, the forced frequency is that of the boundary condition variation, and the natural frequency of the system is that of the undamped oscillation in the absence of oscillatory boundary condition; this natural frequency is independent of external disturbances, as evidenced by Figure 8-4 (a-c) & Figure 8-7 (a-c). Its practical implication is that a large amplitude oscillation with the low frequency may be induced by a undamped oscillatory disturbance in the combustion system as a result of "resonance".

The existence of the "resonance" under imposed oscillatory disturbance has been shown by the experiments (Blackshear 1956).

Remarks on the Model

The predictions presented in the last chapter and this chapter show that with the appropriate input parameters, the experimentally observed features of combustion oscillations have been simulated by the two-fluid model, with, at least, qualitative realism.

The explanation of the "buzz"-phenomenon, by reference to the two-fluid model, is restricted to the model assumptions adopted in this study.

In order to make predictions with the model fit the experimental data, some aspects still need to be explored; particularly the fragmentation formula , the suitability of which is not well represented by the one-dimensional simulation, needs to be further refined by a systematic comparison with experiments.The information on the fragmentation process may be also provided by computational fluid dynamics. The work presented in the first part of this thesis, where the single-fluid theory has been applied to the simulation of wrinkled laminar flames, may provide useful information on the fragment-formation, -distortion and -interaction processes, which are necessary to formulate the interfluid transfer and fragmentation formulae which appear in the two-fluid model. The combined use of the single-fluid theory and two-fluid theory may contribute to the understanding of complex combustion process such as combustion oscillations and give a complete description of the phenomena.

Although refinements of the model are required, it is believed that a step has been taken to lead, in the end, to the quantitative understanding of combustion oscillation.

## 8.7 Closure

The ability of the two-fluid model has been demonstrated by simulating combustion oscillations through the exploration of two types of disturbance to the flow. It is the present auther's opinion that the potential of the two-fluid model is much greater than that demonstrated in this thesis.

In order to make predictions with the two-fluid model fit the experimental data quantitatively, further refinements on the model and an extension of the application of the model to the unsteady flames in two dimensions are required.

# CHAPTER 9 - CONCLUSIONS

This, the last chapter of the thesis, provides a summary of the main conclusions of the present investigation on wrinkled laminar flames and unsteady turbulent flame propagation in Sections 9.1 and 9.2; Section 9.3 contains some suggestions for future research.

## 9.1 Experimental Work

An experimental study of the flame wrinkling in a vented combustion chamber has been performed to supplement the theoretical analysis.

The effects of various experimental factors, such as the gravity force, the mixture ratio, the initially covered vent opening, the vent lay-out and size have been investigated in comparative isolation. A preliminary investigation on the effect of obstacle is also included.

The experimental results indicate that the Rayleigh-Taylor instability due to the effect of gravity force has been overshadowed by the Landau instability due to the thermal expansion of gases in the present series of experiments. In comparison with the rich or lean mixture, the near-stoichiometric mixture favours the flame wrinkling. The flame wrinkling may augment the total area of the flame leading to an increase in the volumetric burning rate;

besides, the results also show a local increase of burning rate in the cusps of wrinkled flame fronts.

The phenomena of flame wrinkling under various operating conditions have been recorded by means of motion pictures and still photographs. The latter has been used for the comparison with the corresponding predictions.

## 9.2 Theoretical Work

### (a) Single-Fluid Computation

A mathematical model and solution procedure, i.e. the single-fluid approach developed by Spalding and Awn (1978) has been refined to predict two-dimensional, unsteady, reacting flows with a "fragmentary character".

The particle-tracking technique and a density calculation method, as a supplement to the combustion model adopted in the present study, have been introduced into the solution scheme. These method provide a valuable tool for the study of the flows under consideration, which allows numerical simulation of the interaction between flow fields and flames. The use of a volumetric continuity equation instead of the customary mass continuity equation is another important feature in the present computational procedure, which is effected by the GALA algorithm

embodied in PHOENICS.

The present computational procedure has been tested by the predictions, which are compared with the experimental results obtained in the present investigation. The agreement in trends between the predictions and experiments is found; and the effect of gravity on the flows has been well predicted. The velocity field in the unburned-gas region presented appears to be realistic. However, the small-scale wrinkles have not successfully been predicted; the reason may attribute to the numerical errors resulting from the extrapolation scheme in evaluating the particle velocity in the particle-tracking technique.

The usefulness of the above approach in providing information on the flame wrinkling has been also well demonstrated by the simulation of the wrinkled flames in simpler circumstances, as summarized below :

(i) The detailed calculations of formation of the wrinkled flame-front presented clearly confirm that the wrinkling is caused by the combustion-induced flow due to the thermal expansion of gases.

(ii) The effect of the gravitational force on the flame behaviour is that of the Rayleigh-Taylor instability.

(iii) The rate of the growth of instabilities is found to increase as the burning velocity or the density difference between the unburned gas and the burned gas increases respectively, or as the wavelength of the perturbations decreases.

In conclusion, the prediction procedure described above constitutes a useful approach to the analysis of wrinkled laminar flames. The foundations for such analysis have been laid, although further improvements are needed.

(b) Two-Fluid Computation

The two-fluid model of turbulent combustion has been applied to one-dimensional, unsteady, confined, premixed flames of an idealized character.

Two types of disturbance introduced to the flow system have been investigated, leading to the "stable" oscillation and a "resonance"-phenomenon to be established.

The parametric studies have been performed to establish the instability conditions under which combustion oscillations may occur.

The results presented show that the experimentally

observed features of the combustion oscillations have been plausibly simulated and compile the information to understand the mechanism of oscillation as follows:

The oscillation is a combined consequence of acoustic oscillation and non-acoustic interaction between flow field and heat release. The mean pressure oscillation coupling with the movement of the flame modulates the acoustic oscillation. The former is characterised by a low frequency and is often referred to as "buzz". The large amplitude oscillation with the low frequency may be induced by a undamped oscillatory disturbance in the combustion system as a result of "resonance".

The ability of the two-fluid model to represent such a complex combustion process, therefore, has been demonstrated.

(c) The Significance of Combined Use of the Single-Fluid Theory and the Two-Fluid Theory

As is seen from the present study, both the single-fluid theory and the two-fluid theory may be employed for the computer simulation of the flows with fragmented interfaces.

In the present two-fluid calculation, the "fragmentary character" of the flows under consideration has not been

well represented by the one-dimensional simulation; however, the work presented in the first part of this thesis, where the single-fluid theory has been applied to the simulation of wrinkled laminar flames, has provided useful information on the fragment-formation,-distortion and -interaction processes.

An extension of the application of the two-fluid model to the unsteady flames in two dimensions and then a comparison with the single-fluid predictions may reveal the similarity in fragmentation between the wrinkled laminar flames and unsteady turbulent flames. Therefore, the combined use of the single-fluid theory and the two-fluid theory may contribute to the understanding of complex combustion process such as combustion oscillations and give a complete description of the phenomena. As an exercise, this study has shown the significance of combined use of these two theories in computational fluid dynamics.

## 9.3 Suggestions for Future Work

### Experiment

The present experimental investigation has been restricted to the visualization of flames; the pressure measurement will be very useful to map the variation of flame

behaviour with the pressure.

In order to provide the information on the fragmentation process for the two-fluid model, a new experiment, designed in such a way that the pressure gradient is the dominant factor responsible for the flame wrinkling leading to a smaller-scale fragmentation, is needed.

In order to obtain the detailed information on flame wrinkling it is desirable to record the phenomena by a high speed framing camera instead of the video-cassette recorder used in the present investigation, and it is particularly true of the investigation on a smaller-scale fragmentation.

Single-Fluid Computation

The potential of the basic numerical procedure for simulating wrinkled laminar flames has been demonstrated in this thesis. Following suggestions are for improving the present predictions and for extending its capability.

(i) As described in Section 4.5.2 and discussed in Section 5.5, the numerical errors may result from the extrapolation scheme in evaluating the velocity components of the particles in the particle-tracking technique. An improvement on this scheme is needed. One of the possible methods is to take the weighted

average value from all the velocity components of the unburned gas surrounding the particle , as shown in Figure 9-1.

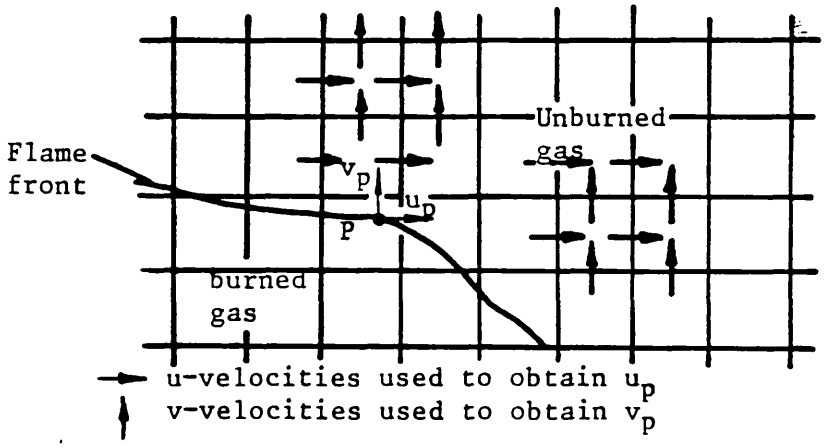



Figure 9-1 Velocities used in the evaluation of the particle velocity.

(ii) Although the present procedure is developed mainly for simulating the two-fluid flows, it may be extended for the simulation of a multi-fluid flow; two flames propagating in the combustion chamber such as the flame propagation over an obstacle shown in Figure 2-11 is an example. In that case, the basic procedure embodied in the particle tracking and the density calculation needs to be repeatedly used.

Two-Fluid Computation

(i) In the present model, the interfluid heat transfer and the reaction within the hot-gas region have been

neglected; their influences should be explored. It requires the solution of the energy equation.

(ii) Now that the one-dimensional two-fluid model has been developed and explored, it is desirable to extend its application to the unsteady flames in two dimensions in order to make the prediction with the two-fluid model fit the experimental data quantitatively and to give a more complete description of the flows under unsideration.

REFERENCES

1. Andrews G.E. and Bradley D. (1972)
"The Burning Velocity of Methane-Air Mixtures",
Combustion and Flame, Vol.19, pp275-288,1972.

2. Andrews M.J. (1986)
"A Study of Mixing by Rayleigh-Taylor Instabilities",
Ph.D Work in Progress, Imperial College, London.

3. Awn A.G. and Spalding D.B. (1978)
"Laminar Flame Propagation in Tubes",
Second Conference of Mechanical Power Engineering, Ain Shames University, Cairo, 1978.

4. Awn A.G. (1979)
"Numerical Modelling of Flows with Moving Interfaces",
Ph.D Thesis, London University, 1979.

5. Barrere M. and Williams F.A. (1969)
"Comparison of Combustion Instabilities Found in Various Types of Combustion Chambers",
12th Symposium (International) on Combustion, The Combustion Institute, Pittsburgh, PP169-181, 1969.

6. Blackshear P.L.,Jr. (1956)
"Growth of Disturbances in a Flame Generated Shear Region",

NACA TN3830, 1956.

7. Campbell I.G. (1982)
"Combustion Oscillations in a Ducted Burner",
Ph.D Thesis, University of Southampton, 1982.

8. Campbell I.G., Bray K.N.C. and Moss J.B. (1983)
"Combustion Oscillations in a Ducted Premixed Flame",
IMechE Conference on Combustiom in Engineering, Vol.2, pp85-94, 1983.

9. Castrejio A. (1984)
"Unsteady Free-Convection Heat Transfer Inside an Annuler Cavity",
Ph.D Thesis, London University, 1984.

10. Daly B.J (1969)
"A Technique for Including Surface Tension Effects in Hydrodynamic Calculations",
J. Compt. Phys., 4, pp97-117, 1969.

11. Damköhler G.Z. (1947)
"The Effect of Turbulence on the Flame Velocity in Gas Mixture",
NACA TM1112 1947.

12. Eckhaus W. (1961)
"Theory of Flame-Front Stability",
J. Fluid Mech.,10, p80, 1961.

13. Harrje D.T. (1972)
"Liquid Propellant Rocket Combustion Instability",
NASA SP-194, 1972.

14. Heitor M., Taylor A.M.K.P. and Whitelaw J.H. (1984)
"I fluence of Confinement on Combustion Instabilities of Premixed Flames Stabilized on Axisymmetric Baffles",
Combustion and Flame 57, pp109-121, 1984.

15. Istratov A.G. and Librovich V.V. (1969)
"Stability of Flames",
Army Foreign Science and Technology Centre, Washington D.C., FSTC-23-952-68, 1969.

16. Jones W.P. and Whitelaw J.H. (1984)
"Modelling and Measurements in Turbulent Combustion",
20th Symposium (International) on Combustion, The Combustion Institute, Pittsburgh, pp233-249, 1984.

17. Karim G.A. and Singh R. (1967)
"A Thermodynamic Investigation of the Combustion of Methane",
Imperial College, London, Mech. Eng. Dept. Report

No.C/TN/3, 1967.

18. Keller J.O., Vaneveld L., Korschelt D., Hubbard G.L., Ghoniem A.F., Daily J.W. and Oppenheim A.K.(1981) "Mechanism of Instabilities in Turbulent Combustion Leading to Flashback", J. AIAA Vol.20, p254,1981.

19. Landau L. (1944) "Theory of Slow Combustion", Acta Physicochim, (URSS) 19, 77, 1944.

20. Lewis B. and Von Elbe G. (1964) "Combustion, Flame and Explosions of Gases", New York, Academic Press, 1964.

21. Libby P.A. and Williams F.A. (1981) "Some Implications of Recent Theoretical Studies in Turbulent Combustion", J. AIAA, Vol.19, No.3, p261, 1981.

22. Markstein G.H. (1949) "Interaction of Flame Propagation and Flow Disturbances", 3rd Symposium on Combustion, Flame and Explosion Phenomena, Williams & Wilkins, Baltimore, p162, 1949.

23. Markstein G.H. (1951)
"Experimental and theoretical Studies of Flame-Front Stability",
J. Aero. Sci. 18, p199, 1951.

24. Markstein G.H. (1964)
"Nonsteady Flame Propagation",
Pergamon Press, London, 1964.

25. Maxwell T.T. (1977)
"Numerical Modelling of Free-Surface Flows",
Ph.D Thesis, London University, 1977.

26. McCann D.P.J., Thomas G.O. and Edwards D.H. (1985)
"Gasdynamics of Vented Explosions Part I : Experimental Studies", Combustion and Flame, 59, pp233-250, 1985.

27. Palm-Leis A. and Strehlow R.A.(1969)
"On the propagation of Turbulent Flames",
Combustion and Flame, 13, p111, 1969.

28. Patankar S.V. and Spalding D.B.(1972)
"A Calculation Procedure for Heat Mass and Momentum Transfer in Three-Dimensional Parabolic Flows",
Int. J. Heat Mass Transfer Vol.15, p1787, 1972.

29. Patankar S.V. (1980)
"Numerical Heat Transfer and Fluid Flow",

Series in Computational Methods in Mechanics and Thermal Sciences, McGraw-Hill Book Company, 1980.

30. Petersen R.E. and Emmons H.W. (1961)
"Stability of Laminar Flames",
Physics of Fluids, Vol.4, No.4, 1961.

31. Qin H.Q. (1984)
"Computer and Water-Model Simulation of Flow Through Poppet Valves",
Ph.D Thesis, London University, 1984.

32. Rayleigh J. (1945)
"The Theory of Sound",
Vol.II, Dover Publications, Second Edition, 1945.

33. Schlichting H. (1968)
"Boundary Layer Theory",
McGraw-Hill, New York, 1968.

34. Shepherd I.G., Moss J.B. and Bray K.N.C., (1982)
"Turbulent Transport in a Confined Premixed Flame",
The Paper Submitted for Presentation at 19th International Symposium on Combustion, The Combustion Institute, Pittsburgh, pp423-431, 1982.

35. Shonerd D.E. (1952)
"Studies of Flame-Front Oscillations",

Jet Prop. Lab., C.I.T., No.3-18, 1952.

36. Solberg D.M., Pappas J.A. and Skranstad E. (1981)
"Observations of Flame Instabilities in Large Scale Vented Gas Explosions",
18th Symposium (International) on Combustion, The Combustion Institute, Pittsburgh, P1607, 1981.

37. Spalding D.B. (1972)
"A Novel Finite-Difference Formulation for Differential Equations Involving First and Second Derivatives",
Int. J. Num. Mech. in Eng. Vol.4, 1972.

38. Spalding D.B. (1974)
"A Method for Computing Steady and Unsteady Flows Possessing Discontinuities of Density",
CHAM Report 910/2, 1974.

39. Spalding D.B. (1976)
"The Calculation of Free-Convection Phenomena in Gas-Liquid Mixtures",
Imperial College, HTS Report 76/11, 1976.

40. Spalding D.B. (1981)
"A General Purpose Computer Program for Multi-Dimesnional One and Two-Phase Flow",
Mathematics and Computers in Simulation, North Holland Press, Vol.XIII, p267,1981.

41. Spalding D.B. (1982a)
"Four Lectures on the PHOENICS Computer Code",
Imperial College, CFD/82/5, 1982.

42. Spalding D.B. (1982b)
"Chemical Reaction in Turbulent Fluids",
Imperial College, CFDU Report 82/8, 1982.

43. Spalding D.B. (1983a)
"Towards a Two-Fluid Model of Turbulent Combustion in Gases with Special Reference to the Spark-Ignition Engine",
IMechE Conf. on Combustion in Engineering, Vol. 1, paper C53/83, 1983.

44. Spalding D.B. (1983b)
"Turbulence Modelling : A State-of-the-Art Review",
Imperial College, CFDU Report CFD/83/3, 1983.

45. Spalding D.B. (1984a)
"The Two-Fluid Model of Turbulence Applied to Combustion Phenomena",
AIAA 22nd Aerospace Science Meeting, Reno, Nevada, 1984.

46. Spalding D.B. (1984b)
"Turbulent Combustion with Special Reference to Diesel and Gasoline Engines",
Research Proposal Submitted to SERC, 1984.

47. Spalding D.B. (1985)
"Two-Fluid Model of Turbulence",
Imperial College, CFDU Report CFD/85/4, 1985.

48. Stewart D.G. and Nesbitt M.V. (1953)
"An Investigation of Oscillations of the Type Found in Ramjet and Reheat Combustion Chambers",
National Gas Turbine Establishment, Report No,R134, 1953.

49. Welch J.E., Harlow F.H., Shannon J.P. and Daly B.J. (1965)
"The MAC Method - A Computing Technique for Solving Viscous, Incompressible, Transient Fluid Flow Problems Involving Free Surface",
Los Alamos Scientific Lab. Report LA-3425, 1965.

50. Williams G.C., Hottel H.C. and Scurlock A.C. (1949)
"Flame Stabilization and Propagation in High Velocity Gas Streams",
3rd Symposium on Combustion, Flame and Explosion Phenomena, p21, Williams & Wilkins, 1949.

51. Wu Z.Y.J. (1984a)
"Plane Flame Propagation",
Imperial College, PDR/CFD IC/12, 1984.

52. Wu Z.Y.J. (1984b)
"Organ Pipe Oscillation",

Imperial College, PDR/CFD IC/14, 1984.

53. WU Z.Y.J (1984c)
"The Two-Fluid Model of Turbulent Combustion Applied to an Idealised One-Dimensional, Unsteady, confined, Premixed Flame",
Imperial College, PDR/CFD IC/21, 1984.

54. Yoshida A. and Tsuji H. (1984)
"Mechanism of Flame Wrinkling in Turbulent Premixed Flames",
20th Symposium on Combustion, The Combustion Institute, Pittsburgh, p445, 1984.

55. Zeldovich Ya.B., Istratov A.G., Kidin N.I. and Librovich V.B. (1980)
"Flame Propagation in Tubes : Hydrodynamics and Stability", Combustion Science and Technology, Vol.24, No.1&2, p1,1980.

56. Zeldovich Ya.B., Barenblatt G.I., Librovich V.B., and Makhviladze G.M. (1985)
"The Mathematical Theory of Combustion and Explosion",
Consultant Bureau/Plenum, New York, London, 1985

NOMENCLATURE

| SYMBOL | MEANING | LOCATION OF FIRST APPEARANCE |
|---|---|---|
| a | Coefficient of the finite-equation | Eg. (4.8) |
| A | Constant in Eg. (6.1) | Eg. (6.1) |
| C | Constant in Eg. (6.1) | Eg. (6.1) |
| Cf(=Kf/l) | Dimensional parameter | Chapter 7 |
| Cm(=Km/l) | Dimensional parameter | Chapter 7 |
| $f_{12}$ | Interfluid friction factor | Eg. (7.6) |
| $g_y$ | Body-force component in the y-direction | Eg. (3.4) |
| k | Constant in Eg. (6.1) | Eg. (6.1) |
| Kf | Dimensionless constant in the interfluid-friction factor | Eg. (7.7) |

| | | |
|---|---|---|
| Km | Dimensionless constant in the interfluid mass transfer rate | Eg. (7.9) |
| l | Fragment size | Eg. (7.7) |
| L | Duct length | Chapter 7 |
| $L_{fl}$ | Length of the flame-front lying inside a cell | Eg. (4.14) |
| $\dot{m}$ | Interfluid mass transfer rate | Eg. (7.6) |
| Ma | Mach number | Chapter 7 |
| P | Pressure | Eg. (3.3) |
| $r_1$ | Volume fraction of Fluid 1 | Eg. (7.1) |
| $r_2$ | Volume fraction of Fluid 2 | Eg. (7.3) |
| $\vec{S}b$ | Burning velocity normal to flame front | Eg. (3.7) |
| Sr | Volumetric source for the continuity equation | Eg. (4.12) |

| | | |
|---|---|---|
| $S_\phi$ | Source of the equation for $\phi$ | Eg. (3.5) |
| t | Time | Eg. (3.1) |
| $t^*(=t^*u_0/L)$ | Dimensionless time | Chapter 7 |
| u | Velocity component in the x-direction | Eg. (3.1) |
| $u_p$ | Velocity component of the particle in the x-direction | Eg. (3.6a) |
| $\vec{U}$ | Velocity vector | Eg. (3.5) |
| $\vec{U}p$ | Velocity vector of the particle | Eg. (3.7) |
| $\vec{U}unb$ | Velocity of the unburned gas at the head of flame | Eg. (3.7) |
| v | Velocity component in the y-direction | Eg. (3.1) |

| | | |
|---|---|---|
| $v_p$ | Velocity component of the particle in the y-direction | Eg. (3.6b) |
| V | cell volume | Eg. (4.1) |
| x | Distance coordinate aligned with u | Eg. (3.1) |
| $x_p$ | Distance coordinate of the particle | Eg. (3.6a) |
| y | Distance coordinate aligned with v | Eg. (3.1) |
| $y_p$ | Distance coordinate of the particle | Eg. (3.6b) |

GREEK SYMBOLS

| SYMBOL | MEANING | LOCATION OF FIRST APPEARANCE |
|---|---|---|
| $\alpha$ | Ratio of the volume of the cell occupied by the burned gas to the total volume of the cell | Eg. (4.11) |
| $\gamma$ | Ratio of specific heat at constant pressure to that at constant volume | Eg. (7.15) |
| $\rho$ | density | Eg. (3.1) |
| $\rho_b$ | Density of the burned gas | Eg. (4.11) |
| $\rho_u$ | Density of the unburned gas | Eg. (4.11) |
| $\phi$ | A scalar quantity | Eg. (3.5) |
| $\omega$ | Frequency of the oscillatory boundary condition | Chapter 8 |

SUBSCRIPTS

| SYMBOL | MEANING | LOCATION OF FIRST APPEARANCE |
|---|---|---|
| E,W,N,S,P | In Chapter 4, for east, west, north, south and central nodes respectively of the finite-domain grid | Chapter 4 |
| e,w,n,s | East, west, north and south interfaces of the control volume respectively | Chapter 4 |

# APPENDIX A = THE LISTINGS OF THE PHOENICS COMPUTER CODE FOR THE SINGLE-FLUID COMPUTATION IN PART 1

In this appendix, the PHOENICS-related listings (Q1 & GROUND) are provided. There are two Q1 listings, one of which is for Case 1 of Chapter 5 (the numerical simulation of experiment), another is for the "standard run" of Chapter 6 (numerical studies of propagating flames exhibiting the Landau instability). The GROUND listing is used by all the runs both in Chapter 5 and in Chapter 6.

A full explanation of the items included in listings for the "standard run" of Chapter 6 is also given in order to enable the reader to learn how to set up PHOENICS to solve the flow considered.

The structure and contents of PHOENICS can be found in "Four Lectures on the PHOENICS Computer Code" (Spalding 1982a).

## A.1 Satellite

The PHOENICS satellite PIPPA is used to prepare the input data for the running of EARTH. The problems are specified by way of PIPPA-language settings made in a Q1 file, the summarized listings showing the groups needed both for Case 1 of Chapter 5 and for the "standard run" of Chapter 6 are supplied at the end of the appendix for reference.

In the present section, the noteworthy features of each data group are discussed by reference to the "standard run" of Chapter 6.

Group 2. Transience; Time-Step Specification

STEADY is set to .FALSE., in order that a transient calculation may be performed. The time-step size is set to 2.E-3 and a maximum of 80 time steps is specified.

Group 3. X-direction Grid Specification

20 grid cells are equally spaced in the x-direction to cover the extent of 0.1m.

Group 4. Y-direction Grid Specification

20 grid cells are uniformly spaced in the y-direction to subdivide the dimension of 0.1m.

Group 7. Variables Stored, Solve & Named

The variables solved for are : pressure P1 and two velocity components in x-and y-directions respectively, U1 & V1. Storage for the density field is provided in this group through the use of SOLUTN.

Group 8. Terms and Devices

The command TERMS is employed to eliminate the diffusion terms from the differential equations.

Group 9. Properties of the Medium

The density is calculated in GROUND by calling the subroutine for the particle tracking and density calculation as described in Section 4.3 and Section 4.5.2. RHO1 is set to GRND for this purpose.

Group 12. Convection and Diffusion Adjustments

GALA is set to .TRUE. in this group so as to activate the GALA procedure for the continuity equation (3.1). Correspondingly, the source term, $(-\frac{1D\rho}{\rho Dt})$, is set in Group 19 of the GROUND subroutine.

Group 13. Boundary Conditions and Special Sources

Subroutines PATCH and COVAL are used to set boundary conditions and source terms. The first pair of PATCH and COVAL is to set zero pressure gradient at the open end of the chamber. The second one is to set the gravitational force.

Group 15. Termination of Sweeps

A maximum of 20 sweeps of the domain are specified for each time step. The RESREF for each solved variable is set to 1.E-5.

Group 19. Special Calls from EARTH to GROUND

All special data are transferred to GROUND to change the value for the parametric study. They are defnied in the Q1 listing.

Group 20. Preliminary Print-Out

NOHEAD is set to .TRUE., so as to de-activate the printing-out of input data at the top of the results listing.

Group 22. Field Print-Out and Plot Control

Field values for solved variables and density are printed out by calling command OUTPUT. NTPRIN=20 activates the field printout every 20 time steps. PATCH and COVAL settings are used to plot the contour of the pressure throughout the domain.

## A.2 GROUND

The relevant aspects of the GROUND subroutine are listed at the end of the appendix. This listing is used by all calculations made in Chapter 5 and Chapter 6. The noteworthy features of GROUND for the "standard run" of Chapter 6 are described below.

Preliminary Section

The appropriate dimensions are set.

Subroutine GREX1 is deactivated by C in column 1.

USEGRD is set to .TRUE. in order to visit necessary group in GROUND.

Group 1. RUN Title

Subroutine MAKE is used for activate storage in EARTH of the quantities indicated. Index EASP1 is needed as working-space store for the source term of the continuity equation.

Group 9. Properties of the Medium

The fluid value of density calculated by subroutines in Group 19 is set in this group by way of calling subroutine SETYX.

Group 19. Special Calls to GROUND from EARTH

Section 1

ICASE is set to 2 for this run.

Special data transferred from PIPPA are re-named here.

Cell geometrical quantities are obtained from EARTH and stored in local arrays for use in the particle tracking and density calculation.

The initial interface is specified.

The initial density distribution is determined from the initial interface location by calling the density

calculation subroutine, DENXY.

Section 8

The field values of the velocity components in the x-direction and the y-direction respectively are obtained at the end of each time step and stored in local arrays for use of the particle tracking.

The particle-tracking subroutine, TRKXY, is called to track the flame front.

Section 9

The source term described in Equation (4.12) is set in this section by the calling of subroutine SETYX and the built-in function FN34.

Q1 Listing for Case 1 of Chapter 5

```
   LINE 2 SETS TALK, RESTRT, FIRST RUN & LAST RUN NUMBER...
TALK=.F. ,RESTRT=.T. ,IR1=1 ,IR2=1
    GROUP 1. RUN title
    GROUP 2. Transience; time-step specification
STEADY=.FALSE.
GRDPWR(T,250,1.0,1.0)
LSTEP=120
    GROUP 3. x-direction grid specification
NX=20,XULAST=0.5
XFRAC(1)=-2.0,XFRAC(2)=0.02
XFRAC(3)=16.0,XFRAC(4)=0.0575
XFRAC(5)=2.0,XFRAC(6)=0.02
    GROUP 4. y-direction grid specification
NY=20,YVLAST=0.5
YFRAC(1)=-2.0,YFRAC(2)=0.02
YFRAC(3)=16.0,YFRAC(4)=0.0575
YFRAC(5)=2.0,YFRAC(6)=0.02
    GROUP 5. z-direction grid specification
    GROUP 6. Body-fitted coordinates or grid distortion
    GROUP 7. Variables stored, solved & named
DEN1=18,NAME(18)=RHO
SOLUTN(RHO,Y,N,N,N,N,N)
SOLUTN(P1,Y,Y,N,N,N,N)
SOLUTN(U1,Y,Y,N,N,N,N)
SOLUTN(V1,Y,Y,N,N,N,N)
    GROUP 8. Terms (in differential equations) & devices
TERMS(U1,Y,Y,N,Y,Y,N)
TERMS(V1,Y,Y,N,Y,Y,N)
    GROUP 9. Properties of the medium (or media)
RHO1=GRND
    GROUP 10. Inter-phase-transfer processes and properties
    GROUP 11. Initialization of variable or porosity fields
    GROUP 12. Convection and diffusion adjustments
GALA=.T.
    GROUP 13. Boundary conditions and special sources
PATCH(1,CELL,1,1,1,1,1,1,1,1000)
COVAL(1,P1,FIXP,0.0)
PATCH(2,PHASEM,1,20,1,20,1,1,1,1000)
COVAL(2,V1,FIXFLU,0.0)
INIADD=.F.
    GROUP 14. Downstream pressure for PARAB=.TRUE.
    GROUP 15. Termination of sweeps
LSWEEP=20
RESREF(P1)=1.E-5
RESREF(U1)=1.E-5
RESREF(V1)=1.E-5
    GROUP 16. Termination of iterations
    GROUP 17. Under-relaxation devices
RELAX(U1,FALSDT,0.01)
RELAX(V1,FALSDT,0.01)
    GROUP 18. Limits on variables or increments to them
    GROUP 19. Special calls from EARTH to GROUND
        C----RG(1) & RG(2)--cold-& hot-gas densities
        C----RG(3)  --  burning velocity
        C----RG(4)  --  initial location of particles
        C----RG(5) & RG(6) --DISMIN &  DISMAX for particle addition
```

```
        C----RG(7)--  DXMIN to delete particles
        C----IG(1)  NTPRIN
        C----IG(3)  NPMAX for RESTRT
        C----IG(4)=1    IRESTA
        C----IG(6)=1  for compressible flow
RG(1)=1.08
RG(2)=0.19
RG(3)=0.4
RG(5)=5.E-4
RG(6)=1.0E-3
RG(7)=8.E-4
RG(8)=0.5
RG(9)=0.8
IG(1)=20
IG(3)=87
IG(4)=1
IG(6)=3
    GROUP 20. Preliminary print-out
NOHEAD=.T.
    GROUP 21. Print-out of variables
OUTPUT(P1,Y,Y,Y,Y,Y,Y)
OUTPUT(U1,Y,Y,Y,Y,Y,Y)
OUTPUT(V1,Y,Y,Y,Y,Y,Y)
OUTPUT(RHO,Y,Y,Y,Y,Y,Y)
    GROUP 22. Spot-value print-out
IXMON=10
IYMON=10
    GROUP 23. Field print-out and plot control
IPLTL=50
NTPRIN=20
    GROUP 24. Dumps for restarts
SAVE=.F.
STOP
```

Q1 Listing for the "standard run" of Chapter 6

```
   LINE 2 SETS TALK, RESTRT, FIRST RUN & LAST RUN NUMBER...
TALK=.F., RESTRT=.F., IR1=1 , IR2=1
    GROUP 1. Run title
    GROUP 2. Transience; time-step specification
STEADY=.F.
GRDPWR(T,500,1.0,1.0)
LSTEP=80
    GROUP 3. X-direction grid specification
GRDPWR(X,20,0.1,1.0)
    Group 4. Y-direction grid specification
GRDPWR(Y,20,0.1,1.0)
    GROUP 5. Z-direction grid specification
    GROUP 6. Body-fitted coordinates or grid distortion
    GROUP 7. Variables stored, solved  & named
DEN1=18,NAME(18)=RHO
SOLUTN(P1,Y,Y,N,N,N,N)
SOLUTN(U1,Y,Y,N,N,N,N)
SOLUTN(V1,Y,Y,N,N,N,N)
SOLUTN(RHO,Y,N,N,N,N,N)
    GROUP 8. Terms (in differential equations) & devices
TERMS(U1,Y,Y,N,Y,Y,N)
TERMS(V1,Y,Y,N,Y,Y,N)
    GROUP 9. Properties of the medium (or media)
RHO1=GRND
    GROUP 10. Inter-phase-transfer processes and properties
    GROUP 11. Initialization of variable or porosity fields
    GROUP 12. Convection and diffusion adjustments
GALA=.T.
    GROUP 13. Boundary conditions and special sources
PATCH(1,CELL,1,20,1,1,1,1,1,1000)
COVAL(1,P1,FIXP?0.0)
PATCH(2,PHASEM,1,20,1,20,1,1,1,1000)
COVAL(2,V1,FIXFLU,0.0)
    GROUP 14. Downstream pressure for PARAB=.TRUE.
    GROUP 15. Termination of sweeps
LSWEEP=20
RESREF(P1)=1.E-5
RESREF(U1)=1.E-5
RESREF(V1)=1.E-5
    GROUP 16. Termination of iterations
    GROUP 17. Under-relaxation devices
    GROUP 18. Limits on variables or increments to them
    GROUP 19. Special calls from EARTH to GROUND
         C----RG(1) &RG(2)--cold- &hot-gas densities
         C----RG(3)--burning velocity
        C----RG(4) & RG(10)--DATA for initial interface
         C----RG(5) & RG(6)--DISMIN & DISMAX for particle addition
         C----RG(7) DXMIN to delete particles
         C----IG(1) NTPRIN
RG(1)=1.0
RG(2)=0.2
RG(3)=0.4
RG(4)=-0.0025
```

```
RG(5)=8.E-4
RG(6)=1.2E-3
RG(7)=8.E-4
RG(10)=1.0
IG(1)=10
     GROUP 20. Preliminary print-out
NOHEAD=.T.
    GROUP 21. Print-out of variables
OUTPUT(P1,Y,Y,Y,Y,Y,Y)
OUTPUT(U1,Y,Y,Y,Y,Y,Y)
OUTPUT(V1,Y,Y,Y,Y,Y,Y)
OUTPUT(RHO,Y,Y,Y,Y,Y,Y)
    GROUP 22. Spot-value print-out
IXMON=10
IYMON=10
    GROUP 23. Field print-out and plot control
IPLTL=50
NTPRIN=20
    GROUP 24. Dump for restarts
SAVE=.F.
STOP
```

GROUND Listing

```
C***********************************************************
      SUBROUTINE GROUND
$INCLUDE SATEAR/G
$INCLUDE GRDLOC/G
$INCLUDE GRDEAR/G
CXXXXXXXXXXXXXXXXXXXXXXXXXXXXXXXXXXXXXXXX USER SECTION STARTS:
C
C 1  Set dimensions of satellite-to-GROUND data arrays to those
C    of the satellite.
     COMMON/LGRND/LG(10)/IGRND/IG(10)/RGRND/RG(10)/CGRND/CG(10)
     LOGICAL LG,USEGRD
     CHARACTER*4 CG
C
C 2  User dimensions own arrays here, for example:
C    DIMENSION UUH(10,10),UUC(10,10),UUX(10,10),UUZ(10,10)
C    DIMENSION
     COMMON/SET1/XP(500),YP(500),NPMAX
     COMMON/SET3/XU(20),YV(20),GVOL(20,20),XG(20),YG(20)
     COMMON/SET4/GDENS(20,20),U(20,20),V(20,20),SORCE(20,20)
     COMMON/SET6/SFL,CIRC,NPT,RHOC,RHOH,DXMIN,DSP,IRESTA,ND
    &     ,DLIMI,ICASE
     COMMON/SET7/IAG
     DIMENSION GXG(20,20),GXU(20,20),GYG(20,20),GYV(20,20)
     DIMENSION GD1DP(20,20),GP1(20,20),GDENF(20,20)
C=============
C
C 3  User places his data statements here, for example:
C    DATA NXDIM,NYDIM/10,10/
C
C 4  De-activate next statement if GREX1 (ie. GRound EXample 1)
C    is not required
C    CALL GREX1
C
C 5  Set USEGRD=.TRUE. in order to visit sequences below.
     USEGRD=.TRUE.
         IF(.NOT.USEGRD) RETURN
C
         IF(IGR.EQ.13) GO TO 13
     GO TO (1,2,3,4,5,6,7,8,9,10,11,12,13,14,15,16,17,18,19,20,21,
    122,23,24), IGR
C***********************************************************************
C
C----GROUP 1. Run title
C
   1 GO TO (101,102),ISC
 101 CONTINUE
     CALL MAKE(XG2D)
     CALL MAKE(XU2D)
     CALL MAKE(YV2D)
     CALL MAKE(YG2D)
     CALL MAKE(VOL)
     CALL MAKE(EASP1)
     RETURN
 102 CONTINUE
     RETURN
C***********************************************************************
```

```
C--- GROUP 9. Properties of the medium (or media)
    9 CONTINUE
      DO 936 IY=1,NY
      DO 936 IX=1,NX
      GDENF(IY,IX)=GDENS(IY,IX)
  936 CONTINUE
      IF(ICASE.EQ.2) GO TO 937
C----For compressible flow-- to set DRHDP
      IF(IG(6).EQ.1) THEN
      CALL GETYX(P1,GP1,NY,NX)
      BR=1./1.4
      DO 935 IY=1,NY
      DO 935 IX=1,NX
      GP=GP1(IY,IX)+1.E5
      GD1DP(IY,IX)=BR/GP
      GDENF(IY,IX)=GDENS(IY,IX)*(GP/1.E5)**BR
  935 CONTINUE
      CALL SETYX(D1DP,GD1DP,NY,NX)
      ENDIF
  937 CONTINUE
      CALL SETYX(AUX(DEN1),GDENF,NY,NX)
      RETURN
C*****************************************************************
C
C--- GROUP 19. Special calls to GROUND from EARTH
C
   19 GO TO (191,192,193,194,195,196,197,198),ISC
  191 CONTINUE
C   * ------------------- SECTION 1 ---- START OF TIME STEP
      ICASE=2
C---Special data transfered from Q1
      RHOC=RG(1)
      RHOH=RG(2)
      SFL=RG(3)
      AMP=RG(4)
      CIRC=RG(4)
      GLAMT=RG(10)
      DXMIN=RG(7)
      DSP=RG(8)
      DLIMI=RG(9)
      NPT=IG(1)
      ND=IG(3)
      IRESTA=IG(4)
      IDRDP=IG(6)
C----To get geometry
      CALL GETYX(VOL,GVOL,NY,NX)
      CALL GETYX(XU2D,GXU,NY,NX)
      CALL GETYX(XG2D,GXG,NY,NX)
      DO 888 IX=1,NX
      XU(IX)=GXU(1,IX)
      XG(IX)=GXG(1,IX)
  888 CONTINUE
      CALL GETYX(YV2D,GYV,NY,NX)
      CALL GETYX(YG2D,GYG,NY,NX)
      DO 999 IY=1.NY
      YV(IY)=GYV(IY,1)
      YG(IY)=GYG(IY,1)
  999 CONTINUE
```

```
      IF(ICASE.EQ.2) THEN
C---To set initial interface for Case 2
      IF(ISTEP.EQ.1) THEN
      IF(IRESTA.NE.1) THEN
      NPMAX=180
      OMAG=(3.14159/180.0)*GLAMT
      DO 1910 IP=1,NPMAX
      XP(IP)=FLOAT(IP-1)*XULAST/FLOAT(NPMAX)
      YP(IP)=0.1/36.+AMP*SIN(FLOAT(IP-1)*OMAG)
 1910 CONTINUE
      XP(NPMAX)=XU(NX)
      YP(NPMAX)=0.1/FLOAT(NX)
      ENDIF
      ENDIF
C---Initial interface for restart run
      IF(IRESTA.EQ.1) THEN
      NPMAX=ND
      DO 789 IP=1,ND
      READ(12,689) XP(IP),YP(IP)
  689 FORMAT(1X,1PE11.3,2X,1PE11.3)
  789 CONTINUE
      DO 889 IP=1,NPMAX
      WRITE(6,589) XP(IP),YP(IP)
  589 FORMAT(1X,1PE11.3,2X,1PE11.3)
  889 CONTINUE
      WRITE(6,*) "NPMAX",NPMAX
      ENDIF
C---To set initial density field
      IF(ICASE.EQ.2) THEN
      IF(IRESTA.EQ.1) GO TO 933
      DO 934 IY=1,1
      DO 934 IX=1,NX
      GDENS(IY,IX)=RHOC
  934 CONTINUE
      DO 937 IY=1,1
      DO 937 IX=1,NX
      GDENS(IY,IX)=RHOH
  937 CONTINUE
  933 CONTINUE
C---To calculate volumetric source for GALA for first time-step
      IAG=1
      CALL DENXY(ISTP)
      IAG=0
      ENDIF
      ENDIF
C---To get density field for restart run
      IF(IRESTA.EQ.1.AND.ISTEP.EQ.1) THEN
      READ(13,1911) GDENS
 1911 FORMAT(1X,1P5E11.3)
      ENDIF
      RETURN
  192 CONTINUE
C   * -------------------- SECTION 2 ----- START OF SWEEP
C---To set source for GALA
      IF(IG(9).EQ.1) THEN
      CALL SETYX(EASP1,SORCE,NY,NX)
      CALL FN34(4*NPHI+72,EASP1,1.0)
      ENDIF
      RETURN
```

```
  198 CONTINUE
C   * ------------------ SECTION 8 --- FINISH OF TIME STEP
      CALL GETYX(U1,U,NY,NX)
      CALL GETYX(V1,V,NY,NX)
C---To track the interface
      CALL TRKXY(ISTEP,RG(5),RG(6))
C---Arrow data for plotting velocity vector
      IF(MOD(ISTEP,IG(1)).EQ.0) THEN
      CALL GETYX(U1,GU1,NY,NX)
      CA_L GETYX(V1,GV1,NY,NX)
      WRITE(19,*) ((GXG(IY,IX),IY=1,NY),IX=1,NX)
      WRITE(19,*) ((GYG(IY,IX),IY=1,NY),IX=1,NX)
      WRITE(19,*) ((GU1(IY,IX),IY=1,NY),IX=1,NX)
      WRITE(19,*) ((GV1(IY,IX),IY=1,NY),IX=1,NX)
      ENDIF
      RETURN
C*************************************************************
```

# APPENDIX B - INTERFACE-TRACKING AND DENSITY-CALCULATION SUBROUTINES

In this appendix, the set of subroutines used for the tracking of the interface and for the density calculation, as described in Chapter 4, is presented. These subroutines do not require any action from the user except the setting of the required storage for the variables used in DIMENSION statements. Comments are made in these listings.

The Listing of SUBROUTINE TRKXY

```
       SUBROUTINE TRKXY(ISTP,DISMIN,DISMAX)
C*****************************************************************
C   FUNCTION : TO TRACK THE INTERFACE
C*****************************************************************
$INCLUDE SATEAR/G
$INCLUDE GRDLOC/G
$INCLUDE GRDEAR/G
      COMMON/SET1/XP(500,YP(500),NPMAX
      COMMON/SET3/XU(20),YV(20),GVOL(20,20),XG(20),YG(20)
      COMMON/SET4/GDENS(20,20),U(20,20),V(20,20),SORCE(20,20)
      COMMON/SET5/UP(500),VP(500)
      COMMON/SET6/SFL,CIRC,NPT,RHOC,RHOH,DXMIN,
     &     DSP,IRESTA,ND,DLIMI,ICASE
      COMMON/SET7/IAG
      LOGICAL TESTIN
      TESTIN=.FALSE.
C*****************************************************************
C  To insert the time-step size
      DELTAT=DT
C
C*****************************************************************
C---To set initial interface
      IF(ICASE.EQ.2) GO TO 1910
      IF(ISTP.EQ.1) THEN
      IF(IRESTA.NE.1) THEN
      NPMAX=90
      DO 1901 IP=1,NPMAX
      IPN=NPMAX-IP+1
      XP(IP)=CIRC*COS(FLOAT(IPN)*3.14159/180.0)
      YP(IP)=CIRC*SIN(FLOAT(IPN)*3.14159/180.0)
 1901 CONTINUE
      XP(1)=0.0
      YP(NPMAX)=0.0
      ENDIF
      ENDIF
C*****************************************************************
C--- To adjust the distance between particles of the new track
 1910 CONTINUE
      IAG=0
      IF(IRESTA.EQ.1.AND.ISTP.EQ.1) GO TO 124
      IF(ISTP.EQ.1) THEN
      IF(IAG.EQ.0) GO TO 124
      ENDIF
  123 CONTINUE
      IF(DISMIN.EQ.0.0) GO TO 300
      IP=1
  310 IF(IP.GE.NPMAX+1) GO TO 300
      IDE=0
      IAD=0
      IP=IP+1
      IPM1=IP-1
  320 DIST=SQRT((YP(IP)-YP(IPM1))**2+(XP(IP)-XP(IPM1))**2)
      IF(IDE.GT.0.AND.IAD.GT.0) GO TO 310
      IF(.NOT.TESTIN) GO TO 2958
      WRITE(6,2959) DIST,IP,IPM1
 2959 FORMAT(5X,"DIST(IP,IPM1)= ",1PE10.3,1X,I3,1X,I3,/)
```

```
 2958 CONTINUE
      IF(DIST.LT.DISMIN) GO TO 340
      IF(DIST.LT.DISMAX) GO TO 310
      IF(IP.GE.NPMAX+1) GO TO 300
      IAD=IAD+1
      NPMAX=NPMAX+1
      NPMAX1=NPMAX-2
      IF(.NOT.TESTIN) GO TO 2113
      WRITE(6,1999) IP
 1999 FORMAT(1X,"ADD PARTICLE WHEN IP= ",IX,I3)
 2113 CONTINUE
      DO 350 INS1=NPMAX1,IP,-1
      INS1P1=INS1+1
      XP(INS1P1)=XP(INS1)
      YP(INS1P1)=YP(INS1)
  350 CONTINUE
      XP(IP)=0.5*(XP(IP)+XP(IPM1))
      YP(IP)=0.5*(YP(IP)+YP(IPM1))
      GO TO 320
  340 CONTINUE
      IF(IP.GE.NPMAX) GO TO 300
      IDE=IDE+1
      NPMAX=NPMAX-1
      DO 360 IDEL=IP,NPMAX
      IDELP1=IDEL+1
      XP(IDEL)=XP(IDELP1)
      YP(IDEL)=YP(IDELP1)
  360 CONTINUE
      IF(.NOT.TESTIN) GO TO 2116
      WRITE(6,2111) NPMAX
      WRITE(6,2112) (YP(IA),IA=1,NPMAX)
      WRITE(6,2112) (XP(IA),IA=1,NPMAX)
 2112 FORMAT(1X,"NEW PARTICLE DISTRIBUTION ",/,12(1PE10.3,1X))
 2116 CONTINUE
      GO TO 320
 2111 FORMAT(1X,"NPMAX= ",I3,/)
  300 CONTINUE
C*****************************************************************
C--- DElete the particles in the hot region when interface intersects
      IPF=1
      IA=0
 1001 CONTINUE
      IF(IPF.GE.NPMAX-1) GO TO 1006
      XPF=XP(IPF)
      YPF=YP(IPF)
      DO 1002 IPL=IPF+1,NPMAX
      XPL=XP(IPL)
      YPL=YP(IPL)
      DXY=SQRT((XPL-XPF)**2.+(YPL1YPF)**2.)
      IF(DXY.LT.DXMIN) THEN
      IF(IPL-IPF).GT.2) THEN
      GO TO 1003
      ENDIF
      ENDIF
 1002 CONTINUE
      IPF=IPF+1
```

```
      GO TO 1001
 1003 CONTINUE
      IA=IA+1
      DO 1004 IJ=IPF+1,IPL
      NPMAX=NPMAX-1
      DO 1005 IDEP=IPF+1,NPMAX
      IDEP1=IDEP+1
      XP(IDEP)=XP(IDEP1)
      YP(IDEP)=YP(IDEP1)
 1005 CONTINUE
 1004 CONTINUE
      IF(IA.GT.0) GO TO 123
 1006 CONTINUE
C
C
      IF(MOD(ISTP,NPT).NE.0) GO  TO 810
      WRITE(6,802) ISTP
  802 FORMAT(5X,"*** OUTPUT FROM TRACK AT ISTEP= ",1X,I3)
      DO 800 IP=1,NPMAX
      WRITE(6,806) XP(IP),YP(IP)
  806 FORMAT(1X,1PE12.4,2X,1PE12.4)
  800 CONTINUE
      WRITE(6,*) "NPMAX= ",NPMAX
  810 CONTINUE
  124 CONTINUE
C*************************************************************
C---To calculate densities
      CALL DENXY(ISTP)
C
      IF(ISTP.EQ.LSTEP.AND.IAG.EQ.1) THEN
      IF(IAG.EQ.1) THEN
      WRITE(6,1912) GDENS
 1912 FORMAT(1X,1P5E11.3)
      ENDIF
      ENDIF
      IF(IAG.EQ.1) GO  TO 710
C---To compute the new position of the particle
      DO 777 IP=1,NPMAX
      XP(IP)=XP(IP)+UP(IP)*DELTAT
      YP(IP)=YP(IP)+VP(IP)*DELTAT
      IF(XP(IP).LT.1.E-4) XP(IP)=0.0
      IF(YP(IP).LT.1.E-4) YP(IP)=0.0
      IF(XP(IP).GT.XU(NX)-1.E-4) XP(IP)=XU(NX)
      IF(YP(IP).GT.YV(NY)-1.E-4) YP(IP)=YV(NY)
  777 CONTINUE
    6 CONTINUE
C--- Delete the particles which reach walls
      ID=0
      DO 3 IPD=1,NPMAX
      IF(XP(IPD).LT.1.E-4.OR.YP(IPD).LT.1.E-4.OR.XP(IPD).
     &  GT.XU(NX)-1.E-4.OR.YP(IPD).GT.YV(NY)-1.E-4) THEN
      NPMAX=NPMAX-1
      ID=ID+1
      DO 4 IDEL=IPD,NPMAX
      IDELP1=IDEL+1
      XP(IDEL)=XP(IDELP1)
      YP(IDEL)=YP(IDELP1)
    4 CONTINUE
```

```
      ENDIF
      IF(ID.GT.0) GO TO 6
    3 CONTINUE
      YP(1)=YP(2)+1.E-6
      IF(XP(1).LT.XU(1)) XP(1)=0.0
      IF(YP(NPMAX).LT.YV(1)) YP(NPMAX)=0.0
      IF(ICASE.EQ.2) THEN
      XP(1)=0.0
      XP(NPMAX)=XU(NX)
      ENDIF
      IAG=IAG+1
      GO TO 123
  710 CONTINUE
C*****************************************************************
C
      RETURN
      END
```

The Listing of SUBROUTINE DENXY

```
      SUBROUTINE DENXY(ISTP)
C*****************************************************************
C    FUNCTION: TO CALCULATE DENSITIES AND PARTICLE VELOCITY
C*****************************************************************
$INCLUDE SATEAR/G
$INCLUDE GRDLOC/G
$INCLUDE GRDEAR/G
      COMMON/SET1/XP(500),YP(500),NPMAX
      COMMON/SET3/XU(20),YV(20),GVOL(20,20),XG(20),YG(20)
      COMMON/SET4/GDENS(20,20),U(20,20),V(20,20),SORCE(20,20)
      COMMON/SET5/UP(500),VP(500)
      COMMON/SET6/SFL,CIRC,NPT,RHOC,RHOH,DXMIN,DSP,IRESTA,ND,
     &    DLIMI,ICASE
       COMMON/SET7/IAG
      DIMENSION AREAH(20,20),XPC(100),YPC(100),GLENG(20,20)
      DIMENSION US(500),VS(500),VF(500),UF(500),VFO(500),UFO(500)
C*****************************************************************
C---- To set density for whole domain to that of the cold gas
      DO 10 IY=1,NY
      DO 10 IX=1,NX
      AREAH(IY,IX)=0.0
      IF(IAG.EQ.1) THEN
      SORCE(IY,IX)=0.0
      GLENG(IY,IX)=0.0
      ENDIF
   10 CONTINUE
C*****************************************************************
C---To locate particle and start from left or top wall
      DO 20 IXIN=1,NX
      IF(XP(1).LT.XU(IXIN)) GO TO 30
   20 CONTINUE
   30 DO 40 IYIN=1,NY
      IF(YP(1).LT.YV(IYIN)) GO TO 50
   40 CONTINUE
   50 XIN=XP(1)
      YIN=YP(1)
      IFIN=3
      IF(IYIN.EQ.NY.AND.XP(1).GE.0.0) THEN
      IF(YP(1).GT.YV(NY)-1.E-4) THEN
      XIN=XP(1)
      YIN=YV(NY)
      IFIN=4
       ENDIF
      ENDIF
C
C
      IPIN=1
C---Main loop starts here
   60 CONTINUE
      IFO=0
       DO 70 IPOUT=IPIN,NPMAX
      IF(XU(IXIN).LT.XP(IPOUT)) IFO=1
      IF(XU(IXIN).LT.XP(IPOUT).AND.YV(IYIN).LT.YP(IPOUT)) IFO=5
      IF(IXIN.NE.1) THEN
```

```
      IF(XU(IXIN-1).GT.XP(IPOUT)) IFO=3
      IF(XU(IXIN-1).GT.XP(IPOUT).AND.YV(IYIN).LT.YP(IPOUT)) IFO=8
      ENDIF
      IF(YV(IYIN).LT.YP(IPOUT)) IFO=4
      IF(IYIN.NE.1) THEN
      IF(YV(IYIN-1).GT.YP(IPOUT)) IFO=2
      IF(XU(IXIN).LT.XP(IPOUT).AND.YV(IYIN-1).GT.YP(IPOUT)) IFO=6
      ENDIF
      IF(IYIN.NE.1.AND.IXIN.NE.1) THEN
      IF(XU(IXIN-1).GT.XP(IPOUT).AND.YV(IYIN-1).GT.YP(IPOUT)) IFO=7
      ENDIF
      IF(IFO.NE.0) GO TO 80
   70 CONTINUE
C--- The out-face is south or east
      IFO=2
      IF(IXIN.EQ.NX.AND.YP(NPMAX).GE.0.0) THEN
      IF(XP(NPMAX).GT.XU(NX)-1.E-4) THEN
      IFO=1
      ENDIF
      ENDIF
   80 CONTINUE
C--- To locate position where track across cell faces
      IF(IPOUT.EQ.1) GO TO 3301
      IPM1=IPout-1
      XD=XP(IPOUT)-XP(IPM1)
      YD=YP(IPOUT)-YP(IPM1)
      GO TO (90,100,110,120,120,90,110,120) IFO
   90 RATIO=(XU(IXIN)-XP(IPM1))/(XD+1.E-10)
      GO TO 399
  100 RATIO=(XU(IXIN-1)-XP(IPM1))/(XD+1.E-10)
      GO TO 399
  110 RATIO=(XU(IXIN-1)-XP(IPM1))/(XD+1.E-10)
      GO TO 399
  120 RATIO=(YV(IYIN)-YP(IPM1))/(YD+1.E-10)
  399 CONTINUE
      XOUT=XP(IPM1)+XD*RATIO
      YOUT=YP(IPM1)+YD*RATIO
      IF(IPOUT.GE.NPMAX) XOUT=XP(NPMAX)
      IF(IPOUT.GE.NPMAX) YOUT=YP(NPMAX)
 3301 CONTINUE
C---------------
      IF(IAG.EQ.0) GO TO 332
      XPC(1)=XIN
      YPC(1)=YIN
      NPTS=IPOUT-IPIN+2
      DO 130 IP=1,NPTS-2
      XPC(IP+1)=XP(IPIN+IP-1)
      YPC(IP+1)=YP(IPIN+IP-1)
  130 CONTINUE
      XPC(NPTS)=XOUT
      YPC(NPTS)=YOUT
C*****************************************************************
C--- To calculate the area of the cell occupied by the hot gas
      DX=XU(1)
      DY=YV(1)
      XS=0.0
      YS=0.0
      XL=XU(IXIN)
```

```
      YL=YV(IYIN)
      IF(IXIN.NE.1) DX=XU(IXIN)-XU(IXIN-1)
      IF(IXIN.NE.1) XS=XU(IXIN-1)
      IF(IYIN.NE.1) DY=YV(IYIN)-YV(IYIN-1)
      IF(IYIN.NE.1) YS=YV(IYIN-1)
      AREAT=DX*DY
      IF(IFIN.EQ.1.AND.IFO.EQ.2) GO TO 140
      IF(IFIN.EQ.1.AND.IFO.EQ.7) GO TO 140
      IF(IFIN.EQ.1.AND.IFO.EQ.8) GO TO 160
      IF(IFIN.EQ.1.AND.IFO.EQ.6) GO TO 170
      IF(IFIN.EQ.1.AND.IFO.EQ.5) GO TO 170
      IF(IFIN.EQ.1.AND.IFO.EQ.3) GO TO 150
      IF(IFIN.EQ.1.AND.IFO.EQ.4) GO TO 160
      IF(IFIN.EQ.1.AND.IFO.EQ.1) GO TO 170
      GO TO 180
  140 AREAH1=AREAT-AREA(XPC,YPC,NPTS,YS,1.0)
      GO TO 330
  150 AREAH1=AREA(XPC,YPC,NPTS,YL,-1.0)
      GO TO 330
  160 AREAH1=AREA(XPC,YPC,NPTS,YL,-1.0)
      GO TO 330
  170 AREAH1=AREAT-AREA(YPC,XPC,NPTS,XL,-1.0)
      IF(YOUT.GT.YIN) AREAH1=AREA(YPC,XPC,NPTS,XL,1.0)
      GO TO 330
  180 IF(IFIN.EQ.2.AND.IFO.EQ.1) GO TO 190
      IF(IFIN.EQ.2.AND.IFO.EQ.3) GO TO 200
      IF(IFIN.EQ.2.AND.IFO.EQ.4) GO TO 210
      IF(IFIN.EQ.2.AND.IFO.EQ.2) GO TO 220
      IF(IFIN.EQ.2.AND.IFO.EQ.5) GO TO 190
      IF(IFIN.EQ.2.AND.IFO.EQ.8) GO TO 200
      IF(IFIN.EQ.2.AND.IFO.EQ.6) GO TO 220
      IF(IFIN.EQ.2.AND.IFO.EQ.7) GO TO 220
      GO TO 230
  190 AREAH1=AREA(YPC,XPC,NPTS,XL,1.0)
      GO TO 330
  200 AREAH1=AREAT-AREA(XPC,YPC,NPTS,YS,1.0)
      GO TO 330
  210 AREAH1=AREA(YPC,XPC,NPTS,XL,1.0)
      GO TO 330
  220 AREAH1=AREAT-AREA(XPC,YPC,NPTS,YS,1.0)
      IF(XOUT.GT.XIN) AREAH1=AREA(XPC,YPC,NPTS,YS,-1.0)
      GO TO 330
  230 IF(IFIN.EQ.3.AND.IFO.EQ.1) GO TO 240
      IF(IFIN.EQ.3.AND.IFO.EQ.2) GO TO 250
      IF(IFIN.EQ.3.AND.IFO.EQ.4) GO TO 260
      IF(IFIN.EQ.3.AND.IFO.EQ.3) GO TO 270
      IF(IFIN.EQ.3.AND.IFO.EQ.6) GO TO 250
      IF(IFIN.EQ.3.AND.IFO.EQ.5) GO TO 260
      IF(IFIN.EQ.3.AND.IFO.EQ.8) GO TO 270
      IF(IFIN.EQ.3.AND.IFO.EQ.7) GO TO 270
      GO TO 280
  240 AREAH1=AREA(XPC,YPC,NPTS,YS,-1.0)
      GO TO 330
  250 AREAH1=AREA(XPC,YPC,NPTS,YS,-1.0)
      GO TO 330
  260 AREAH1=AREAT-AREA(XPC,YPC,NPTS,YL,1.0)
      GO TO 330
  270 AREAH1=AREA(YPC,XPC,NPTS,XS,1.0)
```

```
      IF(YOUT.GT.YIN) AREAH1=AREAT-AREA(YPC,XPC,NPTS,XS,-1.0)
      GO TO 330
  280 IF(IFIN.EQ.4.AND.IFO.EQ.1) GO TO 290
      IF(IFIN.EQ.4.AND.IFO.EQ.2) GO TO 300
      IF(IFIN.EQ.4.AND.IFO.EQ.3) GO TO 310
      IF(IFIN.EQ.4.AND.IFO.EQ.4) GO TO 320
      IF(IFIN.EQ.4.AND.IFO.EQ.6) GO TO 290
      IF(IFIN.EQ.4.AND.IFO.EQ.7) GO TO 310
      IF(IFIN.EQ.4.AND.IFO.EQ.5) GO TO 320
      IF(IFIN.EQ.4.AND.IFO.EQ.8) GO TO 320
      GO TO 330
  290 AREAH1=AREAT-AREA(XPC,YPC,NPTS,YL,1.0)
      GO TO 330
  300 AREAH1=AREAT-AREA(YPC,XPC,NPTS,XL,-1.0)
      GO TO 330
  310 AREAH1=AREA(XPC,YPC,NPTS,YL,-1.0)
      GO TO 330
  320 AREAH1=AREA(XPC,YPC,NPTS,YL,-1.0)
      IF(XOUT.GT.XIN) AREAH1=AREAT-AREA(XPC,YPC,NPTS,YL,1.0)
  330 CONTINUE
C*****************************************************************
C--- To calculate the length lying inside the cell for the source
C     of GALA
C
      DIS1A=XP(IPIN)-XIN
      DIS1B=YP(IPIN)-YIN
      DIS1=SQRT(DIS1A**2.+DIS1B**2.)
      DIS2A=XOUT-XP(IPM1)
      DIS2B=YOUT-YP(IPM1)
      DIS2=SQRT(DIS2A**2.+DIS2B**2.)
      GLENG(IYIN,IXIN)=GLENG(IYIN,IXIN)+DIS1+DIS2
      DO 331 IP=IPIN,IPM1-1
      DISA=XP(IP+1)-XP(IP)
      DISB=YP(IP)-YP(IP+1)
      DISC=SQRT(DISA**2.+DISB**2.)
      GLENG(IYIN,IXIN)=GLENG(IYIN,IXIN)+DISC
  331 CONTINUE
  332 CONTINUE
C*****************************************************************
C--- To calculate velocity of particles
      IF(IAG.EQ.1) GO TO 345
C--- Burning velocity
      DO 400 IP=IPIN,IPM1
      DISA=XP(IP+1)-XP(IP)
      DISB=YP(IP)-YP(IP+1)
      IF(IP.EQ.NPMAX) DISA=XP(IP)-XP(IP-1)
      IF(IP.EQ.NPMAX) DISB=YP(IP-1)-YP(IP)
      DISC=SQRT(DISA**2.+DISB**2.)
      US(IP)=SFL*(DISB/DISC)
      VS(IP)=SFL*(DISA/DISC)
C--- UNburned-gas velocity
      VF(IP)=0.0
      UF(IP)=0.0
C--- Vp calculation
      IF(ICASE.EQ.2) THEN
      DO 1002 IYA=NY,1,-1
      DO 1002 IXA=1,NX
      IF(GDENS(IYA,IXA).LT.1.0) GO TO 1003
```

```
1002 CONTINUE
1003 CONTINUE
     INDYV=IYA
     INDXU=IXIN
     IF(XP(IP).GT.XG(IXIN)) THEN
     INDXU=IXIN+1
     ENDIF
     IF(IXIN.EQ.1) THEN
     IF(XP(IP).LT.XG(IXIN)) THEN
     IF(INDYV.GE.NY) THEN
     VV1=0.0
     GO TO 1001
     ENDIF
     VV1=V(INDYV,INDXU)
1001 CONTINUE
     IF(INDYV+1.GE.NY) THEN
     VFN=0.0
     VFS=0.0
     GO TO 3014
     ENDIF
     VFN=V(INDYV+1,INDXU)
     VFS=VV1
     GO TO 3014
     ENDIF
     ENDIF
     IF(IXIN.EQ.NX) THEN
     IF(XP(IP).GT.XG(IXIN)) THEN
     IF(INDYV+1.GE.NY) THEN
     VV1P1=0.0
     GO TO 1301
     ENDIF
     VV1P1=V(INDYV+1,NX)
1301 CONTINUE
     IF(INDYV.GE.NY) THEN
     VFN=VV1P1
     VFS=0.0
     GO TO 3014
     ENDIF
     VFN=VV1P1
     VFS=V(INDYV,NX)
     GO TO 3014
     ENDIF
     ENDIF
     IF(INDYV.GE.NY) THEN
     VV1=0.0
     VV2=0.0
     GO TO 1005
     ENDIF
     VV1=V(INDYV,INDXU-1)
     VV2=V(INDYV,INDXU)
1005 CONTINUE
     IF(INDYV+1.GE.NY) THEN
     VV1P1=0.0
     VV2P1=0.0
     GO TO 307
     ENDIF
     VV1P1=V(INDYV+1,INDXU-1)
     VV2P1=V(INDYV+1,INDXU)
     GO TO 307
```

```
C--- Up calculation
      INDYV=IYA
      INDXU=IXIN
      IF(YP(IP).GT.YG(IYIN)) THEN
      INDYV=IYA+1
      INDXU=IXIN
      ENDIF
      IF(IXIN.EQ.1) THEN
      FRAC1=(XU(1)-XP(IP))/XU(1)
      FRAC2=1.0-FRAC1
      IF(INDYV.GE.NY) THEN
      UU2=0.0
      GO TO 1101
      ENDIF
      UU2=U(INDYV,1)
 1101 CONTINUE
      IF(INDYV+1.GE.NY) THEN
      UU2P1=0.0
      UFS=UU2*FRAC2
      GO TO 4046
      ENDIF
      UU2P1=U(INDYV+1,1)
      UFN=UU2P1*FRAC2
      UFS=UU2*FRAC2
      GO TO 4046
      ENDIF
      IF(IXIN.EQ.NX) THEN
      FRAC1=(XU(NX)-XP(IP))/(XU(NX)-XU(NX-1))
      FRAC2=1.0-FRAC1
      IF(INDYV.GE.NY) THEN
      UU1=0.0
      GO TO 1103
      ENDIF
      UU1=U(INDYV,NX-1)
 1103 CONTINUE
      IF(INDYV+1.GE.NY) THEN
      UFN=0.0
      UFS=UU1*FRAC1
      GO TO 4046
      ENDIF
      UU1P1=U(INDYV+1,NX-1)
      UFN=UU1P1*FRAC1
      UFS=UU1*FRAC1
      GO TO 4046
      ENDIF
      IF(INDYV.GE.NY) THEN
      UU1=0.0
      UU2=0.0
      GO TO 1105
      ENDIF
      UU1=U(INDYV,INDXU-1)
      UU2=U(INDYV,INDXU)
 1105 CONTINUE
      IF(INDYV+1.GE.NY) THEN
      UU1P1=0.0
      UU2P1=0.0
      GO TO 4045
      ENDIF
```

```
      UU1P1=U(INDYV+1,INDXU-1)
      UU2P1=U(INDYV+1,INDXU)
      GO TO 4045
      ENDIF
C--- Case 1 ---
      IF(XP(IP).LT.YP(IP)) GO TO 101
      IF(IYIN.EQ.1) THEN
      INDYV=IYIN
      INDXU=IXIN
      IF(XP(IP).GT.XG(IXIN)) THEN
      INDXU=IXIN+1
      ENDIF
      VV2=0.0
      VV2P1=0.0
      VV1=V(1,INDXU)
      VV1P1=V(1,INDXU+1)
      FRAC1=YP(IP)/YV(1)
      FRAC2=1.0-FRAC1
      IV3=0
 1032 CONTINUE
      IF(GDENS(1,INDXU+1).GE.1.0) GO TO 1033
      IF(INDXU+1.GE.NX) GO TO 1034
      IF(IV3.GT.3) GO TO 1031
      INDXU=INDXU+1
      VV2=0.0
      VV2P1=0.0
      VV1=V(1,INDXU)
      VV1P1=V(1,INDXU+1)
      IV3=IV3+1
      GO TO 1032
 1033 CONTINUE
      VFW=VV1
      VFE=VV1P1
      VF(IP)=(VFW*(XG(INDXU+1)-XP(IP))-VFE*(XG(INDXU)-XP(IP)))/
     &       (XG(INDXU+1)-XG(INDXU))
      GO TO 1000
 1034 CONTINUE
      IF(INDXU.GE.NX) THEN
      VF(IP)=VFO(IP)
      GO TO 1000
      ELSE
      VV1=V(1,INDXU)
      VF(IP)=VV1
      GO TO 1000
      ENDIF
      ENDIF
      INDYV=IYIN
      INDXU=IXIN
      IF(XP(IP).GT.XG(IXIN)) THEN
      INDXU=IXIN+1
      ENDIF
      VV1=V(INDYV,INDXU)
      VV2=V(INDYV-1,INDXU)
      VV1P1=V(INDYV,INDXU+1)
      VV2P1=V(INDYV-1,INDXU+1)
      IV1=0
  102 CONTINUE
      IF(GDENS(INDYV,INDXU+1).EQ.1.0.AND.GDENS(INDYV-1,INDXU+1).
     &    EQ.1.0) GO TO 103
```

```
      IF(INDXU+1.GE.NX) GO TO 103
      IF(IV1.GT.3) GO TO 1031
      INDXU=INDXU+1
      VV1=V(INDYV,INDXU)
      VV2=V(INDYV-1,INDXU)
      VV1P1=V(INDYV,INDXU+1)
      VV2P1=V(INDYV-1,INDXU+1)
      IV1=IV1+1
      GO TO 102
  103 CONTINUE
      IF(INDXU+1.LT.NX) GO TO 107
      INDYV=IYIN
      INDXU=IXIN
      IF(XP(IP).GT.XG(IXIN)) THEN
      INDXU=IXIN+1
      ENDIF
      VV1=V(INDYV,INDXU)
      VV2=V(INDYV-1,INDXU)
      VV1P1=V(INDYV,INDXU+1)
      VV2P1=V(INDYV-1,INDXU+1)
 1031 CONTINUE
      IF(IXIN.EQ.NX) THEN
      VF(IP)=VFO(IP)
      GO TO 1000
      ELSE
      VF(IP)=0.0
      GO TO 1000
      ENDIF
  107 CONTINUE
      FRAC1=(YP(IP)-YV(INDYV-1))/(YV(INDYV)-YV(INDYV-1))
      FRAC2=1.0-FRAC1
      VFW=VV1*FRAC1+VV2*FRAC2
      VFE=VV1P1*FRAC1+VV2P1*FRAC2
      VF(IP)=(VFW*(XG(INDXU+1)-XP(IP))-VFE*(XG(INDXU)-XP(IP)))/
     &    (XG(INDXU+1)-XG(INDXU))
      GO TO 1000
  101 CONTINUE
      INDYV=IYIN
      INDXU=IXIN
      IF(XP(IP).GT.XG(IXIN)) THEN
      INDXU=IXIN+1
      GO TO 306
      ENDIF
      IF(IXIN.EQ.1) THEN
      FRAC1=XP(IP)/XG(1)
      FRAC2=1.0-FRAC1
      VV2=0.0
      VV2P1=0.0
      VV1=V(INDYV,1)
      VV1P1=V(INDYV+1,1)
      IV3=0
 3012 CONTINUE
      IF(GDENS(INDYV+1,1).GE.1.0) GO TO 3013
      IF(INDYV+1.GE.NY) GO TO 3013
      IF(IV3.GT.3) GO TO 305
      INDYV=INDYV+1
      VV2=0.0
      VV2P1=0.0
```

```
      VV1=V(INDYV,1)
      VV1P1=V(INDYV+1,1)
      GO TO 3012
 3013 CONTINUE
      IF(INDYV+1.GE.NY) GO TO 3011
      VFN=VV1P1*FRAC1
      VFS=VV1*FRAC1
 3014 VF(IP)=(VFS*(YV(INDYV+1)-YP(IP))-VFN*(YV(INDYV)-YP(IP)))/
     &    (YV(INDYV+1)-YV(INDYV))
      GO TO 1000
 3011 CONTINUE
      IF(INDYV.GE.NY) THEN
      VF(IP)=VFO(IP)
      GO TO 1000
      ELSE
      VV1=V(INDYV,1)
      VF(IP)=VV1
      GO TO 1000
      ENDIF
      ENDIF
  306 CONTINUE
      VV1=V(INDYV,INDXU-1)
      VV2=V(INDYV,INDXU)
      VV1P1=V(INDYV+1,INDXU-1)
      VV2P1=V(INDYV+1,INDXU)
      IV1=0
  302 CONTINUE
      IF(GDENS(INDYV+1,INDXU-1).EQ.1.0.AND.GDENS(INDYV+1,INDXU).
     &   EQ.1.0) GO  TO 303
      IF(INDYV+1.GE.NY) GO TO 303
      IF(IV1.GT.3) GO TO 3021
      INDYV=INDYV+1
      VV1=V(INDYV,INDXU-1)
      VV2=V(INDYV,INDXU)
      VV1P1=V(INDYV+1,INDXU-1)
      VV2P1=V(INDYV+1,INDXU)
      IV1=IV1+1
      GO TO 302
  303 CONTINUE
      IF(INDYV+1.LT.NY) GO TO 307
      INDYV=IYIN
      INDXU=IXIN
      IF(XP(IP).GT.XG(IXIN)) THEN
      INDXU=IXIN+1
      ENDIF
      VV1=V(INDYV,INDXU-1)
      VV2=V(INDYV,INDXU)
      VV1P1=V(INDYV+1,INDXU-1)
      VV2P1=V(INDYV+1,INDXU)
 3021 CONTINUE
      VF(IP)=0.0
      GO TO 1000
  307 CONTINUE
      FRAC1=(XG(INDXU)-XP(IP))/(XG(INDXU)-XG(INDXU-1))
      FRAC2=1.0-FRAC1
      IF(INDYV+1.GE.NY) GO TO 304
      VFN=VV1P1*FRAC1+VV2P1*FRAC2
      VFS=VV1*FRAC1+VV2*FRAC2
```

```
      VF(IP)=(VFS*(YV(INDYV+1)-YP(IP))-VFN*(YV(INDYV)-YP(IP)))/
     &   (YV(INDYV+1)-YV(INDYV))
      GO  TO 1000
  304 CONTINUE
      IF(INDYV.GE.NY) THEN
      VF(IP)=0.0
      GO TO 1000
      ELSE
      VV1=V(INDYV,INDXU-1)
      VV2=V(INDYV,INDXU)
      VF(IP)=VV1*FRAC1+VV2*FRAC2
      GO TO 1000
      ENDIF
  305 CONTINUE
      VF(IP)=0.0
 1000 CONTINUE
      IF(IP.GT.1) THEN
      IF(ABS(VF(IP)-VF(IP-1)).GT.DSP) VF(IP)=VF(IP-1)
      ENDIF
      VP(IP)=VF(IP)+VS(IP)
      VFO(IP)=VF(IP)
C----- Up  calculation --
      IF(YP(IP).GT.YG(IYIN)) THEN
      INDYV=IYIN+1
      INDXU=IXIN
      GO  TO 2011
      ENDIF
      IF(IYIN.EQ.1)  THEN
      FRAC1=YP(IP)/YG(1)
      UU1=U(1,INDXU)
      UU1P1=U(1,INDXU+1)
      UU2=0.0
      UU2P1=0.0
      IU1=0
 2012 CONTINUE
      IF(GDENS(1,INDXU+1).GE.1.0) GO TO 2013
      IF(INDXU+1.GE.NX) GO TO 2013
      IF(IU1.GT.3) GO TO 206
      INDXU=INDXU+1
      UU1=U(1,INDXU)
      UU1P1=U(1,INDXU+1)
      IU1=IU1+1
      GO TO 2012
 2013 CONTINUE
      IF(INDXU+1.GE.NX) GO TO 2014
      UFW=UU1
      UFE=UU1P1
      UF(IP)=(UFW*(XU(INDXU+1)-XP(IP))-UFE*(XU(INDXU)-XP(IP)))/
     &  (XU(INDXU+1)-XU(INDXU))
      GO  TO 2000
 2014 CONTINUE
      IF(INDXU.GE.NX) THEN
      UF(IP)=UFO(IP)
      GO TO 2000
      ELSE
      UU1=U(1,INDXU)
      UF(IP)=UU1
      GO TO 2000
```

```
      ENDIF
      ENDIF
 2011 CONTINUE
      UU1=U(INDYV,INDXU)
      UU2=U(INDYV-1,INDXU)
      UU1P1=U(INDYV,INDXU+1)
      UU2P1=U(INDYV-1,INDXU+1)
      IU1=0
  202 CONTINUE
      IF(GDENS(INDYV,INDXU+1).EQ.1.0.AND.GDENS(INDYV-1,INDXU+1).
     & EQ.1.0)  GO  TO 203
      IF(INDXU+1.GE.NX) GO TO 203
      IF(IU1.GT.3) GO TO 2041
      INDXU=INDXU+1
      UU1=U(INDYV,INDXU)
      UU2=U(INDYV-1,INDXU)
      UU1P1=U(INDYV,INDXU+1)
      UU2P1=U(INDYV-1,INDXU+1)
      IU1=IU1+1
      GO TO 202
  203 CONTINUE
      IF(INDXU+1.LT.NX) GO  TO 207
      INDYV=IYIN
      INDXU=IXIN
      IF(YP(IP).GT.YG(IYIN)) THEN
      INDYV=IYIN+1
      ENDIF
      UU1=U(INDYV,INDXU)
      UU2=U(INDYV-1,INDXU+1)
      UU2P1=U(INDYV-1,INDXU+1)
 2041 CONTINUE
  206 CONTINUE
      UF(IP)=0.0
      GO TO 2000
  207 CONTINUE
      FRAC1=(YP(IP)-YG(INDYV-1))/(YG(INDYV)-YG(INDYV-1))
      FRAC2=1.0-FRAC1
      UFW=UU1*FRAC1+UU2*FRAC2
      UFE=UU1P1*FRAC1+UU2P1*FRAC2
      UF(IP)=(UFW*(XG(INDXU+1)-XP(IP))-UFE*(XG(INDXU)-XP(IP)))/
     &  (XG(INDXU+1)-XG(INDXU))
      GO TO 2000
  201 CONTINUE
      IF(IXIN.EQ.1) THEN
      INDYV=IYIN
      INDXU=IXIN
      IF(YP(IP).GT.YG(IYIN)) THEN
      INDYV=IYIN+1
      ENDIF
      FRAC1=XP(IP)/XU(1)
      FRAC2=1.0-FRAC1
      UU2=0.0
      UU2P1=0.0
      UU1=U(INDYV,1)
      UU1P1=U(INDYV+1,1)
      IU4=0
 4012 CONTINUE
      IF(GDENS(INDYV+1,1).GE.1.0) GO  TO 4013
      IF(INDYV+1.GT.NY) GO TO 4011
```

```
      IF(IU4.GT.3) GO TO 206
      INDYV=INDYV+1
      UU1=U(INDYV,1)
      UU1P1=U(INDYV+1,1)
      IU4=IU4+1
      GO TO 4012
 4013 CONTINUE
      UFN=UU1P1*FRAC1
      UFS=UU1*FRAC1
      UF(IP)=(UFS*(YG(INDYV+1)-YP(IP))-UFN*(YG(INDYV)-YP(IP)))/
     &    (YG(INDYV+1)-YG(INDYV))
      GO TO 2000
 4011 CONTINUE
      IF(INDYV.GE.NY) THEN
      UF(IP)=UFO(IP)
       GO  TO 2000
      ELSE
      UU1=U(INDYV,1)
      UF(IP)=UU1
      GO  TO 2000
       ENDIF
      ENDIF
      INDYV=IYIN
      INDXU=IXIN
      IF(YP(IP).GT.YG(IYIN)) THEN
      INDYV=IYIN+1
      ENDIF
      UU1=U(INDYV,INDXU-1)
      UU2=U(INDYV,INDXU)
      UU1P1=U(INDYV+1,INDXU-1)
      UU2P1=U(INDYV+1,INDXU)
      IU1=0
  402 CONTINUE
      IF(GDENS(INDYV+1,INDXU-1).EQ.1.0.AND.GDENS(INDYV+1,INDXU).
     &  EQ.1.0) GO TO 403
       IF(INDYV+1.GE.NY) GO TO 403
      IF(IU1.GT.3)  GO TO 4031
      INDYV=INDYV+1
      UU1=U(INDYV,INDXU-1)
      UU2=U(INDYV,INDXU)
      UU1P1=U(INDYV+1,INDXU-1)
      UU2P1=U(INDYV+1,INDXU)
      IU1=IU1+1
      GO TO 402
  403 CONTINUE
      IF(INDYV+1.LT.NY) GO  TO 4045
      INDYV=IYIN
       INDXU=IXIN
      IF(YP(IP).GT.YG(IYIN)) THEN
      INDYV=IYIN+1
      ENDIF
      UU1=U(INDYV,INDXU-1)
      UU2=U(INDYV,INDXU)
      UU1P1=U(INDYV+1,INDXU-1)
      UU2P1=U(INDYV+1,INDXU)
 4031 CONTINUE
      IF(IYIN.EQ.NY) THEN
      UF(IP)=UFO(IP)
      GO TO 2000
```

```
      ELSE
      UF(IP)=0.0
      GO TO 2000
      ENDIF
 4045 CONTINUE
      FRAC1=(XU(INDXU)-XP(IP))/(XU(INDXU)-XU(INDXU-1))
      FRAC2=1.0-FRAC1
      UFN=UU1P1*FRAC1+UU2P1*FRAC2
      UFS=UU1*FRAC1+UU2*FRAC2
 4046 UF(IP)=(UFS*(YG(INDYV+1)-YP(IP))-UFN*(YG(INDYV)-YP(IP)))/
     &  (YG(INDYV+1)-YG(INDYV))
      GO TO 2000
 2000 CONTINUE
      IF(IP.GT.1) THEN
      IF(ABS(UF(IP)-UF(IP-1)).GT.DSP)  UF(IP)=UF(IP-1)
      ENDIF
      UP(IP)=UF(IP)+US(IP)
      UFO(IP)=UF(IP)
      UP(1)=0.0
      VP(NPMAX)=0.0
  400 CONTINUE
  345 CONTINUE
C*****************************************************************
C--- Sum areas --
      IF(AREAH1.GT.AREAT-AREAH(IYIN,IXIN)) THEN
      AREAH(IYIN,IXIN)=AREAH1-AREAT+AREAH(IYIN,IXIN)
      ELSE
      AREAH(IYIN,IXIN)=AREAH(IYIN,IXIN)+AREAH1
      ENDIF
C------- To set new cell --
      IF(IFO.EQ.1) THEN
      IXIN=IXIN+1
      IFIN=3
      ELSE
      IF(IFO.EQ.2) THEN
      IYIN=IYIN-1
      IFIN=4
      ELSE
      IF(IFO.EQ.3) THEN
      IXIN=IXIN-1
       IFIN=1
      ELSE
      IF(IFO.EQ.4) THEN
      IYIN=IYIN+1
      IFIN=2
      ELSE
      IF(IFO.EQ.5) THEN
      IF(XOUT.LT.XU(IXIN))  XOUT=XU(IXIN)
      IF(YOUT.LT.YV(IYIN)) YOUT=YV(IYIN)
      IXIN=IXIN+1
      IYIN=IYIN+1
      IFIN=3
      ELSE
      IF(IFO.EQ.6) THEN
      IF(XOUT.LT.XU(IXIN)) XOUT=XU(IXIN)
      IXIN=IXIN+1
      IYIN=IYIN-1
      IF(YOUT.GT.YV(IYIN)) YOUT=YV(IYIN)
```

```
      IFIN=4
      ELSE
      IF(IFO.EQ7) THEN
      IXIN=IXIN-1
      IYIN=IYIN-1
      IF(XOUT.GT.XU(IXIN)) XOUT=XU(IXIN)
      IF(YOUT.GT.YV(IYIN)) YOUT=YV(IYIN)
      IFIN=4
      ELSE
      IF(IFO.EQ.8) THEN
      IF(YOUT.LT.YV(IYIN)) YOUT=YV(IYIN)
      IXIN=IXIN-1
      IYIN=IYIN+1
      IF(XOUT.GT.XU(IXIN)) XOUT=XU(IXIN)
      IFIN=1
      ENDIF
      ENDIF
      ENDIF
      ENDIF
      ENDIF
      ENDIF
      ENDIF
      ENDIF
      IPIN=IPOUT
      XIN=XOUT
      YIN=YOUT
      IF(IPOUT.GT.NPMAX) GO TO 340
      GO TO 60
C---- Main loop end here --
  340 CONTINUE
      IF(IAG.EQ.0) GO TO 346
C--- To calculate area ratio and to set density
      DO 350 IY=1,NY
      DO 350 IX=1,NX
      IF(AREAH(IY,IX).NE.0.0) THEN
      ABC=GVOL(IY,IX)
      ALPHA=AREAH(IY,IX)/ABC
      DEN=RHOC*(1.0-ALPHA)+RHOH*ALPHA
      GDENS(IY,IX)=DEN
      SORCE(IY,IX)=SFL*GLENG(IY,IX)*RHOC*(1.0/RHOH-1.0/RHOC)
      ELSE
      IF(GDENS(IY,IX).LT.DLIMI) THEN
      GDENS(IY,IX)=RHOH
      ELSE
      GDENS(IY,IX)=RHOC
      ENDIF
      ENDIF
  350 CONTINUE
      IF(ICASE.EQ.2) THEN
      DO 351 IY=1,NY
      DO 351 IX=1,NX
      SORCE(IY,IX)=SORCE(IX,IY)
  351 CONTINUE
      ENDIF
  346 CONTINUE
      RETURN
      END
C
```

```
      FUNCTION AREA(XP,YP,NPTS,YY,SWAP)
      DIMENSION XP(100),YP(100)

      AREA=0.0
      DO 10 IP=1,NPTS-1
      XOLD=XP(IP)
      XNEW=XP(IP+1)
      YOLD=YP(IP)
      YNEW=YP(IP+1)
      AREA=AREA+0.5*(2.0*YY-YNEW-YOLD)*(XNEW-XOLD)*SWAP
   10 CONTINUE
      RETURN
      END
```

# APPENDIX C - LISTINGS OF THE Q1 AND GROUND FILES FOR THE TWO-FLUID COMPUTATION IN PART 2

## Q1 Listing

All values listed are those used for the "stable"-oscillation case in Section 7.6.2; and they will be changed accordingly when parametric studies are performed.

```
TALK=F;RUN(1,1)
    GROUP 1.Run title
    GROUP 2.Transience; time-step specification
STEADY=.F.
TLAST=GRND
LSTEP=150
    GROUP 3. X-direction grid specification
GRDPWR(X,40,1.0,1.0)
    GROUP 4. Y-direction grid specification
    GROUP 5. Z-direction grid specification
    GROUP 6. Body-fitted coordinates or grid distortion
    GROUP 7. Variables stored, solved & named
ONEPHS=.F.
SOLUTN(P1,Y,Y,N,N,N,N)
SOLUTN(U1,Y,Y,N,N,N,N)
SOLUTN(U2,Y,Y,N,N,N,N)
SOLUTN(R1,Y,Y,N,N,N,N)
SOLUTN(R2,Y,Y,N,N,N,N)
INTMDT=20
NAME(20)=MDOT
SOLUTN(MDOT,Y,N,N,N,N,N)
    GROUP 8. Terms (in differential equations) & devices
TERMS(U1,Y,Y,N,Y,Y,Y)
TERMS(U2,Y,Y,N,Y,N,Y)
    GROUP 9. Properties of the medium (or media)
RHO1=GRND,RHO2=GRND
DRH1DP=GRND,DRH2DP=GRND
    GROUP 10. Inter-phase-transfer processes and properties
CFIPS=GRND
CMDOT=GRND
    GROUP 11. Initialization of variable or porosity fields
FIINIT(P1)=500.
FIINIT(U1)=10.,FIINIT(U2)=20.
FIINIT(R1)=0.8,FIINIT(R2)=0.2
    GROUP 12. Convection and diffusion adjustments
    GROUP 13. Boundary conditions and special sources
PATCH(INF,WEST,1,1,1,1,1,1,1,1000)
COVAL(INF,P2,FIXFLU,GRND)
```

```
COVAL(INF,P1,FIXFLU,GRND)
COVAL(INF,U1,ONLYMS,GRND)
COVAL(INF,U2,ONLYMS,GRND)
PATCH(FIX,EAST,NX,NX,1,1,1,1,1,1000)
COVAL(FIX,P1,FIXVAL,GRND)
    GROUP 14. Downstream pressure for PARAB=.TRUE.
    GROUP 15. Termination of sweeps
      *** LSWEEP is set only for the first time-step
LSWEEP=300
    GROUP 16. Termination of iterations
RESREF(P1)=1.E-4,RESREF(U1)=1.E-4
RESREF(U2)=1.E-4,RESREF(U2)=1.E-4
RESREF(R1)=1.E-4,RESREF(R2)=1.E-4
    GROUP 17. Under-relaxation devices
RELAX(R1,LINRLX,0.3)
RELAX(R2,LINRLX,0.3)
RELAX(U1,FALSDT,1.E-3)
RELAX(U2,FALSDT,1.E-3)
RELAX(MDOT,LINRLX,0.5)
    GROUP 18. Limits on variables or increments to them
    GROUP 19. Data communicated by satellite to GROUND
     *** RG(1) - Coefficient Cf in the interfluid friction term
         RG(2) - Coefficient Cm in the interfluid mass transfer rate
         RG(3) - DT set in GROUND for the first time step
         RG(5) - Density of Fluid 1
         RG(6) - Density of Fluid 2
         IG(1) Index for two types of boundary conditions
         IG(2) - LSWEEP after the second time step
RG(1)=23.0
RG(2)=100.0
RG(3)=50.
RG(5)=1.0
RG(6)=0.2
IG(1)=1
IG(2)=50
    GROUP 20. Preliminary print-out
NOHEAD=.T.
    GROUP 21. Print-out of variables
OUTPUT(P1,Y,Y,Y,Y,Y,Y)
OUTPUT(U1,Y,Y,Y,Y,Y,Y)
OUTPUT(U2,Y,Y,Y,Y,Y,Y)
OUTPUT(R2,Y,Y,Y,Y,Y,Y)
OUTPUT(MDOT,Y,Y,Y,Y,Y,Y)
    GROUP 22. Spot-value print-out
NPRMON=30,IXMON=NX/2
    GROUP 23. Field print-out and plot control
NTPRIN=20,IPLTL=200
USEGRD=.T.,USEGRX=.F.,NAMGRD=DULL
    GROUP 24. Dumps for restarts
STOP
```

GROUND Listing

```
     SUBROUTINE GROUND
$INCLUDE SATEAR/G
$INCLUDE GRDLOC/G
$INCLUDE GRDEAR/G
      INTEGER HIGH,OLD,AUX
      LOGICAL STORE,SOLVE,PRINT
CXXXXXXXXXXXXXXXXXXXXXXXXXXXXXXXXXX USER SECTION STARTS:
      COMMON/LGRND/LG(20)/IGRND/IG(20)/RGRND/RG(20)/CGRND/CG(10)
      LOGICAL LG
      CHARACTER*4 CG
C
      DIMENSION GP1(1,40),GP(1,40),GDRDP1(1,40),GDRDP2(1,40)
      DIMENSION GRHO1(1,40),GRHO2(1,40),GMCO(1,40),GCFP(1,40)
      DIMENSION GVOL(1,40),GR1(1,40),GR2(1,40),GXAXIS(150),GYAXIS(150)
      DIMENSION GPP1(1,40),GMASS2(1,40),GUO(1,40),GU1(1,40),GU2(1,40)
      DIMENSION GPB(1,40),GMASS1(1,40)
      LOW(I)=NPHI+I
      HIGH(I)=2*NPHI+I
      OLD(I)=3*NPHI+I
      IN(I)=4*NPHI+I
      STORE(I)=MOD(ISLN(I),2).EQ.0
      SOLVE(I)=MOD(ISLN(I),3).EQ.0
      PRINT(I)=MOD(IPRN(I),2).EQ.0
C
C
      IXL=IABS(IXL)
          IF(IGR.EQ.13) GO TO 13
          IF(IGR.EQ.19) GO TO 19
      GO TO (1,2,3,4,5,6,7,8,9,10,11,12,13,14,15,16,17,18,19,20,21,
     122,23,24),IGR
C*********************************************************************
C
C---GROUP 1. Run title
C
    1 GO TO (1001,1002),ISC
 1001 CONTINUE
      CALL MAKE(VOL)
      RETURN
 1002 CONTINUE
      RETURN
C*********************************************************************
C
C--- GROUP 2. Transience; time-step specification
C
    2 CONTINUE
      DT=RG(3)
      IF(ISTEP.GT.1) DT=1.E-3
      RETURN
C*********************************************************************
C
C--- GROUP 9. Properties of the medium (or media)
C
C************
    9 CONTINUE
C--- To set densities for the cold gas
      PRES=1.E5
```

```
      BR=1.0/1.4
      CALL GETYX(P1,GP1,1,NX)
      DO 911 IX=1,NX
      GP(1,IX)=PRES+GP1(1,IX)
  911 GRHO1(1,IX)=RG(5)*(GP(1,IX)/PRES)**BR
      CALL SETYX(AUX(DEN1),GRHO1,1,NX)
      DO 921 IX=1,NX
      GP(1,IX)=PRES+GP1(1,IX)
  921 GDRDP1(1,IX)=BR/GP(1,IX)
      CALL SETYX(D1DP,GDRDP1,1,NX)
C--- To set densities for the hot gas
      DO 931 IX=1,NX
      GP(1,IX)=PRES+GP1(1,IX)
  931 GRHO2(1,IX)=RG(6)*(GP(1,IX)/PRES)**BR
      CALL SETYX(AUX(DEN2),GRHO2,1,NX)
      DO 941 IX=1,NX
      GP(1,IX)=PRES+GP1(1,IX)
  941 GDRDP2(1,IX)=BR/GP(1,IX)
      CALL SETYX(D2DP,GDRDP2,1,NX)
      RETURN
C*****************************************************************
C
C--- GROUP 10. Inter-phase-transfer processes and properties
C
   10 GO TO (101,102),ISC
  101 CONTINUE
C--- for CFIPS.LE.GRND---  . inter-phase friction coeff. AUX(INTFRC).
C
      CALL GETYX(U1,GU1,1,NX)
      CALL GETYX(U2,GU2,1,NX)
      CALL GETYX(R1,GR1,1,NX)
      CALL GETYX(R2,GR2,1,NX)
      CALL GETYX(VOL,GVOL,1,NX)
      CALL GETYX(AUX(DEN2),GRHO2,1,NX)
C
      DO 1011 IX=1,NX
      DU=ABS(GU1(1,IX)-GU2(1,IX))
      BDU=AMAX1(1.0,DU)
      GCFP(1,IX)=GCF*GVOL(1,IX)*GR1(1,IX)*GR2(1,IX)*GRHO2(1,IX)
     &   *BDU
C
 1011 CONTINUE
C
C
      CALL SETYX(AUX(INTFRC),GCFP,1,NX)
      RETURN
  102 CONTINUE
C--- for CMDOT.EQ.GRND- inter-phase mass transfer Index AUX(INTMDT).
C
C
      DO 1021 IX=1,NX
      DU=ABS(GU1(1,IX)-GU2(1,IX))
      BDU=AMAX1(1.0,DU)
      GMCO(1,IX)=-GCM*GVOL(1,IX)*GR1(1,IX)*GR2(1,IX)*GRHO2(1,IX)*BDU
 1021 CONTINUE
C
      CALL SETYX(AUX(INTMDT),GMCO,1,NX)
      RETURN
```

```
C*****************************************************************
C
C--- GROUP 13. Boundary conditions and special sources
C
   13 CONTINUE
C------------------------------------ value= GRND
C--- Boundary conditions for a sudden change in back pressure
C
      DO 1391 IX=1,NX
      GPB(1,IX)=0.0
      IF(ISTEP.GT.1.AND.IG(1).EQ.1) GPB(1,NX)=1.E3
 1391 CONTINUE
      CALL ONLYIF(P1,P1,"FIX")
      CALL SETYX(VAL,GPB,1,40)
C
C--- Boundary conditions for the oscillatory mass inflow rate
      UO=10.
      OME=100.
      GK=3.14159*OME*DT*FLOAT(ISTEP-1)
      GK=GK-IFIX(GK/3.14159)*3.14159
      DO 1392 IX=1,NX
      GUU(1,IX)=UO
      IF(ISTEP.GT.1.AND.IG(1).EQ.2) GUO(1,IX)=UO*(1.+COS(GK))
      GMASS1(1,IX)=0.9*RG(5)*GUO(1,IX)
      GMASS2(1,IX)=0.1*RG(6)*GUO(1,IX)
 1392 CONTINUE
      CALL ONLYIF(U1,U1,"INF")
      CALL SETYX(VAL,GUO,1,40)
      CALL ONLYIF(U2,U2,"INF")
      CALL SETYX(VAL,GUO,1,40)
C
      CALL ONLYIF(P1,P1,"INF")
      CALL SETYX(VAL,GMASS1,1,40)
      CALL ONLYIF(P2,P2,"INF")
      CALL SETYX(VAL,GMASS2,1,40)
      RETURN
C*****************************************************************
C
C--- GROUP 19. Special calls to GROUND from EARTH
C
   19  GO TO (191,198),ISC
  191 CONTINUE
C   *--------------- SECTION 1 -- START of TIME STEP
      IF(ISTEP.GT.1) LSWEEP=IG(2)
      GCF=RG(1)
      GCM=RG(2)
      CALL GETYX(P1,GP1,1,NX)
      RETURN
C
  198 CONTINUE
C  *---------------- SECTION 8 -- FINISH of TIME STEP
C-- To print out pressure variation with time at mid-duct section
C
      CALL GETYX(P1,GPP1,1,NX)
      ISTPM=ISTEP-1
      IHNX=NX/2
      IF(ISTEP.NE.1) GO TO 1981
      GPLOW=GPP1(1,IHNX)
      GPREF=GPLOW
 1981 CONTINUE
```

```
      GXAXIS(ISTEP)=0.0
      GYAXIS(ISTEP)=0.0
      IF(ISTEP.EQ.1) GO TO 1982
      GXAXIS(ISTEP)=DT*UO*ISTPM/XULAST
      GYAIXS(ISTEP)=(GPP1(1,IHNX)-GPLOW)/GPREF
 1982 CONTINUE
      IF(ISTEP.NE.LSTEP) GO TO 1983
      WRITE(6,1984) GXAXIS,GYAXIS
 1984 FORMAT(2E11.3)
 1983 CONTINUE
      RETURN
```